EXTENDED FRAMEWORK FOR EARTHQUAKE AND TSUNAMI RISK ASSESSMENT: PADANG CITY A CASE STUDY

A thesis submitted for the degree of Doctor of Philosophy
in the Faculty of Engineering of the University of Sheffield

By

Rini Mulyani

BSc. Civil Eng. (Indonesia), MSc. Structural Eng. (Sheffield)

Earthquake Engineering Group
Department of Civil and Structural Engineering
The University of Sheffield

January 2013

ACKNOWLEDGMENTS

I offer my sincerest gratitude and appreciation to my supervisor, Professor Kypros Pilakoutas, who has supported me throughout this project with his patience, guidance and outstanding knowledge. I would like to express gratitude and appreciation to my co-supervisor, Dr. Maurizio Guadagnini, for his continuous help and guidance during this project.

I want to acknowledge Prof. Dr. Ahmet Cevdet Yalciner for providing me with NAMI-DANCE software and for his valuable assistance in tsunami numerical modelling of this project.

My appreciation also extends to Dr. Shaukat Ali Khan for his technical assistance of my work at its early stages and Dr Iman Hajirasouliha for his advice. I am indebted to my colleagues who supported me in particular Raudhah, Yasser Jemaa, Yaser Helal, Tamim, Yasser Eljajeh, Reyes, Humberto, Naeimeh, Ali Reza, Sohaib, Harris, Andreea, Panos and Van Hien. I also want to thank Anggun, Mbak Linda, Kak Lin, Ita, Saila and Ain for providing a friendly environment and continuous supports.

I'm also thankful for the financial support provided to me by the Indonesian Ministry of Higher Education and Bung Hatta University, Padang.

Most of all I thank my parents Dr. Martibas Mara and Arnelys Arlina, my sisters and brothers as well as Asril Aboet family for their love and encouragement throughout everything. Without their continuous supports, this thesis would not have been possible.

This thesis is dedicated to my lovely husband Anas who has always stood by me and dealt with all of my absence throughout my PhD tenure.

ABSTRACT

The Great Sumatra earthquake and resulting devastating tsunami in 2004 have highlighted the significance of earthquake risk assessment that can effectively include all main associated hazards, such as tsunami. An integrated quantification of earthquake and tsunami risk is challenging due to mathematical and computational issues as well as limited data, and as such it has not been done before in developing countries. In addition, the conventional Probabilistic Seismic Hazard Assessment (PSHA) generally assumes a Poissonian earthquake model with a stationary rate of hazard. However, hazard rates increase with elapsed time since last large earthquake, or when a seismic gap is present along a fault, and thus, a time dependent (non-Poissonian) PSHA model is generally more suitable.

The Earthquake Risk Assessment (ERA) Framework developed at the University of Sheffield is extended in this study to account for tsunami and to include a time dependent hazard assessment. The ERA Framework is based on a stochastic approach that utilizes readily available seismological information. Hence, it is suitable for use in developing countries.

The extended framework is used to carry out earthquake and tsunami hazard assessments for Sumatra. This study finds that a maximum PGA of 0.65g on bedrock is expected in the area, a value comparable with that found in other recent studies, but higher than the Indonesian seismic code SNI 03-1726-2002 (the code uses a value of 0.3g). In addition, the time dependent model of this study captured the increased rate of hazard in the middle segment of the Sumatra Subduction Zone, which is consistent with the location of the seismic gap. Currently, the seismicity of this region has increased about 2 times above that of the long term rates. An average tsunami height of 20.7 m is estimated for Padang city at 10% probability of exceedance in 50 years.

This study estimates that total earthquake and tsunami risks for buildings in Padang are approximately £54.5 million and £30.8 million per annum, respectively. The annual fatality risk due to tsunamis is much higher than that due to earthquakes, which is approximately 2000 and 8 fatalities, respectively.

Total earthquake premiums for the existing building stock of Padang are estimated to be 36.4‰, 16.6‰, 8.1‰ and 3.1‰ for UBM, CBM, RCI and steel structures, respectively. For tsunami hazard, the recommended premium rates are 11.7‰, 9.9‰ and 7‰ for UBM, CBM, RCI/steel structures, respectively. For seismically designed structures, the premium rates decrease about 80% and 25% for earthquake and tsunami hazards, respectively. Earthquake insurance rates applied by insurance companies in Indonesia are comparable with those estimated for seismically designed structures (1.9‰ for RC/steel buildings and 4.7‰ for other buildings).

Mitigation strategies to minimize the risks are proposed including the enforcement of seismic design provisions for all buildings in Padang, nationwide obligatory seismic insurance for buildings, tsunami vertical evacuations shelters and tsunami energy dissipation efforts (e.g. offshore barriers, coastal vegetation). At least 17 points of tsunami evacuations refuges are proposed for Padang city, to increase the survival probability of the residents in the area.

TABLE OF CONTENTS

CHAPTER 3
METHODOLOGY FOR EARTHQUAKE AND TSUNAMI RISK ASSESSMENT FRAMEWORK

CHAPTER 4

DATA COLLECTION AND ANALYSIS FOR EARTHQUAKE AND TSUNAMI RISK ASSESSMENTS

CHAPTER 5

THE PROBABILISTIC SEISMIC HAZARD ASSESSMENT OF SUMATRA

CHAPTER 6

THE PROBABILISTIC TSUNAMI HAZARD ASSESSMENT OF SUMATRA

CHAPTER 7
EARTHQUAKE AND TSUNAMI RISK ASSESSMENTS AND MITIGATION STRATEGIES FOR PADANG CITY

CHAPTER 8
CONCLUSIONS AND RECOMMENDATIONS FOR FUTURE WORKS

APPENDIX A

APPENDIX B

APPENDIX C

APPENDIX D

APPENDIX E

APPENDIX F

LIST OF FIGURES

CHAPTER 1

CHAPTER 2

CHAPTER 3

CHAPTER 4

CHAPTER 5

CHAPTER 6

CHAPTER 7

LIST OF TABLES

CHAPTER 2

CHAPTER 3

CHAPTER 4

CHAPTER 5

CHAPTER 7

ABBREVIATIONS

AFE	Annual Frequency of Exceedance
ASEAN	Association of Southeast Asian Nations
AU	Area Unit
BAKORSURTANAL	Indonesian government agency for surveying and mapping
BMKG	Indonesian Agency for Meteorology, Climatology and Geophysics
BN	Bayesians Network
BPT	Brownian Passage Time
CBM	Confined Brick Masonry
EADR	Expected Annual Damage Ratio
EEFIT	Earthquake Engineering Field Investigation Team
EFL	Earthquake Fault Length
EM-DAT	Emergency Events Database
EQ-RACY	Earthquake Risk Assessment Cyprus
ERA	Earthquake Risk Assessment
FEM	Finite Element Method
FEMA	Federal Emergency Management Agency
GEBCO	General Bathymetric Chart of the Oceans
GESI	Global Earthquake Safety Initiative
GITEWS	German Indonesia Tsunami Early Warning System
GPS	Global Positioning System
HAZUS	Hazards United States
HRC	Homogeneous Reinforced Concrete
IDNDR	International Decade of Natural Disaster Reduction
InaTEWS	Indonesian Tsunami Early Warning System
IOC	Intergovernmental Oceanographic Commission

LF	Load Factor
MDR	Mean Damage Ratio
NCEDC	Northern California Earthquake Data Centre
NEIC	National Earthquake Information Centre
NOAA	National Oceanic and Atmospheric Administration
OCHA	Office for the Coordination of Humanitarian Affairs
PGA	Peak Ground Acceleration
PDF	Probability Distribution Function
PMEL	Pacific Marine Environmental Laboratory
PRP	Pure Risk Premium
PSHA	Probabilistic Seismic Hazard Assessment
PSTHA	Probabilistic Seismic and Tsunami Hazard Assessment
PTHA	Probabilistic Tsunami Hazard Assessment
RA	Rupture Area
RADIUS	Risk Assessment tools for Diagnosis of Urban areas against Seismic disasters
RC	Reinforced Concrete
RCI	Reinforced Concrete frame structures with masonry Infill
RLD	Sub-surface Rupture Length
RW	Rupture Width
SCHEMA	Scenarios for Tsunami Hazard Induced Emergency Management
SFZ	Sumatra Fault Zone
SNI	Indonesian National Standard
SPT	Standard Penetration Test
SRL	Surface Rupture Length
SSZ	Sumatra Subduction Zone
STWAVE	Steady-State Spectral Wave

TP	Total Premium
UBC	Uniform Building Code
UBM	Unreinforced Brick Masonry
USA	United States of America
USGS	United States Geological Survey
WGCEP	Working Group on California Earthquake Probabilities

CHAPTER 1

INTRODUCTION

1.1. INTRODUCTION

As a result of rapid growth in population, seismic risk across moderate and high seismicity regions increases continuously. It is estimated that until now, in the 21st century, more than 700,000 people were killed due to earthquakes, which affected more than 90 million people and resulted in over $ 450 billion of economic losses (EM-DAT, 2011). Spence (2007) points out that developing countries are more likely to be exposed to higher risk. This is mostly due to unpreparedness or inadequate mitigation strategies to deal with the hazards. However, the concern in devising seismic mitigation strategies in developing countries is generally low either due to ignorance, lack of human resources and detailed seismological data, or to other pressing natural needs. To address this problem, a cost effective and simple seismic risk framework is required, so that it can be easily adopted and implemented in developing countries (Khan, 2011; Kythreoti, 2002).

A key element for developing good mitigation strategies is to identify the potential hazard and risk. Experience from past earthquakes demonstrates that hazards triggered by earthquakes such as tsunami, liquefaction and landslides pose serious dangers. Recent examples include the M_w 9.0 Japan earthquake in 2011 and the M_w 9.1 great Sumatra earthquake in 2004. Both events triggered large tsunami leading to very high death tolls and displaced millions of people. The devastating effects of the tsunami in Japan are shown in Figure 1.1. Another example is the M_w 7.6 West Sumatra Earthquake in 2009 which resulted in more than 1,000 fatalities mostly caused by a massive landslide (Wilkinson et al., 2009). Despite rigorous research conducted in addressing earthquakes and associated hazards, most studies rarely include their combination into a risk assessment framework (Dominey-Howes et al., 2010; FEMA, 2009; IDNDR, 1990-2000; Khan, 2011; Kythreoti, 2002; Moharram et al., 2008; Mouroux and Le Brun, 2006). Hence, the overall risk for regions prone to these hazards is likely to be underestimated.

(a) (b)

Figure 1.1. Tsunami hazard: (a). Inland penetration of Tsunami wave train (Shimbun, 2011); (b). Shattered buildings and debris following the earthquake and tsunami in Japan (Kyodo, 2011)

To focus on tsunami hazard, the massive consequences of the Great Sumatra Earthquake in 2004 could have been reduced had there been tsunami mitigation strategies. Tsunami mitigation strategies must be developed based on tsunami hazard assessment. Therefore, an integrated quantification of earthquakes and associated tsunamis is required, which remains a challenge. A “scenario” or “deterministic” approach is generally adopted to evaluate tsunami hazard. However, the scenario approach has limited applications for broader policy and planning decisions (Burbidge et al., 2008). This highlights the importance of a probabilistic approach. Nevertheless, undertaking Probabilistic Tsunami Hazard Assessment (PTHA) is difficult.

For seismic hazard, the Probabilistic Seismic Hazard Assessment (PSHA) method pioneered by Cornell (1968) is widely used. This conventional PSHA is used to identify earthquake ground motions for a particular site. The method has four components which include the identification of seismic zones, earthquake recurrence functions, ground motion attenuation relationships and distance from seismic zones to site. The expected ground motion level is obtained by integrating probability density functions for the last 3 components above for all seismic zones. In this approach, a Poissonian model is generally assumed to characterise earthquake distribution. Musson (2000) states that the use of a Poissonian model is convenient, as the mathematical and computational solutions for earthquake occurrence probability are technically simple. However, if a non-Poissonian model is adopted,

the difficulty of the mathematical and computational solutions may increase since it involves more complex and a non-uniform seismicity models (Musson, 2000). Nevertheless, the problems are likely no longer prohibitive given the expansion of modern statistical methods (i.e. Bayesian integrals) as well as rapid development of computer power in the last decade. The non-Poissonian model is compulsory for a time-dependent PSHA, which takes into account the Elastic Rebound Theory, with a varying rate of hazard over time. Hazard rate increases extensively when the elapsed time since the last large earthquake has almost reached its return period or when seismic gaps are present in a region. For this case, a time independent (Poissonian model) PSHA model is not satisfactory, as people are unaware of the increasing upcoming hazards.

Musson (2000) proposed an alternative method to perform seismic hazard assessment in the UK. He adopted a stochastic technique using Monte Carlo simulations to produce synthetic earthquakes. This method does not require the integration procedure as that of the conventional PSHA. Consequently, the method has the adaptability to utilise different seismicity models including the non-Poissonian. In addition, this stochastic approach can also be extended to directly estimate the associated risk and to incorporate earthquake associated hazards such as tsunami, liquefaction and landslides. The approach was utilised by Kythreoti (2002) and Khan (2011) to develop an Earthquake Risk Assessment Framework (ERA Framework) that contains a PSHA module and seismic risk module. Nevertheless, earthquake associated hazards were not taken into account in this framework.

The generation of synthetic events in the Musson's approach was based on long term seismicity using earthquake recurrence relationships. The synthetic events were randomly generated over seismic zones defined in a particular area. However, Khan et al. (2010) argued that this approach would result in arbitrarily smearing the seismicity over the seismic zones. Hence, Khan (2011) generated synthetic earthquakes based on real events in an earthquake catalogue and utilised a fault rupture mode for each event as a defined location for the synthetic events. It was assumed that the fault rupture was oriented along the predominant fault line for a given zone. Khan (2011) showed that the generation of synthetic events within a defined boundary could maintain the known seismicity distribution in the investigated region.

However, Khan's approach heavily relied on an instrumental earthquake catalogue, which was assumed to represent the regional seismicity well, as it was the case for the Islamabad-Peshawar region, his case study area. As a result, the reliability of Khan's approach depends on the completeness of earthquake catalogues. Nevertheless, such complete earthquake catalogues are often lacking, particularly in developing countries.

1.2. RESEARCH AIM AND OBJECTIVES

The main aim of this research is to extend the ERA Framework developed by Khan (2011) at the University of Sheffield to account for tsunami and time-dependency of hazards. It should be noted that this study only takes into account earthquake-generated tsunami. Any tsunamis trigger by other hazards such as landslide, volcanic eruptions and meteorite impact are beyond the scope of this study.

Padang city, the capital of West Sumatra Province, in Indonesia is selected as the case study area. The case study region has a long history of earthquakes and tsunami with the presence of a seismic gap, which may lead to a mega thrust tsunamigenic earthquake in the near future. The accomplishment of the main aim requires several objectives as follows:

1. Extend the existing earthquake catalogue to appropriately characterise the seismicity of the case study region.
2. Extend the existing Probabilistic Seismic Hazard Assessment (PSHA) method to account for time independent and time dependent seismicity models.
3. Perform tsunami numerical analysis methods to complement tsunami databases, which are lacking for the examined area.
4. Develop a Probabilistic Tsunami Hazard Assessment (PTHA) module to complement the modified ERA Framework.
5. Carry out a risk assessment by taking into account all probable levels of earthquake and tsunami hazards in the case study region.
6. Propose mitigation strategies for Padang city.

1.3. LAYOUT OF THE THESIS

Chapter 2 presents a review of the literature available on the various aspects of seismology, earthquake hazard assessment, tsunami hazard assessment, vulnerability of existing structures, risk assessment, as well as earthquake mitigation strategies.

Chapter 3 describes the methodology adopted to upgrade the existing ERA Framework including the development of a time dependent seismicity model, the incorporation of the tsunami hazard assessment, and the estimation of the risks associated with earthquake and tsunami hazards.

Chapter 4 presents data collection for ERA Framework as well as preliminary analyses of the obtained data.

Chapters 5 and 6 present the outcomes and discussions of earthquake hazard assessment (PSHA) and tsunami hazard assessment (PTHA), respectively.

Chapter 7 presents the results of risk assessment and proposes earthquake and tsunami mitigation strategies that are suitable for Padang city.

In Chapter 8, the main conclusions from the present study are drawn, along with recommendations for further work.

CHAPTER 2

LITERATURE REVIEW

2.1. INTRODUCTION

The following sections present a literature review as a background for the development of the earthquake and tsunami risk assessment framework. This subject is multi-disciplinary and involves seismology, geophysics and structural engineering expertise. This chapter focuses on seismic risk assessment framework and its components including Probabilistic Seismic Hazard Assessment (PSHA), Probabilistic Tsunami Hazard Assessment (PTHA) and the vulnerability of existing building stock. Mitigation strategies associated with the risk are also presented in this chapter.

2.2. RISK ASSESSMENT FRAMEWORK

In general terms, risk can be defined as potential loss or consequence if exposed to a particular hazard. The determination of risk requires three components including hazard or encounter probability, exposure and vulnerability. Hazard represents any sources of potential damage or adverse effects on any elements at risk such as buildings, people, houses, bridges, etc. (CCOHS, 2009). Exposure denotes the probability that the elements at risk will be present when the hazard occurred. Vulnerability is defined as the reduced capacity of the elements at risk due to a given level of hazard. The probable consequence resulted from the hazard at a particular element is called a specific risk. The specific risk (R_{spec}) is a product of hazard (encounter probability) and vulnerability as shown in Equation 2.1 (Eckert et al., 2012).

$$R_{spec} = \int_0^\infty p(y)\, V(z_w, y)\, dy \qquad 2.1$$

Where,

$p(y)$: hazard or encounter probability of y-hazard

$V(z_w, y)$: the vulnerability of w-element at risk

z_w : the value of the w-element

Based on Equation 2.1, the total risk (R) of the elements can be estimated as follows:

$$R = \sum_{w} p(z_w)\, z_w\, R_{spec} \qquad 2.2$$

where,

$p(z_w)$: the exposure of w-element

The $\sum_w p(z_w)\, z_w$ term of the equation above is also known as probable maximum loss.

Ferson (2003) emphasised the sources of uncertainties in risk analysis including the lack of empirical data, the incorporation of subjective/judgmental information as well as the selection of mathematical model adopted in the analysis. To get reliable outcomes, these uncertainties need to be properly addressed. The use of Bayesian approach to quantify the uncertainty in the risk assessment framework was highlighted by many studies (Eckert et al., 2012; Ferson, 2003; Li et al., 2010; Rüttener et al., 1996) and its applications to deal with imprecise data were given by Egozcue and Rüttener (1996) and Rüttener et al. (1996). The formulation of the Bayesian rule for improving inference in the field of risk assessment was given in Berger (1985 cited in Eckert et al., 2012) as follows:

$$p(\theta|y_{obs}) \propto p(\theta) \times p(y_{obs}|\theta) \qquad 2.3$$

where,

θ : a vector of unknown parameters

$p(\theta)$: a prior distribution representing extra data information

$p(\theta|y_{obs})$: the posterior distribution of the parameters given the available data sample y_{obs}

$p(y_{obs}|\theta)$: the probability of the data as realisations of $p(\theta|y_{obs})$

The posterior distribution given above formally expresses the uncertainty associated with the partial knowledge of θ in the risk equation and its integration will lead to Bayesian risk as follows:

$$R_{BW}(d, y_{obs}) = \int p(\theta|y_{obs}) \times R_w(d, \theta)\, d\theta \qquad 2.4$$

where, $R_w(d, \theta)$ denotes a risk function for the system given a decisional variable d and the type of element at risk w (Eckert et al., 2012). Using the Bayesian method

Eckert et al. (2012) found that the inclusion of uncertainty in the risk model might lead to more cautious recommendation as a consequence of imperfect knowledge.

Ferson (2003) pointed out the main advantages of the Bayesian method including: 1). The method accounts for parameter uncertainty of a probability model; 2). The method allows the incorporation of subjective information (i.e. expert opinion, personal judgement, etc.) often required in the risk assessment; 3). The approach always gives precise answer even when the supporting data are very limited. Nevertheless, Ferson (2003) reviewed the shortcomings of the Bayesian method including: 1). The difficulty of selecting prior distribution and likelihood function for the method; 2). The method sometimes leads to overconfidence and arbitrariness in its solutions; 3). The Bayesian method is computationally difficult particularly for determining the normalizing factor of the Bayes' rule; 4). The Bayesian method does not differentiate between incertitude and equiprobability. Despite of those disadvantages, the Bayesian method provides a robust mathematical model to estimate the distribution of random variables particularly in the field of seismic risk (Rüttener et al., 1996).

2.2.1. Earthquake and Tsunami Risk Assessment

In seismology, seismic risk refers to the expected loss due to earthquake and its following hazards (i.e. tsunami, landslide, and liquefaction) in a region for a specified period of time. To estimate the seismic risk for buildings in Cyprus, Kythreoti (2002) used the following relation:

$$R = \sum_{i=1}^{n}\sum_{j=1}^{m}\left(H_i \times V_{ij}\right) \times C_j \qquad 2.5$$

where,

H_i : the magnitude/quantity of hazard-i, which is equivalent to $p(y)$ in Equation 2.1

V_{ij} : the vulnerability of element-j exposed to the hazard-I, which is equivalent to $V(z_w, y)$ in Equation 2.1

C_j : the value of the exposed type of structure-j (e.g. masonry buildings, steel structures, reinforced concrete structures, etc.) in a particular region, which is equal with z_w in Equation 2.1

It should be noted that the equation above is specifically derived for buildings. Therefore, the exposure is taken as 1 assuming that the buildings will remain in their place when the hazard occurred. The $(H_i \times V_{ij})$ element in Equation 2.5 denotes the specific risk (R_{spec}) as given in Equation 2.1.

If the hazard, vulnerability functions and the value of an element at risk in the examined area are available, the seismic risk can be easily estimated. The quantification of hazards is discussed in Sections 2.3 and 2.4. The vulnerability function for earthquake and tsunami hazards are discussed in Section 2.5, which, in this study, is limited to vulnerability functions for building. This is to consider that the main monetary losses due to seismic events in Padang are mainly contributed by structural damage, as shown from the M_w 7.6 of the Padang earthquake (Wilkinson et al., 2009).

2.2.2. Probabilistic Risk Assessment and the Insurance Rate for Hazards

Risk assessment can be performed probabilistically by taking into account all probable level of hazards in the examined area. The risk can be estimated annually and the annual risk is generally used as a foundation to determine the insurance rate of hazard. The annual risk is usually expressed in terms of pure risk premiums (PRP) and is a function of expected annual damage ratio ($EADR_k$) and building value (INSV), as shown in Equation 2.6.

$$PRP_k = EADR_k \times INSV \quad (2.6)$$

The $EADR_k$ involves the integration of all hazard levels (SH_j) and the associated mean damage ratio (MDR_k), as shown in Equation 2.7. Different hazard parameters can be incorporated into Equation 2.7. For example, the SH_j can be referred to the annual probability of a particular PGA (Peak Ground Acceleration) for earthquake risk assessment and can be denoted as the annual probability of a particular tsunami height (H_t), if the tsunami risk is the main concern.

$$EADR_k = \sum_j MDR_k(j) \times SH_j \quad (2.7)$$

where,

$EADR_k$: Expected annual damage ratio for k-type of structure

SH_j : The annual probability of a certain level of hazard

MDR_k (j) : Average damage ratio for k-type of structure at certain level of hazard-j

Total insurance premium (TP_k) is determined by applying a load factor (LF) into the pure risk premium. The load factor takes into account hidden uncertainties, administration, taxes and profits for the insurance company (Yucemen, 2005). The relationship between TP_k and PRP_k is defined in Equation 2.8.

$$TP_k = PRP_k / (1 - LF) \quad 2.8$$

where,

TP_k : Total insurance premium for k type of structure

PRP_k : Pure risk premium for k type of structure

LF : Load factor, taken as 0.4 (Yucemen, 2005)

2.2.3. Existing Risk Assessment Frameworks

Several risk assessment frameworks were available including HAZUS (FEMA, 2003; FEMA, 2009), RADIUS, RISK-UE, EQ-RACY and ERA Framework. HAZUS was a Geographic Information System (GIS) based program for analysing potential loss in the United State of America due to earthquake, hurricane and floods (FEMA, 2009). The HAZUS's earthquake model was mainly developed to assess risk subjected to earthquake ground motions and ground failure. The incorporation of tsunami hazard in the HAZUS program is still under development.

RADIUS (IDNDR, 1999) was intended to provide preliminary estimations of earthquake risk, particularly for developing countries. A scenario or deterministic approach was adopted in the RADIUS program. Hence, its application was limited to identify seismic risk for mitigation purposes.

RISK-UE (Mouroux and Le Brun, 2006) was a seismic risk assessment project specifically designed for European cities. A GIS environment was used in the RISK-UE project. However, the risk was estimated based on damage scenarios from some plausible earthquakes in an investigated area; thus, the method did not take probabilistic assessment into account.

EQ-RACY was a probabilistic seismic risk assessment framework developed at the University of Sheffield by Kythreoti (2002). The risk framework was developed for

low to medium seismicity regions such as Cyprus. Afterwards, Khan (2011) developed ERA (Earthquake Risk Assessment) Framework to expand EQ-RACY, so that it could be more generally applicable to include high seismicity areas. The ERA Framework was based on GIS environment and produced a probabilistic hazard and risk estimates due to earthquake ground motions. However, it did not consider earthquake associated hazards such as tsunami, liquefaction and landslides.

2.3. SEISMIC HAZARD ASSESSMENT

Thenhaus and Campbell (2003) define seismic hazard as the probability of experiencing a certain level of earthquake intensity and its consequent hazards (including ground shaking, liquefaction, landslides and tsunami) in a particular region within a period of time. The main outcome of seismic hazard assessment is a hazard curve indicating the probability of exceedance for selected ground motion parameters (i.e. peak ground acceleration (PGA) or spectral acceleration) at a site for a given period of time (Bommer and Abrahamson, 2006).

In the past, seismic hazard was assessed mainly using a deterministic approach considering single or few earthquake scenarios. Nevertheless, this approach has the issue of which earthquake should be selected as the scenario for the hazard assessment (Sabetta, 2005; Thenhaus and Campbell, 2003). Using the worst case scenario, usually a maximum magnitude earthquake expected in a region is appropriate for the design of critical structures, such as nuclear power plants. This is because, in this case, failure could lead to catastrophic consequences. However, using this scenario for all structures may be too conservative, especially since the probability of the occurrence of the resulting ground motion may be too low or the consequences of failure are less important. For earthquake risk assessment of a large region, as that examined in this study, the deterministic method is not adequate.

Progress in seismological statistics and seismic hazard studies, as well as computational tools, allowed the development of Probabilistic Seismic Hazard Assessment (PSHA). This method was pioneered by Cornell (1968) and it took into account the contribution of all seismic sources for a particular site. In other words, PSHA comprises a large number of deterministic analyses (Abrahamson, 2006). Many other PSHA methods have since been developed including a stochastic PSHA

method and a time-dependent PSHA model; these are discussed further in the following sub-sections after the conventional PSHA method is introduced.

2.3.1. Main Components of Seismic Hazard Assessment

Several steps are required to perform seismic hazard assessment, including identifying seismic sources of the investigated area, defining seismic zones, assessing earthquake recurrence relationships and assigning appropriate ground motion attenuation equations. Seismic source identification requires a basic understanding of the tectonic setting of the assessed region (as discussed in more detail in Chapter 4). The other steps of PSHA are presented in the following sections.

2.3.1.1. Seismic Zone Definition

A seismic zone can be defined as an area that shares comparable type and distribution of earthquakes. Generally, the boundary of a seismic zone is determined by considering the tectonic configuration, seismic source characteristics and seismicity distribution of the examined area. However, the definition of a seismic zone boundary involves subjective decisions (Sabetta, 2005), so different studies with similar case study areas are likely to produce different seismic zones.

Most PSHA models assume that seismicity in a seismic zone is uniformly distributed, which can lead to spatial smoothing of seismicity (see section 2.3.2). To deal with this problem, Khan (2011) proposed a method of generating randomised synthetic earthquakes around real events as will be discussed in section 2.3.3. This approach closely resembles the past seismicity of a region. In Khan's approach, seismic zones are only used to define areas with similar tectonic characteristics, as well as to determine the direction of earthquake ruptures that correspond to the strike angle of main faults. The selection of seismic zones for the study region is shown in Chapter 4.

2.3.1.2. Earthquake Recurrence Relationship

The earthquake recurrence relationship gives the expected number of earthquakes occurring in a region for a defined period of time (Elnashai and Sarno, 2008). The earthquake recurrence relationship is essential for Probabilistic Seismic Hazard

Assessment (PSHA) since it allows all probable magnitudes of earthquakes to be evaluated in PSHA studies. The recurrence relationship is also useful to approximate the seismicity of an investigated area which lacks seismicity records. The simplest and most well-known recurrence relationship was proposed by Gutenberg and Richter (1954) with their frequency-magnitude relationship as follows:

$$\log N = a + b\,.M \qquad 2.9$$

where,

N : the number of earthquakes per year greater than or equal to M

M : earthquake magnitude

a and b : regressed constants from the observed seismological data

The Gutenberg-Richter recurrence distribution assumes a Poissonian process for earthquake occurrence. Therefore, it implies a relatively stationary seismicity and assumes that each earthquake occurs independently. Wesnousky (1994) argued that for some regions, their seismicity did not follow the Gutenberg-Richter distribution. Instead, the Gutenberg-Richter distribution only reflects part of the regional seismicity as revealed in the Characteristic Earthquake Model (see Figure 2.1). The characteristic model applies seismicity data at lower magnitudes and geologic data at higher magnitude earthquakes (Sabetta, 2005). Selecting the most appropriate earthquake recurrence model is critical to conduct a reliable seismic hazard analysis. Applying the Gutenberg-Richter model to an area where its seismicity does not follow the power law distribution may overestimate the hazard (Khan, 2011). Nevertheless, it is reasonable to use the truncated Gutenberg-Richter relation, if available fault information is not sufficient (Sabetta, 2005).

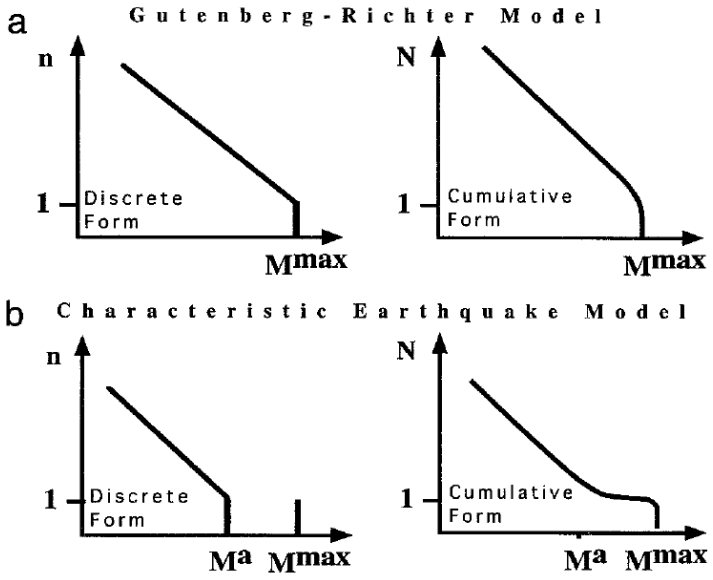

Figure 2.1. Earthquake distribution models: (a) Gutenberg-Richter model; (b) Characteristic earthquake model (Wesnousky, 1994)

2.3.1.3. Ground Motion Attenuation Relationship

Ground motion attenuation relationships estimate ground motion parameters (e.g. peak ground acceleration, velocity and displacement) as seismic waves radiate from the earthquake hypocentre to the surrounding regions. These relationships correlate earthquake parameters to earthquake magnitude, focal distance, soil condition, and fault type. Attenuation relationships can be derived either empirically, using earthquake ground motion records, or theoretically, using a seismological model of synthetic ground motions (Elnashai and Sarno, 2008). Ground attenuation models are generally developed for a specific site. However, if they are not available, attenuation relationships developed for other areas can be adopted, provided both regions have comparable tectonic and geological situations (Irsyam et al., 2008).

Various ground motion attenuation relationships are commonly used for assessing seismic hazard in Indonesia. For a subduction zone environment, attenuation functions produced by Youngs (1997), Atkinson and Boore (2003) are commonly adopted (Asrurifak et al., 2010; Irsyam et al., 2008; Petersen et al., 2004; Sengara et al., 2007; SNI 03-1726-2002, 2002). The attenuation relationships for rock and soil sites developed by Youngs (1997) are shown in Equations 2.10 and 2.11, respectively.

$$\ln Y = 0.2418 + 1.414M + C_1 + C_2\,(10 - M)^3 + C_3 \ln\left(r_{rup} + 1.7818\, e^{0.554M}\right) + 0.00607H + 0.3846Z_T \quad 2.10$$

$$\ln Y = -0.6687 + 1.438M + C_1 + C_2\,(10 - M)^3 + C_3 \ln\left(r_{rup} + 1.097\, e^{0.617M}\right) + 0.00648H + 0.3643Z_T \quad 2.11$$

where,

Y : spectral acceleration (g)

M : earthquake moment magnitude

r_{rup} : the closest distance to rupture surface (km)

H : depth (km)

Z_T : source type (0 for interface and 1 for intraslab)

C_1, C_2, and C_3: the coefficients to be determined (see Youngs, 1997)

For a shallow crustal environment, the equations from Boore et al. (1997) and Sadigh et al. (1997) are frequently used. The attenuation relationship from Boore et al. (1997) is shown in the following equations:

$$\ln Y = b_1 + b_2\,(M - 6) + b_3(M - 6)^2 + b_5\,.\ln r + b_v\,.\ln\frac{V_S}{V_A} \quad 2.12$$

$$r = \sqrt{{r_{jb}}^2 + h^2} \quad 2.13$$

where,

Y : the ground motion parameter (peak horizontal acceleration or pseudo acceleration response in g)

M : earthquake moment magnitude

r_{jb} : distance (km)

h : fictitious depth determine by regression

V_S : average shear-wave velocity to 30 m (m/sec)

$b_1, b_2, b_3, b_5, h, b_v$ and V_A : the coefficients to be determined as shown in Boore et al. (1997)

The attenuation relationships for rock and deep soil sites from Sadigh et al. (1997) are shown in Equations 2.14 and 2.15, respectively.

$$\ln Y = C_1 + C_2 (8.5M)^{2.5} + C_4 \ln\left(r_{rup} + \exp(C_5 + C_6 M)\right) + C_7 \ln\left(r_{rup} + 2\right) \quad 2.14$$

$$\ln Y = C_1 + C_2 M - C_3 \ln\left(r_{rup} + C_4 \mathrm{e}^{(C_5 M)}\right) + C_6 + C_7 (8.5 - M)^{2.5} \quad 2.15$$

where,

Y : peak horizontal acceleration or pseudo acceleration response (g)

M : earthquake moment magnitude

r_{rup} : the closest distance to rupture surface (km)

$C_1, C_2, C_3, C_4, C_5, C_6$ and C_7 : the coefficients to be determined (see Sadigh et al., 1997)

Recently, new attenuation models were developed based on the earthquakes in Indonesia (Megawati and Pan, 2010; Parithusta, 2007). Parithusta (2007) derived an attenuation relationship based on Indonesian earthquake databases to account for deep source events with focal depth up to 150 km. This was considered necessary since most existing attenuation relationships were produced for shallow earthquakes with focal depth around 10–50 km, which were not suitable for deep events commonly found in Indonesia (Parithusta, 2007). The deep source events are generally associated with subduction or Benioff zones in the region. Megawati and Pan (2010) also developed an attenuation relationship for megathrust earthquakes in Sumatra. Their attenuation function was intended for distant regions, about 200-1500 km from earthquake epicentres. Hence, this was not suitable for near field earthquakes (<200 km) for which Megawati and Pan (2010) suggested the use of an attenuation equation derived by Atkinson and Boore (2003).

2.3.1.4. Physical Earthquake Models

A physical earthquake model is a fundamental element for seismic hazard analysis. It allows the computation of earthquake shaking intensity as well as assessing earthquake interactions using rupture scenarios. The standard physical models generally assume an elastic whole space, two dimensional and quasi-static earthquake simulations (Ward, 2000). The models require a complex geometry of major active faults, the specification of failure law (e.g. Coulomb Failure Criterion) as well as rigorous seismological information including, slip distribution, slip rates, stress drop, healing time and the frictional coefficient of fault elements. The

frictional coefficient is the difference between static and dynamic frictional coefficients ($\mu_i^s - \mu_i^d$). The static frictional coefficient (μ_i^s) denotes the ratio of shear to normal stress for surface at rest and the dynamic coefficient (μ_i^d) represents the ratio for surfaces in a relative motion. Failure on a fault segment may occur when the static frictional coefficient is equal to the dynamic coefficient (Rundle, 1988).

Based on an improved standard physical model, Ward (2000) successfully simulated the 1906 San Francisco earthquake and showed fault interactions in San Francisco bay area associated with the event. Ward (2000) found that the released stresses from a fault might accelerate or delay the occurrence of nearby earthquakes. Furthermore, Ward (2000) plotted the earthquake recurrence times produced by the model and obtained a comparable result with those of the existing earthquake catalogue. Consequently, Ward (2000) showed that the physical earthquake model could give realistic outcomes and could be a good alternative for estimating earthquake probabilities and hazard.

Robinson and Benites (1995) used the physical earthquake model to generate long catalogue of synthetic seismicity for faults in Wellington region, New Zealand and obtained detailed rupture histories for the area. Robinson and Benites (1995) found that the clustering of large earthquakes (M>7.2) occurred due to the interaction between the subduction thrust and one of the overlying strike-slip faults in the region. Similar studies were conducted by Rundle et al. (2005). Rundle et al. (2005) developed a physical earthquake model with a simulation based approach and highlighted its significance for estimating the statistical distribution of recurrence times between great earthquakes. Rundle et al. (2005) argued that the estimation of earthquake sequence with a purely field-based approach might not be accurate due to the limited length of earthquake catalogues. Consequently, Rundle et al. (2005) carried out numerical simulations for San Andreas fault that represented the seismicity of the area for over 40,000 years. The outcomes showed that the method approximated the recurrence times better than the field-based approach. The method adopted by Rundle et al. (2005) was initially developed by Rundle (1988). Rundle (1988) treated earthquakes as “perturbations” or short term fluctuations on the long-term motion of plate tectonics and applied interaction among fault segments during slip, which led to the construction of the interaction matrix. Rundle (1988) found that the geometry of fault segments took an effect in the fault interactions. Rundle (1988)

observed that long and slender fault patches were likely to produce regular slip patterns and small interaction coefficient. In contrast, nearly square fault segments would produce more irregular slip patterns and higher interaction coefficient.

2.3.2. Conventional Probabilistic Seismic Hazard Analysis (PSHA)

Cornell (1968) initially developed PSHA to find the desired correlation between ground motion parameters (i.e. Modified Mercalli Intensity, peak-ground velocity, peak-ground acceleration, etc.) and their average return period for a particular site. The method consists of at least four main components including identification of seismic sources, earthquake recurrence functions, ground attenuation relationships and distance from seismic source to the site, as discussed previously. The PSHA technique integrates earthquake magnitude and distance to a hazard site for each seismic source and sums their contribution to the study area as expressed in Equation 2.16 (Thenhaus and Campbell, 2003):

$$\lambda[X \geq x] = \sum_{Sources-i} v_i \int_{M_0}^{M_{max}} \int_{R|M} P(X \geq x|M,R).f_M(m).f_{R|M}(r|m)dr\,dm \qquad 2.16$$

where,

$\lambda[X \geq x]$: the annual frequency of ground shaking exceeding a given level $X = x$

v_i : the annual rate of earthquake for seismic source-i with magnitudes between M_o and M_{max}

$P(X \geq x|M,R)$: probability that certain level of ground motion will be exceeded for a given magnitude M and distance R

$f_M(m)$ and $f_R(r)$: probability density function for magnitude and distance from seismic sources to the site, respectively

The probability of exceedance of an observed ground motion parameter, $P[X \geq x]$, is computed from Equation 2.17.

$$P[X \geq x] = 1 - e^{(-t.\lambda[X \geq x])} \qquad 2.17$$

where, t in the above equation denotes the exposure period of engineering interest.

An important outcome of seismic hazard assessment is to identify design earthquakes that contribute to the hazard. This is generally required for structural design purposes. The standard PSHA characterises earthquake events in terms of probability density functions (see Equation 2.16). As a result, identifying a design earthquake is challenging due to the integration of all seismic sources, magnitudes and distances (Abrahamson, 2006). An alternative procedure, also known as a deaggregation technique, can be performed to obtain the controlling earthquake by computing a fractional contribution of each seismic source to the total hazard. Nevertheless, the deaggregation procedure has some issues regarding selection of bin size, grouping of scenarios and which set of quantities should be chosen as the base for the deaggregation. Abrahamson (2006) showed that the deaggregation procedure could lead to an unrealistic earthquake scenario if the hazard in the area was controlled by two or more seismic sources. In addition, the integration nature of the conventional PSHA has made actual risk difficult to be estimated directly from PSHA. This is because the method requires the integration of vulnerability functions to get conditional probability of damage given by a particular level of ground shaking (Musson, 2000).

It is assumed in the conventional PSHA that seismicity in a seismic source zone is uniformly distributed. Abrahamson (2006) argued that this assumption smoothed the historical seismicity. Very little smoothing would closely represent the historical seismicity, yet it does not allow future earthquakes to take place in a region with no historical seismic activity. On the other hand, very large smoothing would overrate the seismicity in the region with little or no historical earthquakes (Abrahamson, 2006). Therefore, the selection of an appropriate size for seismic source zones or level of spatial smoothing is challenging issues. Inappropriate degree of spatial smoothing will lead to unreliable results (Musson, 2004). Musson (2004) proposed a method to measure optimum smoothing using Monte Carlo simulations. He produced synthetic earthquakes randomly within a seismic zone and compared the result with the historical seismicity of the region. The size of the zone was considered appropriate if the distribution of synthetic events was consistent with historical seismicity. However, this approach only worked well to identify overly sized seismic zones (Musson, 2004).

In addition, the standard PSHA method assumes earthquake events occur randomly and independently. This implies that the earthquake recurrence function follows a Poisson distribution and fore-shock and after-shock events should be discarded from the earthquake catalogue (Petersen et al., 2007b) to minimise the dependency of each event. A method proposed by Gardner and Knopoff (1974) can be utilised to remove aftershocks using a time and distance window as a function of earthquake magnitude. However, whether the main earthquakes are Poissonian or non-Poissonian events remains unclear, thus yielding a certain degree of uncertainty.

The Poissonian model provides ease of the integration process as required in PSHA. This model is time independent, and as a result a constant hazard rate is applied over a given exposure time. However, this assumption does not agree with the Elastic Rebound Theory, which aims to characterise the real behaviour of earthquakes. The elastic rebound approach assumes that earthquake occurrence depends on past seismicity including time, size and location of preceding events (Adnan et al., 2005; Cramer et al., 2000; Ferraes, 2003; Petersen et al., 2007b; WGCEP, 1988; WGCEP, 1995; WGCEP, 2003). Non-Poissonian or time-dependent models with varying hazard rate can be incorporated into PSHA, but would involve the use of more complex mathematical and computational formulations than for the conventional PSHA.

2.3.3. PSHA with Stochastic Method

PSHA using the stochastic method is based on Cornell's approach. However, instead of solving the total probability theorem as required in the conventional PSHA, the stochastic approach directly calculates earthquake ground motions from synthetic earthquake catalogues (Khan, 2011; Kythreoti, 2002; Musson, 2000; Musson, 2004; Shapira, 1983; Weatherill and Burton, 2010).

Musson (2000) used Monte Carlo simulation to generate synthetic events for each seismic zone. The synthetic events were produced randomly within a seismic zone assuming that the seismicity in a seismic zone was uniformly distributed. The Monte Carlo approach allows flexibility in the selection of seismicity models to be adopted in the hazard, including non-Poissonian models for a time dependent PSHA without extensive programming. The uncertainties of input parameters in this method are easier to deal with using distribution functions with observed mean and standard

deviations, as shown by Weatherill and Burton (2010). In addition, the outcome of PSHA with the Monte Carlo approach can be directly incorporated to calculate the risk for each event, which is challenging to achieve in the standard PSHA due to the integration of vulnerability and hazard probability density functions. Musson (2000) compared the results of PSHA obtained from both conventional and Monte Carlo methods and found that, given the same input data, the outcomes of Monte Carlo approach were comparable with those of conventional method. However, the reliability of the Monte Carlo method increased with an increasing number of simulations. As a consequence, this method was computationally slow, especially when it involved a large number of simulations for high seismicity regions. However, this issue is becoming less important with increasing computer power (Musson, 2000).

Alternative stochastic PSHA methods were proposed at the University of Sheffield (Khan, 2011; Kythreoti, 2002). Khan et al. (2010) argued that Musson's approach tended to overestimate the hazard since the locations of synthetic earthquakes were equally smeared over the seismic zones. Therefore, Kythreoti (2002) and Khan (2011) generated synthetic earthquakes based on a defined boundary for each real event in the earthquake catalogue.

Kythreoti (2002) carried out a parametric study for seismic hazard parameters such as earthquake magnitude, epicentral location and focal depth, and showed that uncertainties due to the determination of the hazard parameters can affect the reliability of seismic hazard assessment. Therefore, Kythreoti (2002) took into account those uncertainties to determine the parameters of new synthetic earthquakes (Equation 2.18 and Equation 2.19).

$$M_R = M_0 \pm (e_M . N_R) \quad 2.18$$

$$H_R = H_0 \pm (e_H . N_R) \quad 2.19$$

where,

M_R : the magnitude of a new synthetic event

M_0 : the magnitude of a real earthquake

e_M : the error of earthquake magnitude determination

N_R : a random number within a given range

H_R : the focal depth of a new synthetic event

H_0 : the focal depth of a real earthquake

e_H : the error of focal depth determination

Kythreoti (2002) assessed the seismic hazard for Cyprus, which has low to moderate seismicity. Kythreoti (2002) assumed that seismic waves spread from the earthquake hypocentre in a circular shape (Figure 2.2a) due to the limited rupture length of low to moderate magnitude earthquakes. Based on that assumption, Kythreoti generated synthetic earthquakes within the boundary of the estimated fault rupture. However, the relatively circular mode of fault rupture can only be used to represent low to moderate magnitude earthquakes. Whilst for large magnitude earthquakes, the waves radiate along the rupture line (Garcia-Fernandez and Egozcue, 1989; Khan, 2011; Khan et al., 2010), as illustrated in Figure 2.2b. Khan (2011) extended Kythreoti's method to take into account high magnitude earthquakes and used Pakistan as a case study. Khan produced new synthetic earthquakes along the length and directivity of fault ruptures, as illustrated in Figure 2.2b and Figure 2.3, and calculated fault rupture characteristics such as rupture length, width and area using empirical equations developed by Wells and Coppersmith (1994). Most recent empirical relations to scale earthquake source parameters have been proposed by various studies (Blaser et al., 2010; Strasser et al., 2010); however, the relations are only derived for subduction environments.

To minimise the incompleteness of instrumental earthquake catalogues, Khan (2011) merged historical and instrumental earthquake catalogues. He divided the earthquake magnitudes into 7 magnitude ranges (M_w 0-6, M_w 6-6.5, M_w 6.5-7, M_w 7-7.5, M_w 7.5-8, M_w 8-8.5 and $M_w \geq 8.5$) and produced new synthetic earthquakes by randomising earthquake parameters in the combined catalogue. The randomisation of earthquake magnitude and focal depth was carried out over the error margins e_M and e_H as expressed in Equations 2.18 and 2.19, respectively. Afterwards, Khan (2011) selected the new synthetic events randomly to produce the same number of events for each magnitude category in the instrumental catalogue. In brief, Khan (2011) used the number of events in the instrumental catalogue to represent seismicity of a region and to prevent the overestimation of hazard due to the inclusion of historical earthquakes. The selected synthetic events were then simulated to obtain a ground motion response using ground motion attenuation relationships.

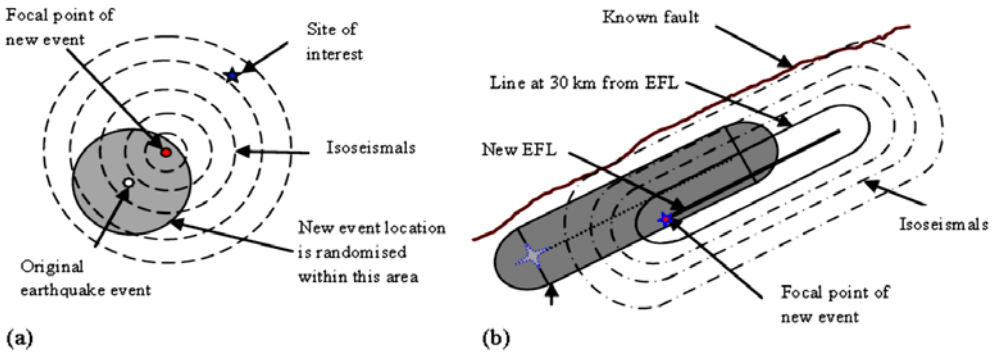

Figure 2.2. Generation of new random event and earthquake intensity: (a). spreading from focal point; (b). spreading from the rupture line or EFL (Khan, 2011)

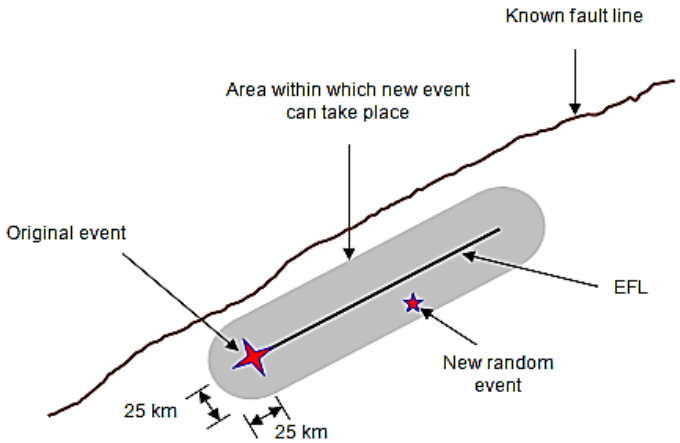

Figure 2.3. Area of synthetic earthquake event and its orientation related to the fault line (Khan, 2011)

The reliability of Khan's approach depends strongly on the completeness of the earthquake catalogues. A minimum duration of instrumental catalogue, which covers at least one sequence of the longest earthquake return period of the area, is required for this method. Otherwise, the method may underestimate the return period of higher magnitude earthquakes, which could result in a higher hazard; it can also underrate earthquake rates, particularly for lower magnitude events. For example, an area with a history of mega magnitude earthquakes may require a few hundred years of instrumental catalogue to represent its seismicity well. This extensive instrumental catalogue is rarely, if ever, available, particularly for developing countries. In addition, unexpectedly large magnitude earthquakes such as those that hit Japan in 2011 (M_w 9.0) and Sumatra in 2004 (M_w 9.1) have shown that sometimes the historical records do not contain all probable earthquakes in a region. Therefore, a method should be developed to take into account potential earthquakes, especially along seismic gaps. This topic is discussed in Chapter 3.

2.3.4. Time Dependent Seismic Hazard Assessment

The development of a time dependent seismic hazard model is intended to extend conventional PSHA by applying a varying hazard rate to the PSHA model. It is assumed that in a time dependent model, the probability of earthquake occurrence depends on the time since last large earthquake (WGCEP, 1995). In other words, major or characteristic earthquakes might occur if the elastic strains on a fault segment have re-accumulated to the amount that was released in previous large earthquakes (WGCEP, 2003). This assumption agrees with the Elastic Rebound Theory, which explains the earthquake mechanism. Consequently, the hazard rate increases when elapsed time since the last large earthquake has almost reached its return period or when seismic gaps are present in a region. For both cases, a time independent PSHA model is not satisfactory as it does not recognise the increased rate of upcoming hazards. Thus, the time dependent model is more effective for identifying short-term hazard (Akinci et al., 2009).

Petersen et al. (2007) compared time independent and time dependent PSHA for California, assuming a 10% probability of exceedance for 30 years since 2006. They found that the differences of PGA values between time dependent and time independent were approximately 10-15%. The distinctions were more obvious near time dependent sources, where seismicity of the areas clearly showed a periodic nature. The PGA values for areas distant from the time dependent sources were comparable with those of the time independent model.

A time-dependent PSHA requires several parameters to be known, including elapsed time since last large earthquake, as well as the definition of the fault segments. Appropriate fault segmentation is essential to get reliable earthquake recurrence interval parameters for hazard assessment. Inadequate segmentation may lead to inaccurate results (WGCEP, 1988). Fault segments are defined based on earthquake slip rate, fault creep, historical earthquakes and the geometry of examined faults (Field, 2007; WGCEP, 1988). A basic assumption to determine segment ruptures is that the total slip rate produced by the estimated earthquake rate is equivalent to the slip rate of long term seismicity (WGCEP, 1995). In general, a single segment, or multi segment ruptures, can be used for estimating rupture probabilities. The single segment rupture produces a lower recurrence interval that leads to higher hazard

probabilities (2007 WGCEP, 2008). However, this approach results in more practical calculations, as presented in the earlier versions of the WGCEP's models (WGCEP, 1988; WGCEP, 1990). The multi segment rupture approach requires extensive calculations, more seismological information and produces more uncertainties.

There are various models for assessing time dependent seismic hazards. Most models utilise the probability density function (pdf) of earthquake recurrence intervals. Figure 2.4 illustrates the underlying principles of probability calculation for a time dependent seismic hazard, which can be described as follows (WGCEP, 2003):

$$F(T)=\int_T^\infty f(t)dt \qquad 2.20$$

$$h(t)=f(t)/F(t) \qquad 2.21$$

where,

$F(T)$: probability that at least time T will elapse between successive events

$f(T)$: probability density function indicating the likelihood of failure from T to T+ΔT with condition that the major event has not occurred prior to T

T : elapsed time since last earthquake

ΔT : time interval

$h(t)$: hazard function

Conditional probability that one or more earthquake will occur on a seismic source during a particular time interval is defined as follows:

$$P(T \le t \le T+\Delta T | t > T) = \frac{F(T) - F(T+\Delta T)}{F(T)} \qquad 2.22$$

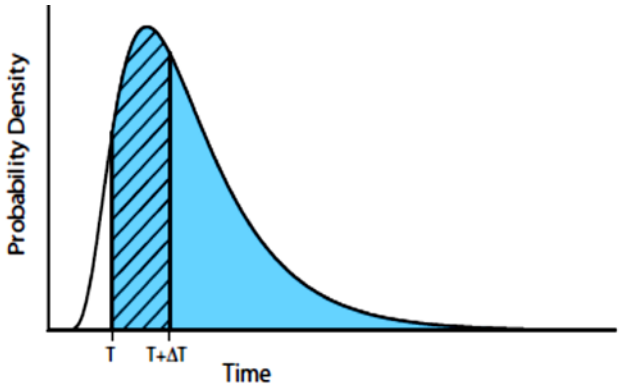

Figure 2.4. Illustration of conditional probability calculation based on a probability density function (WGCEP, 2003)

As mentioned earlier, the probability distribution of hazard rate in the time dependent approach is assumed to be varied with time. Accordingly, renewal models of probability distributions are generally used including gamma, Weibull, log-normal (Petersen et al., 2007b; WGCEP, 1988; WGCEP, 1990; WGCEP, 1995) and Brownian Passage Time (2007 WGCEP, 2008; Akinci et al., 2009; Matthews et al., 2002; WGCEP, 2003). The renewal models take into account the statistical distribution of rupture times (WGCEP, 2003). Generally, the models require at least two parameters including mean recurrence intervals (μ) and the variability of the recurrence interval. The mean recurrence interval is defined as follows:

$$\mu = 1/\lambda \qquad 2.23$$

where, λ is the mean rate of events per unit time.

The probability distribution function (PDF) of gamma distribution is shown in Equation 2.24 with a shape parameter k and scale parameter λ. The density function of gamma distribution resembles the exponential distribution as k=1.

$$f(t) = \frac{\lambda^k \, t^{k-1} \, e^{-\lambda t}}{\Gamma(k)}, \qquad k, \lambda > 0, \; t \geq 0 \qquad 2.24$$

Where, $\Gamma(k)$ is the gamma function $\left(\Gamma(k) = \int_0^\infty t^{k-1} \, e^{-t} \, dt\right)$.

Equation 2.25 shows the PDF of Weibull distribution. Similar with the gamma distribution, the behaviour of the Weibull distribution depends on the value of shape parameter k. A value of $k < 1$ indicates a decreased rate of hazard over time, $k = 1$ shows a constant rate and $k > 1$ indicates an increased rate with time.

$$f(t) = \frac{k}{\lambda} \left(\frac{t}{\lambda}\right)^{k-1} e^{-(t/\lambda)^k}, \qquad k, \lambda > 0, \; t \geq 0 \qquad 2.25$$

Other commonly used distributions in the time dependent approach are lognormal and Brownian Passage Time (BPT). The lognormal distribution is generally applicable for circumstances with multiplicative random effects (Soong, 2004). The lognormal distribution contains two parameters, σ and μ, which denote standard deviation and mean recurrence interval, respectively. The shape of the lognormal distribution depends on the value of σ. Smaller values of σ will produce higher peak of distribution. The PDF of the lognormal distribution is shown in Equation 2.26.

$$f(t) = \frac{1}{t\sqrt{2\pi\sigma^2}}\, e^{\frac{-(\ln t-\mu)^2}{2\sigma^2}}, \qquad \sigma^2 > 0,\ t \geq 0 \tag{2.26}$$

The shape of lognormal distribution is really close to that of the BPT, as seen in Figure 2.5b. However, after reaching a maximum value, the hazard function of the BPT distribution is not abruptly decreased as that observed in the lognormal model. The key parameters to determine the BPT distribution are the mean recurrence interval (μ) and aperiodicity (α). Aperiodicity characterises the irregularity of the length of interval between successive events (WGCEP, 2003). Smaller values of α indicate a relatively regular sequence of events and the distribution becomes more Poisson-like with increasing values of α. The PDF of the BPT distribution is shown in Equation 2.27.

$$f(t) = \sqrt{\frac{\mu}{2\pi\alpha^2 t^3}}\, e^{-\frac{(t-\mu)^2}{2\mu t\alpha^2}}, \qquad \alpha, \mu > 0,\ t \geq 0 \tag{2.27}$$

Where,

μ : mean recurrence interval

σ : standard deviation of the distribution

α : the variability of recurrence interval $(\alpha = \sigma/\mu)$

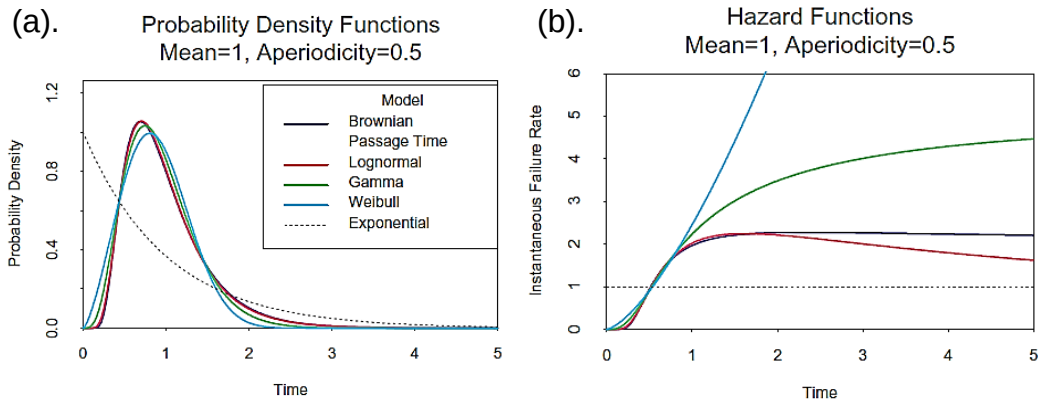

Figure 2.5. Comparison of several probability models used in long-term earthquake forecasting (WGCEP, 2003)

Figure 2.5 plots the probability models commonly used for PSHA. It shows that the exponential or Poissonian models do not take into account elapsed time since the last large earthquake and it applies a constant hazard rate over the exposure time (Figure 2.5b). This means that the probability of a large earthquake occurring the next day after a recent event is equivalent to the probability of such event happening a

hundred years later on the fault segment. This assumption does not represent the physics of the earthquake process well. Therefore, the Poissonian model is only appropriate to be used in the case of limited availability of seismological information (WGCEP, 2003).

In contrast, the renewal models, such as Brownian Passage Time (BPT), lognormal, gamma and Weibull, apply zero failure rates instantaneously after an event and assume varying hazard rate over time (see in Figure 2.5). Nishenko and Buland (1987) assessed the distribution of earthquake recurrence intervals using empirical data. They concluded that the lognormal model gave the best fit to the normalised recurrence interval distribution compared with the exponential, gamma and Weibull models. However, WGCEP (2003) argued that a hazard function based on the lognormal distribution always goes to zero as time (t) reaches infinity (Figure 2.5b). This condition does not satisfy the long-term behaviour of the earthquake renewal cycle (Matthews et al., 2002). Therefore, WGCEP (2003) adopted the BPT distribution for their time dependent PSHA model. To consider that the shape of the BPT distribution is really close to that of lognormal (see Figure 2.5b), hence, the BPT function represents well the distribution of earthquake recurrence interval (WGCEP, 2003).

Ellsworth et al. (1999) estimated aperiodicity based on 37 series of recurrent earthquakes, which ranged from 3 to 13 sequences of events and found that a finite length of sequences (two or three intervals between events) could lead to unreliable aperiodicity values. Akinci et al. (2009) limited their aperiodicity calculations to the sequences that had at least three and four close intervals (i.e. 5 events). It means that, to get acceptable values of aperiodicity, a long duration of earthquake catalogues that contain a few sequences of major earthquakes is required. This information is rarely available for most regions, even more so for developing countries.

Reasenberg et al. (2003) argued that the previous time dependent models did not appropriately account for the stress shadow effect of the 1906 earthquake in California. Consequently, their results could overestimate the hazard. Therefore, Reasenberg et al. (2003) proposed an alternative method for assessing earthquake probabilities. The so-called empirical model is based on earthquake rates from historical earthquake activity and is basically a variant of the Poisson model.

However, it modulates the long-term mean rate of earthquakes in the Poisson distribution to be non-stationary and time dependent, as illustrated in Figure 2.6. Future seismicity can be estimated by extrapolating $\gamma(t)$ forward in time (Reasenberg et al., 2003; WGCEP, 2003).

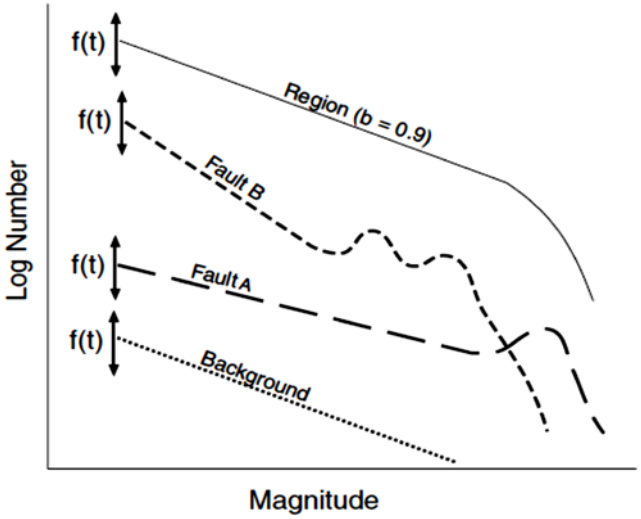

Figure 2.6. Modulation of the long-term mean regional rates using the time-varying rate function, *f(t)* (Reasenberg et al., 2003)

The time varying rate function $\gamma(t)$ (similar to $f(t)$ in Figure 2.6) is given by Equation 2.28 and earthquake probability for fault-i with mean rate λ_i is shown in Equation 2.29 (WGCEP, 2003).

$$\gamma(t) = \lambda(t)/\lambda \qquad 2.28$$

$$P_i^{Emp} = 1 - e^{-\bar{\gamma}\,\lambda_i\,\Delta t} \qquad 2.29$$

where,

$\lambda(t)$: varying rate estimated from historical earthquake records

λ : long term mean rate of earthquakes in the region

$\bar{\gamma}$: average of $\gamma(t)$ over $(t, t + \Delta t)$

The empirical approach complements other models since it takes into account moderate size earthquakes (M≥5.5), which are not considered in the BPT, Poisson or time-predictable probability models (WGCEP, 2003). Moreover, the method can be easily adapted for upgrading the existing stochastic PSHA models (Khan, 2011; Kythreoti, 2002; Musson, 2000) to be time dependent. The empirical model has been implemented in various studies to estimate seismic hazard empirically (2007

WGCEP, 2008; WGCEP, 2003). The empirical model will adequately fit the observed regional seismicity rates considering that there are no significant altering events (Felzer, 2008). Reasenberg et al. (2003) calculated seismicity rates in ten different models for the San Francisco Bay region and took the average of those for the final seismicity rates (see Table 2.1). Model A to D were performed by taking mean rate of earthquakes over certain time periods and magnitude ranges. Model E and F assumed a linear increase of seismicity. Model G to J adopted a seismic cycle model so that seismicity rates would drop immediately after large earthquakes. Felzer (2008) only took into account Reasenberg's mean method to develop the empirical model for California. Felzer (2008) argued that the seismicity rate in San Francisco Bay region did not linearly increase as suggested by Reasenberg's model E and Felzer (2008) added that the G to J models were also lacking accuracy, since the seismicity rates were likely to be dropped after the end of aftershock sequence and most foreshock sequences were short; thus they did not represent the long term seismicity of the San Francisco region well, which was hypothesised by a seismic cycle model. However, seismicity characteristics are different among regions; therefore, further investigations are recommended to enhance the use of the linear trend or the seismic cycle models for a time dependent seismic hazard model.

Table 2.1. Extrapolation of Regional Rate (Reasenberg et al., 2003)

Model	Data	Time Period	Method	Mean rate (M≥6.7) in 2002-2031[1]	Mean of f(t) in 2002-2031[2]	Mean of f(t) over one cycle
A	M ≥ 3.0	1942-1998	Mean	0.014	0.47	-
B	M ≥ 3.0	1984-1998	Mean	0.016	0.53	-
C	M ≥ 5.5	1906-2000	Mean	0.011	0.37	-
D	M ≥ 5.5	1979-2000	Mean	0.020	0.67	-
E	M ≥ 3.0	1942-1998	Linear trend	0.016	0.53	-
F	M ≥ 3.0	1970-1998	Linear trend	0.020	0.67	-
G	M ≥ 5.5	1970-2156	Seismic cycle-linear rise	0.027	0.90	1.00
H	M ≥ 5.5	1970-2351	Seismic cycle-linear rise	0.020	0.67	1.15
I	M ≥ 5.5	1970-2156	Seismic cycle-exponential rise	0.019	0.63	0.96
J	M ≥ 5.5	1970-2351	Seismic cycle-exponential rise	0.014	0.47	0.74

Rundle et al. (2005) performed numerical simulations to estimate time dependent probability of great earthquakes in San Francisco region using a physical earthquake

[1] Rates are extrapolated to M ≥ 6.7 by assuming a Guntenberg-Richter relation with b=0.9.
[2] Based on a long-term mean annual rate (M ≥ 6.7) of 0.031.

model (see Section 2.3.1.4). The simulation based method was different with those given by WGCEP (2003) since it did not directly use the probability distribution of recurrence times. Instead, the probability distribution was characterized by modelling the slip on fault segments; thus, fault interactions and frictional physics were taken into account (Rundle et al., 2005). In the method, detailed slip history of fault segments for longer duration of seismicity and the interaction among neighbouring faults could be obtained, which were difficult to be achieved in the conventional field-based approach. Nevertheless, the numerical simulation models require rigorous seismological information (see Section 2.3.1.4), which is rarely available in developing countries.

2.3.5. Previous PSHA studies of Sumatra

An early seismic hazard study of Indonesia was presented in the first Indonesian Earthquake Resistant Design Code for Buildings (PPTI-UG-1983). The hazard map was produced by Beca Carter Hollings and Ferner, in 1978, as part of the bilateral collaboration between Indonesia and New Zealand (Irsyam et al., 2010; Sutjipto, 1994). The seismic hazard map was developed based on a 200 year earthquake recurrence period and divided the Indonesian region into 6 seismic zones. Almost two decades later, the seismic code was revised to comply with the American Uniform Building Code (UBC) 1997. The code was ratified in 2002 and is known as SNI 03-1726-2002. In this code, an earthquake return period of 500 years was assumed for the seismic hazard assessment and the hazard map basically consists of 6 seismic zones with 0.30g as the maximum value for base rock accelerations (Figure 2.7). Presently, the SNI 03-1726-2002 is still the official seismic design code for buildings in Indonesia.

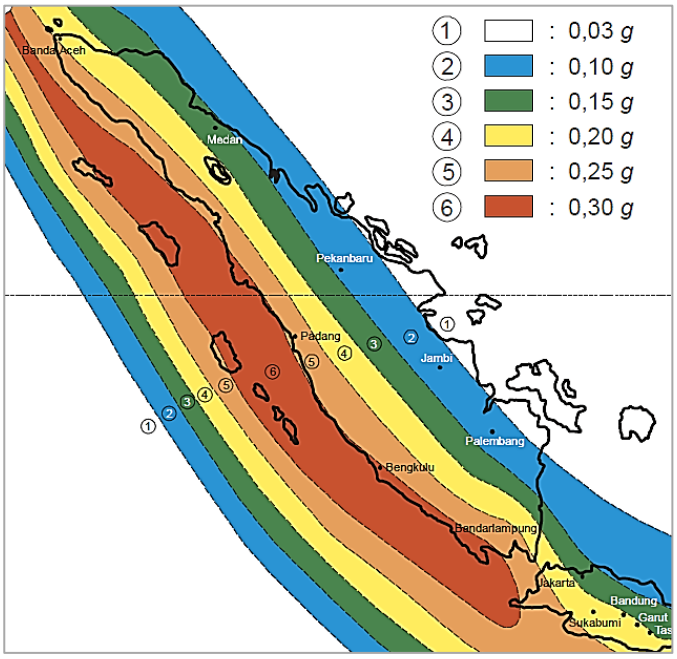

Figure 2.7. Seismic hazard map of Sumatra (SNI 03-1726-2002, 2002)

The seismic activity in Indonesia has increased significantly in the past decades. The Great Sumatra earthquake with M_w 9.1 struck northern part of Sumatra in 2004. This was followed by a destructive tsunami and resulted in more than 200,000 fatalities. This event highlighted the importance of identifying potential hazard, particularly for the susceptible regions. Since then, more seismic hazard studies were carried out for the Indonesian regions (Asrurifak et al., 2010; Briggs et al., 2008; Chlieh et al., 2008; Irsyam et al., 2008; Irsyam et al., 2010; Petersen et al., 2007a; Petersen et al., 2004; Sengara et al., 2007; Sieh, 2005; Sieh, 2007; Sieh et al., 2008) and most of them recommended seismic hazard maps with higher PGA values than currently applied in the Indonesian seismic codes. Figure 2.8 and Figure 2.9 show seismic hazard maps for the Sumatra area developed by Petersen et al. (2004) and Irsyam et al. (2008), respectively.

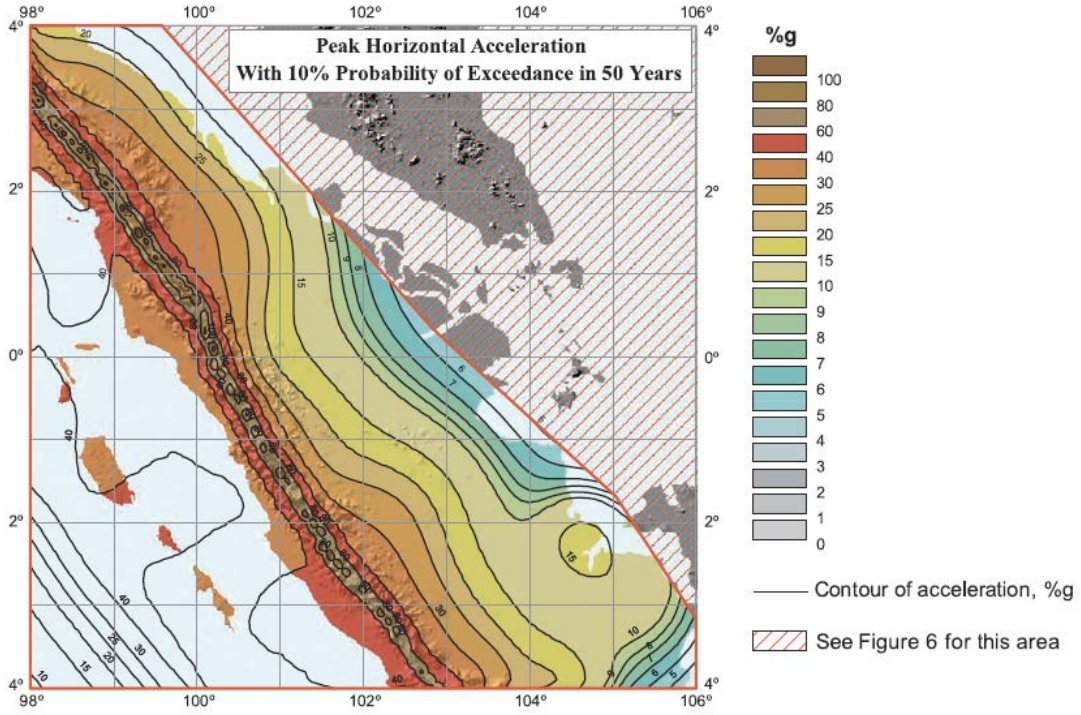

Figure 2.8. Seismic hazard map of Sumatra at 10% probability of exceedance in 50 years on rock site (Petersen et al., 2004)

Figure 2.9. Seismic hazard map of Sumatra at 10% probability of exceedance in 50 years on rock site (Irsyam et al., 2008)

Considering the recent seismicity of Indonesia as well as recently available seismological data, the Indonesian Ministry of Public Works initiated a revision of the Indonesian seismic code in 2006. A revision team was formed that consisted of government agencies, academics, and professionals with various expertise including geology, seismology, tomography, crustal deformation, earthquake geotechnical and structural engineering (Irsyam et al., 2010). The team proposed new hazard maps of Indonesia for 10% and 2% probability of exceedance in 50 years. The seismic hazard assessment was carried out using the conventional PSHA method with constant hazard rate over the exposure period (a time independent PSHA model). Figure 2.10 illustrates the proposed hazard maps, which shows higher acceleration values than those of the former code. The increase of hazard values is due to the use of three dimensional (3D) fault models as well as the adoption of higher maximum magnitude as a result of mega magnitude earthquakes occurring in the recent years (Asrurifak et al., 2010).

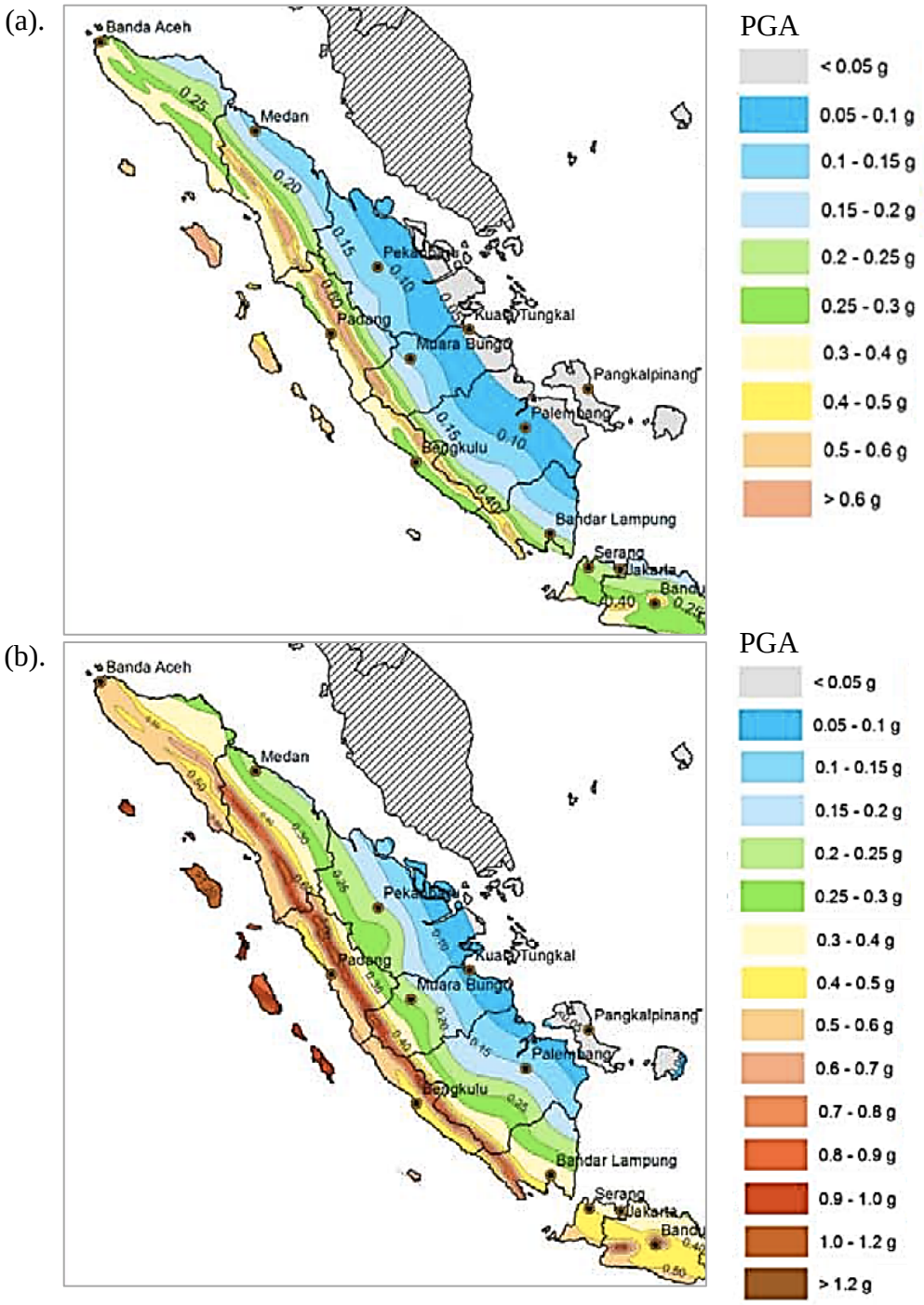

Figure 2.10. Maps of Peak Ground Acceleration (PGA) of Sumatra: a). for 10% probability of exceedance in 50 years; and b). for 2% probability of exceedance in 50 years (Irsyam et al., 2010)

2.4. TSUNAMI HAZARD ASSESSMENT

2.4.1. Introduction to Tsunami Hazard

"*Tsunami"* in Japanese means "harbour wave"' ("*tsu"*= harbour, "*nami*" = wave) as cited in IOC (2008). Tsunami can be defined as a series of travelling waves associated with impulsive disturbances in the oceans (i.e. earthquake, volcanic eruptions, submarine landslide or meteorite impact), which has a great wave length and period (IOC, 2008). In deep oceans, the length of tsunami waves can exceed 500 km with period between 100 to 2000 seconds. In deep sea, the height of tsunami waves is relatively small (less than 0.4 m) and sometimes goes unnoticed (Bryant, 2001). However, the tsunami height increases considerably in shallow water. Tsunami waves travel very quickly, depending on the depth of sea water. The waves move around 600-900 km/hour in deep ocean, about 100-300 km/hour in continental shelf and around 36 km/hour on shore (Bryant, 2001). The velocity of tsunami at sea (assumed as long and linear waves) can be estimated using Equation 2.30 and the velocity on shore can be approximated by Equation 2.31 (Bryant, 2001).

$$C = \sqrt{g\,d} \qquad 2.30$$

$$v_r = 2\sqrt{g\,H_s} \qquad 2.31$$

where,

C : celerity of the wave (m/s)

g : gravitational acceleration (9.81 m/s^2)

d : water depth (m)

v_r : velocity of run-up (m/s)

H_s : wave height at shore or the toe of the beach (m)

In addition, the tsunami waves are not travelling at the same speed. Long-period waves travel faster than the shorter ones and reach the shore earlier. As a result, there could be a series of tsunami waves in one tsunami event. This phenomenon is known as dispersion. Tsunami waves can be idealised into several forms, as illustrated in Figure 2.11. In deep oceans, the waves suit the sinusoidal form. However, as the waves approach the shoreline, the waves are better modelled as solitary or N-waves (Bryant, 2001).

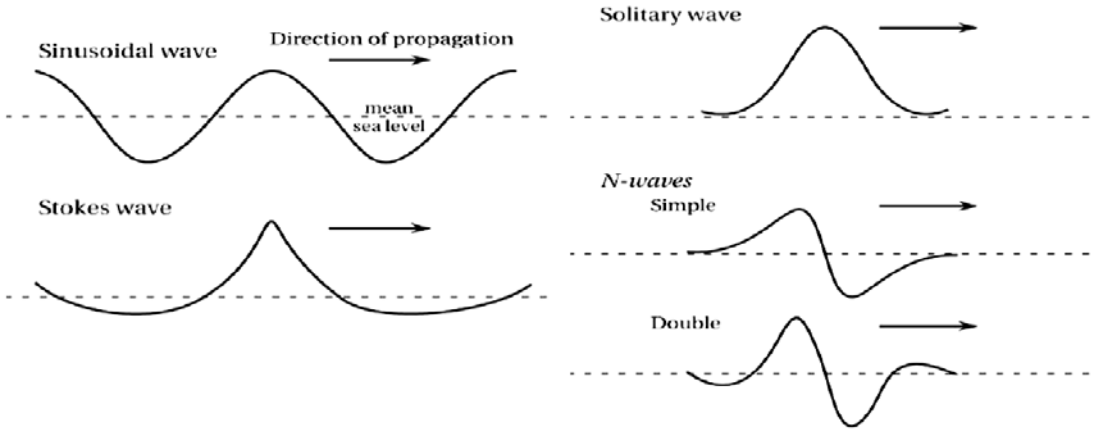

Figure 2.11. Idealised models of tsunami waves (Bryant, 2001)

The mechanism of a tsunami can be described in a few stages including initiation, split, amplification and run-up (Figure 2.12). The initiation process begins as the sea floor suddenly deforms and vertically displaces the overlying water. The displaced water is pushed above mean sea level and exerts potential energy. The potential energy is then transformed into kinetic energy through the propagation of tsunami waves. At the latter stage, the tsunami waves split and move into two opposite directions. The waves that travel landward may cause local tsunami (< 100 km of travel distance) and the waves that move seaward may result in regional (100-1000 km) and distant tsunami (> 1000 km of travel distance). As the tsunami reaches the continental shelf, tsunami amplitude increases, but the period of the wave decreases. As a result, the waves would be steepened and create run-up onshore (USGS, 2008). A tsunami run-up (H_r) characterises the height of a tsunami onshore, above mean sea level (see Figure 2.13). A tide gauge record in Japan, due to a distant tsunami, is shown in Figure 2.14. The figure illustrates the determination of tsunami amplitude and wave height from tide data.

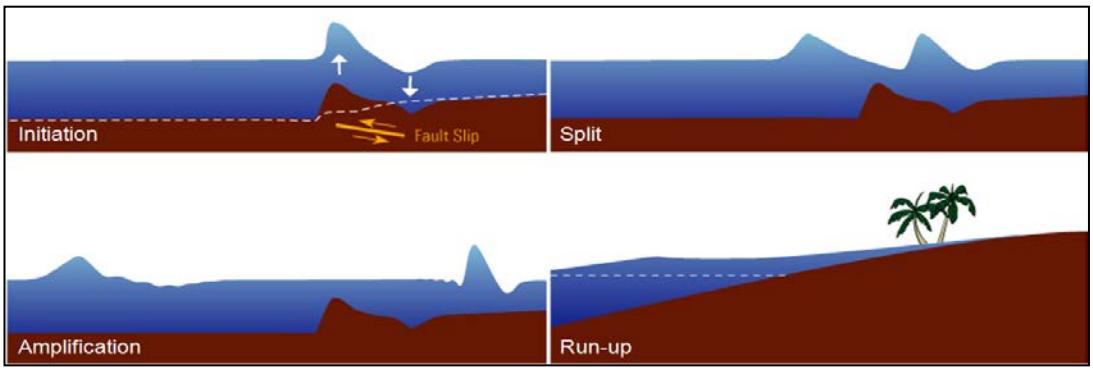

Figure 2.12. The illustration of Tsunami Mechanism, unscaled (USGS, 2008)

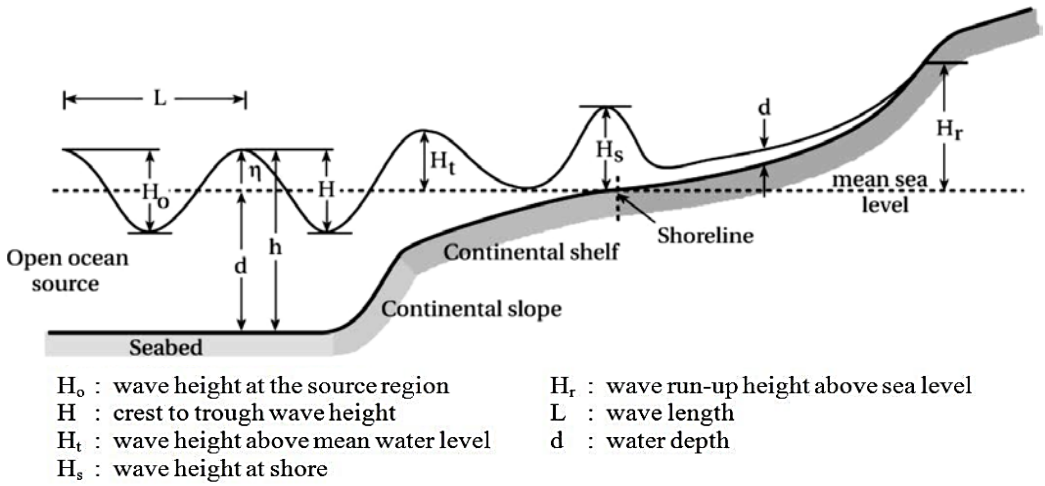

Figure 2.13. Various terms associated with tsunami (Bryant, 2001)

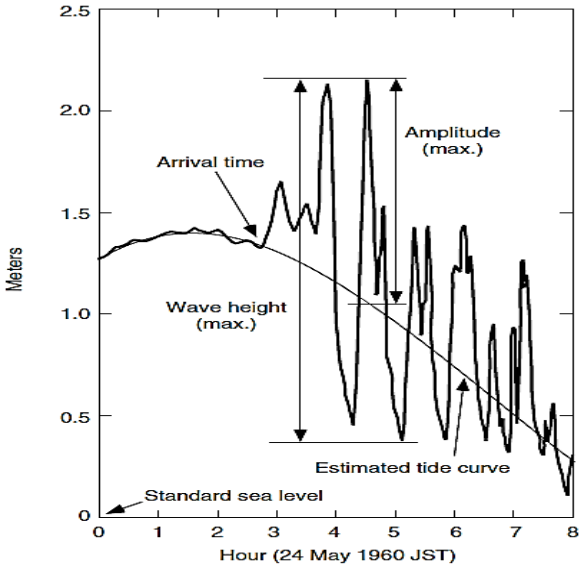

Figure 2.14. Tide gauge record at Miyako, Japan due to the 1960 Chilean earthquake that triggered distant tsunami (Satake, 2002)

2.4.2. Magnitude Scale of Tsunami

The intensity scale of tsunami was initially proposed by Sieberg in 1927 and then modified by Ambraseys in 1962 (Levin and Nosov, 2009). The Sieberg-Ambraseys tsunami intensity scale categorises tsunami in terms of their destructive effect on coastal areas. These early generations of tsunami scales do not contain any tsunami physical parameters such as tsunami run-up height and wave length.

In 1942, Imamura developed a tsunami magnitude based on tsunami run-up height. The method was later improved by Iida (Levin and Nosov, 2009) and has since been known as the Imamura-Iida scale. The Imamura-Iida scale is widely used in tsunami

catalogues. The Imamura-Iida scale is defined in Equation 2.32 and presented in Table 2.2.

$$m_{II} = \log_2(H_{r\max}) \qquad 2.32$$

where,

m_{II} : Imamura-Iida's tsunami magnitude scale

H_{rmax} : maximum tsunami run-up height (m)

Table 2.2. Tsunami magnitude scale (Iida, 1963 cited in Bryant, 2001)

Earthquake Magnitude (Richter Scale)	Tsunami Magnitude	Maximum Run-up (m)
6.0	-2	< 0.3
6.5	-1	0.50 – 0.75
7.0	0	1.00 – 1.50
7.5	1	2.00 – 3.00
8.0	2	4.00 – 6.00
8.2	3	8.00 – 12.0
8.5	4	16.0 – 24.0
8.8	5	> 32

The maximum run-up heights of tsunami along coastlines are likely to be varied. Hence, Soloviev modified the Imamura-Iida scale to take into account the variability of tsunami heights along a coast. Instead of using maximum tsunami run-up height, Soloviev utilised mean run-up height as seen in Equation 2.33 and Table 2.3. The scale was later known as the "Soloviev-Imamura Tsunami Intensity Scale".

$$I = 1/2 + \log_2(H) \qquad 2.33$$

where,

I : Soloviev's tsunami intensity

H : mean tsunami run-up height on the coast closest to tsunami source (m)

Table 2.3. Soloviev's tsunami intensity scale (Horikawa and Shuto, 1983 cited in Bryant, 2001)

Tsunami Intensity	Mean Run-up Height (m)	Maximum Run-up Height (m)
-3.0	0.1	0.1
-2.0	0.2	0.2
-1.0	0.4	0.4
0.0	0.7	0.9
1.0	1.5	2.1
2.0	2.8	4.8

Tsunami Intensity	Mean Run-up Height (m)	Maximum Run-up Height (m)
2.5	4.0	7.9
3.0	5.7	13.4
3.5	8.0	22.9
4.0	11.3	40.3
4.5	16.0	73.9

Abe (1979) developed a tsunami magnitude scale (M_t) based on the maximum amplitude of tsunami waves recorded by tide gauges. Abe observed that the maximum tsunami amplitudes (H) in the Pacific region were strongly related to the earthquake moment magnitudes (M_w). This suggested that tsunami magnitude scale (M_t) could also be correlated to M_w. Abe (1979) calibrated the instrumental tsunami data in the Pacific region and equated $M_t = M_w$ to obtain a constant "C". Initially, the method was applied for far-field tsunami. Then, the method was improved to include near-field events. Abe defined the tsunami magnitude formula as the following (Abe, 1981; Abe, 1985; Abe, 1995):

$$M_t = \log(H) + a.\log(R) + D \qquad 2.34$$

where,

H : maximum tsunami amplitude (m)

M_t : earthquake moment magnitude

R : epicentral distance (km)

a : a constant to characterise tsunami amplitude-decay relation with distance

D : a constant required to fulfil $M_t = M_w$ on the average for the calibration data set

Abe (1989) demonstrated that the M_t scale represents the seismic moment and the physical parameters of tsunamigenic earthquakes, as discussed in the next section.

2.4.3. Estimation of Tsunami Wave Height from Earthquake Magnitude

Further research was conducted to determine the correlation of the tsunami parameters such as wave amplitude and distance with the tsunami magnitude scale M_t (Abe, 1981; Abe, 1985; Abe, 1995). An empirical approach was adopted and the tsunami data from the tide stations in Japan were assessed. Abe (1981, 1985 and 1995) found that the maximum amplitude of tsunami waves corresponded to seismic moment (M_o) produced by the earthquake, which was related to rupture areas,

average sea floor displacement, as well as shear modulus of the rocks where the area ruptured. The M_w scale was related to the seismic moment as follows:

$$M_w = (\log M_o - 16.1)/1.5 \quad 2.35$$

$$M_o = \mu D S \quad 2.36$$

where,

M_w : earthquake moment magnitude

M_o : seismic moment (dyne.cm)

μ : rigidity (dyne/cm^2)

D : the average displacement of fault (cm)

S : the area of the fault (cm^2)

Tsunami amplitude can be estimated from Equation 2.34 by assuming M_t=M_w. Through a regression procedure, Abe (1981) obtained a relation for tsunami propagation distance in Japan, as shown in Equation 2.37.

$$\log(H_t) = M_w - \log(R) - 5.55 + C \quad 2.37$$

where,

H_t : tsunami height (m)

M_w : earthquake moment magnitude

R : distance (km)

C : constant (C = 0.00 for tsunami in the fore arc and C = 0.2 for tsunami in the back arc)

Equation 2.37 is applicable for regional data of 100-3500 km. However, the equation would produce extremely large wave heights for near field events. In this case, Abe (1995) proposed a minimum distance (R_o) and limited the tsunami height near tsunami source, as shown in equations 2.38 and 2.39.

$$\log(R_o) = 0.5M_w - 2.25 \quad 2.38$$

$$\log(H_r) = 0.5M_w - 3.30 + C \quad 2.39$$

where,

R_o : the radius of a circular fault (km)

H_r : limiting tsunami height near the source (m)

Based on tsunami observation data, Abe (1995) reported that for a local tsunami, H_t actually represents local mean of tsunami run-up height and $2H_t$ corresponds to the maximum run-up of local tsunami at each segment. For regional tsunami, H_r represents the maximum of local tsunami height and $2H_r$ characterises the maximum of all data (H_{max}). Verification against tsunami observation data shows that Equation 2.39 tends to overestimate tsunami run-up heights. However, the method is applicable for near-field tsunami warning systems that require rapid evaluation of tsunami amplitudes (Abe, 1995). Abe's approach is relatively simple and takes into account the quantitative parameters of tsunami including wave heights and epicentral distance. Nevertheless, the method does not take into account the effect of bathymetry or topography of an area. Abe (1995) argued that the mean-height of tsunami was less responsive to topographic irregularities than the tsunami maximum height, thus the method is acceptable for tsunami hazard analysis for mitigation purposes. Moreover, Abe (1989) showed that regional variation has a negligible effect on the amplitude-distance relation, with the condition that the number of stations is considerable and well distributed.

Nevertheless, Abe's amplitude-distance relation is not applicable to tsunami earthquakes. A tsunami earthquake refers to an earthquake that produces immensely large tsunami despite its weak seismic waves (Abe, 1989). Kanamori (1972) characterises the tsunami earthquake as an earthquake that has long period of fault rupture, moderately small rupture zone, but exceptionally large average displacement. Abe (1989) compared the earthquake surface wave magnitude (M_s) and the tsunami magnitude of the tsunamigenic events in Japan. The result shows that most tsunamigenic events produce a good correlation between M_t and M_s. However, the trend tends to deviate for tsunami earthquakes. Based on this finding, Abe (1989) categorises an event as tsunami earthquake if $(M_t - M_s) \geq 0.5$.

There are several factors affecting run-up heights such as configuration of the shore, diffraction, standing wave resonance, edge wave that moves at right angles to the shoreline and refraction energy (Bryant, 2001). Generally, a tsunami dissipates its energy through a frictional attenuation with the seabed. Steep shoreline has lesser amount of frictional attenuation, and therefore, dissipates less energy than that of the lower slope coastline. Abe (1985) observed that the tsunami potential in the Japan sea is larger than that in the Pacific ocean. Abe discovered that the difference is

contributed by the assumed rigidity of the source medium between the Japan Sea and Pacific Ocean for determining their seismic moments. The difference leads to about 0.2 unit of M_t. In addition, the geometry of a fault rupture plays a significant role for tsunami potential. Bryant (2001) reveals three types of faults that can trigger tsunami including a vertical strike-slip fault and a dip-slip fault, which includes normal and thrust fault types. However, an event on a thrust fault has more potential for generating tsunami.

2.4.4. Tsunami Inland Penetration

The extent of tsunami inundation depends on the volume of water passing onshore. Long periods of tsunami waves usually produce greater inundation. The cross-sectional area of inundated shoreline is equal to the cross-sectional area under the tsunami as shown in Figure 2.15. Inland penetration of tsunami can be estimated, as the following (Bryant, 2001):

$$x_{\max} = (H_s)^{1.33} n^{-2} k \qquad 2.40$$

where,

x_{max} : limit of inland incursion (m)

H_s : water height onshore

n : Manning coefficient, which reflects surface roughness of penetrated lands (see Table 2.4).

k : denotes a constant (=0.06)

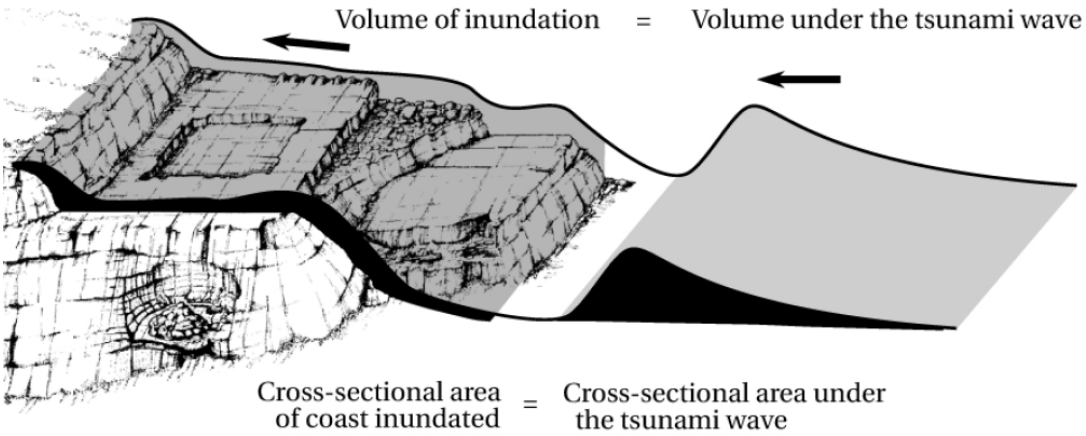

Figure 2.15. Cross sectional area of inundated coast and volume of tsunami (Bryant, 2001)

Table 2.4. Manning's coefficient associated with land surface (Bryant, 2001)

No.	Coast Surface Type	Manning's Coefficient
1.	Very smooth terrain such as mud flats or pastures	0.015
2.	Areas covered by buildings	0.03
3.	Densely treed landscapes	0.07

2.4.5. Probabilistic Tsunami Hazard Analysis (PTHA)

In the past, tsunami hazard assessment mainly relied on scenario or deterministic models. Deterministic hazard analysis is usually used to assess tsunami hazard prior to the development of the probabilistic model. As is also the case for the deterministic seismic hazard model; the deterministic tsunami model is known for its conservatism in terms of selecting maximum credible events. The method is likely to set higher limits of input parameters, especially when the scenarios do not consider the historical events (Geist and Parsons, 2006). However, the approach has been improved by the development of Probabilistic Tsunami Hazard Analysis (PTHA), which is based on the PSHA method. The PTHA has distinct principles from those of PSHA. The PTHA must consider far field sources to take into account regional tsunamis (about 100 to 1000 km of travel distance) as well as distant tsunamis (more than 1000 km of tsunami travel distance). PSHA depends on attenuation relationships; whereas PTHA is based on tsunami propagation models (Geist and Parsons, 2006). Empirical and computational models of PTHA are generally used in tsunami hazard assessments. The empirical method is suitable for a region with relatively complete tsunami catalogue (Brizuela, 2005; Burbidge et al., 2008; Geist and Parsons, 2006) and the computational method is preferable for areas with lack of tsunami data (Appuhamy, 2007; Løvholt et al., 2008; Parsons and Geist, 2009; Power et al., 2007; Puspito and Gunawan, 2005). The empirical method is easier to implement and requires moderate modelling capabilities. However, the method is unable to appropriately characterise local characteristics of tsunamis, which results in increased uncertainty (Strunz et al., 2011). On the other hand, the numerical method involves tsunami numerical simulations to obtain tsunami parameters, including tsunami wave heights in an examined area. The method requires a physical model of tsunamis including hydraulic parameters so that more detailed analysis of tsunami hazard can be obtained (Strunz et al., 2011). Furthermore, the tsunami numerical

models can be integrated with Monte Carlo simulations to generate a synthetic tsunami catalogue (Geist and Parsons, 2006; Power et al., 2007). Synthetic tsunamigenic earthquakes are produced to complement tsunami data in the investigated study areas.

Latief et al. (2008) proposed an integrated probabilistic seismic and tsunami hazard analysis (PSTHA) method. The method was based on the well-established PSHA that consisted of a recurrence model for potential tsunami sources, maximum magnitude, total probability theorem and the wave propagation to the investigated site. Latief et al. (2009) carried out a probabilistic tsunami hazard assessment for the city of Banda Aceh in Sumatra. The method used a PSHA computer program, called EZ-FRISK, to find the relationship of subduction earthquake magnitude, peak acceleration and tsunami height, which corresponded to various return periods (Latief et al., 2008; Latief et al., 2009). To assess the tsunami hazard probabilistically, Latief et al. (2009) only activated the subduction zone as the main tsunami source of the area. Hence, the return period of the tsunamigenic earthquakes could be obtained. Nevertheless, the study did not take into account far field tsunami sources and applied a constant rate of tsunami occurrence for every earthquake magnitude considered in the analysis. In fact, not every earthquake in the subduction area could produce a tsunami. Larger earthquakes (M_w > 7.5) are more likely to generate tsunami than the smaller ones; thus, they have different rates. As a consequence, this method is valid if the minimum threshold of earthquake magnitude is sufficiently high to ensure the occurrence of tsunami, and the contribution of far field tsunami sources to the hazard in the area is negligible.

2.4.6. Tsunami Numerical Simulations

Various tsunami numerical propagation models can be utilised for tsunami hazard assessment including MOST (Titov and Gonzalez, 1997), SAGE Model (Gisler et al., 2006; Løvholt et al., 2008), TUNAMI (Imamura et al., 2006), NAMI-DANCE (Zaytsev et al., 2002).

The MOST (Method of Splitting Tsunami) model was developed by Titov of PMEL (Pacific Marine Environmental Laboratory) and Synolakis of University of Southern California. The program had been used as standard tools for tsunami estimations for NOAA (National Oceanic and Atmospheric Administration) Centre for Tsunami

Research in the USA. The program was based on a finite difference method. The MOST propagation model accounted for numerical dispersion scheme, Coriolis force and non-linear shallow water wave equations in spherical coordinates, which were numerically solved using a splitting method (Titov and Gonzalez, 1997). The MOST had the capability to compute all stages of tsunami process such as tsunami generation, propagation and run-up and the model was used to simulate the 1996 Andreanov tsunami and the resulted runup distributions were comparable with those of the actual observations (Titov and Gonzalez, 1997). In tsunami numerical simulations, relatively coarse grids can approximate the wave in deep water well; however, as the wave reached shallow water, high-resolution grids are required. Hence, nested computational grids were utilized in the MOST model to allow better approximation of wavelength in the area of interest with minimum errors. Nevertheless, the MOST model was only made available to close collaborators of the NOAA (NOAA, personal communication, 2010).

The SAGE model is a multi-material adaptive grid Eulerian code based on a high resolution Godunov scheme initiated by Michael Gittings for Science Applications International (SAIC) and Los Alamos National Laboratory or LANL (Gisler et al., 2006). The SAGE model allowed the simulations of landslide model and the resulted tsunami generation. Løvholt et al. (2008) used the SAGE model to simulate La Palma Island tsunami, which was triggered by submarine landslide. Nevertheless, the tsunami triggered by submarine landslides has different characteristics from those generated by the displacement of seafloor due to earthquake (Bryant, 2001). First, the direction of landslide tsunami is more focus than that of the earthquake tsunami. Second, the waves of landslide tsunami are asymmetric near tsunami source and better characterized by N-waves (see Figure 2.11), while the earthquake tsunami waves tend to be symmetrical near source. Therefore, an analytical formula to compute the fault rupture and the displacement of seabed is required for the SAGE model to be applicable for simulating tsunami generated by earthquakes. Hence, Løvholt et al. (2012) extended the SAGE model to include tsunami generated by earthquake and utilised the analytical formula of Okada (1985) to determine the fault rupture characteristics of earthquakes. Løvholt et al. (2012) then used the SAGE model to assess tsunami hazard in eastern Indonesia deterministically. However, the dry land inundation of tsunami in the investigated area has not been taken into

account in the model. Instead, wave surface elevations near the shoreline were considered as a good approximation for the coastal inundation (Løvholt et al., 2012).

The TUNAMI (Tohoku University's Numerical Analysis Model for Investigation of Near field tsunamis) model was developed by the Disaster Control Research Centre of Tohoku University in Japan for TIME (Tsunami Inundation Modelling Exchange) project (Imamura et al., 2006). The TUNAMI model solved Nonlinear Shallow Water equations (NSW) using leap frog scheme numerical solution procedures (Goto and Ogawa, 1991; Imamura, 1989; Shuto et al., 1990). Zaytsev et al. (2002) stated that the Nonlinear Shallow Water equations provided acceptable error limit as well as reasonable computational time and memory. The numerical algorithm of TUNAMI was adopted by the NAMI-DANCE model (Zaytsev et al., 2002). In addition, the NAMI-DANCE extended the model to include the calculation of current velocity distributions and their directions at selected time interval, relative damage levels associated with drag and impact forces as well as equipped the model with more interactive interface (e.g. 3D plots, tsunami animations, etc.). However, a nested domain system had just integrated in the new version of NAMI-DANCE model (Yalciner, personal communication, January 17th, 2012). Detailed information on the mathematical and numerical basis of the NAMI-DANCE model can be found in Appendix F of this thesis.

2.4.7. Previous Tsunami Hazard Assessments for Sumatra

Borrero et al. (2006) carried out tsunami inundation modelling for western Sumatra. Few tsunami simulations were conducted, including the 1797 events, the 1833 events and four other tsunami scenarios with earthquake magnitude up to M_w 9.3. The magnitudes of the 1797 and 1833 events were estimated between M_w 8.4-8.6 and M_w 8.6-8.9 respectively. Borrero et al. (2006) used the patterns of uplifted coral on the Mentawai Islands to model seafloor deformations based on the works of Natawidjaja et al. (2004). The study assumed that the 1797 event produced a rupture length about 300 km with average slip around 6 m; and the 1833 event produced a rupture length of about 320 km, with slip up to 18 m. The resulting wave heights and inundation distances were compared for Padang city and Bengkulu city in western Sumatra. The outcomes showed that Bengkulu was likely to experience greater tsunami inundation than Padang. It appears that the Mentawai islands shield the Padang area from the

direct impact of the region's maximum seafloor uplift. These large adjacent offshore islands do not exist for Bengkulu; thus the area is exposed to the direct impact of the region maximum uplift (Borrero et al., 2006). Nevertheless, Borrero et al. (2006) only considered local tsunamis and the analysis was based on few tsunami scenarios (deterministic tsunami hazard assessment). Therefore, the approach is only suitable for mitigation purposes. For wider application (i.e. design criteria, etc.), a probabilistic tsunami hazard analysis should be conducted.

Latief et al. (2009) carried out a probabilistic tsunami hazard assessment (PTHA) for the city of Banda Aceh in Sumatra. They found that the M_w 9.2 tsunamigenic earthquake in Aceh has a corresponding return period of 520 years and generates a tsunami height of 9.10 m in the case study area. Tsunami inundation modelling for several probable scenarios obtained from the PTHA was conducted for the city of Banda Aceh. The outcomes were useful for tsunami mitigation strategy, tsunami design criteria for building and infrastructures as well as tsunami warning system (Latief et al., 2009).

The estimation of tsunami hazard for some regions in Indonesia was also conducted through a GITEWS Project (Rudloff et al., 2009). The project was a joint cooperation between German and Indonesian governments as a response to the great Sumatran tsunami in 2004. The project produced tsunami hazard maps for several pilot areas in Indonesia including Padang, Cilacap and Bali (Strunz et al., 2011). In addition, the project helped the Indonesian government develop the Tsunami Early Warning System as well as to estimate the tsunami risk in Indonesia.

2.5. VULNERABILITY FUNCTIONS FOR BUILDINGS

2.5.1. Earthquake Vulnerability Curves

Vulnerability is defined as the loss of a given element at risk subjected to a given level of hazard (Coburn and Spence, 2002). Vulnerability functions relate the probability of exceedance of multiple damage states to a parameter of hazard level (Rossetto and Elnashai, 2003). The hazard parameter can vary for different types of hazards such as PGA for earthquake or tsunami height for tsunami risk assessment. Vulnerability functions can be expressed in many terms including damage states and damage ratios.

There are four fundamental methods to develop vulnerability curves for structures: empirical, judgmental, analytical and hybrid. The empirical methods utilise damage data distribution from post-earthquake surveys. This method is reliable provided that a large quantity of reliable damage data of similar construction is available and the data covers a wide range of ground motions (Rossetto and Elnashai, 2003). However, such damage data are often lacking. As a consequence, various datasets from different countries can be used (Rossetto and Elnashai, 2003; Spence et al., 1992). Nevertheless, heterogeneity of building damage data can be a major source of uncertainty in the empirical approach when used for regions with specific construction practices. Judgemental vulnerability curves can be developed based on estimation, knowledge and experience of structural engineers who are experts in earthquake engineering (Ahmad, 2011). The reliability of this method strongly depends on the experience and opinion of the experts, and therefore, its uncertainty is difficult to measure. Analytical vulnerability curves are obtained through the analytical procedure of structural models under increasing earthquake loads. The resulting deformations are related to damage distributions, which are used to develop the vulnerability functions. This method has gained popularity in recent years, along with the rapid development of computational tools. Many special features of structural response can be taken into account in the analytical model including shear-flexural-axial load interaction, re-bar buckling, bond and shear failure (Ahmad, 2011). However, for some cases, appropriate structural modelling remains a challenge such as the modelling of infill walls, architectural finishes and unexpected brittle failure modes due to poor materials or bad detailing. The hybrid method combines the previous techniques to deal with the uncertainties arising from limited empirical damage data, the subjectivity of judgemental approach and modelling issues in analytical method (Ahmad, 2011).

Numerous studies were conducted to develop vulnerability curves for structures subjected to earthquake hazard. GESI (2001) proposed vulnerability curves for different types of structures based on site observations as well as other existing studies on vulnerability. GESI applied a scoring system to take into account the quality of design, construction and materials; therefore, engineering judgements are required for selecting the appropriate vulnerability curve.

Rossetto and Elnashai (2003) produced fragility functions for European-type Reinforced Concrete (RC) structures based on earthquake post-damage distributions. As many as 99 datasets from 19 earthquakes (340,000 RC structures in total) were utilised, mostly from European countries. The heterogeneous damage data were then transformed into a homogeneous reinforced concrete (HRC) scale, which was calibrated experimentally to obtain seismic resistance for different structural systems (Rossetto and Elnashai, 2003). Vulnerability curves for different building ages-classes were developed using the combined observation and test data.

Kyriakides (2007) carried out analytical vulnerability analyses for typical RC structures by considering different types of buildings stock in Cyprus for different periods of constructions including "pre", "basic" and "modern" seismic structures. The analytical models took into account flexural, shear and bond failures in members and joints of RC buildings. Kyriakides (2007) observed that the damage modes of "pre" and "basic" seismic structures were mainly due to brittle failures. As a consequence, rapid increase in damage took place just before failure. The work of Kyriakides (2007) was extended by Ahmad (2011) to examine the vulnerability of RC structures with low strength concrete, typically found in developing countries (Pakistan as a case study). Ahmad (2011) highlighted that early damage accumulation and brittle failure were the typical problems for low-rise pre-seismic design RC buildings. However, more gradual damage was observed for the 1st generation of seismic design structures.

2.5.2. Tsunami Vulnerability Curves

Tsunami vulnerability curves can be developed using similar methods as for earthquakes. However, it is found that most of the existing tsunami vulnerability functions are based on the empirical approach (Koshimura et al., 2009; Peiris, 2006; Reese et al., 2011; Reese et al., 2007; Suppasri et al., 2012). This can be attributed to the complications of modelling interactions between tsunami waves and the response of structures that would be damaged by the earthquake.

Suppasri et al. (2012) produced fragility curves for wooden houses in Japan. The vulnerability curves were developed based on observations of damage in the Miyagi prefecture after it was hit by the great tsunami of Japan in 2011. Suppasri et al. (2012) found that an inundation depth greater than 4 m would totally demolish

wooden structures and an inundation depth of about 3 m could lead to severe damage.

Reese et al. (2007) developed empirical vulnerability relationships based on the observed damages of buildings due to the 2006 tsunami in South Java, Indonesia. The tsunami was triggered by an earthquake with a magnitude of 7.7 at the southern coast of West Java. It was reported that the event generated an average tsunami run-up in the range of 2-4 m above normal sea level. Therefore, the vulnerability curves proposed by Reese et al. (2007) were limited to a maximum tsunami height of 4 m. Reese et al. (2007) categorised the buildings in the region into four classes: timber/bamboo structure, traditional brick masonry building, brick masonry building with RC columns and RC structure with brick infill walls. It was found that different types of structures produced different levels of damage. Total damage was observed for older brick houses, about 50% for newer buildings of confined brick masonry types and approximately 5-20% for engineered RC structures. However, punch-out of rudimentary brick-walls was generally observed. In addition, Reese et al. (2007) developed relationships for death and injury rates based on the casualty data of the events as a function of water depth.

Other empirical tsunami damage functions were produced as part of the Scenarios for Tsunami Hazard-induced Emergency Management (SCHEMA) project (Scheer et al., 2011; Tinti et al., 2011; Valencia et al., 2011). The vulnerability curves were developed based on damage data collected from field surveys in Banda Aceh (Sumatra), Indonesia after the 2004 Indian Ocean tsunami. Very high resolution (40-60 cm or better) satellite imagery was used to complement the damage database obtained in the field survey (Valencia et al., 2011). Valencia et al. (2011) revealed that the buildings in Indonesia had similarities with the building typology in the European-Mediterranean areas. The SCHEMA project, as cited in Valencia et al. (2011), categorised the buildings in Aceh into 6 types: light construction in wood or timber without any design (A), brick not reinforced masonry (B), brick with reinforced column and masonry infill (C), collective buildings/concrete not reinforced (D) and well-designed buildings with RC columns and infill walls (E) and religious building/mosque (M). However, the vulnerability curve for the RC structures (Type E) was only limited to mid-rise structures up to 3 storeys. The damage datasets for the high rise RC buildings were limited; hence, the vulnerability

function could not be developed. The vulnerability curves for A to E types of building can be seen in SCHEMA technical report (Tinti et al., 2011).

2.6. EXISTING MITIGATION STRATEGIES IN THE CASE STUDY AREA

2.6.1. Indonesian Seismic Design Standard for Buildings

The first Indonesian seismic design standard for buildings was initially developed in 1983 (PPTGIUG-1983). The code was basically adopted from the New Zealand seismic design code and accounted for a 200-year earthquake recurrence period. The code was amended in 1987 (SKBI-1.3.53: 1987) and ratified as one of the Indonesian National Standards in 1989 (Sutjipto, 1994). The 1987 code categorised the Indonesian region into 6 zones. The seismicity level decreased from Zone-1 to Zone-6 and Padang city was part of Zone-3.

In 2002, the code was revised to account for a 500-year earthquake recurrence period (SNI 03-1726-2002, 2002). As a consequence, the PGA values in the former seismic standard were lower than those of the 2002 code. However, comparable values of seismic base shear force could be obtained for both seismic standards, since the 1987 code adopted a lower reduction factor R (SNI 03-1726-2002, 2002). Moreover, some soil types that were classified as soft soil in the former code were considered as medium soil in the latter code. This reduced further the seismic loads obtained from the 2002 code. To some extent, the 2002 code is more similar to the American UBC 1997.

In 2006, a team was formed by the Indonesian Ministry of Public Works to improve the Indonesian seismic design standard for buildings. The team proposed new seismic hazard maps for Indonesia (Irsyam et al., 2010); however, the completion of the new code is still in progress. Typical building standards in Indonesia for different periods of structures are summarised in Table 2.5.

Table 2.5. Typical standards adopted for buildings in Jakarta (Hoedajanto, 2007)

No.	Building Era	Building Code
1.	Before 1970	GBV and PBI 1955 (concrete)
2.	1970-1980	PBI 1971(concrete)
3.	1990-2000	SNI 03-2847-1991 (concrete) and PPTGIUG 1983 (earthquake)
4.	2000-date	SNI 03-2847-2002 (concrete) and SNI 03-1726-2002 (earthquake)

2.6.2. Tsunami Evacuation Maps for Padang City

After the devastating Indian Ocean tsunami in 2004, many studies highlighted the significance of tsunami risk in the city of Padang (Borrero et al., 2006; Chlieh et al., 2008; Sieh, 2005; Sieh, 2007; Sieh et al., 2008). The city is home to about 1 million people and has large infrastructures. Moreover, the most populated area of the city is situated near the coast with low lying areas in which the distance to higher ground with elevation > 5 m is approximately 30 km. High level of hazard, large exposure and the geographical conditions of the city contribute to the high risk in Padang city.

Since the 2004 tsunami, many attempts have been made to minimise tsunami risk in the area. The first tsunami evacuation maps for Padang city were produced a few years after the 2004 Indian Ocean Tsunami (see Figure 2.16). The evacuation maps categorised the city into 5 zones based on their altitudes above mean sea levels. Zone-I was marked as a red zone with elevation of 0-5 m from mean sea level, which has the highest risk to be inundated by tsunami and covers the most populated areas of Padang. Zone-II, Zone-III, Zone-IV and Zone-V are assigned for areas with elevations of 5-10 m, 10-25 m, 25-100 m and >100 m, respectively. Tsunami evacuation routes are also shown in the maps. The routes basically provide the shortest way to reach higher ground.

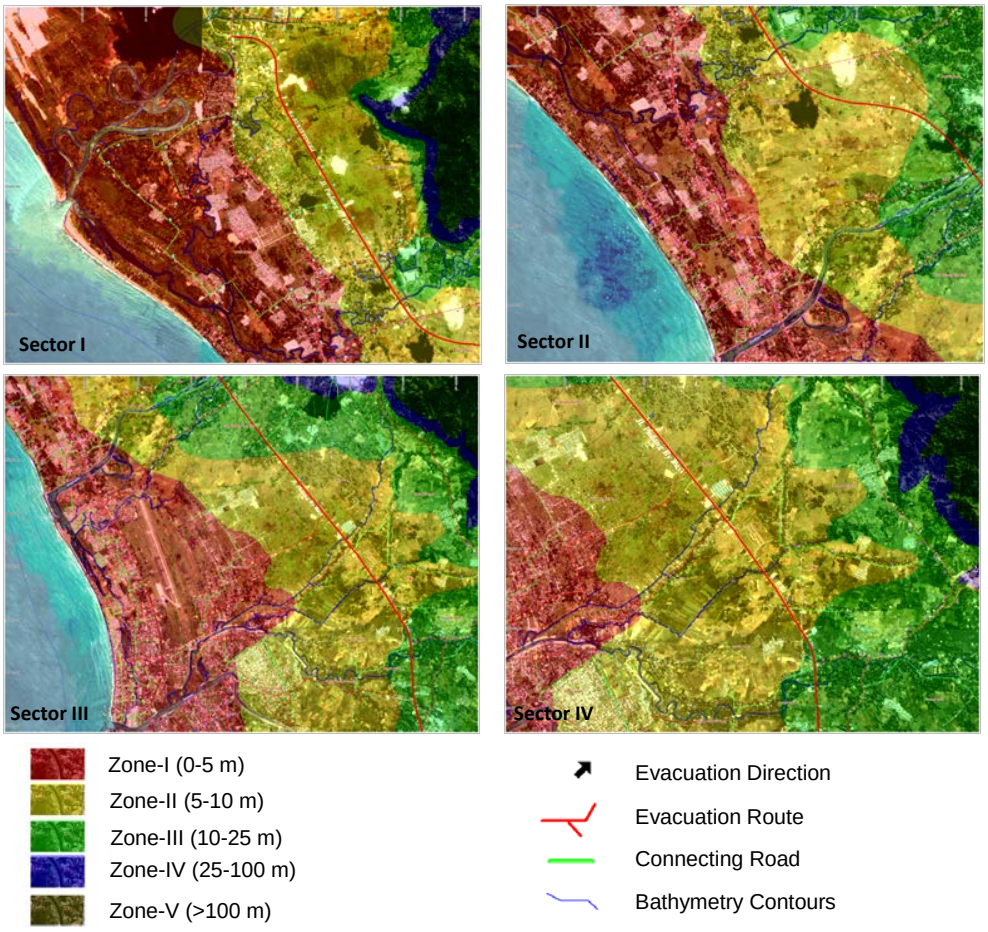

Figure 2.16. Former tsunami evacuation maps for Padang city

In addition, some buildings in the area that could be used as evacuation shelters were also highlighted in the evacuation maps. However, most of the recommended evacuation structures were damaged during the M_w 7.6 earthquake of Padang in 2009. The event was not tsunamigenic; hence, the damage was solely triggered by earthquake ground motions. Therefore, it appeared that the majority of the recommended evacuations structures were not even seismically designed. Consequently, they were not appropriate for tsunami evacuation purposes. Tsunami evacuation shelters should be capable of resisting both earthquake ground motion and tsunami forces. If the 2009 event was tsunamigenic, these buildings could have been a death trap for the evacuees and caused more fatalities.

The tsunami evacuation maps were later revised in 2010. Unlike the former evacuation maps, which were merely based on topography, the new evacuation maps were developed on the basis of the most plausible rupture scenarios in the area. The studies were initiated from a group of scientists from USA, Japan, Germany and

Indonesia. Schlurmann et al. (2010) revealed that the next large earthquake near Padang would probably be associated with a 200 year cycle. Therefore, Schlurmann et al. (2010) suggested the 1833 tsunamigenic earthquake as a realistic and historically proven scenario for Padang city. An accurate modelling of tsunami inundation and run up was performed using a very detailed model of near-shore bathymetry and coastal topography (Schlurmann et al., 2010). The tsunami hazard map for Padang was then officially released in May 2010. Based on the tsunami inundation map, it revealed that approximately 265.000 people in Padang are exposed to tsunami and only 170.000 of them (who live further inland) are likely to reach the evacuation areas within 30 minutes (Schlurmann et al., 2010). The latest version of tsunami evacuation maps in Padang is shown in Figure 2.17.

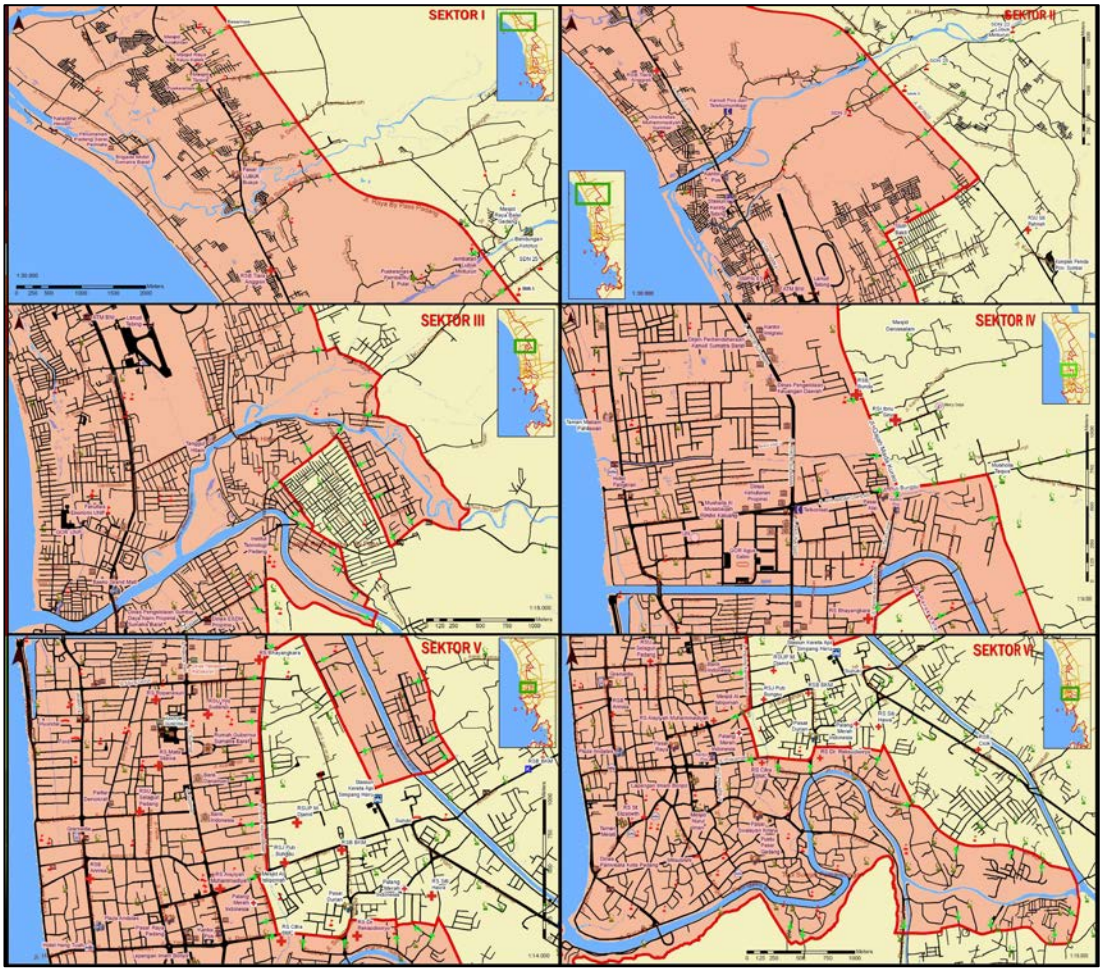

Figure 2.17. The new version of tsunami evacuation maps for Padang city

2.6.3. Tsunami Early Warning System

The Indonesian Tsunami Early Warning System (InaTEWS) was launched in 2008. The InaTEWS was developed with strong collaboration between Indonesia and Germany under the GITEWS Project (German Indonesian Tsunami Early Warning System) from 2005 to 2011 (Münch et al., 2011; Rudloff et al., 2009; Schlurmann and Siebert, 2011; Steinmetz et al., 2010). The operation of InaTEWS is under the management of the Indonesian Meteorological, Climatological and Geophysical Agency (BMKG). The BMKG not only provides a real time tsunami warning for Indonesia, but also for other countries in the Indian Ocean and ASEAN (Prih-Harjadi and Fauzi, 2009). To serve this purpose, massive instrumentation is required that include 160 broadband seismic stations, 500 accelerograph stations, 60 tide gauges, 20 DART buoys and several continuous GPS stations for monitoring purposes. Prih-Harjadi and Fauzi (2009) revealed that about 148 broadband seismograph stations, 85 accelerographs, 57 tide gauges, 19 DART buoys and 19 GPS stations were installed in the region. Therefore, more investment is still required.

The scheme of InaTEWS is illustrated in Figure 2.18. The initial stage of the tsunami warning system involves the determination of earthquake information such as earthquake magnitude, location and any ground movements and shape changes due to the earthquake. The estimation of earthquake magnitude and location is performed with SeisComP3 software (Hanka et al., 2010) and the ground movements are measured by GPS stations. The InaTEWS has a tsunami database that incorporates thousands of tsunami scenarios in the region. Based on the earthquake information, the best correlated scenario is selected from the database to predict whether the event is tsunamigenic or not; and if tsunamigenic, tsunami heights on the affected coast are estimated. At the same time, pressure sensors installed on the ocean floor measure the earthquake shock and report it to nearby buoys. The buoys then measure the lengthened-stretched peak of tsunami wave and raise the alarm via telecom satellite to the tsunami warning headquarter. To avoid false alarm, further verification is conducted through the observation of tide gauges. A sudden drop in sea level indicates that a tsunami is heading to the coasts. Once all information is collected and the occurrence of tsunami is highly plausible, the chief officer at the tsunami headquarter will raise a tsunami warning.

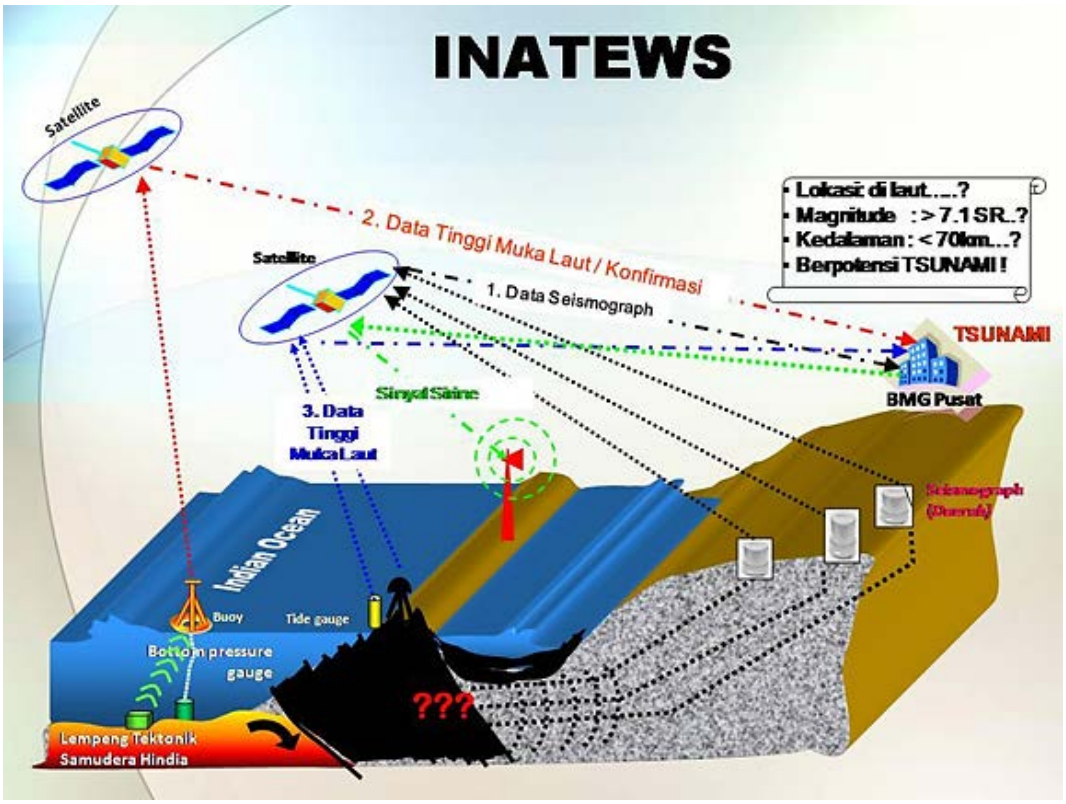

Figure 2.18. An illustration of the tsunami early warning system in Indonesia (InaTEWS)

To deal with the uncertainties of the warning process, Blaser et al. (2012) proposed the incorporation of Bayesians networks (BNs) in a real-time tsunami warning. Details of the approach can be found in Blaser et al. (2011). Blaser et al. (2012) estimated the probability of tsunami occurrence for the 10 recent earthquakes offshore Sumatra. The outcomes were then compared with real-time tsunami warning issued by the Indonesian officials (BMKG), as well as the available tide gauges or observation data in the region. The results showed good correlation with the existing data; however, for some events, discrepancies were considerable. The main problem was due to difficulties in estimating the real-time moment magnitude of earthquake, which had to be obtained very quickly (within 5 minutes after the earthquake). The reliability of BN approach depended on moment magnitude (Blaser et al., 2012). The difference between the real-time and post-processing magnitude estimates could lead to underestimation or overestimation of tsunami probability. In addition, the BN approach was not capable of estimating the probability of tsunami earthquakes. The tsunami earthquakes ruptured really slowly and emitted little high frequency energy, thus reliable real-time moment magnitude estimates were difficult to achieve (Blaser

et al., 2012). Nevertheless, the integration of BN approach in tsunami early warning system provided a more effective way to deal with the uncertainties for estimating the appropriate tsunami warning level.

The main challenge of a tsunami early warning system in Indonesia is to issue the warning immediately after the earthquake. This is because of its geographic and tectonic situation, which is very close to tsunami sources. As a consequence, the region is susceptible to local tsunamis that can reach the coast within 20-40 minutes after the earthquake. A quick decision may result in false alarm that can affect the credibility of tsunami warning in the future. However, late warning can result in insufficient time for the evacuation procedure. The InaTEWS can issue the first tsunami warning within 5 minutes after the earthquake (see Figure 2.19).

The dissemination of the warning is conducted in many ways, including: sirens, electronic media (TV/radio) and automatic SMS to the affected residence. Tsunami evacuation drills have been conducted in many prone regions in Indonesia. However, the systematic and periodic evacuation drills have to be maintained by the government and local authorities.

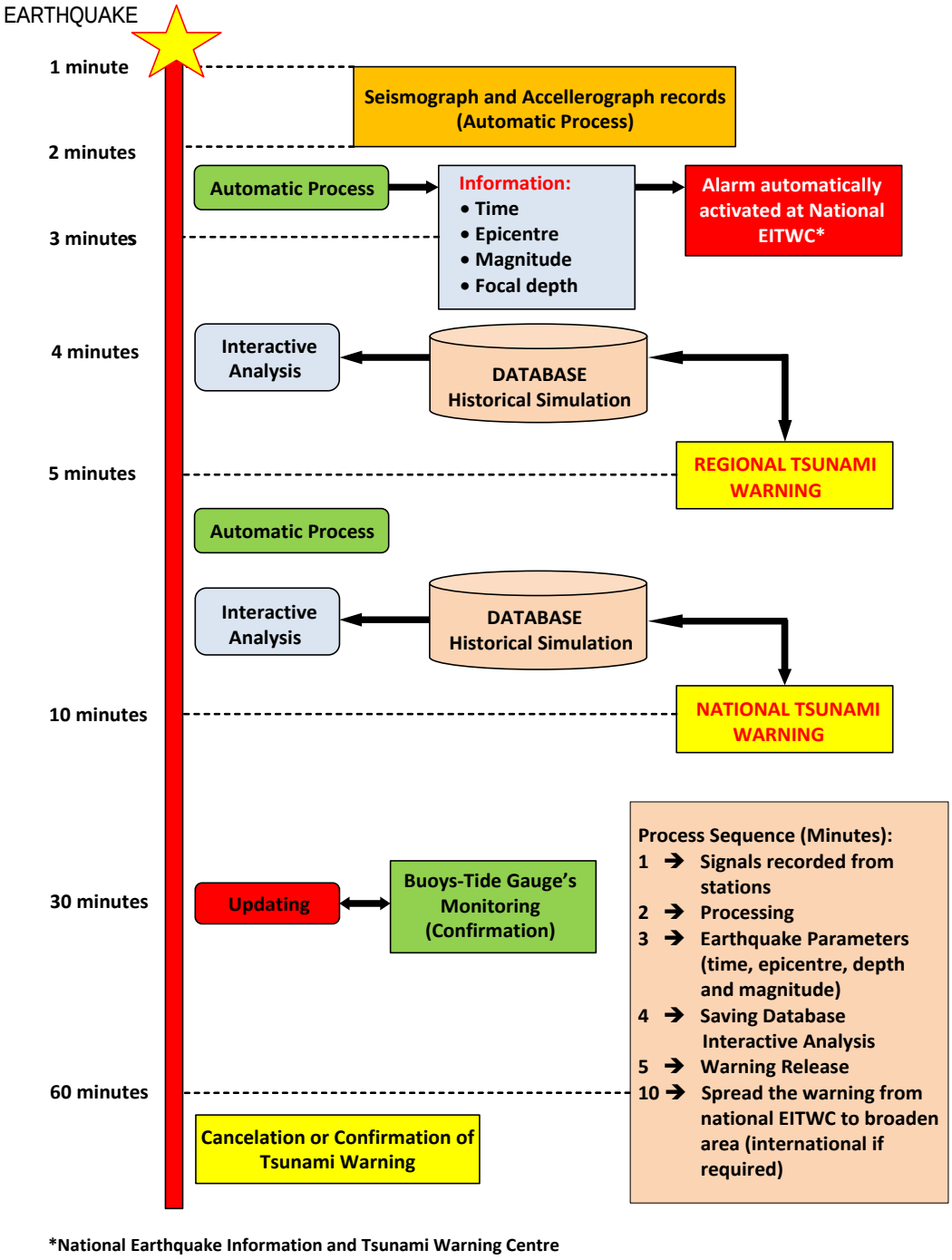

Figure 2.19. The procedure of the Tsunami Early Warning System in Indonesia (InaTEWS) based on the information from BMKG-Padang Panjang, Indonesia (Wilkinson, Alarcon, Mulyani, Chian, and Whittle, 2009)

2.7. SUMMARY

- The significance of probabilistic seismic hazard method (PSHA) is highlighted and compared with deterministic/scenario approach.

- The conventional PSHA method requires an integration of PSHA components for each seismic zone including earthquake recurrence function, ground motion attenuation relationship and distance from a seismic zone to a particular site (see Equation 2.16).

- A Poissonian seismicity model is generally adopted in the conventional PSHA by assuming a stationary hazard rate with time. The integration nature of the conventional PSHA restricts its adaptability to utilise a non-Poissonian seismicity model, which is compulsory for a time dependent hazard assessment.

- The conventional method requires a deaggregation procedure to obtain the contribution of each seismic source to total hazard in an area. The deaggregation procedure may lead to uncertainties due to the selection of bin size, the grouping of scenario and the selection of quantities utilized in the deaggregation process.

- A stochastic PSHA method is developed based on the conventional approach. However, instead of solving the total probability theorem, the stochastic approach directly calculates earthquake ground motions for all events in earthquake catalogue. Consequently, other seismicity models including the non-Poissonian can be easily utilized in the stochastic method.

- A risk assessment can be directly conducted in the stochastic PSHA method, which is difficult to perform in the conventional approach.

- A deterministic tsunami hazard assessment is generally adopted prior to the development of probabilistic model (PTHA). The PTHA commonly uses empirical and computational methods. The empirical method requires an extended tsunami catalogue, which is limited for most regions. For areas with limited tsunami data, the computational method is more suitable. However, the computational method requires a sophisticated hydrodynamic modelling of tsunamis.

- Existing risk assessments frameworks are reviewed including HAZUS, RADIUS, RISK-UE, EQ-RACY and ERA Framework. These frameworks are mainly developed to assess risk associated with earthquake ground motions. Therefore, earthquake associated hazards (e.g. tsunami, liquefaction and landslides) are not

taken into account. As a result, the overall risk for regions prone to these hazards is likely to be underestimated.

- Existing Indonesian seismic design standard for buildings, tsunami evacuation maps and tsunami early warning system are reviewed as part of earthquake and tsunami mitigation strategies in Indonesia.

CHAPTER 3

METHODOLOGY FOR EARTHQUAKE AND TSUNAMI RISK ASSESSMENT FRAMEWORK

3.1. INTRODUCTION

This chapter discusses the methodology used to extend the earthquake risk assessment framework (ERA Framework) developed at the University of Sheffield. The extension includes the incorporation of a time dependent seismic hazard (PSHA) as well as the estimation of tsunami hazard (PTHA). A time dependent PSHA model is proposed to account for the variability of hazard rate due to seismic gaps. Tsunami hazard triggered by earthquakes is also incorporated into the ERA Framework. The quantification of risk associated with earthquake and tsunami is performed probabilistically to take into account all probable level of hazard in the area. The extended modules are discussed in the following sections.

3.2. PROBABILISTIC EARTHQUAKE HAZARD ASSESSMENT (PSHA)

The seismic hazard assessment in this study is an extension of the stochastic PSHA model developed by Khan (2011) who used the instrumental earthquake catalogue to characterise the seismicity of the region. As discussed in Section 2.3.3, the reliability of this method depends strongly on the completeness of earthquake catalogues. As information on instrumental earthquakes for the case study area is scarce (Mulyani et al., 2010), the existing earthquake catalogue is extended using synthetic events. The synthetic events are generated by randomising the uncertainties of earthquake parameters in the earthquake catalogue, which is discussed in Section 3.2.1. To appropriately characterise the seismicity of the region, earthquake recurrence relationships are incorporated in the PSHA module, which is presented in Section 3.2.2. This approach is relatively similar to that proposed by Musson (2000). However, unlike Musson's approach, the locations of synthetic earthquakes in this study are not equally smeared over the seismic zones, but radiate along the rupture line, as suggested by Khan (2011). As a result, the probability of earthquakes

occurring along seismic sources is higher than other areas, which is consistent with the real distribution of earthquakes.

In addition, the stochastic PSHA model developed by Khan (2011) is expanded to include time dependency. The time dependent model takes into account elapsed time since the last large earthquake to comply with the Elastic Rebound Theory. The model foresees the increase of earthquake hazard due to the existence of seismic gaps in the region of West Sumatra. A non-stationary rate of hazard, as suggested by Reasenberg et al. (2003), is utilised. The modulation of earthquake rates in the investigated area is discussed in Section 3.2.3. The procedure of the PSHA module of this study and the development of hazard curves for the case study area are presented in Sections 3.2.4 and 3.2.5, respectively.

3.2.1. Generation of Synthetic Earthquakes

It is assumed in the conventional PSHA method that seismicity distribution is uniformly distributed over a seismic zone. However, Abrahamson (2006) argues that the approach tends to spatially smear the seismicity, which may lead to spatial inaccuracies in hazard values (Khan, 2011). Hence, a stochastic method that utilise existing earthquake catalogue to generate synthetic events is adopted in this study as proposed by Khan (2011). This approach randomises the locations of synthetic events within a certain boundary of real events as shown in Figure 3.1; hence, the spatial distribution of seismicity in the examined region can be maintained (Khan, 2011).

The synthetic earthquakes are generated by randomising the uncertainties of earthquake parameters such as earthquake magnitude, focal depth and epicentral location. The randomisation is performed over the margin of the parameter uncertainties as shown in Equation 2.18 and Equation 2.19. The magnitude of the synthetic events is estimated from magnitude determination and conversion errors, which are taken as ±0.20 for events initially recorded in moment magnitude (M_w), and ±0.41 for converted M_w (Khan, 2011). Focal depth is randomised ±15% from the original values (Khan, 2011; Kythreoti, 2002). The location of the new earthquakes is placed around the Epicentre Fault Length (EFL) of the past events with an orientation parallel to the strike angle of the main fault (Khan et al., 2010). Fault

rupture characteristics are estimated using Wells and Coppersmith (1994) empirical relationships as shown below:

$$\log(SRL) = -3.22 + 0.69\, M_w \quad 3.1$$

$$\log(RLD) = -2.44 + 0.59\, M_w \quad 3.2$$

$$\log(RW) = -1.01 + 0.32\, M_w \quad 3.3$$

$$\log(RA) = -3.49 + 0.91\, M_w \quad 3.4$$

where,

SRL : surface rupture length

RLD : sub-surface rupture length

RW : rupture width

RA : rupture area

The standard deviations for Equations 3.1, 3.2, 3.3 and 3.4 are 0.22, 0.16, 0.15 and 0.24, respectively. The errors of these empirical equations are incorporated in estimating the fault rupture characteristics, which are required to generate synthetic events.

Khan (2011) uses a constant value of ±25 km along the EFL to define the area for generating new randomised events. However, the characteristics of fault ruptures are not constant and strongly depend on the magnitude of earthquakes (M_w). Instead of using a constant width value, this study utilises the fault rupture width (RW), as defined in Equation 3.3, to determine the area for new synthetic events (Figure 3.1).

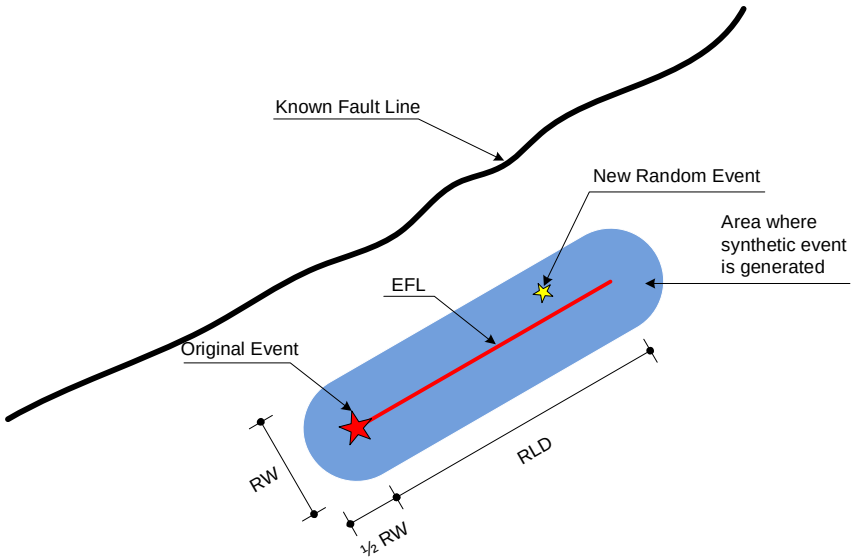

Figure 3.1. Definition of area for generating randomised synthetic events

3.2.2. Integration of Earthquake Recurrence Relationship into the PSHA Module

The stochastic PSHA involves direct simulations of all probable earthquakes in a region to obtain the possible ground motions in the area. The reliability of this approach depends strongly on the characterisation of earthquake rates as well as the number of simulations performed. Khan (2011) used the number of earthquakes in the instrumental catalogue to represent the rate of seismicity of Pakistan. Khan used this approach to avoid using the recurrence relationships in PSHA. As pointed out in Chapter 2, Khan's assumption is valid providing that the earthquake catalogue is complete and the length of the catalogue should at least correspond to one seismic cycle. This issue is highlighted in Chapter 4, section 4.6.

To address this issue, earthquake recurrence relationships are incorporated into the PSHA module to characterise the seismicity of the investigated area. The number of earthquakes for every simulation is determined based on earthquake recurrence relationships. The event number is obtained by multiplying the annual rate of earthquakes (N) with a specified time period (T), as illustrated in Figure 3.2. The time period expresses the length of seismicity considered in the study and should at least correspond to one seismic cycle, which is equivalent to the maximum return period of earthquakes in the area.

In this approach, all events in the earthquake catalogue are categorised into several magnitude ranges ($0 \leq M_w < 6$, $6 \leq M_w < 6.5$, $6.5 \leq M_w < 7$, $7 \leq M_w < 7.5$, $7.5 \leq M_w < 8$, $8 \leq M_w < 8.5$, $M_w \geq 8.5$). The number of events for each magnitude range is calculated using Equation 3.5, and this procedure is performed for all seismic zones, as discussed in Section 4.3. The synthetic events are generated based on the event number $\left(N_{M-(M+\Delta M)}\right)$, the number of simulations performed, varying rate (see Section 3.2.3) as well as the number of events in the existing catalogue. The original and synthetic earthquake catalogues are then merged to create an earthquake database for the area. A randomised earthquake catalogue is generated for each simulation considered in the analysis by randomly selecting the events in the database according to the number of events obtained from the recurrence relationship $\left(N_{M-(M+\Delta M)}\right)$.

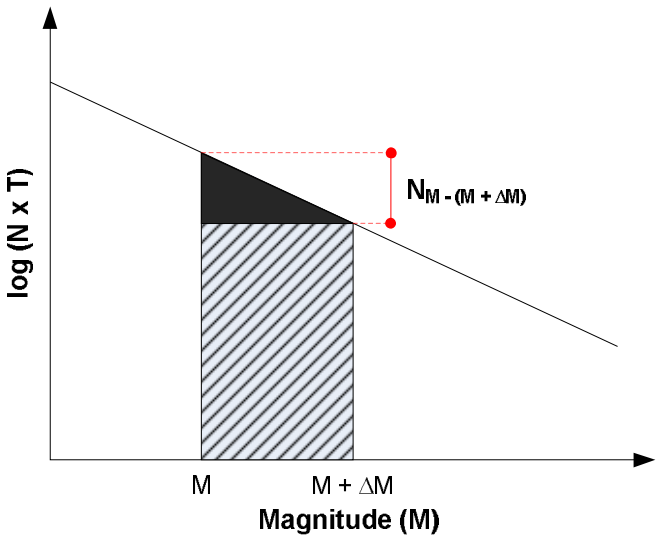

Figure 3.2. Calculation of earthquake occurrence for a magnitude range using the Gutenberg-Richter recurrence relationship

$$N_{M-(M+\Delta M)} = N_M - N_{M+\Delta M} \quad 3.5$$

where,

$N_{M-(M+\Delta M)}$: the total number of events for a magnitude range $(M \leq M_w < (M+\Delta M))$ in a seismic zone

N_M : the cumulative number of events for $M_w \geq M$

$N_{M+\Delta M}$: the cumulative number of events for $M_w \geq (M+\Delta M)$

3.2.3. Modulation of Seismicity Rate

An empirical model proposed by Reasenberg et al. (2003) is adopted to include time dependency in the PSHA module. This approach is a time-varying Poisson model, which allows a non-stationary seismicity rate (Matthews and Reasenberg, 1988; Reasenberg et al., 2003). It is assumed that a seismicity rate follows a regional earthquake cycle, which corresponds to the recurrences of the largest earthquake in a region (WGCEP, 2003). A time-varying function $\gamma(t)$ is applied to modulate the average long-term rate as discussed in Chapter 2. The varying rate is calculated using Equation 2.28.

This approach employs the Gutenberg-Richter distribution $(\log N = a - b.M_w)$ to obtain the long term rate of seismicity for each region or fault segment. The initial stage involves estimating the *"b"* value of the recurrence relationship using the

instrumental catalogue with a magnitude range and time period for which the catalogue is complete. It is assumed that this "b" value is constant over time. The variability of seismicity rate is then taken into account by assigning "a" as a free parameter (Reasenberg et al., 2003). Therefore, the value of "a" is adjusted to fit the seismicity for a specified period, as illustrated in Figure 3.3.

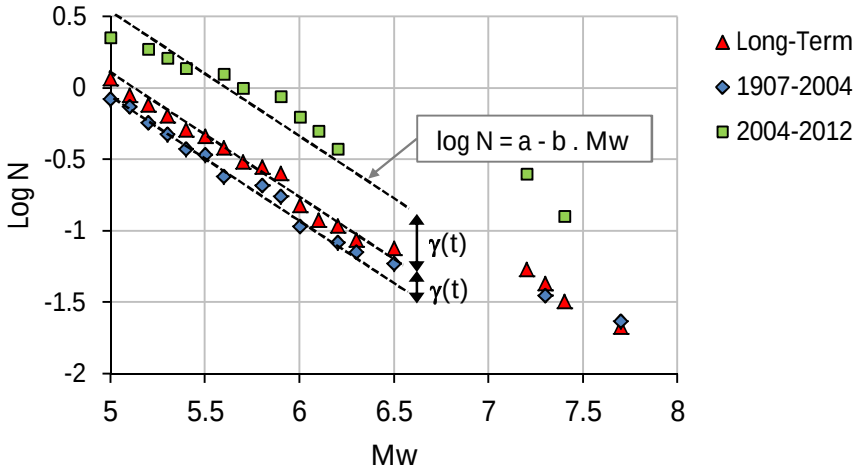

Figure 3.3. Recurrence relationship for the Sumatra Subduction Zone with different periods of time

The figure compares the average seismicity for different periods in the Sumatra Subduction Zone (SSZ). The period 1907-2004 gives the average seismicity before the M_w 9.1 mega-thrust earthquake, which is lower than the long term rate. The period 2004-2012 implies that the seismicity after the event increases significantly, up to 5 times that of the long term rate. The varying rate $\gamma(t)$ of the SSZ since 1963 is plotted in Figure 3.4. The value of $\gamma(t)$ is obtained by using the annual frequency of earthquakes in the magnitude range of 4.0-5.5. The magnitude range is selected to consider that the earthquakes in that interval occur more frequently; thus, the data is sufficiently available. The annual rate for different magnitude ranges can also be estimated based on $\gamma(t)$ and the Gutenberg-Richter distribution with fixed "b" value.

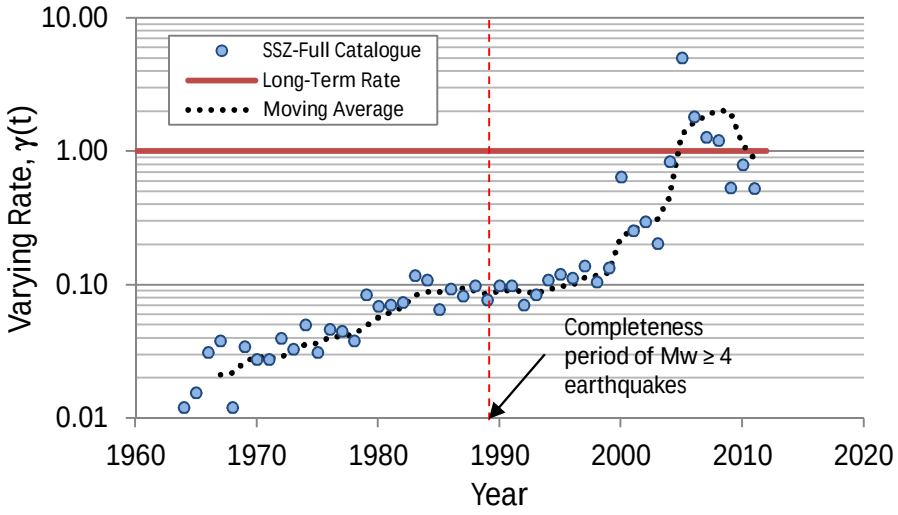

Figure 3.4. The varying rate of the Sumatra Subduction Zone

In addition, the $\gamma(t)$ function can be extrapolated with time to estimate the seismicity in the near future (t_{est}), as suggested by Reasenberg et al. (2003). The extrapolated varying rate of Sumatra for the next 5 years can be found in Table 5.3. Once the varying rate is obtained, the long term recurrence function can be modulated for a time dependent PSHA by multiplying the $N_{M-(M+\Delta M)}$ value with $\gamma(t)$. It should be pointed out that assigning the $\gamma(t)$ value as "1" indicates a time independent hazard assessment.

3.2.4. The Procedure of PSHA Module

The PSHA module requires some input data including earthquake catalogue, soil parameters, geographic information, seismic zones, seismicity rates and the number of events for each magnitude range (see Table 3.1). The initial procedure begins with screening the earthquake catalogue to remove any events that produce PGA less than the minimum PGA threshold. This step is addressed to remove unnecessary events (e.g. low magnitude earthquakes with long distance to the investigated site), which can prolong the duration of the analysis. The screened catalogue is also useful to determine the minimum threshold of the earthquake magnitude considered in the analysis.

Table 3.1. Input data required for the PSHA module

Input Data	Input Files[1]	Description
Study Area	Area.shp	Polygon shapefile of the investigated area that consists of Area Units (AUs)
Earthquake Catalogue	InstCatA.csv	Combination of historical and instrumental catalogues that contains earthquake information including date, time, location, focal depth and magnitude (Mw)
Soil Information	UCSoil.csv	Soil type information for each AU
Geographical Information	UCGeo.csv	Geographical information for each AU
Seismic Zones	SZones.csv	Tectonic information (strike angle, fault mechanism) and the boundary definition for each seismic zone
Recurrence Relationship	EqRec.csv	The number of earthquakes for each magnitude range and each seismic zones for T period of time $\left(N_{M-(M+\Delta M)}\right)$.
Hazard Rate $\boldsymbol{\gamma(t)}$	ZonRate.csv	Hazard rate for each magnitude range and each seismic zones for a particular period of time (t_{est}).

The next stage involves categorising the screened events into a magnitude range and seismic zone, which are defined in Section 5.2 and Section 4.3, respectively. These categorised events are utilised to generate synthetic earthquakes in the investigated area. The number of synthetic events is computed based on the total number of events $\left(N_{M-(M+\Delta M)}\right)$, varying rate $\gamma(t)$, the number of simulations (S) as well as the number of events in the existing catalogue. The synthetic events are generated within a defined area, as shown in Figure 3.1, and then merged with the categorised events to create an earthquake database. This database corresponds to (T x S) years of earthquake catalogue.

Subsequently, randomised earthquake catalogues for each simulation is produced by randomly selecting the events in the earthquake database to the number of events in the recurrence relationship multiplied by the varying rate $\left(N_{M-(M+\Delta M)} \cdot \gamma(t)\right)$. For a time dependent PSHA, a time dependency factor $\gamma(t)$ is applied to modulate the seismicity for a particular time (t_{est}). However, the value of $\gamma(t)$ can also be assigned as "1" for a time independent PSHA.

The last stage of the PSHA module requires the estimation of earthquake ground accelerations (PGA) for all events in the randomised earthquake catalogues. The

[1] Suffix '.csv' denotes comma separated file and 'shp' denotes a shapefile of GIS program.

PGA is calculated using ground attenuation relationships, which are selected based on tectonic environments in the case study area. The PGA calculations are performed for every Area Unit (AU) in the examined area. The flowchart of the PSHA module can be seen in Figure 3.5.

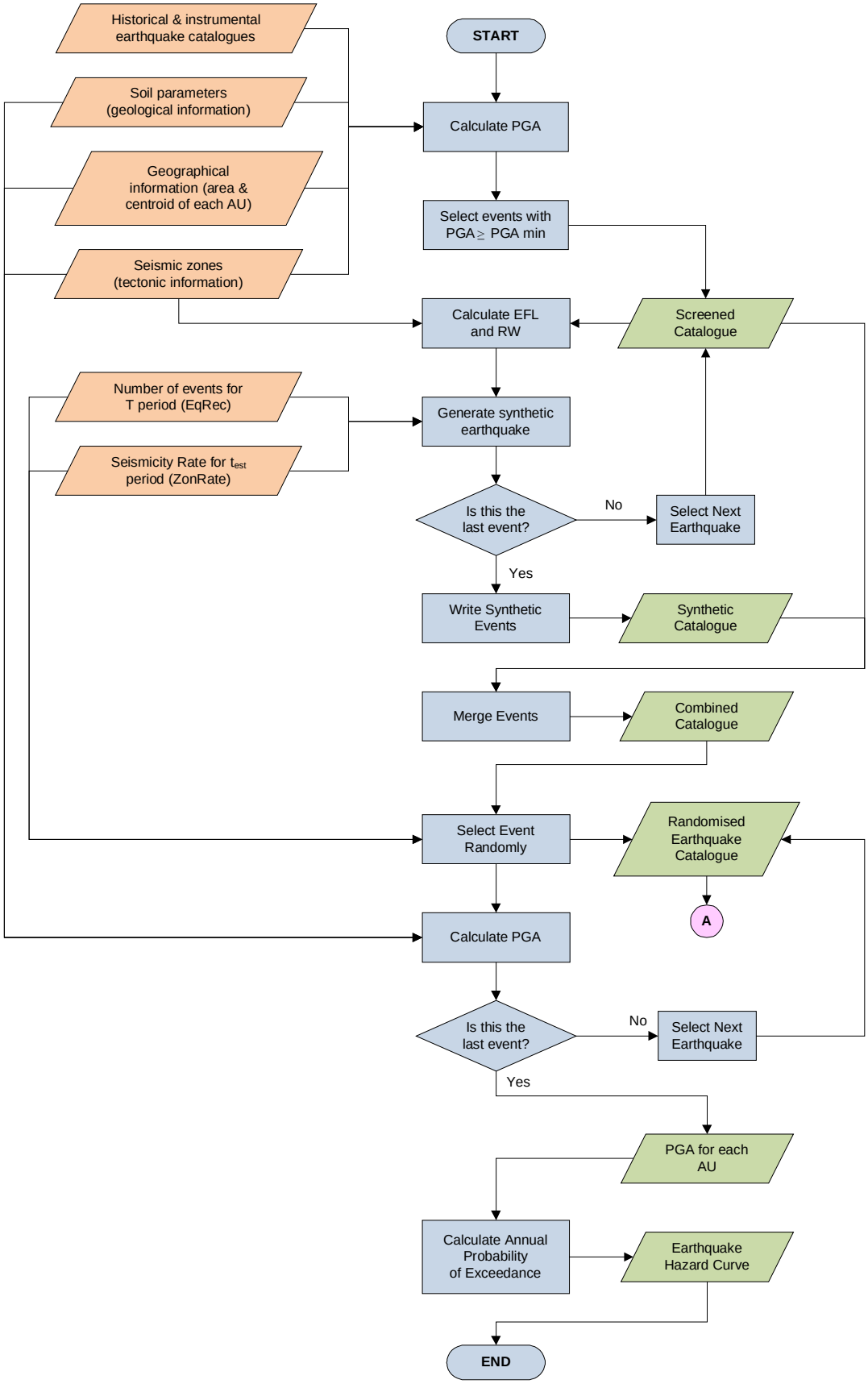

Figure 3.5. Flow chart for the PSHA module

3.2.5. Development of a Hazard Curve

The hazard curve is useful to show the distribution of ground motions for a particular period of time in an area. The hazard curve allows the flexibility to select the level of hazard to be used for many applications, including determining seismic performance objectives for structural designs (e.g. 10% and 2% probability of exceedance in 50 years that correspond to 475 and 2500 years of earthquake return periods, respectively) as well as mitigation strategies. The proposed PSHA method requires a relatively straightforward technique for developing the hazard curve; however, this is not done in the previous version of the ERA Framework. The previous version of the ERA Framework mainly produces a seismic hazard map for a particular probability of exceedance in a given exposure time. Hence, the PGA values associated with other exceedance probabilities (or return periods) are not computed and the hazard curve is not drawn. The hazard curve involves the calculation of annual frequency for each value of PGA for each Area Unit (AU), as described in Equation 3.6.

$$n_{PGA-Annual} = \frac{n_{PGA-T}}{T \cdot S} \qquad 3.6$$

where,

$n_{PGA-Annual}$: the annual frequency of occurrence of a particular PGA.

n_{PGA-T} : the frequency of occurrence of a particular PGA for T period of time.

T : the length of seismicity considered in the study

S : the number of simulations performed in the analysis

The cumulative distribution of the PGA (N) can be obtained by cumulatively summing up the annual frequency of PGA values $(n_{PGA-Annual})$ in descending order. The return period of the earthquake, which produces the PGA value, can be determined from the cumulative annual frequency using the relationship $T_r = 1/n_{PGA-Annual}$. The correlation between PGA and the associated return period denotes the rate of hazard as show in Figure 3.6(a). The time interval of this Poisson process follows an exponential distribution with a cumulative distribution function (CDF) as shown in Equation 3.7. The equation indicates earthquake probability of exceedance that corresponds to a particular exposure period, which is required to develop a hazard curve as shown in Figure 3.6(b).

$$P(PGA \geq PGA_i) = 1 - e^{-t/T_r} \quad 3.7$$

where,

$P(PGA \geq PGA_i)$: the probability that PGA will be greater than or equal to PGA_i in the next t years (the probability of exceedance)

t : exposure time

T_r : the return period of PGA_i

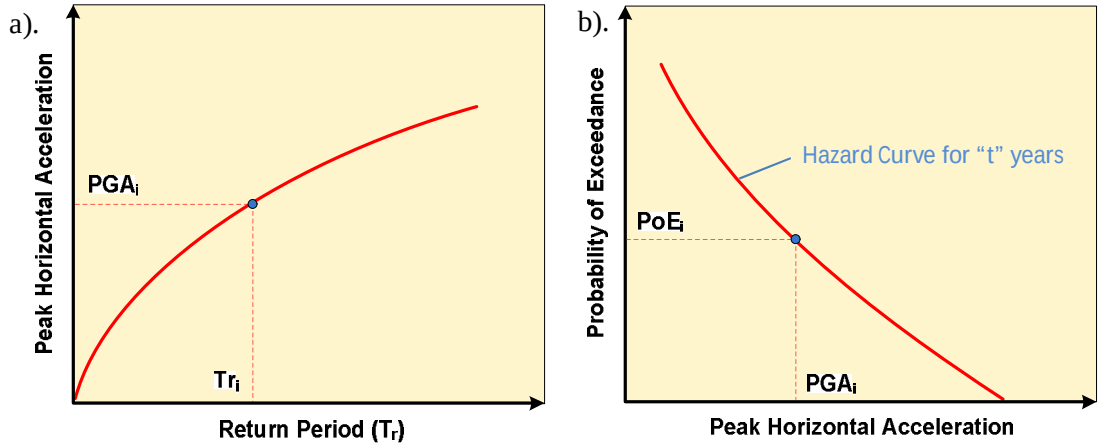

Figure 3.6. Determination of hazard curve based on the outcomes of PSHA: a). the rate of hazard; b). hazard curve

3.3. PROBABILISTIC TSUNAMI HAZARD ASSESSMENT (PTHA)

Tsunami hazard assessment in this study is an extension of the PSHA discussed in the previous chapter. The method is based on a stochastic approach and combines a few methodologies from previous studies (Abe, 1995; Khan, 2011; Musson, 2000). Tsunami numerical analysis is performed to complete tsunami data that is lacking for Sumatra. The numerical analysis simulates tsunami propagation to coastal areas to obtain tsunami heights. Tsunami numerical analysis is conducted using NAMI-DANCE software (Zaytsev et al., 2002). The simulations are carried out for significant tsunami events in the tsunami catalogue of Sumatra (BMKG, 2010; Gusiakov, 2001; NOAA, 2011). Some synthetic events are also included in the analysis to complement the data.

It is assumed that earthquake epicentres for each tsunami model are located in the middle of a fault rupture line. Although the directivity and the propagation of fault rupture from earthquake epicentres are unknown and varied, this assumption is fairly reasonable for this study. It is found from the preliminary numerical analysis that earthquakes with a magnitude below 7 trigger very small tsunami; thus, the tsunami heights are likely to be negligible. Therefore, the earthquake magnitude range considered in the analysis is between M_w 7.0 and M_w 9.1. Detailed information of the tsunami models can be found in Appendix B and the corresponding fault ruptures are plotted in Figure 3.7.

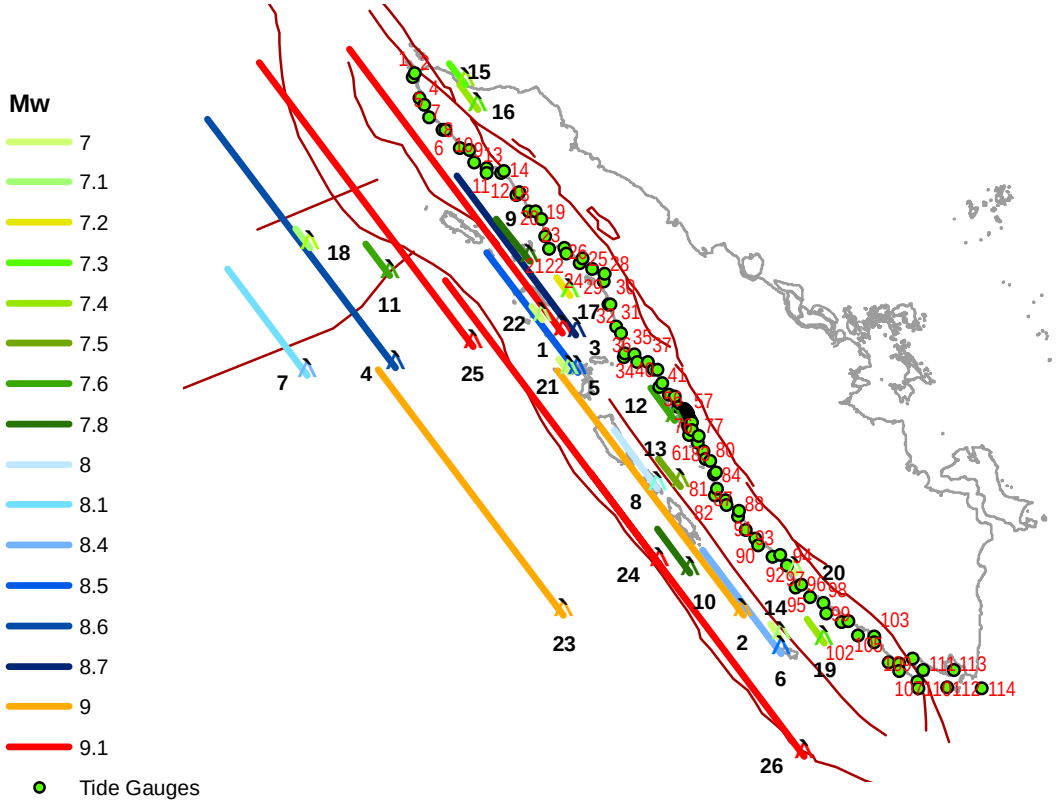

Figure 3.7. The fault ruptures of the tsunami models for Sumatra

3.3.1. Estimation of Tsunami Run-Up Heights for Sumatra

The outcomes of tsunami numerical simulations are examined to study the relationship among earthquake moment magnitudes (M_w), closest distances and tsunami wave heights at the case study area. This method was introduced by Abe (1995, 1985, and 1981), as discussed in Chapter 2 Section 2.4.3. However, Abe's approach requires past tsunami data recorded by tide stations installed at an

investigated area, which are not available for Sumatra. Therefore, instead of using past tide gauge records of tsunamis, this study utilises tsunami wave heights obtained from the tsunami numerical analyses. The initial form of Abe's equation (see Equation 2.34) is used to correlate earthquake magnitude with various distances and tsunami wave heights.

Abe (1981, 1995) assumes that the "R" variable in Equation 2.34 is the distance from earthquake epicentre to the tide stations along the shortest oceanic path, due to the uncertainty in tsunami sources in past events. In this study, the tsunami source for each simulation is defined for each tsunami numerical model; hence, the closest distance from tsunami source to tide station can be obtained.

The constant *"a"* in Equation 2.34 represents the attenuation of tsunami wave amplitude with distance. The value is obtained through a linear least square regression analysis of *log (H)* and *log (R)* dataset. Once the *"a"* value is found, the constant "D" can be calculated by equating M_t with M_w as follows:

$$D = M_w - \log(H) - \log(R) \tag{3.8}$$

The relationship between earthquake moment magnitude and tsunami parameters is necessary for quick estimation of tsunami heights in this study. This is the simplest method for determining the heights of all probable tsunamis in a tsunami framework. The integration of tsunami numerical analysis into the tsunami framework is hard to achieve in this study for several reasons. First, most tsunami numerical analyses are based on a finite difference method to solve the long wave equation of tsunami. The analysis basically requires a 3D model to take into account many components, including the deformation of a tsunami source as well as the bathymetry of the sea. As a result, the analysis requires extensive calculation for each tsunami simulation; therefore, it is not suitable for the stochastic technique adopted in this study. Second, tsunami numerical simulation is time consuming. Thus, simulating the thousands of probable tsunamis in this study is not time efficient and is computationally expensive.

3.3.2. The Rate of Tsunami for Each Magnitude of Earthquakes

In this study, the rate of tsunami for each magnitude of earthquakes is examined. The tsunami rate basically represents the ratio between the number of tsunamigenic

events and the number of all earthquakes for every earthquake magnitude. This ratio is required to estimate the proportion of tsunamigenic events in the randomised earthquake catalogue, which is generated from the PSHA framework. The rate of tsunami for Sumatra is shown in Figure 3.8. The correlation in Figure 3.8 is developed from thrust fault events at the Sumatra Subduction Zone (SSZ), which is the main source of tsunami in the region. Figure 3.8 also shows that lower earthquake magnitudes would have lower tsunami rate and the rate would linearly increase up to M_w 7.5. The tsunami rate remains constant afterwards.

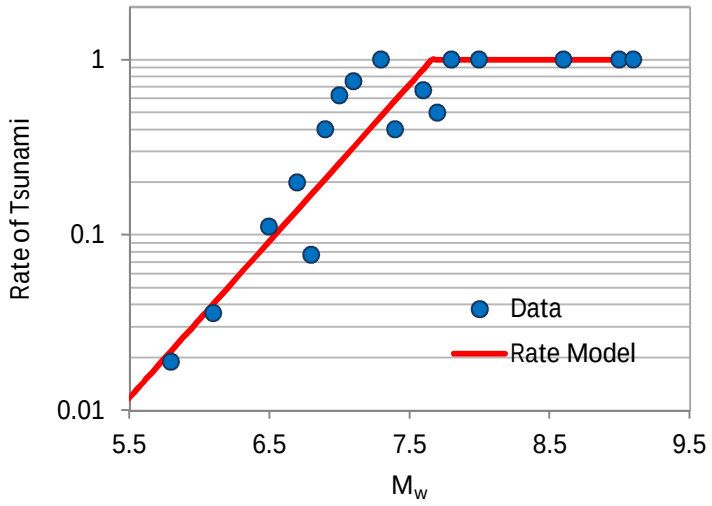

Figure 3.8. Probability of tsunami occurrence in terms of the moment magnitude of earthquake (M_w) based on the tsunami catalogue of Sumatra

3.3.3. The Procedure of PTHA Module

The tsunami module requires some additional input data, including tide gauge locations and tsunami rate, as shown in Table 3.2. The tide gauge data specify the points where the tsunami hazard would be assessed and should be placed onshore. The tsunami rate represents the proportion of tsunamigenic events from the total events occurring in the SSZ for each magnitude range of earthquakes. Hence, the number of tsunamigenic events can be estimated simply by multiplying the tsunami rate with the number of events in the earthquake catalogue for each magnitude range.

Table 3.2. Input data required for the PTHA module

Input Data	**Input Files**[2]	**Description**
Tide gauges	TideGauges.csv	The coordinates (longitude and latitude) of tide gauges in an investigated area
Tsunami Rate	TRate.csv	The rate of tsunami for each magnitude range and each seismic zone
Random Catalogue	Cat####.csv	Randomised earthquake catalogue from "RandCat" folder

The procedure of the PTHA module is shown in Figure 3.9. It starts with selecting the potentially tsunamigenic events as explained below from the randomised earthquake catalogue (previously generated in the PSHA module). The tsunamigenic events are then stored in a tsunami catalogue. It is observed from the data (Figure 4.2.3) that 90% of tsunamis in Sumatra are triggered by thrust fault earthquakes in the Sumatra subduction zone, with a focal depth of $\leq$ 80 km and an earthquake magnitude of $M_w \geq 6.5$. Therefore, the tsunamigenic earthquakes in this study are selected based on these criteria. Moreover, the PTHA method proposed in this study is only applicable to ordinary tsunamigenic earthquakes. The anomalous tsunami earthquakes, as defined in Section 2.4.3, are beyond the scope of this study.

The events in the tsunami catalogue are selected randomly from the number of tsunamis estimated from the tsunami rate, which is saved into Randomised Tsunami Catalogue. The tsunami heights for each randomised event are then calculated using Equation 2.34 for every location of tide gauges. Hence, the tsunami height at each tide gauge for a defined return period can be determined using a similar procedure used in PSHA (see Section 3.2.5). Following the same procedure, the tsunami hazard curve for the region can also be obtained.

[2] Suffix '.csv' denotes comma separated file.

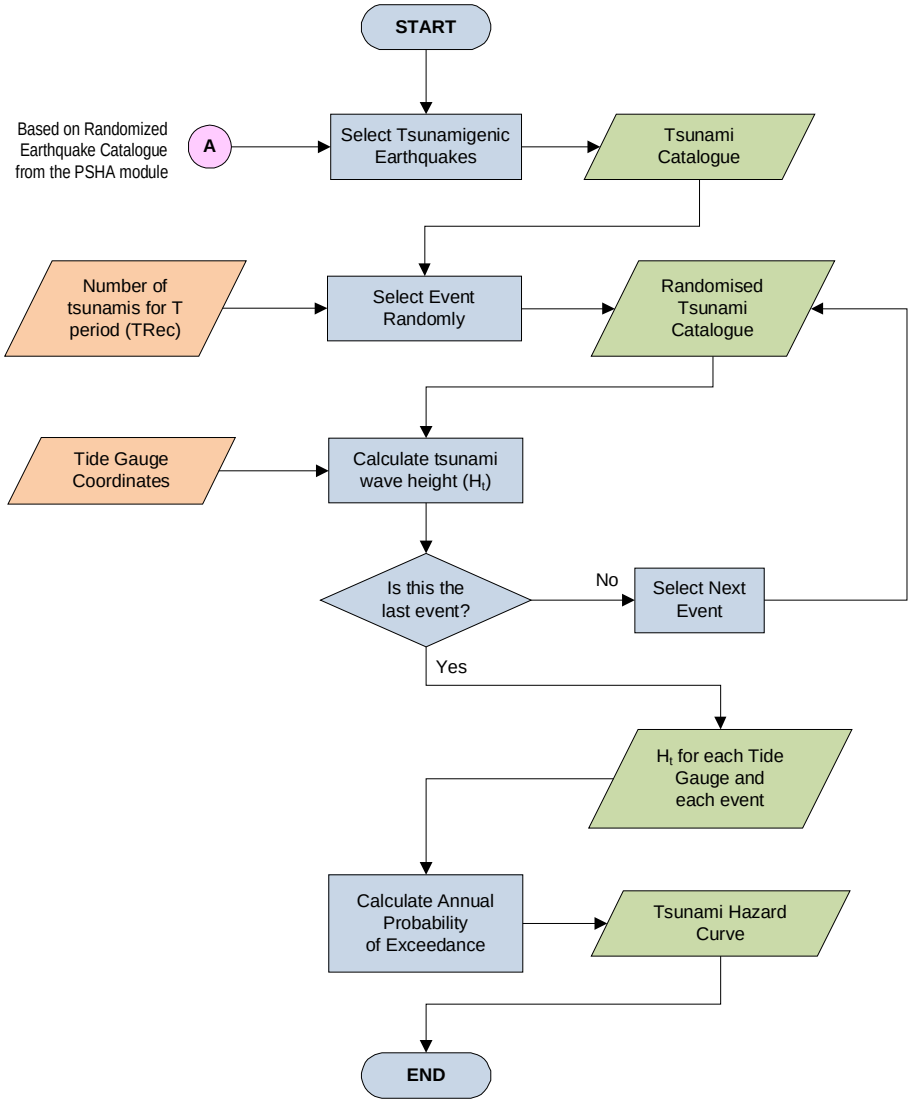

Figure 3.9. Procedure for Probabilistic Tsunami Hazard Assessment (PTHA)

3.4. EARTHQUAKE AND TSUNAMI RISK ASSESSMENT FRAMEWORK

3.4.1. The Selection of Vulnerability Functions for the Building Stock in Padang

To determine the earthquake and tsunami risk, vulnerability curves for each type of structures in Padang are required. The vulnerability curves correlate the expected ground motions (or tsunami heights) with the mean damage ratio of the existing building stock in the region. For earthquake risk, this study adopts vulnerability curves proposed by GESI (2001), since GESI provides flexibility in selecting the class of construction in terms of design, quality and material. In addition, the GESI

project includes data from many countries including Indonesia. The assignment of vulnerability curves to represent building stock in Padang is discussed in Appendix E, and the chosen vulnerability curves are shown in Figure 3.10. Vulnerability curves for improved seismic performance to the level of modern seismic design standard are shown in Figure 3.11. GESI vulnerability curves comprise 4 damage states, which are defined in Table 3.3.

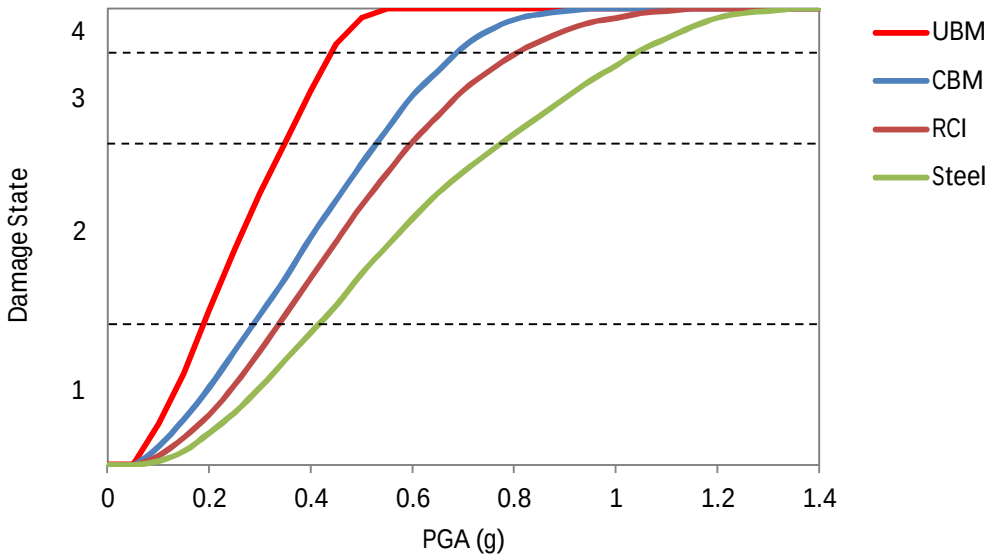

Figure 3.10. Correlation between ground acceleration and damage state for existing building stock in Padang (GESI, 2001)

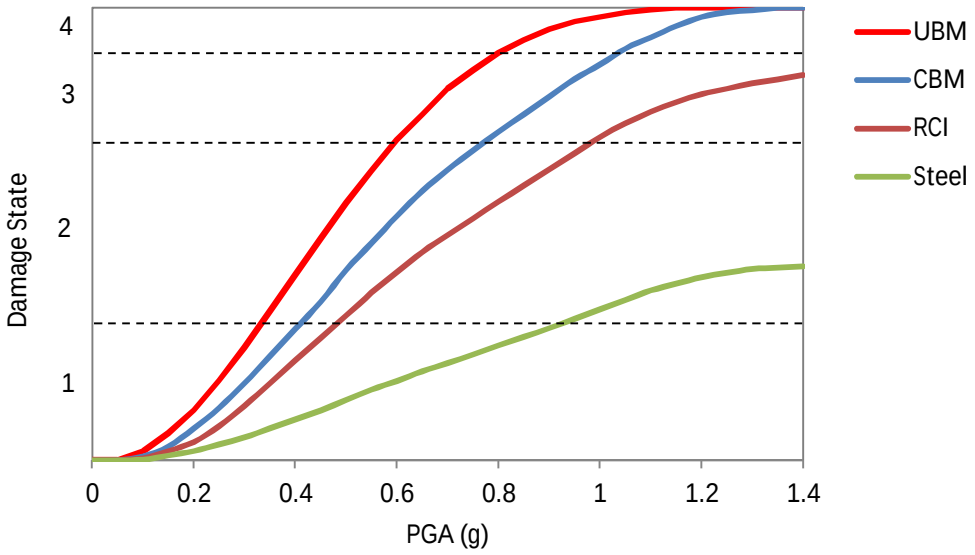

Figure 3.11. Correlation between ground acceleration and average damage state for seismically strengthened structures in Padang (GESI, 2001)

Table 3.3. GESI building damage states (GESI, 2001)

Damage State	Description
None, slight or moderate	Ranging from no damage to non-structural damage and minor structural damage.
Extensive	Extensive structural and non-structural damage. Localised life-threatening situations are common.
Partial collapse	Building is entirely structurally compromised and on the verge of collapse or small portion of the building has collapsed.
Complete collapse	Building is entirely destroyed, with significant portions of the building collapsed.

In addition, vulnerability curves developed by Kyriakides (2007) for reinforced concrete structures are also utilised in this study. It is assumed that Kyriakides's low pre-seismic and modern seismic RC structures comply with the existing and seismic designed buildings in Padang. Kyriakides's vulnerability curves in comparison with those of GESI (2001) are shown in Figure 3.12.

Table 3.4 shows the estimated mean damage ratio (MDR) of existing RCI buildings in Padang subjected to M_w 7.6 earthquake occurring in the area. The event produced a MDR of 18% in the area. The vulnerability curves proposed by GESI (2001) and Kyriakides (2007) for reinforced concrete structures appear to be comparable with the value of this empirical MDR, as seen in Figure 3.12, and therefore, are suitable for this study.

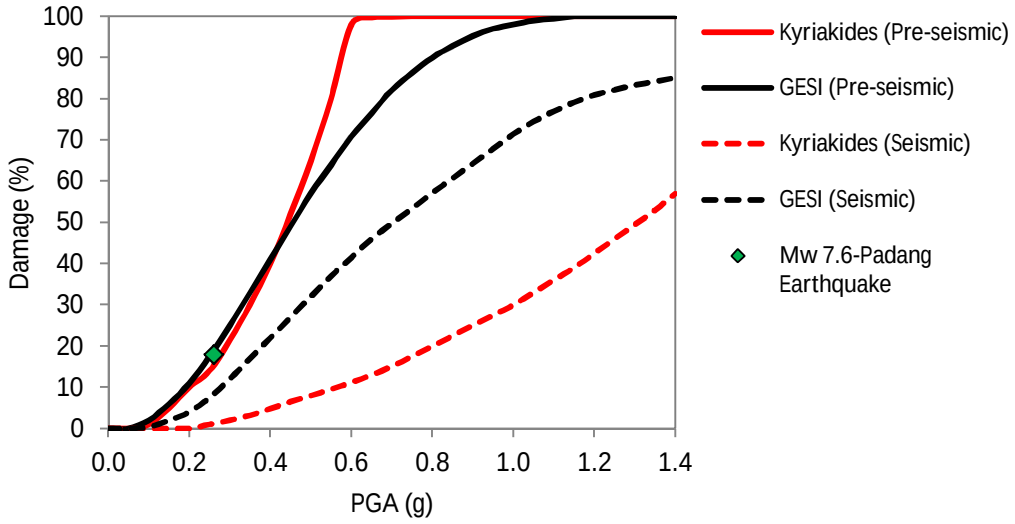

Figure 3.12. The comparison of GESI (2001) and Kyriakides (2007) vulnerability functions with the empirical MDR for reinforced concrete buildings in Padang

Table 3.4. The estimation of mean damage ratio for RCI buildings in Padang based on the damage data of the M_w 7.6 earthquake

Damage State (DS)	Central Damage Ratio (CDR) % - HAZUS (1999)	Probability of DS (PGA 0.26g at Padang city)
None	0	0.606
Light	20	0.173
Moderate	55	0.125
Extensive	80	0.096
	MDR =	**0.180**

For tsunami hazard assessment, the vulnerability curves proposed by (Tinti et al., 2011) are used. The vulnerability curves were developed as part of the SCHEMA project (a consortium of 11 organisations in the European Union, Turkey and Morocco) aiming to build up tsunami hazard, vulnerability and impact damage maps for Europe and Mediterranean. The project used post tsunami data from Banda Aceh (Sumatra, Indonesia) after the Indian Ocean tsunami in 2004 (Valencia et al., 2011). Therefore, the vulnerability curves are perfectly applicable for this study. The adopted vulnerability curves are shown in Figure 3.13. No data exist for improved structures. However, it is accepted that the forces from ground motion (PGA) and tsunami at height (H_t) have similar effects on structures. Vulnerability curves for the seismically strengthened structures can be developed by using the ratios from Figure 3.10 and Figure 3.11. These curves are seen in Figure 3.14 and the description for each damage scale is shown in Table 3.5.

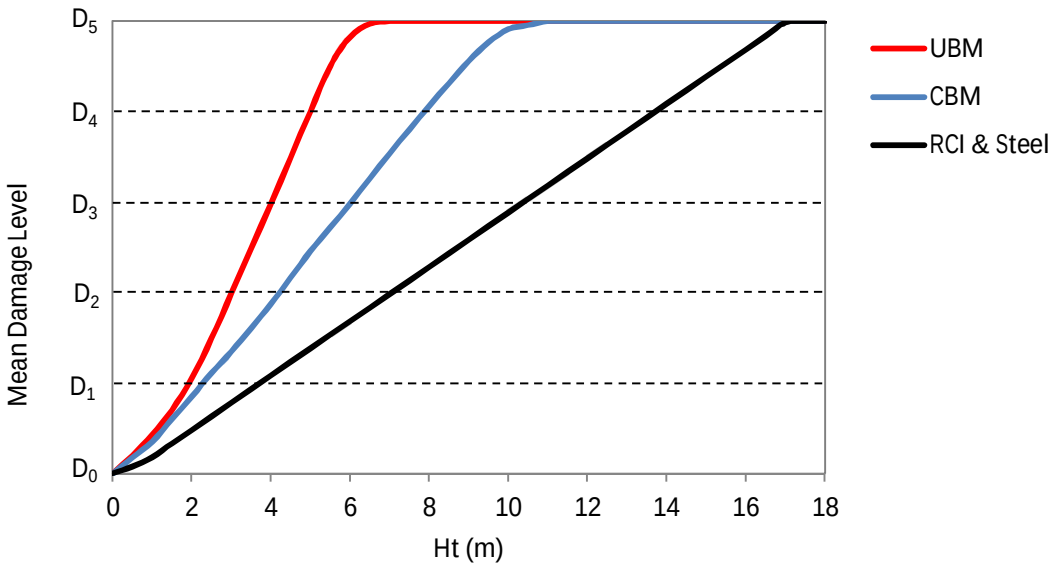

Figure 3.13. Correlation between tsunami height and mean damage level for existing building stock in Padang (Tinti et al., 2011)

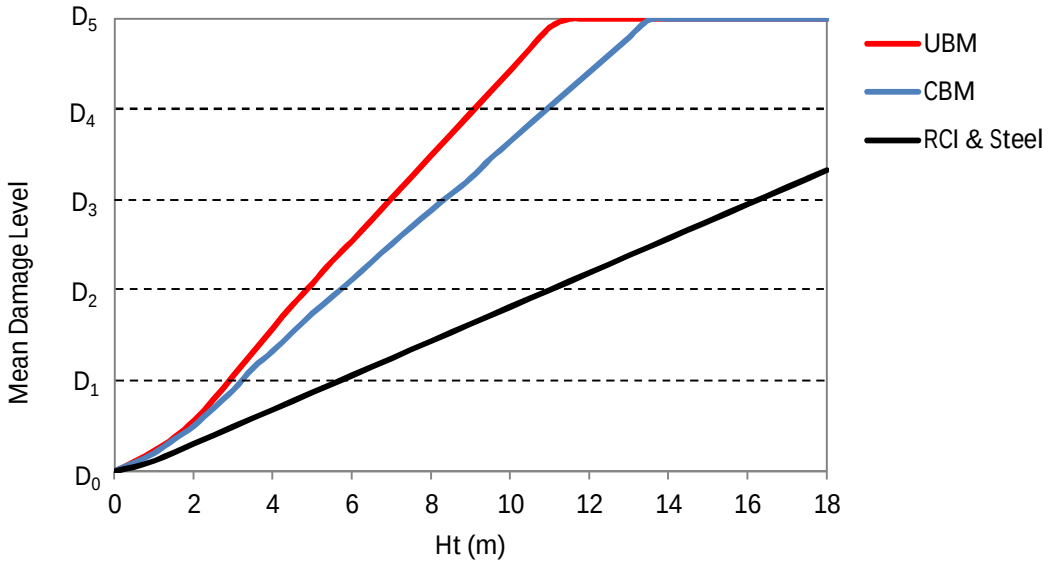

Figure 3.14. Correlation between tsunami height and mean damage level for seismically strengthened structures in Padang

Table 3.5. Damage levels for buildings (Tinti et al., 2011)

Damage Level	Damage on Structure	Use as shelter/ post crisis use	Detection by Earth observation
D0 No damage	No significant damage	Shelter/ immediate occupancy	No sign of damage visible on building and surrounding environment. The absence of damage cannot be proved only through space imagery.
D1 Light damage	No structural damage - minor damage, repairable: *chipping of plaster, minor visible cracking, damage to windows, doors.*	Shelter / immediate occupancy	Barely visible
D2 Important damage	Important damage, but no structural damage: *out-of-plane failure or collapse of parts of wall sections or panels without compromising structural integrity, leaving foundations partly exposed.*	Evacuation / Unsuitable for immediate occupancy, but suitable after repair	Damage on roof hardly visible. Other damage not visible.
D3 Heavy damage	Structural damage that could affect the building stability: *out-of-plane failure or collapse of masonry, partial collapse of floors, excessive scouring and collapse of sections of structure due to settlement.*	Evacuation / Demolition required since unsuitable for occupancy	Not or hardly visible if roofs have not been removed
D4 Partial failure	Heavy damages compromising structural integrity, partial collapse of the building	Evacuation / Complete demolition required	Visible
D5 Collapse	Complete collapse: *foundations and floor slabs visible and exposed.*	Evacuation	Very visible

3.4.2. The Procedure Adopted in the Earthquake and Tsunami Risk Assessment Module

The main outcomes of the risk assessment module are loss and casualty estimation. The loss estimation requires building inventory, vulnerability curves and the estimated ground motion parameter corresponding to a particular period of time. The prediction of casualty involves death and injury rate functions, building inventory, as well as population data (Khan, 2011). In this case, the population data must at least contain the rate of occupancy at any time in the investigated area. This information is not available for the case study region. Hence, the risk assessment module in this

study only includes the loss estimation for building damage subjected to earthquake and tsunami hazards.

The risk assessment takes into account the annual frequency of exceedance for all events, which are generated in the PSHA and PTHA modules. It should be noted that this study only takes into account mean damage ratio (MDR) ≥ 2%, which represents the minimum threshold of damage covered by earthquake insurance (Deniz, 2006).

3.4.2.1. Probabilistic Earthquake Risk Assessment

The procedure of earthquake risk assessment begins with reading the building inventory data for each area unit (AU), as given in Appendix C. In this case study, the data contain only the area of buildings for each building category in the region. Hazard data files for all AUs calculated in the PSHA module are incorporated into the risk assessment module. The hazard data files summarise the outcomes of PSHA in terms of PGA and its return period (T) and arrange them in a descending order. Therefore, it is more convenient, for computation, to utilise the hazard curves instead of reading the raw data from the PSHA module. Afterwards, the annual frequency of exceedance (AFE) associated with a particular PGA is calculated from its return period (AFE = 1/T). Then, the corresponding mean damage ratio (MDR) for each building category is obtained from the vulnerability curves. The annual MDR at a certain level of ground motion can be obtained simply by multiplying the annual rate of occurrence (computed from AFE) with the MDR. The summation of the annual MDR for all events represents the total annual MDR for the area unit. The multiplication of building inventory data, building value and the total annual MDR produces the annual losses for each building category in the area unit. The input data for the earthquake risk module are shown in Table 3.6, whilst the flowchart of the earthquake risk module is shown in Figure 3.15.

Table 3.6. Input data for the earthquake risk assessment module

Input Data	**Input Files**[3]	**Description**
Building inventory	UCInv.csv	Building inventory data for each type of structure in every AU
Earthquake Hazard Data Files	HazCur####.csv	Ground motion rate (PGA vs. its return period) for every AU
Earthquake vulnerability curves	VULCUR.csv	Earthquake vulnerability curves for every typology of structures

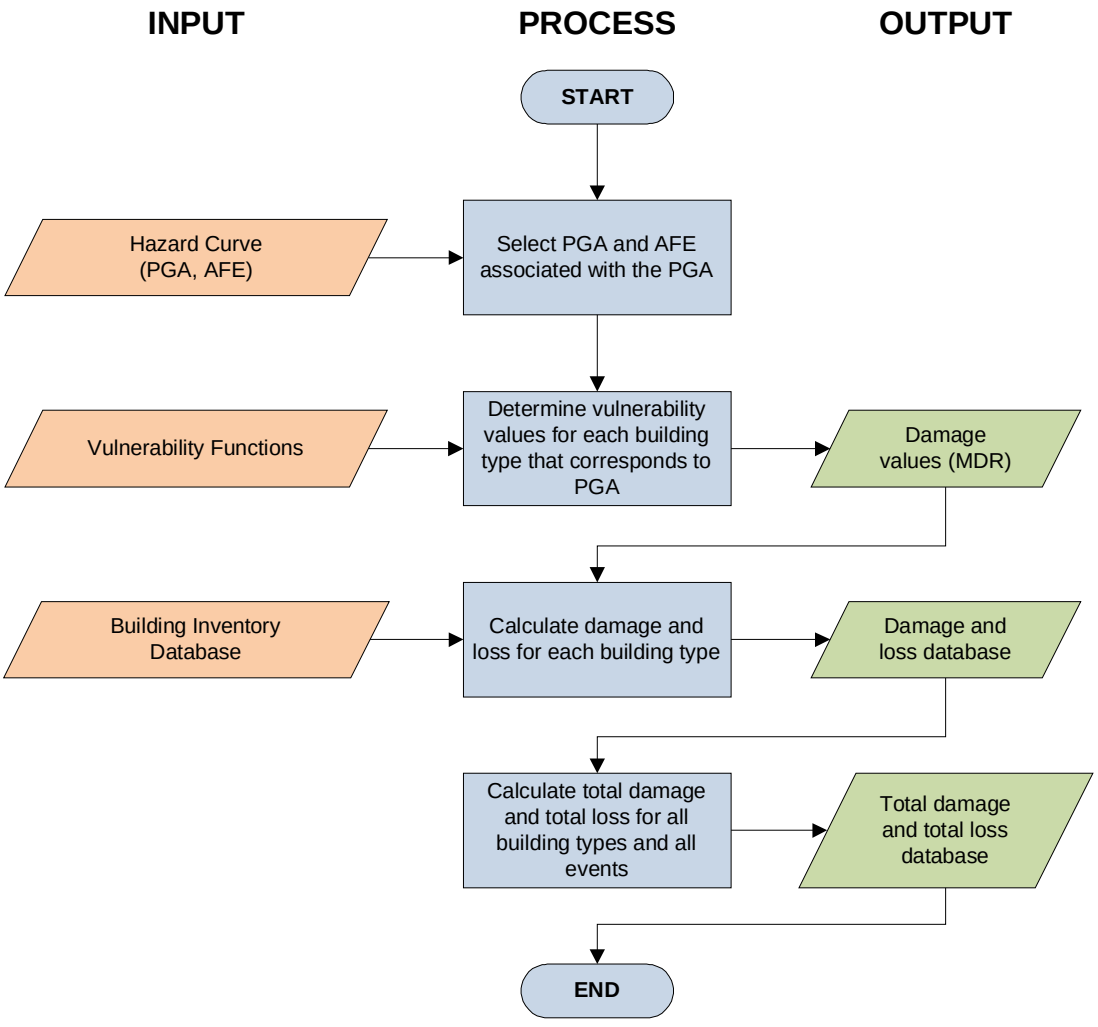

Figure 3.15. Flow chart of the earthquake risk module

[3] Suffix '.csv' denotes comma separated file.

3.4.2.2. Probabilistic Tsunami Risk Assessment

A similar method to the earthquake risk module is applied to estimate tsunami risk. However, instead of using ground motion response (PGA), tsunami risk calculation involves tsunami height (H_t) as the parameter to determine the level of damage. The tsunami heights are the main outcome of the PTHA module. In addition, ground elevation information for each area unit is required to determine the maximum water height above the base of structure (h_{max}). The structural damage for each building category is predicted using tsunami vulnerability curves proposed by (Tinti et al., 2011). The tsunami vulnerability functions correlate h_{max} with MDR; and hence, the damage value can be predicted. The input data for the tsunami risk module are shown in Table 3.7 and the flowchart is shown in Figure 3.16.

Table 3.7. Input data for tsunami risk assessment module

Input Data	Input Files[4]	Description
Building inventory	UCInv.csv	Building inventory data for each type of structure in every AU
Tsunami Hazard Data Files	HazCur####.csv	The rate of tsunami height in the area
Tsunami vulnerability curves	VULCUR-Tsu.csv	Tsunami vulnerability curves for every typology of structures
Elevation data	UCElv.csv	Elevation information at the centroid of each AU

[4] Suffix '.csv' denotes comma separated file.

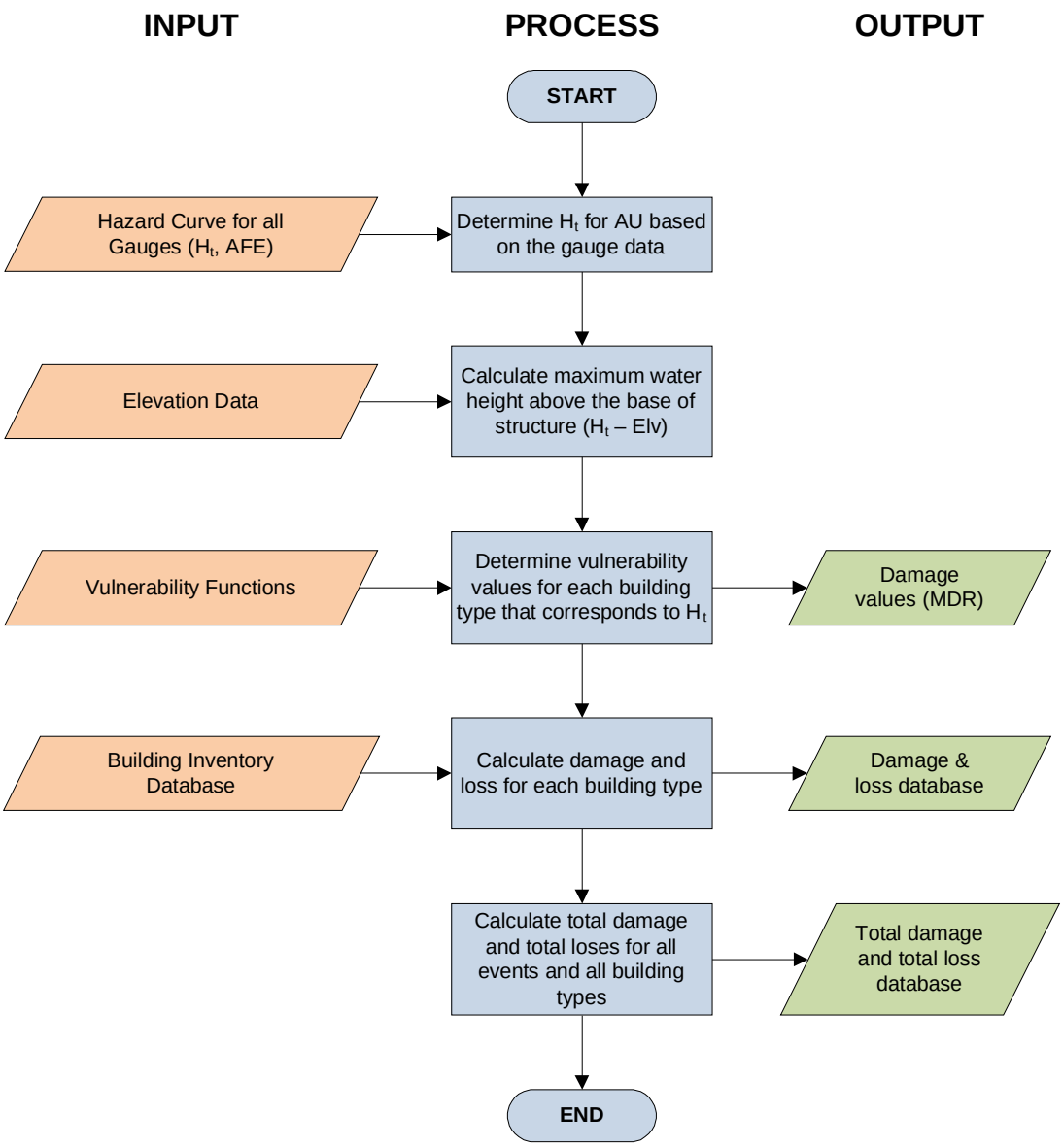

Figure 3.16. Flowchart of the tsunami risk module

3.5. SUMMARY

- An earthquake risk assessment framework (ERA Framework), developed at the University of Sheffield, is extended to take tsunami hazard and time dependent hazard assessment into account. The framework consists of three main tasks, PSHA module, PTHA module and risk module. These modules are developed based on stochastic approach with readily available seismological information.
- For the PSHA module, a method is developed to extend the existing earthquake catalogue by generating synthetic events. The synthetic events are produced using a method by Khan (2011). However, this study also integrates earthquake recurrence relationships, as proposed by Musson (2000), to characterise seismicity. In addition, a method to include a time dependent approach for hazard assessment is proposed to consider the non-stationary rate of hazard with time.
- The integration of PTHA module in the framework is conducted by selecting tsunamigenic events in the randomised earthquake catalogue based on defined criteria. To take into account tsunami probability for different magnitudes of earthquakes, a tsunami rate is applied in the random selection procedure. Tsunami heights are computed for these randomised events.
- Probabilistic risk assessments are conducted for both earthquake and tsunami hazards. The risk is determined using hazard curves obtained from the hazard modules, vulnerability functions and inventory database in the investigated area. The risk assessment in this study foresees the expected building loss and fatalities due to earthquake and tsunami hazards.

CHAPTER 4

DATA COLLECTION AND ANALYSIS FOR EARTHQUAKE AND TSUNAMI RISK ASSESSMENTS

4.1. INTRODUCTION

This chapter presents the data collection and analysis required to perform the seismic risk assessment. Key parameters such as the tectonic setting of Sumatra, earthquake zones, earthquake catalogue, magnitude conversion as well as selection of attenuation relationships are presented for conducting seismic hazard assessment. Tsunami catalogue, bathymetry and topography maps are also collected, as required in tsunami hazard assessment. Population data and building inventory are obtained and utilised as main parameters to determine seismic risk.

4.2. TECTONIC SITUATION OF SUMATRA

Sumatra has high seismicity due to the collision between the Indian-Australian and Eurasian tectonic plates. The process was initiated around ~100 Ma when the northern edge of the Indian-Australian plate subducted beneath the Sunda continental margin. Consequently, the Sunda trench was formed as a result of the northward movement of the Indian-Australian into Eurasian plate, as illustrated in Figure 4.1 and Figure 4.2. The slip rate along the plate boundary is around 52-60 mm/year (Natawidjaja, 2002). This subduction area has become one of the major seismic sources for Sumatra and is known as the Sumatra Subduction Zone (SSZ). The SSZ can be distinguished into 2 zones: interface and intraplate. The interface zone is close to the subduction trench and is known for producing large and shallow earthquakes due to its low-dip-angle of about 13-15° (Irsyam et al., 2008). The most notable earthquake ever recorded in this zone was the M_w 9.1 Great Sumatra Earthquake in 2004. In contrast, the intraplate zone (also known as the Benioff zone) is located further away from the Sunda trench. This zone has a dip angle of around 40°-45° and consequently, generates deeper earthquakes with focal depth up to 200 km (Newcomb and McCann, 1987). Earthquakes with magnitude up to M_s 8.1 were recorded in this intraplate region (Irsyam et al., 2008).

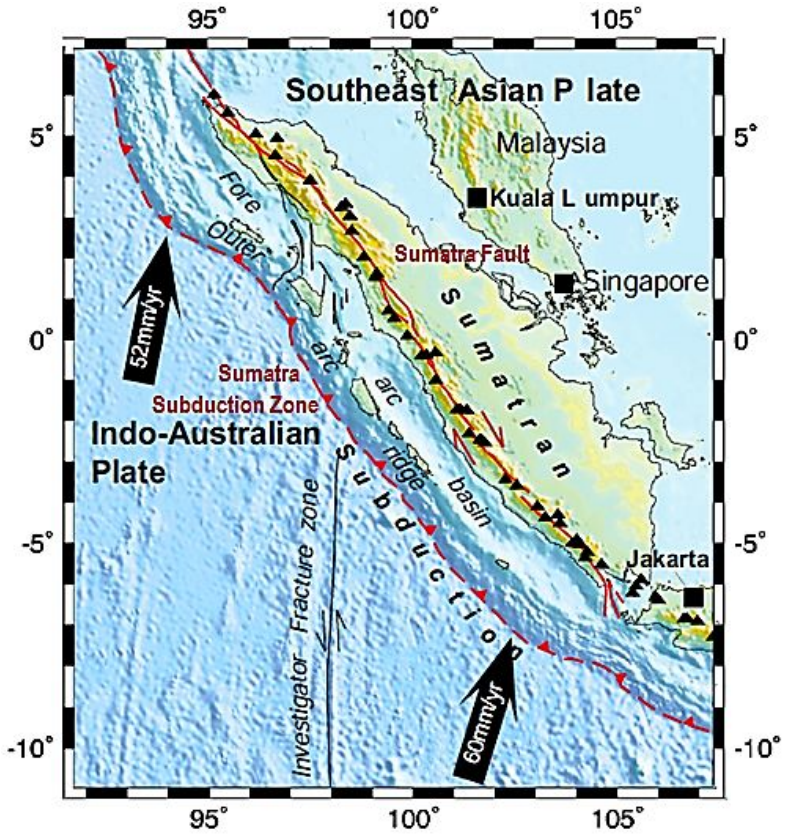

Figure 4.1. Primary tectonic elements of Sumatra (Natawidjaja, 2002)

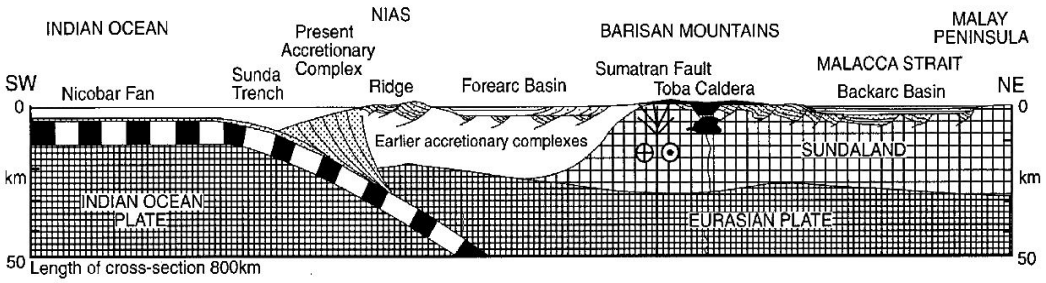

Figure 4.2. Sumatra Subduction System from the floor of Indian Ocean to Malay Peninsula, drawn to scale (Barber et al., 2005)

Beetham (2009) estimated the cross section of the subduction zone facing Padang city as shown in Figure 4.3, which appears to be consistent with the observed seismicity of West Sumatra (see Figure 4.4).

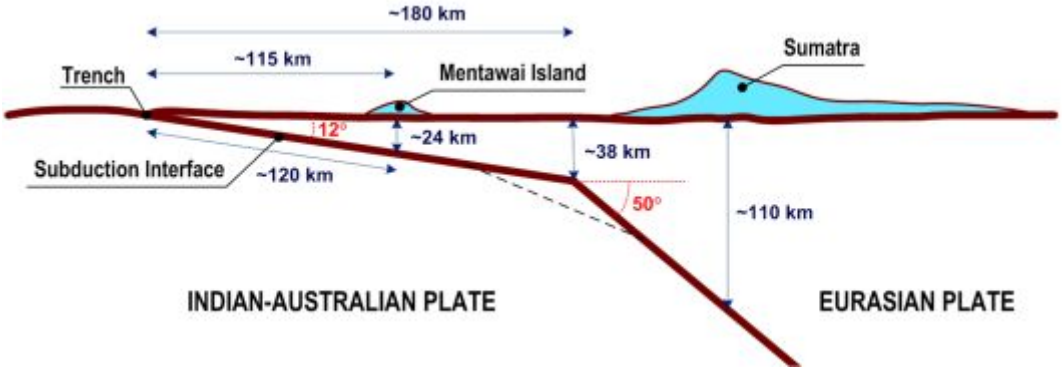

Figure 4.3. The great subduction zone interface facing Padang city in West Sumatra, figure redrawn from Beetham (2009)

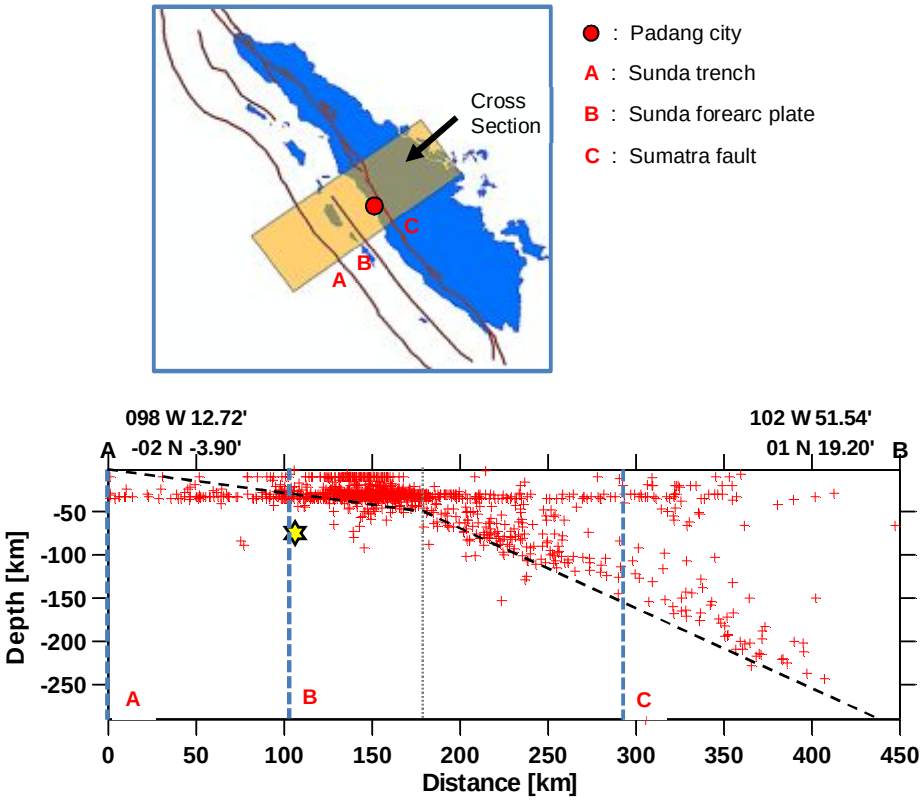

Figure 4.4. Seismicity of Sumatra in a cross section perpendicular to Padang city plotted by ZMAP software developed by Wiemer (2001)

A series of large magnitudes earthquakes have occurred in the SSZ since the M_w 9.1 Great Sumatra Earthquake in 2004. A few months after the large earthquake, another major event of M_w 8.6 struck the SSZ with the epicentre slightly downward that of the 2004 event. Other major events with magnitudes of M_w 8.4 and M_w 7.9 hit further south of the SSZ in 2007. These series of large earthquakes have left a segment in the Mentawai area, which remains unruptured for nearly 2 centuries, as shown in Figure

4.5. The existence of the unruptured segment, as known as a seismic gap, is highlighted by many studies (Borrero et al., 2006; Chlieh et al., 2008; Konca et al., 2008; Sieh, 2005; Sieh, 2007; Sieh et al., 2008). This seismic gap may lead to a mega thrust earthquake that is potentially tsunamigenic in a near future.

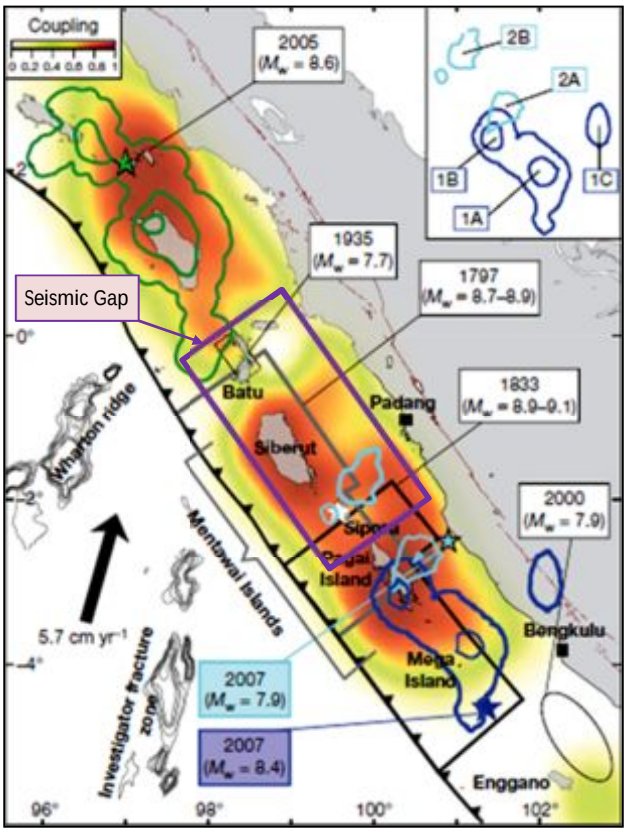

Figure 4.5. Patches with strong inter-seismic coupling on the Sunda megathrust associated with large seismic ruptures (Konca et al., 2008) and the estimated location of seismic gap

The Sumatra Fault Zone (SFZ) is another important seismic source for Sumatra. The SFZ runs from the north to the south of Sumatra Island for about 1900 km. The oblique convergence between Indian-Australian and Eurasian Plates of the Sumatra subduction zone had formed the SFZ to take up the shear components of the plate movements (McCaffrey, 2009), as illustrated in Figure 4.6. The SFZ is characterised as a strike slip fault with dextral movement. The slip rates across the SFZ vary around 6 mm/year near Sunda strait, 25 mm close to the equator and 50 mm/year near the Andaman sea (Genrich et al., 2000). Other studies revealed that the Sumatra fault moved westward with slip rates between 11-27 mm/year (Natawidjaja, 2002). In addition, Natawidjaja (2002) showed that the Sumatra fault was highly segmented.

At least 19 segments were identified and most of the segments were shorter than 100 km. Only two segments were observed longer than 200 km (Natawidjaja, 2002). A highly segmented fault and a wide step-over had limited the areas of slip ruptures in the SFZ, which consequently produced lower magnitude earthquakes. Historical records showed that this fault was capable of producing $M_w \leq 7.5$ (McCaffrey, 2009).

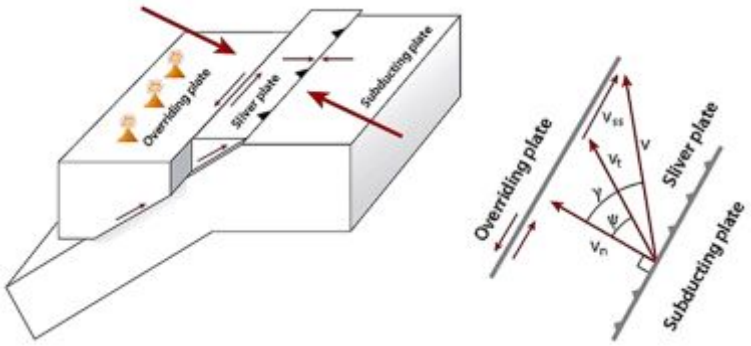

Figure 4.6. Geometry of sliver plate as a result of plate slip partitioning process (McCaffrey, 2009)

4.3. EARTHQUAKE ZONES

As discussed earlier, the seismic sources of Sumatra are characterised into two main categories: subduction and strike slip zones. The subduction zone has a thrust slip mechanism located along the Sumatra Subduction Zones (SSZ). While the strike slip zone is situated along the Sumatra fault (SFZ) as well as the Sumatra volcanic arc. To consider areas with undefined fault characteristics, one more category of seismic sources is added, which is classified as a background seismicity zone.

The SSZ, SFZ and the background zones are then divided into smaller sections to account for different levels of seismicity along the main seismic sources. The boundary of the smaller zones is determined based on the tectonic configuration, seismicity level, seismicity distribution as well as fault segmentation collected from previous studies. Consequently, it is assumed that each earthquake zone follows an earthquake recurrence relationship. This is a standard procedure for conventional PSHA. However, in this project, a method proposed by Khan (2011) is adopted by generating synthetic earthquakes randomly within an estimated rupture area of real earthquakes. Unlike the conventional method that tends to smooth seismicity, this approach produces more realistic earthquake distribution, which is scattered around

main faults. As a result, seismicity in a zone boundary is not uniformly distributed. Therefore, this solves the problem of smoothing seismicity in conventional PSHA. However, it should be pointed out that in Khan's method, the directivity of fault rupture follows the strike angle of the main fault. Consequently, a seismic zone should only cover an area with similar tectonic characteristics. Figure 4.7 shows the earthquake zones used for this project.

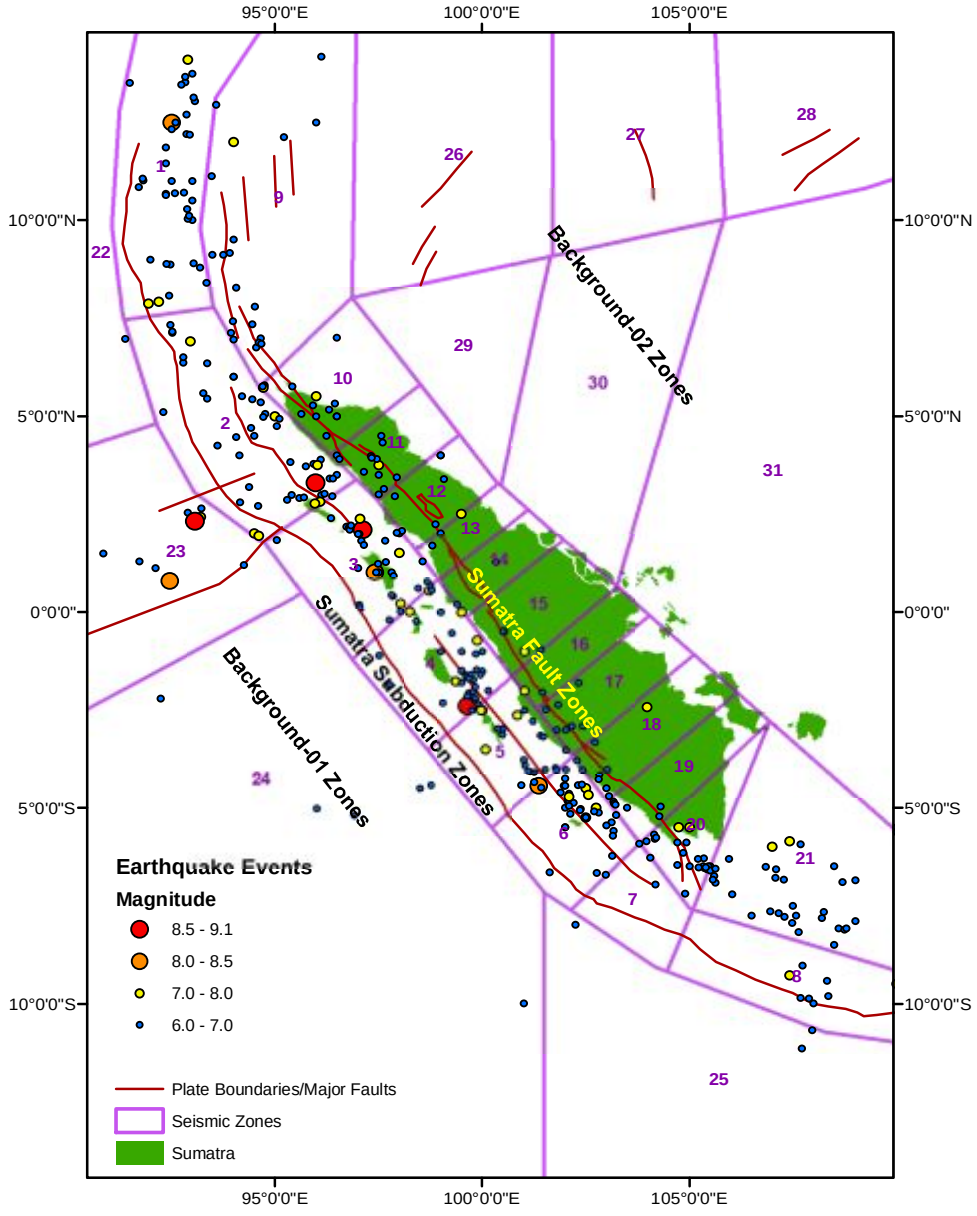

Figure 4.7. Earthquake zones of Sumatra ($M_w \geq 6.0$)

4.4. EARTHQUAKE CATALOGUE

Earthquake catalogues are freely accessible on various international seismological databases such as National Earthquake Information Centre-United State Geological Survey (NEIC-USGS), Northern California Earthquake Data Centre-United State Geological Survey (NCEDC-USGS), International Seismological Centre (ISC) and the Indonesian Meteorology, Climatology and Geophysics Agency (BMKG). The extent of catalogue completeness varies among different sources and different regions. For example, the ISC catalogue has recorded historical earthquakes of Sumatra since 1907, the NCEDC catalogue since 1963 and the NEIC catalogue since 1973. The BMKG has provided online access for earthquake databases in Indonesia since 2004. Hendriyawan (2007 cited in Irsyam, et al., 2008) revealed that earthquake catalogues for the Southeast Asia regions were relatively complete since 1978 for magnitude interval $5 \leq M_w < 6$, since 1972 for magnitude interval $6 \leq M_w < 7$ and since 1900s for $M_w \geq 7$.

Figure 4.8 shows the cumulative number of earthquakes for different earthquake catalogues. The figure indicates that the level of seismic recording for Sumatra can be separated into 3 main periods: 1907-1963, 1963-2004, and 2004-date. The steeper gradient at the latter period indicates that earthquake recording in Sumatra improved significantly since the M_w 9.1 Great Sumatra earthquake in 2004. The figure also reveals that ISC catalogue contains more events compared with NEIC and NCEDC catalogues. However, the events in the NEIC and NCEDC catalogues have been reviewed by removing duplicate solutions for similar events. In addition, most of the existing earthquake catalogues lack detailed information, particularly for historical earthquakes occurring when instrumental seismic observations are not available. In such a case, any information from paleoseismological studies is utilised to fill in the missing information. Therefore, the earthquake catalogue used for this project is basically a compilation of the ISC, NEIC and NCEDC catalogues combined with historical events from paleoseismological studies (Gusiakov, 2001; Natawidjaja, 2002; NOAA, 2011).

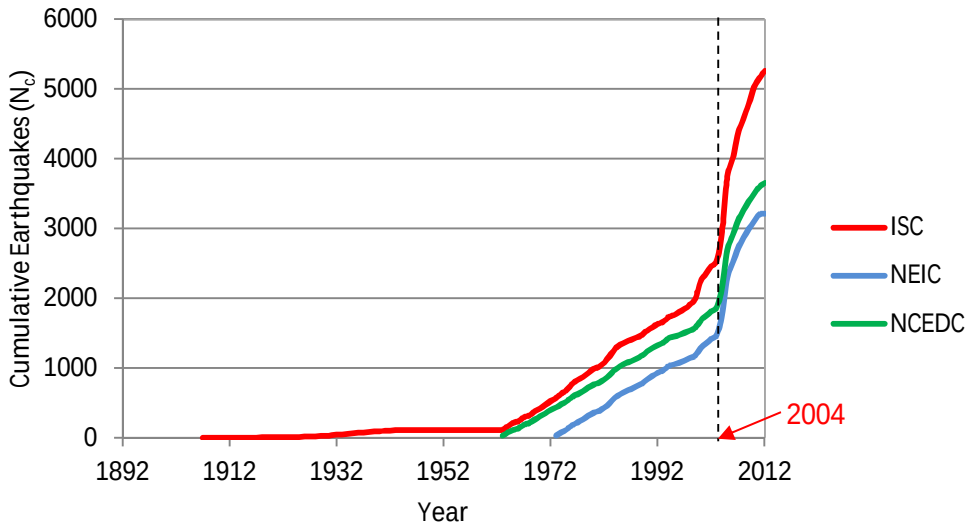

Figure 4.8. Comparison of earthquake catalogues of Sumatra for $M_w \geq 5$

4.5. CONVERSION OF EARTHQUAKE MAGNITUDES

Earthquake catalogues usually contain various magnitude scales including Richter/local magnitude (M_L), body-wave magnitudes (m_b), duration magnitude (M_D), surface-wave magnitudes (M_S) energy magnitude (M_E) and moment magnitudes (M_W). For this study, M_w scale is used since the other magnitude scales have limitations in measuring large earthquakes (see Figure 4.9). However, the number of events measured in M_w is relatively limited; therefore, earthquakes recorded in other magnitude scales are utilised and converted to M_w using earthquake magnitude conversion equations. Asrurifak et al. (2010) performed regression analysis to obtain magnitude conversion equations for earthquakes in Indonesia (Table 4.1). These equations are used in this study.

Table 4.1. Magnitude conversion equations for Indonesia (Asrurifak et al., 2010)

Conversion Correlation	Number of Data	Range of Magnitude	Consistency (R^2)
$M_w = 0.143M_s^2 - 1.051M_s + 7.285$	3173	$4.5 \leq M_S \leq 8.6$	93.9%
$M_w = 0.114m_b^2 - 0.556m_b + 5.560$	978	$4.9 \leq m_b \leq 8.2$	72.0%
$M_w = 0.787M_E + 1.537$	154	$5.2 \leq M_E \leq 7.3$	71.2%
$m_b = 0.125M_L^2 - 0.389\ M_L + 3.513$	722	$3.0 \leq M_L \leq 6.2$	56.1%

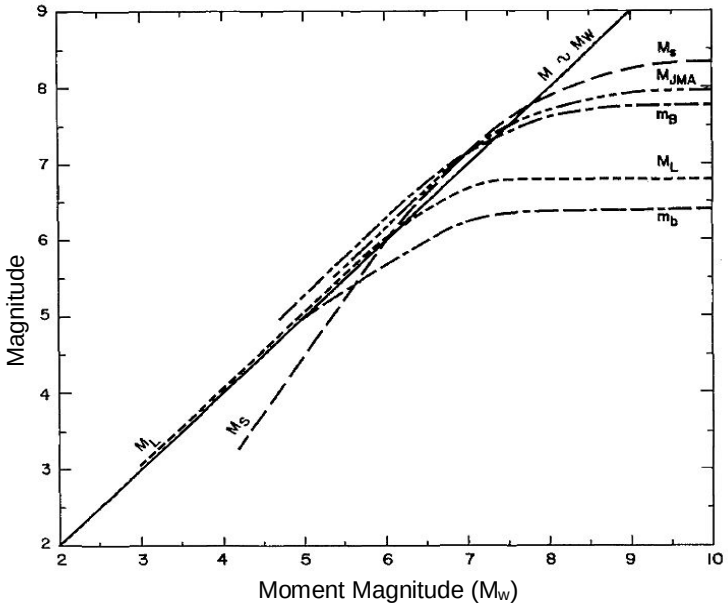

Figure 4.9. Comparison of some magnitude scales with moment magnitude scale (Heaton et al., 1986)

4.6. EARTHQUAKE RECURRENCE RELATIONSHIP

The PSHA method adopted for this study requires the estimation of seismicity rate for the case study area. The ISC catalogue provides earthquake records for Sumatra since 1907 (105 years). The catalogue contains one event of M_w 9.1. If Khan's assumption is adopted, the annual rate of 0.0095 is obtained with an assumed return period of 105 years. This means that on average, about four earthquakes with M_w 9.1 are expected in 475 years. A simple method to estimate earthquake recurrence time is proposed by Wallace (1970) by dividing the displacement of the event with the average slip rate of the fault. Using Wells and Coppersmith (1994) empirical equations, the displacement associated with the M_w 9.1 event is approximately 30 m. By assuming a fault slip rate of 60 mm/year, the average recurrence interval of the event is about 500 years. Hence, Khan's approach is likely to underestimate the recurrence interval of high magnitude earthquakes. Moreover, Khan's method may also underestimate the rate of small magnitude events. If the completeness period of $M_w \geq 4$ for Sumatra is since 1990s, calculating the rate of $M_w \geq 4$ based on the 105 year catalogue (since 1907) may result in a lower seismicity rate. To solve this problem, the rate of seismicity can be approximated using earthquake recurrence relationships as recommended by Musson (2000). The comparison of seismicity rate

and the expected number of events computed with and without earthquake recurrence relationship is presented in Figure 4.10 and Figure 4.11, respectively.

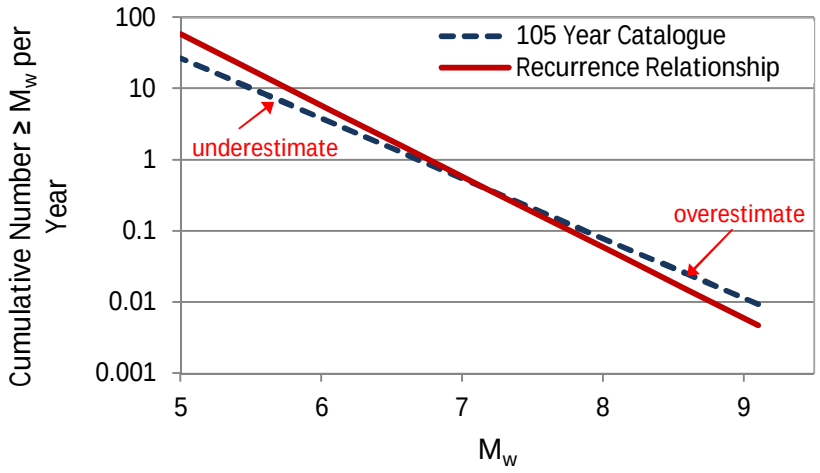

Figure 4.10. Comparison of seismicity rate estimated using earthquake recurrence relationship and the instrumental catalogue of Sumatra (105 years)

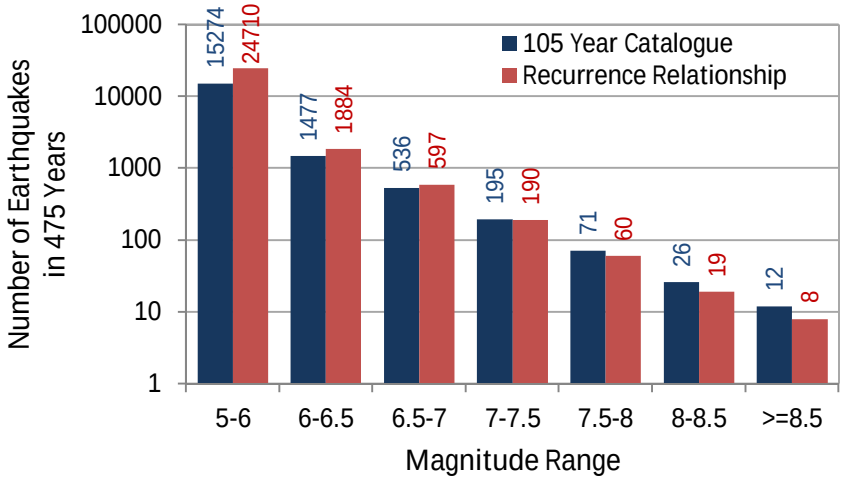

Figure 4.11. Estimated number of earthquakes for 475 years based on recurrence relationship and 105 years of instrumental catalogue

There are several recurrence models usually adopted for seismic hazard assessment including the “characteristic” and the “Gutenberg-Richter” relationships. Youngs and Coppersmith (1985) showed that the characteristic recurrence model can characterise individual faults and fault segments better than the exponential magnitude distribution (Gutenberg-Richter recurrence relationship). However, the model requires the geological data of seismic sources, which is limited for the sources in this study. Hence, the Gutenberg-Richter recurrence relationship is adopted in this

study (see Equation 2.9). An improved recurrence model can be easily utilised in the PSHA module when the required data become available.

The PSHA model adopted in this study assumes that each earthquake occurs independently, and therefore, follows the Poisson process. To achieve this, various methods are proposed to decluster the earthquake catalogue (Gardner and Knopoff, 1974; Reasenberg, 1985). The declustering process basically removes the accessory shocks (preshocks and aftershocks) from the catalogue; thus enabling to obtain a better approximation for the rate of main earthquakes. However, experience from past earthquakes shows that accessory shocks can cause damage and should not be excluded from risk studies.

The comparison of recurrence relationships for non-declustered and declustered earthquake catalogues for Sumatra is presented in Figure 4.12. For the declustered catalogues, a time and distance window proposed by Gardner & Knopoff (1974) and a declustering criteria used by Reasenberg (1985) are adopted. It is observed that Gardner & Knopoff's algorithm tends to eliminate low magnitude events (about 75% of the events discarded) resulting in lower "b" values (see Equation 2.9). The Reasenberg's method removes around 25% of the earthquakes and the resulted "b" value is closer to the non-declustered approach. Lower "b" value indicates a higher ratio of large to small earthquakes.

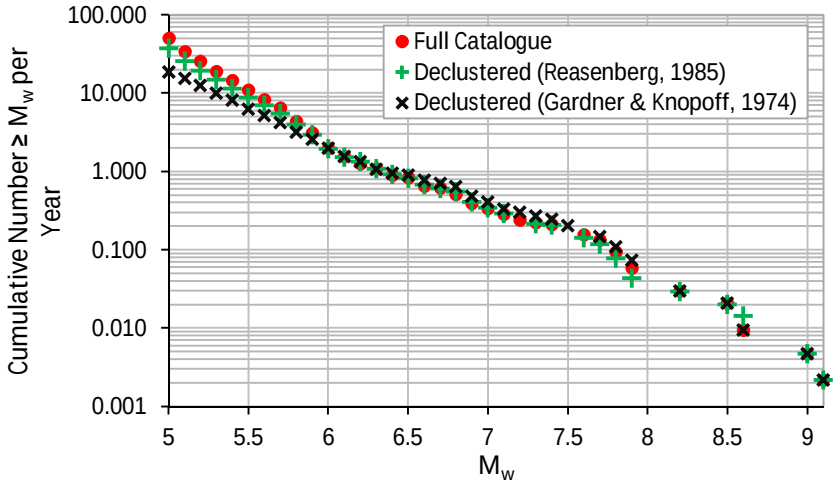

Figure 4.12. Recurrence relationships for the Sumatra Subduction Zone developed based on the full and declustered earthquake catalogues

Figure 4.13 illustrates the recurrence relationships for major seismic sources of Sumatra. The figure shows that the Sumatra Subduction Zone (SSZ) has the highest seismicity rate compared with the Sumatra Fault Zone (SFZ) and the background seismicity zones. The SSZ and Background-01 zone have a lower gradient (lower absolute "b" value) and a higher proportion of large events. The SSZ is notable for producing mega magnitude earthquakes such as the M_w 9.1 earthquake in 2004. The Background-01 zone is a transform zone located on the Indian Ocean near the subduction zone, and it is also known to produce large magnitude earthquakes. Two consecutive large earthquakes (M_w 8.6 and 8.2) occurred in this zone in 2012. The SFZ produces smaller magnitude events ($\leq M_w$ 7.7). However, the SFZ is located in the mainland of Sumatra, so it has the potential to produce high earthquake intensities in the region. The Background-02 zone is considered as a low seismicity area, which is located on the eastern part of Sumatra and around the Malay Peninsula.

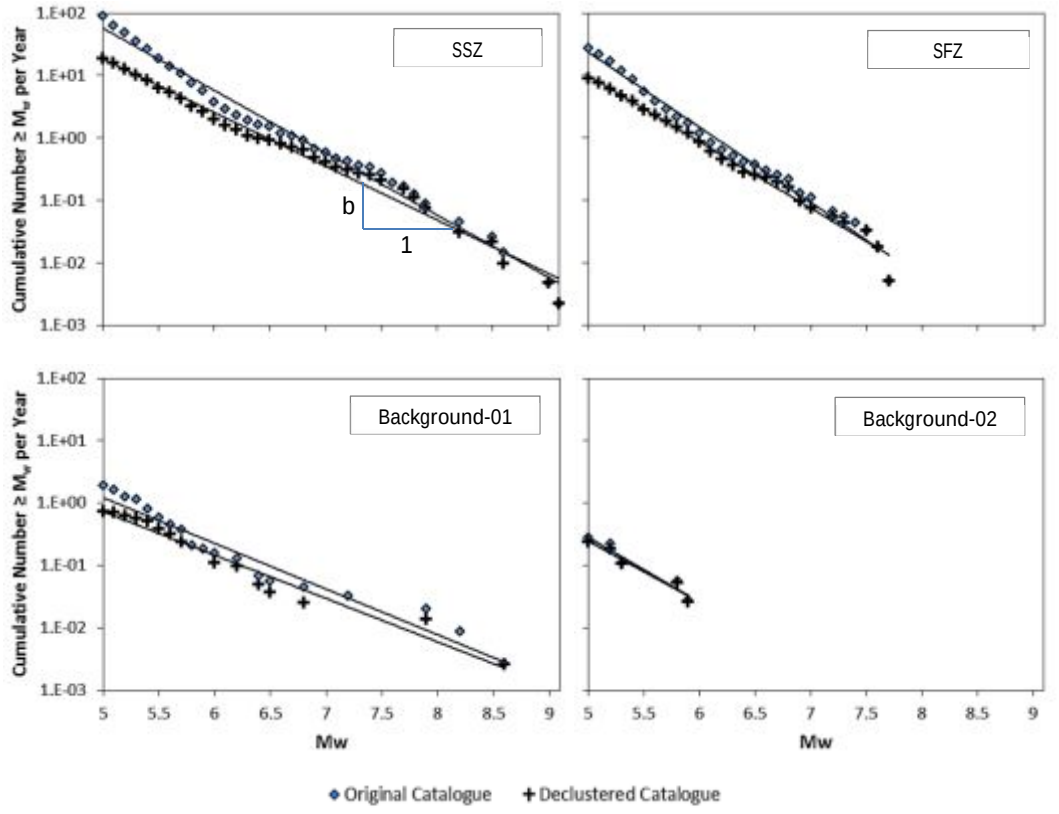

Figure 4.13. Recurrence relationships for typical seismic sources in Sumatra for full and declustered (based on Gardner & Knopoff's algorithm) earthquake catalogues

4.7. GROUND MOTION ATTENUATION RELATIONSHIP

Ground motion attenuation relationships are selected by comparing suitable equations with earthquake strong motion data. A 3-D fault source model is adopted in this study for better modelling of fault source geometries including dip angle, strike angle and fault rupture characteristics, as shown in Figure 4.14. The interface and intraslab events in the subduction area are differentiated based on their faulting mechanism, as proposed by Youngs et al. (1997). It is reported that the focal depth of interface earthquakes are mostly shallower than 50 km and the intraslab events typically occur at depths below 50 km (Atkinson and Boore, 2003; Youngs et al., 1997).

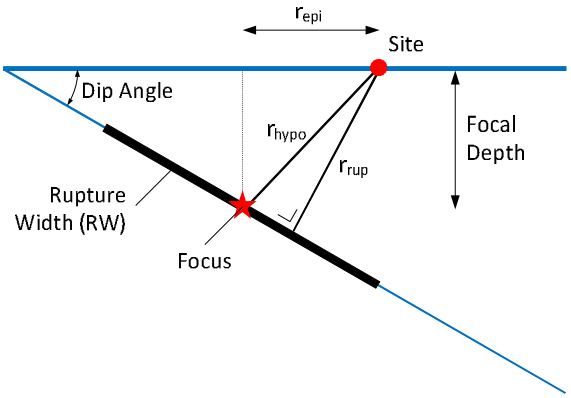

Figure 4.14. Definition of fault source geometries for ground motion calculation

For the Sumatra subduction area, attenuation equations are verified with the ground motion data of M_w 7.6 West Sumatra earthquake in 2009 provided by BMKG (2009). The earthquake occurred deep in the Sumatra Subduction Zone with a focal depth of 71 km. The soil information of the recording stations is not available.

The comparison shown in Figure 4.15 demonstrates that Parithusta (2007) equations tend to overestimate the ground motion at close distance. In addition, the Parithusta‘s equations do not distinguish the interface and in-slab events in subduction zone. The Atkinson and Boore (2003) attenuation equations provide reasonable estimates of ground accelerations. However, Atkinson and Boore (2003) equations are saturated at M_w 8.5 for interface events and at M_w 8.0 for in-slab events. Consequently, the equations are not suitable for Sumatra, which has a long history of mega magnitude earthquakes (up to M_w 9.1). Youngs et al. (1997) equations compare well with the data, but provide a lower estimate at close distances. To consider the location of

subduction area, which is away from the mainland of Sumatra, it is reasonable to select Youngs et al. (1997) ground motion attenuation relations for the Sumatra Subduction Zone.

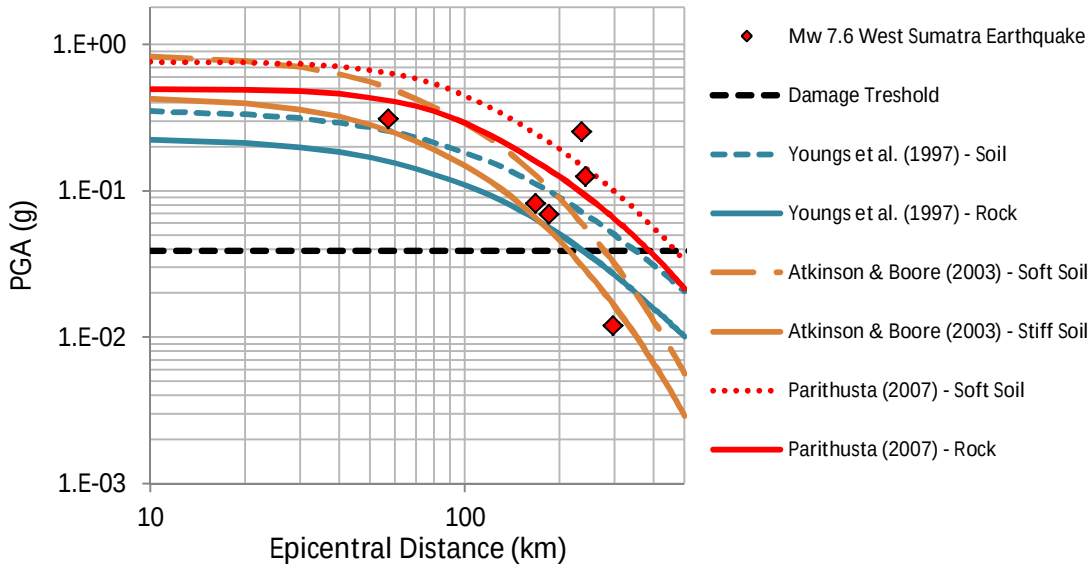

Figure 4.15. Ground Attenuation predictions vs. real strong motion records for the M_w 7.6 West Sumatra earthquake in 2009

Unlike for the Sumatra subduction zone, the strong motion data are not available for the Sumatra Fault Zone. However, BMKG provided earthquake data from 2008 to 2009 recorded by a seismic station in Padang Panjang, West Sumatra. The ratio of predicted to recorded accelerations is shown in Figure 4.16. Based on these data, the Boore et al. (1997) attenuation equation appears to overestimate the ground motions. In contrast, Sadigh et al. (1997) equation fits the earthquake data better. Hence, Sadigh's attenuation equation is used to calculate earthquake ground motions for the Sumatra fault zone.

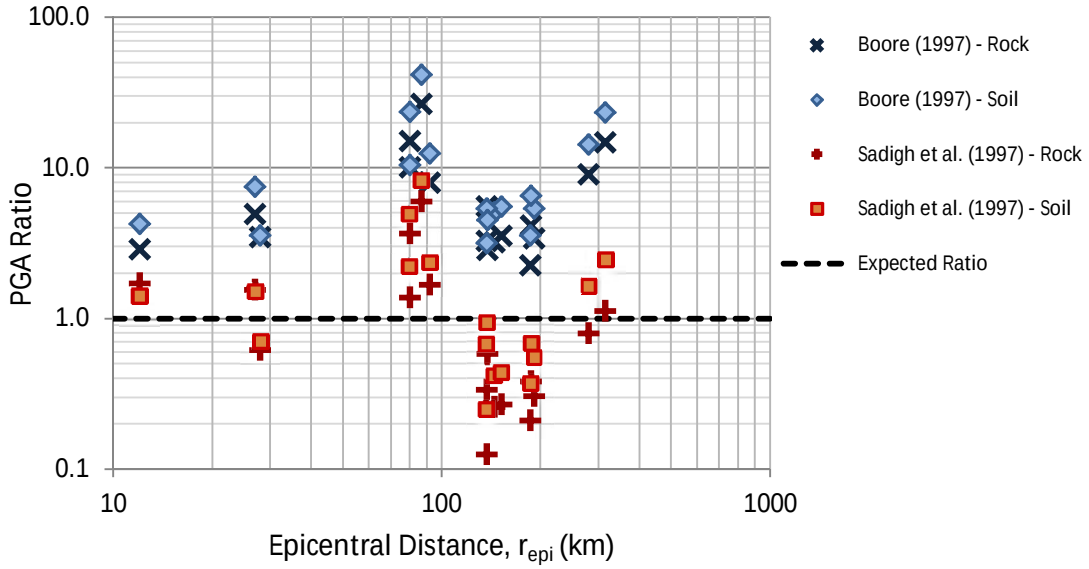

Figure 4.16. Ratio between the estimated ground attenuation and the real strong motion records for various earthquakes occurred in the Sumatra Fault

4.8. GEOLOGICAL MAP AND SOIL TYPES OF PADANG CITY

The identification of soil types is necessary for seismic hazard assessment since the intensity of earthquake ground motions is strongly correlated to the soil condition in an area. For this project, the soil type of Padang city is taken from a local geological map obtained from the Indonesian Geological Agency, Department of Energy and Mineral Resources, as shown in Figure 4.17. The map reveals that Padang area is mostly based on alluvium deposits, which cover the low lying part of the city. EERI (2009) reported that the subsurface of the alluvium deposits primarily consists of medium dense to dense silty sand and stiff to very stiff silt with relatively low ground water levels. Near river banks, the soil is typically loose and saturated fine sand. On the other hand, the soil types on the eastern side of Padang are mostly stiff soil and rock. This highland area is formed by the Barisan Range that is mainly composed of andesite, tuff, granite, limestone and quaternary volcanic deposits. The details of Padang's geology as well as its soil classification can be seen in Figure 4.17.

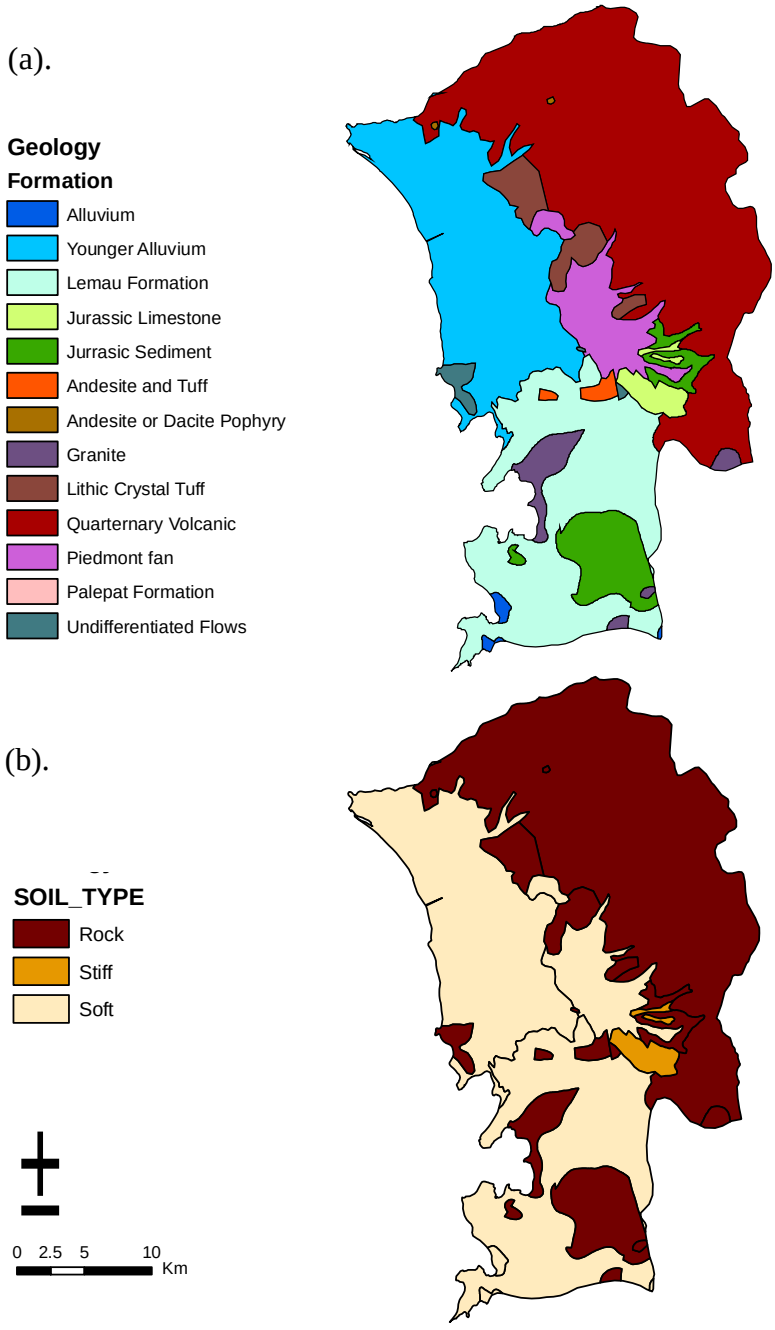

Figure 4.17. Geological map (a) and soil classification (b) of Padang city

4.9. TSUNAMI SOURCES IN SUMATRA

Tsunami sources in Sumatra are mainly contributed by major submarine earthquakes in the subduction zone (SSZ). The SSZ is known to produce mega thrust earthquakes triggering regional and distant tsunamis across the Indian Ocean as happened in 2004 (see Figure 4.18). Puspito and Gunawan (2005) reveal that earthquakes in the Sumatra regions tend to produce larger tsunami than those of the Pacific Ocean, as

shown in Figure 4.19, Figure 4.20 and Figure 4.21. Figure 4.19 shows that most tsunamis in Sumatra are triggered by earthquakes with a magnitude range of 6.6-7. Unlike tsunamis in the Pacific Ocean, considerable number of tsunamis in Sumatra is triggered by relatively deep earthquakes as shown in Figure 4.20.

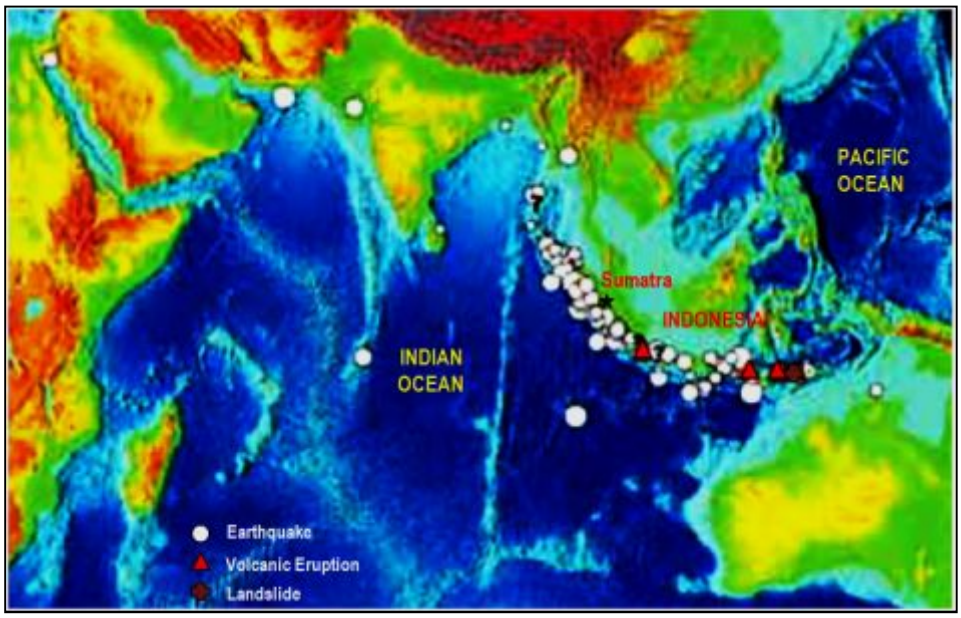

Figure 4.18. Tsunami sources in Indian Ocean (IOC, 2008)

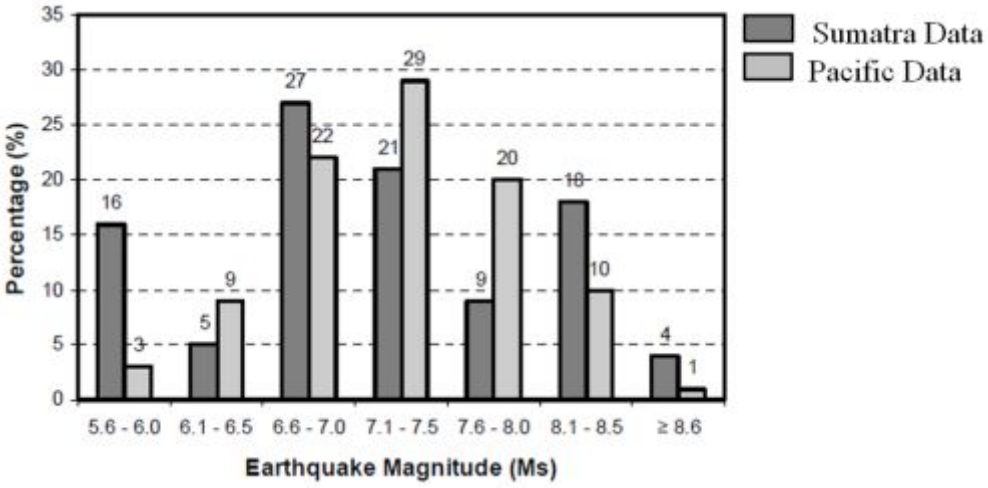

Figure 4.19. Distributions of tsunamigenic earthquakes in Sumatra & Pacific Ocean in terms of earthquake magnitude (Puspito and Gunawan, 2005)

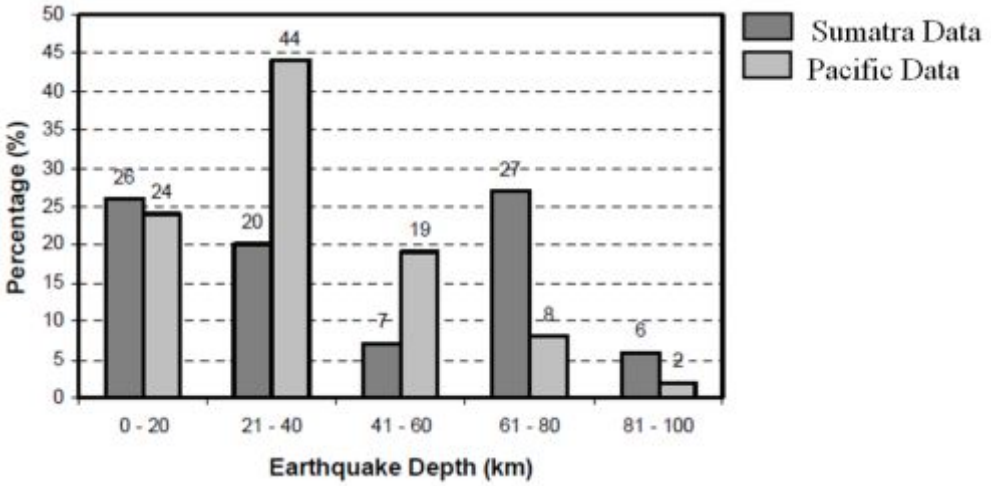

Figure 4.20. Distributions of tsunamigenic earthquakes in Sumatra & Pacific Ocean in terms of earthquake focal depth (Puspito and Gunawan, 2005)

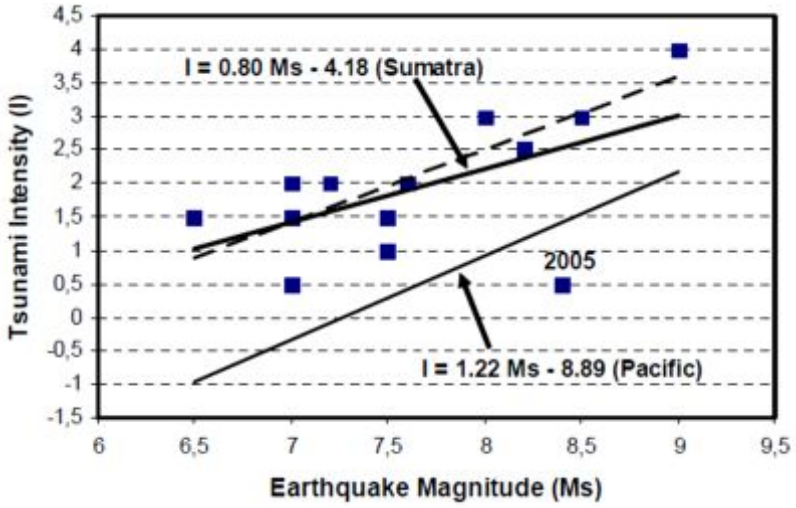

Figure 4.21. Earthquake Magnitude vs. Tsunami Intensity for Sumatra region and Pacific Ocean (Puspito and Gunawan, 2005)

4.10. TSUNAMI CATALOGUE

For this project, the tsunami catalogue of Sumatra is compiled from many sources including the Indonesian national agency (BMKG, 2010), National Oceanic and Atmospheric Administration of USA (NOAA, 2011), the Russian Oceanographic Commission (Tsunami Laboratory Novosibirsk, 2005) as well as various other studies (Gusiakov, 2001; Hamzah et al., 2000; Puspito and Gunawan, 2005). Most tsunamis in Sumatra are triggered by earthquakes; only a few of them are caused by other hazards such as landslides and volcanic eruptions. For that reason, this study

only considers tsunami events triggered by earthquakes. Only reliable records, which have validity codes of 3 (probable tsunami) and 4 (definite tsunami), are included in the tsunami catalogues. The wave heights as well as the spatial distribution of tsunamigenic earthquakes in Sumatra are presented in Figure 4.22 and Appendix A.

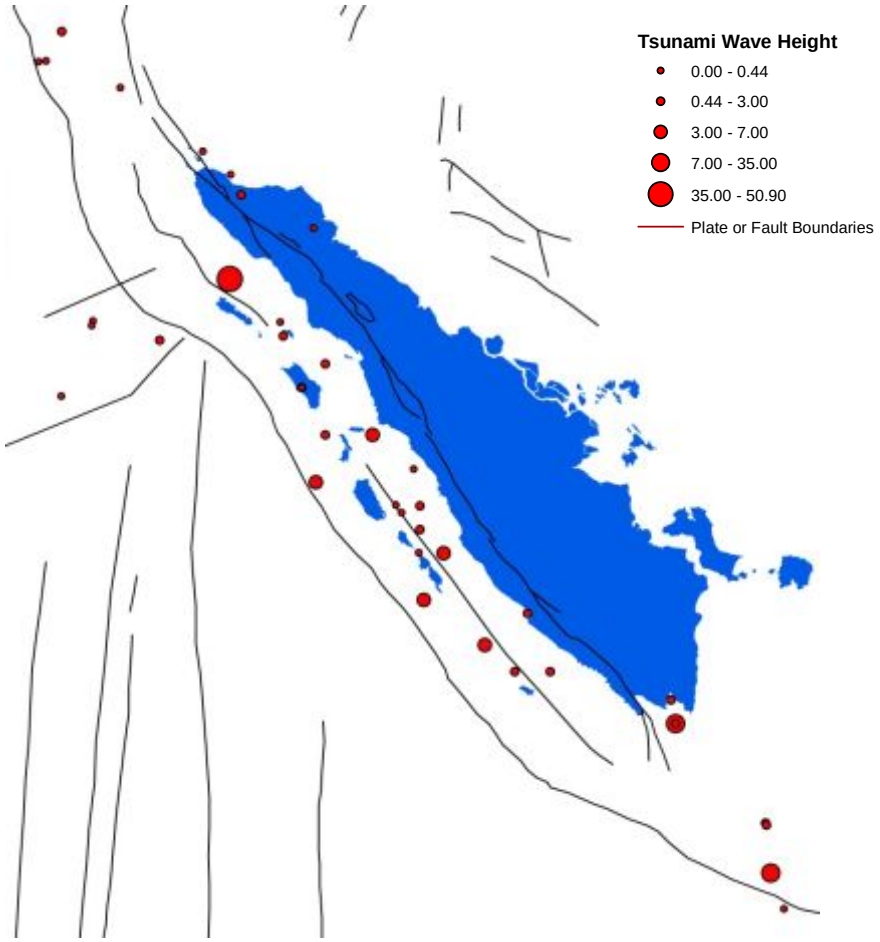

Figure 4.22. Spatial distribution of tsunamigenic earthquakes in Sumatra

The intensity of a tsunami depends, to some extent, on the characteristics of the earthquake. For the Sumatra region, the magnitude of tsunamigenic earthquakes ranges between M_w 5.4 and 9.1. However, the probability that a tsunami would be triggered by an earthquake with magnitude less than M_w 6.5 is only 10%. The weighted average of magnitude is 7.367 with standard deviation of 1.399 (Figure 4.23). Beside the magnitude, the focal depth of the tsunamigenic earthquake is also important for triggering the hazard. The focal depths of tsunamigenic earthquakes in Sumatra are around 10 to 133 km with weighted mean of 41.15 km. However, most of the tsunamigenic earthquakes in Sumatra are generated by shallow events with depth around 20 km.

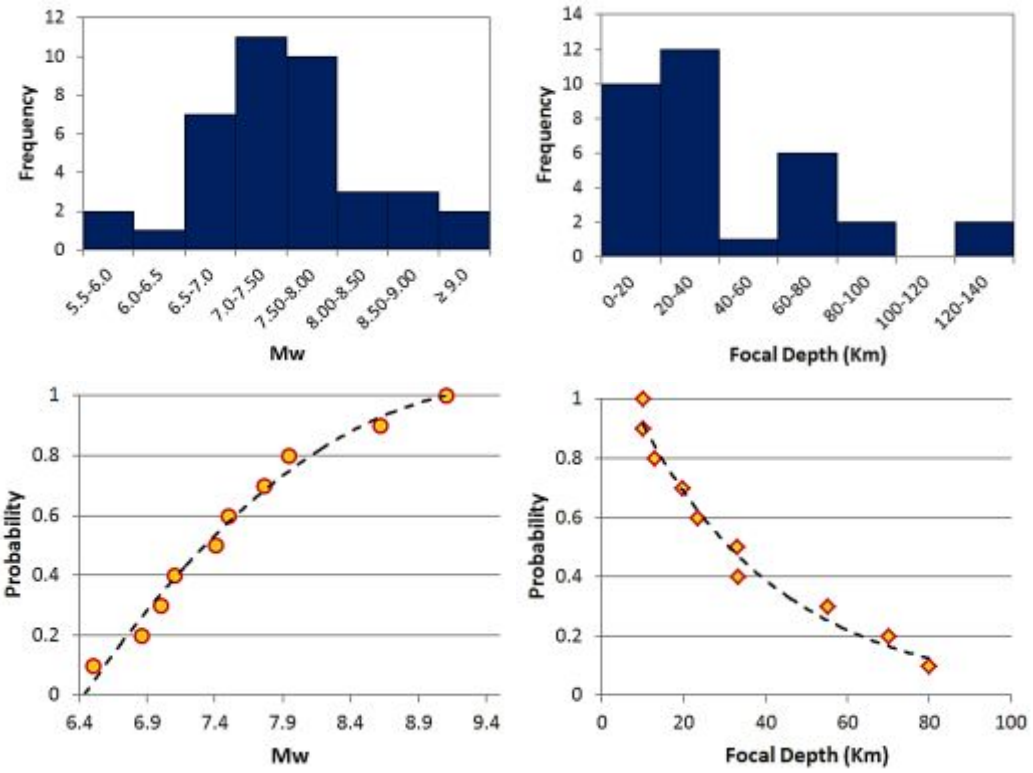

Figure 4.23. Characteristics of tsunamigenic earthquakes in Sumatra

4.11. BATHYMETRY OF SUMATRA

A gridded bathymetry data from GEBCO (2012) is used for the numerical tsunami analysis. The resolution of the data is 30 arc-second grid, which is obtained from a combination of quality-controlled ship depth soundings with interpolation between sounding points guided by satellite-derived gravity data (GEBCO, 2012). Land data is mostly based on the Shuttle Radar Topography Mission (SRTM30) gridded digital elevation model (GEBCO, 2012). The GEBCO data provides a global coverage of bathymetry and can be obtained for free. The GEBCO bathymetry of Sumatra is plotted in Figure 4.24 and a three dimensional plot of the bathymetry is presented in Figure 4.25. It is observed that the subducting plate (the Indo-Australian plate) at the Sumatra Subduction Zone is relatively deep, which is around 5 km below the mean sea level. The depths of the ocean are getting shallower at the overriding plate. In addition, a deep trench (approximately 2000 m below mean sea level) exists between the mainland of Sumatra and the smaller islands near the subduction interface. As a consequence, this creates steep bathymetry at most parts of the western coast of Sumatra.

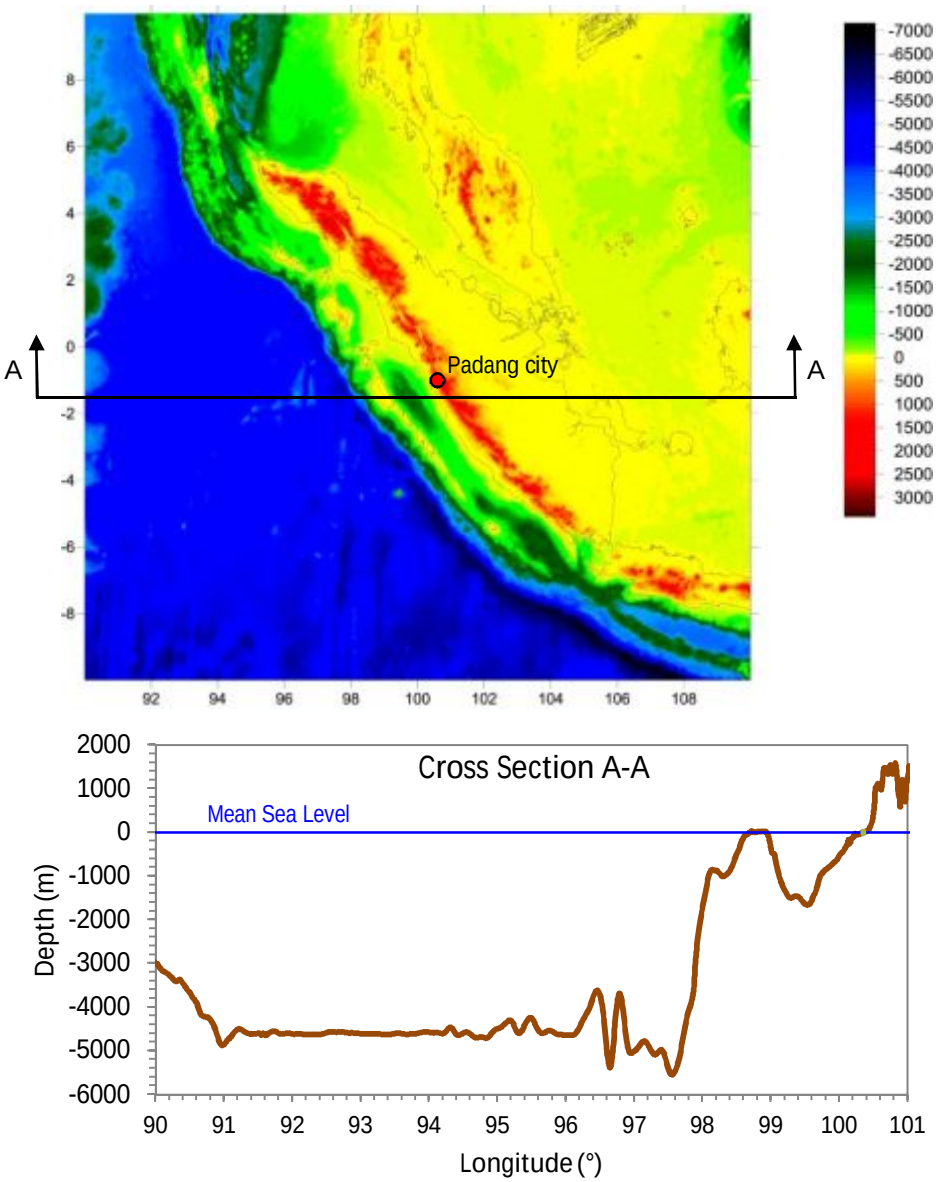

Figure 4.24. Bathymetry of Sumatra (GEBCO, 2012)

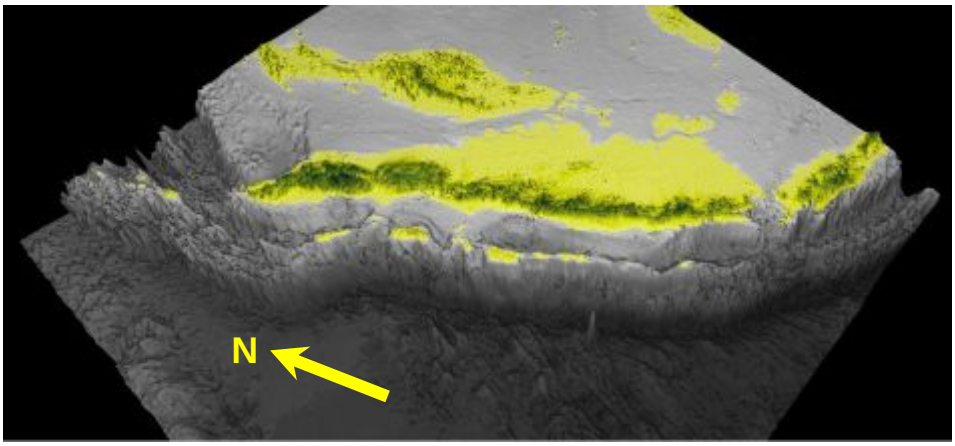

Figure 4.25. A three dimensional view of Sumatra Bathymetry plotted using NAMI-DANCE software (not scaled)

4.12. POPULATION DATA

Population data of Padang city are obtained from Indonesian Central Bureau of Statistics. The data contains population distribution for each sub-district in Padang based on the census conducted in 2010. Total area of Padang city is 698 km^2 with an estimated population of 833,584; resulting in a population density of 1194 people/km^2. Figure 4.26 shows the population density of the city, which is highly distributed around the low lying coastal areas.

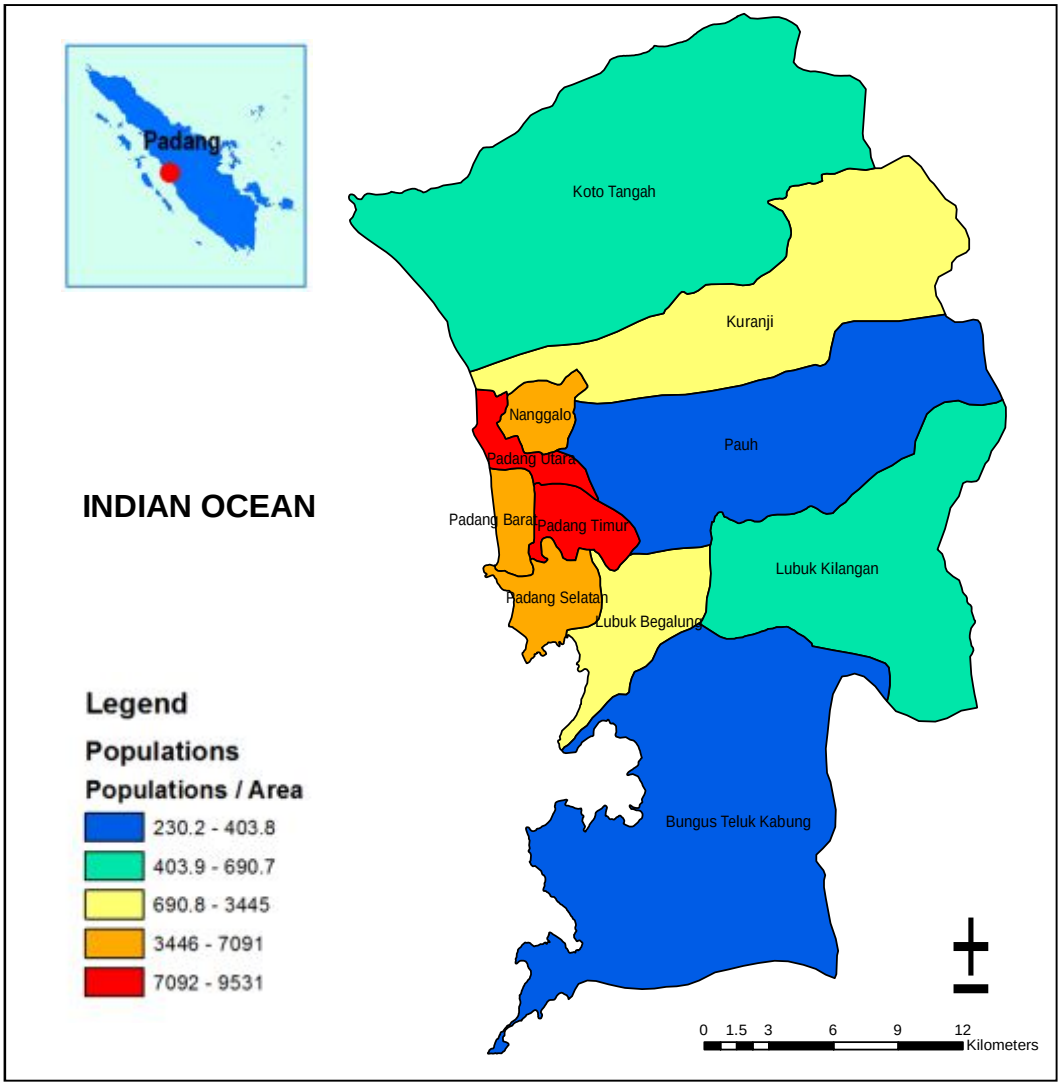

Figure 4.26. Population density of Padang city (total population/km^2)

4.13. BUILDING INVENTORY

Building inventory for Padang is obtained from a digital map produced by PT. Exsa International in collaboration with BAKORSURTANAL (the Indonesian government

agency for surveying and mapping). The map contains a layer with the plans of buildings in the region, as shown in Figure 4.27. However, the map does not provide the number of storeys for each building as well as the typology of structures.

Figure 4.27. An example of a building layer from the BAKOSURTANAL digital map for Padang city (scale 1:10,000)

A field survey by the EEFIT team reveals that the structures in Padang mainly consist of unreinforced masonry, confined masonry and reinforced concrete frames with masonry infill (Chian et al., 2010; Wilkinson et al., 2009; Wilkinson et al., 2012). Based on a personal communication with a government official from the urban planning agency of Padang city, the region currently has 203,450 residential houses and 20% of them are classified as semi-permanent (wood and unreinforced masonry constructions). The other 80% are generally constructed with either brick with reinforced columns (confined masonry) or RC frames with masonry infills and typically have 1 or 2 storeys. The city has about 1,572 buildings for public or commercial purposes, which are mainly constructed from RC frames with masonry infills. The use of steel structures is limited and generally found in large commercial buildings or industrial facilities.

To estimate the distribution for each type of structures in the investigated area, visual inspections from satellite imagery (Google Earth, 2011) are performed. The area is divided into several categories such as residential, commercial, industrial facilities

and combinations of the aforementioned categories (see Figure 4.28). The Padang region is subdivided into small rectangular grids and a category is assigned to each grid. The percentage of each type of structure for every category is determined and its average is shown in Table 4.2. . The assigned building category for each grid is shown in Figure 4.29. The "NA" category in the figure denotes an area with limited or no observed building stock. The estimated area of buildings for each grid in Padang city is shown in Figure 4.30. The figure shows that the building density is higher along the coastal area of Padang. Full details are given in Appendix C.

Residential Area

Commercial Area

Industrial Area

Residential and Commercial Area

Figure 4.28. Typical satellite imagery for residential, commercial and industrial areas in Padang city (Google Earth, 2011)

Table 4.2. Composition of buildings in Padang based on the land use of the areas

Category	% UBM[1]	% CBM[2]	% RCI[3]	% Steel[4]
1. Rural residential area (R-1)	17.3	69.0	13.6	0.1
2. Residential area in the city (R-2)	13.1	52.2	34.6	0.1
3. Residential and commercial area at the outskirt of the city (RC-1)	6.7	26.6	66.5	0.2
4. Residential and commercial area in the city (RC-2)	1.5	6.1	92.0	0.4
5. Residential and industrial area (RI)	11.6	46.6	27.2	14.6
6. Residential, commercial and industrial area (RCI)	3.0	12.1	80.4	4.5

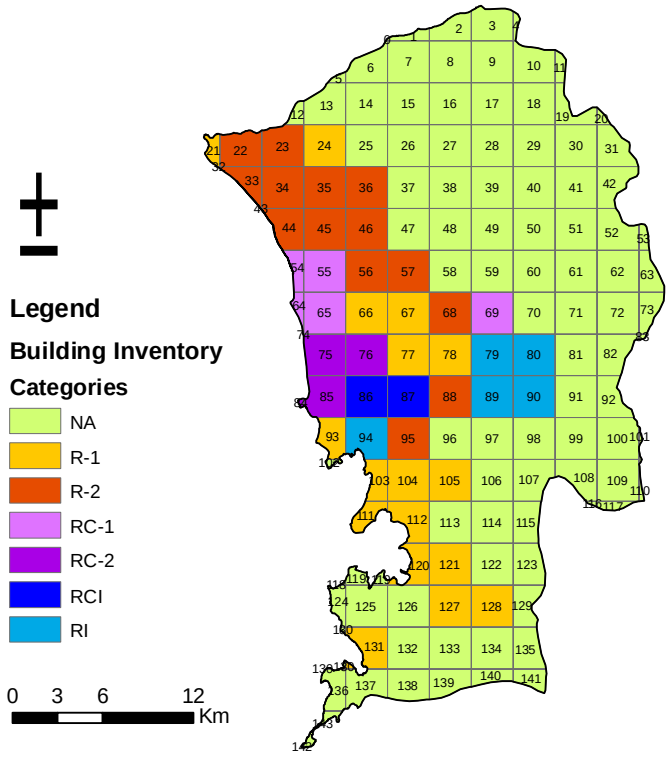

Figure 4.29. Distribution of structural categories within the Padang area

[1] Unreinforced brick masonry (UBM)
[2] Confined brick masonry (CBM)
[3] Reinforced concrete frame structures with masonry infill (RCI)
[4] Steel structures (Steel)

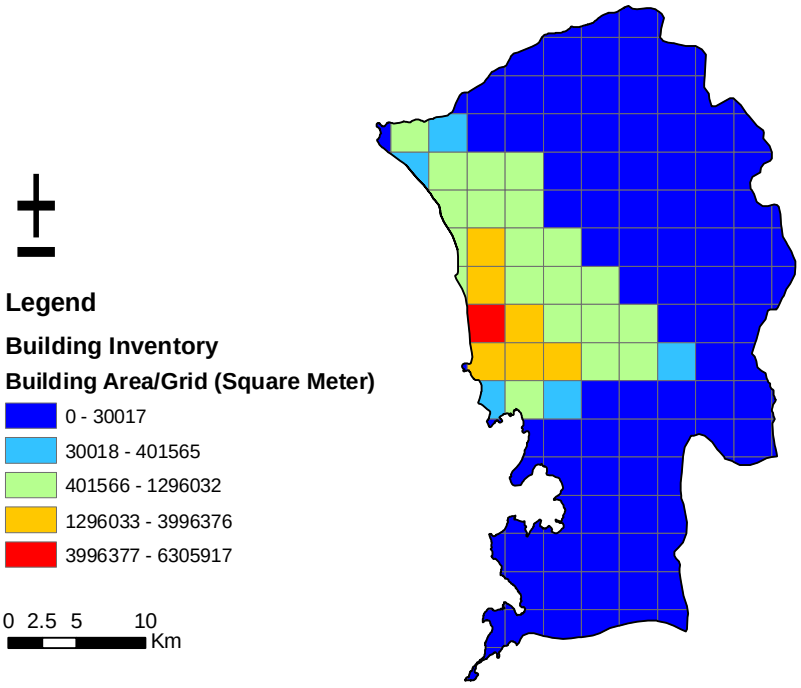

Figure 4.30. Estimated areas of buildings (m^2) for each grid in Padang city

4.14. SUMMARY

- Seismic sources in Sumatra are reviewed and these are dominated by the Sumatra Subduction Zone (SSZ) and the Sumatra Fault Zone (SFZ). The seismic source information is important to determine the seismic zones of the region along with other information including fault slip mechanism, tectonic configuration, seismicity level, seismicity distribution as well as fault segmentations.
- The earthquake catalogue used in this study is compiled from many sources including ISC, NEIC, NCEDC and historical events from paleoseismological studies. The earthquake catalogue is utilized to determine earthquake recurrence relationships in the investigated area as well as to generate synthetic events in the PSHA module.
- Earthquake moment magnitude scale (M_w) is used in this study. Hence, any earthquakes recorded in other scales are converted to M_w using magnitude conversion equations proposed by Asrurifak et al. (2010).
- Ground motion attenuation equations proposed by Youngs et al. (1997) and Sadigh et al. (1997) are utilised in the PSHA module to calculate PGA in the SSZ and SFZ, respectively.

- Detailed soil data for Padang city is not available. Therefore, the soil information is inferred from a geological map issued by the Indonesian Geological Agency, Department of Energy and Mineral Resources. The soil information is required to calculate PGA using the attenuation relationships.
- A tsunami catalogue for Sumatra is compiled from many sources including BMKG (2010), NOAA (2011) and Tsunami Laboratory Novosibirsk (2005). The tsunami catalogue is used to determine tsunami rate (Figure 3.8) and the characteristics of tsunamigenic earthquakes in Sumatra (Figure 4.23).
- A gridded bathymetry data from GEBCO (2012) is utilized for the numerical tsunami analysis.
- Population data of Padang city is obtained from the Indonesian Central Bureau of Statistics based on the census conducted in 2010. This data is necessary for the estimation of fatality risk.
- Building inventory data are required for building loss estimation. Building inventory for Padang is developed based on a digital map produced by PT. Exsa International in collaboration with BAKORSURTANAL. However, the inventory map does not contain the distribution for each type of structure in the investigated area; hence, visual inspections from satellite imagery (Google Earth, 2011) are performed.

CHAPTER 5

THE PROBABILISTIC SEISMIC HAZARD ASSESSMENT OF SUMATRA

5.1. INTRODUCTION

This chapter discusses the main outcomes of the PSHA performed for Sumatra. The use of a magnitude range to represent the earthquake recurrence relation is initially investigated. The success of the declustering procedure to remove accessory shocks in earthquake catalogue is also examined. Several hazard maps are produced based on three different techniques including two based on time independent PSHA (Khan's model and the proposed model) and a time dependent model. A seismic hazard curve and a uniform hazard spectrum are produced for Padang city, West Sumatra.

5.2. VERIFICATION OF PSHA MODULE

5.2.1. The Sensitivity of the PSHA Module to Different Magnitude Ranges

As discussed in Chapter 3, the PSHA module uses specified magnitude ranges to control the seismicity for each zone. However, the outcome of the PSHA module should be consistent, regardless of the magnitude range adopted in the analysis. To investigate this, three simulations are performed using different magnitude ranges, as shown in Table 5.1. An identical earthquake catalogue is used for each simulation, and no synthetic earthquakes are included at this stage. The resulting seismic hazard maps are shown in Figure 5.1, which shows that all simulations produce comparable hazard maps. It can be concluded that the outcomes of the PSHA module do not depend on the assumed magnitude ranges providing that a sufficient number of simulations are conducted, and hence, a magnitude range of 0.5 (Type 2) is selected for this study. It should be pointed out that the hazard maps in Figure 5.1 do not represent the real earthquake hazard of Padang city, since the simulations involve limited events, which do not characterise the seismicity of the region well.

Table 5.1. Different types of magnitude range for assessing the PSHA module

Type	Magnitude Ranges						
	1	**2**	**3**	**4**	**5**	**6**	**7**
1	$0 \leq M_w < 6.5$	$6.5 \leq M_w < 6.75$	$6.75 \leq M_w < 7$	$7 \leq M_w < 7.25$	$7.25 \leq M_w < 7.5$	$7.5 \leq M_w < 8$	$M_w \geq 8$
2	$0 \leq M_w < 6$	$6 \leq M_w < 6.5$	$6.5 \leq M_w < 7$	$7 \leq M_w < 7.5$	$7.5 \leq M_w < 8$	$8 \leq M_w < 8.5$	$M_w \geq 8.5$
3	$0 \leq M_w < 4$	$4 \leq M_w < 5$	$5 \leq M_w < 6$	$6 \leq M_w < 7$	$7 \leq M_w < 8$	$8 \leq M_w < 9$	$M_w \geq 9$

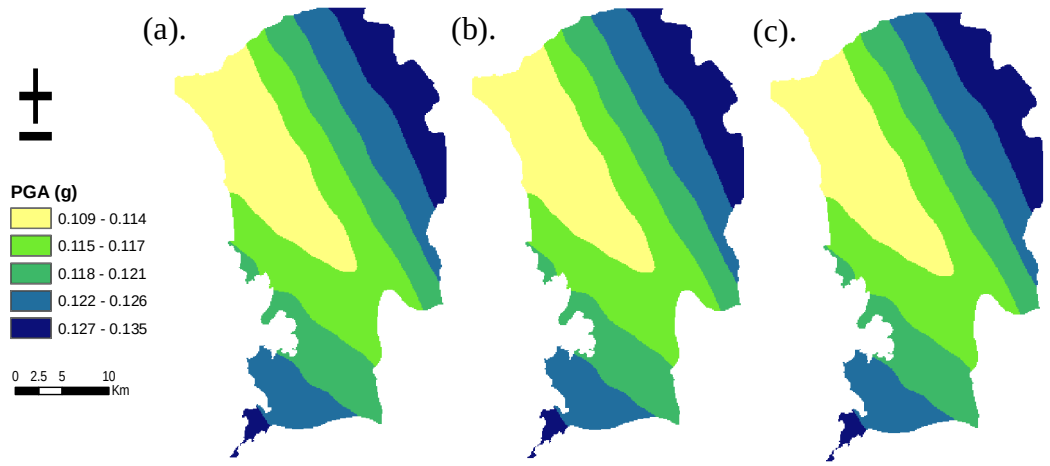

Figure 5.1. Artificial seismic hazard maps of the Padang region at 10% probability of exceedance in 50 years for magnitude range analyses: a). Type 1; b). Type 2; and c). Type 3

5.2.2. The Sensitivity of PSHA to the Number of Simulations

As discussed earlier in Chapter 2, the reliability of the stochastic seismic hazard approach increases with the number of simulations performed. Consequently, this section investigates the acceptable number of simulations that should be conducted in the case study area. Three different numbers of simulations (200, 250 and 300 simulations) are carried out for Padang city and the outcomes are compared in Figure 5.2. It can be seen that the seismic hazard maps for Sumatra region converge after 250 simulations. However, the differences of the outcomes among the three simulations are not significant. The average difference of PGA values between the 200 and 250 simulations is only 1.29%, and the average difference between the 250 and 300 simulations is only 0.72%. Lower seismicity areas may require less simulations since those areas contain less events.

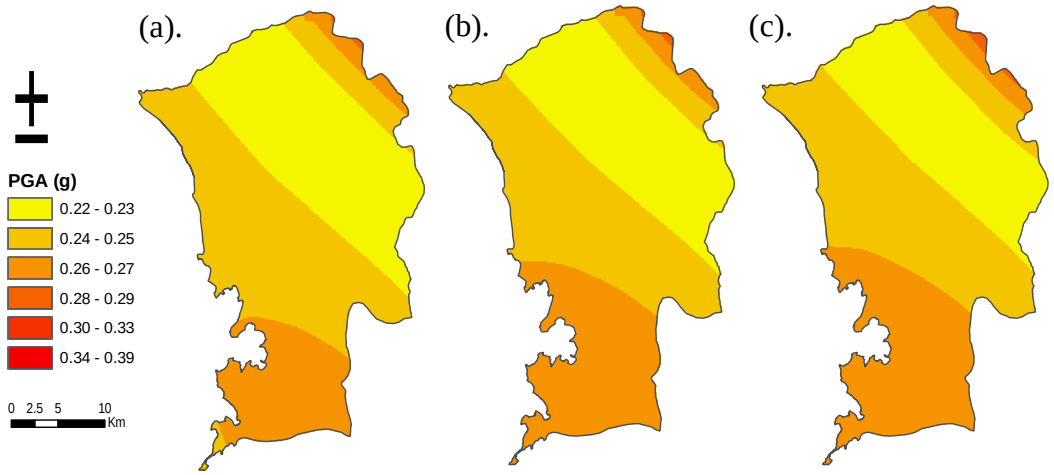

Figure 5.2. Seismic hazard maps of the Padang region at 10% probability of exceedance in 50 years for different number of simulations: a). 200 simulations; b). 250 simulations; c). 300 simulations

5.2.3. The Effects of Seismicity Declustering in Seismic Hazard Assessment

Seismicity declustering is a procedure that removes aftershocks and preshocks from the earthquake catalogue. The procedure mainly removes lower magnitude events from the earthquake catalogue to obtain only independent events. To investigate the effect of the seismicity declustering on the seismic hazard, two PSHA studies are conducted using the declustered and full (non-declustered) earthquake catalogues of Sumatra. The declustered catalogue follows Reasenberg's (1985) algorithm. The outcomes are presented in Figure 5.3(a) and Figure 5.3(b), which show comparable hazard maps. The average difference between the ground motion values calculated using the declustered and the full catalogues is about 5.5%. Since the difference between the two hazard maps is not really significant, in this study, the full earthquake catalogue is adopted for the PSHA simulations.

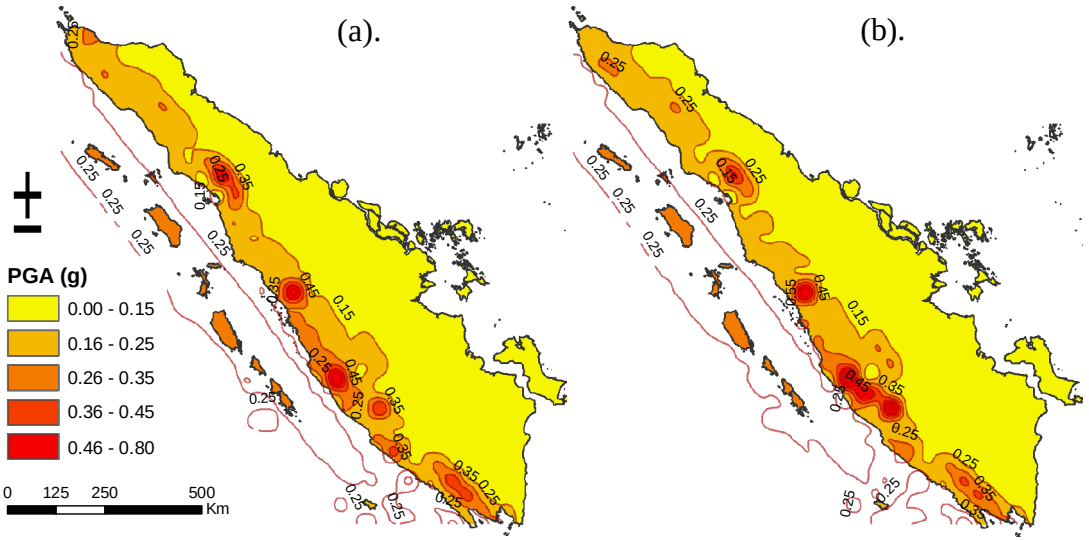

Figure 5.3. Seismic hazard maps of Sumatra at 10% probability of exceedance in 50 years for 100 simulations: a). based on full catalogue; b). based on the declustered catalogue

5.3. TIME INDEPENDENT PSHA

Although spectral acceleration is a better parameter to approximate the motion of structures under earthquake loading, the seismic hazard map produced in this study is expressed in terms of PGA. This is to consider that PGA is still used in the current Indonesian seismic code (SNI 03-1726-2002, 2002) and the majority of buildings in Padang is low rise structures with short natural period and limited ductility. For these reasons, the use of PGA is realistic. In addition, the available vulnerability curves for the buildings in the case study area are expressed in terms of PGA. The vulnerability curves are required to assess earthquake risk in the investigated area as discussed in Chapter 7.

The seismic hazard map in Figure 5.4 is produced based on the stochastic PSHA method proposed in Chapter 3. Three hundred simulations are performed based on the Monte Carlo approach. In comparison with existing hazard maps, the PGA values of the new method are considerably higher than those given in the Indonesian seismic design code for buildings, SNI 03-1726-2002 (shown in Figure 2.7). In the 2002 seismic code, the PGA of the Sumatra Fault Zone (SFZ) ranges between 0.20g and 0.25g. However, the hazard map in Figure 5.3 reveals that the ground motions

for the SFZ can reach up to 0.65g. Despite the fact that the subduction zone is capable of generating greater magnitude earthquakes, at a small source to site distance, the shallow crustal earthquakes in the SFZ may produce higher peak acceleration, as highlighted by Youngs et al. (1997).

The hazard map in Figure 5.4 appears to be comparable with the hazard maps by Petersen et al. (2004), Irsyam et al. (2008) and Irsyam et al. (2010) (see Figure 2.8 Figure 2.9 and Figure 2.10, respectively). Nevertheless, the PGA values of Petersen's and Irsyam's are better distributed around the main Sumatran faults. This is due to the nature of the conventional seismic hazard methods adopted in those studies, which tend to smooth the seismicity over a seismic source. In addition, Petersen et al. (2004) use only interplate attenuation equations for the subduction environment, which result in higher ground motion values for the subduction areas.

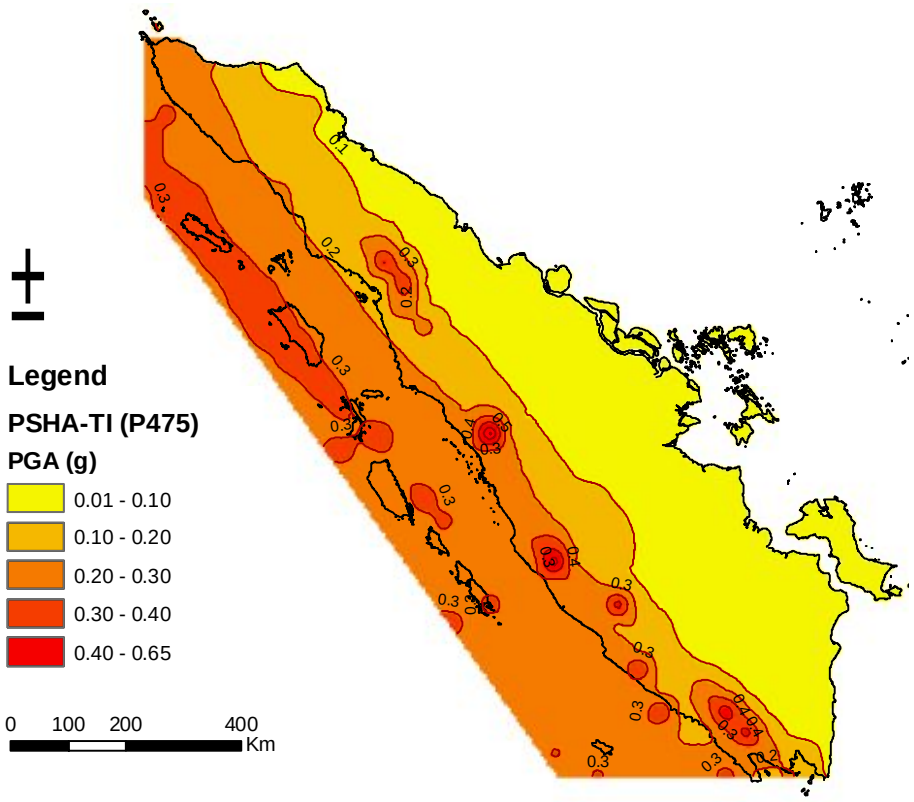

Figure 5.4. Seismic hazard maps for Sumatra for 10% probability of exceedance in 50 years based on the proposed method (300 simulations)

Figure 5.5 presents a hazard map based on Khan's approach. The ground motion values obtained from Khan's and the new method are then compared in terms of PGA ratios, as presented in Figure 5.6. The white colour grids in the figure show the

PGA values with the margin of about 15% difference from the hazard map in Figure 5.4. The 15% range is selected to consider the random nature of the stochastic PSHA, which is not likely to produce identical results for each simulation. The orange grids define the areas where PGA values are underestimated in Khan's method and the blue grids indicate overestimates. Observing the ratio distribution in Figure 5.6, it can be concluded that Khan's method tends to underestimate the hazard in the Sumatra fault area (SFZ). This is because Khan's method uses the instrumental catalogue to represent the seismicity. The instrumental catalogue of Sumatra has only been available in the last 50 years, with varying completeness periods corresponding to the magnitude of earthquakes. It is understood that the early period of the instrumental catalogue lacks low to moderate magnitude earthquakes, which dominate the seismicity in the SFZ. As a consequence, Khan's method underestimates the hazard in the SFZ. In addition, it is observed that the current seismicity of the SFZ is lower than its mean long-term seismicity, which can lead to the underestimation of the hazard in the area.

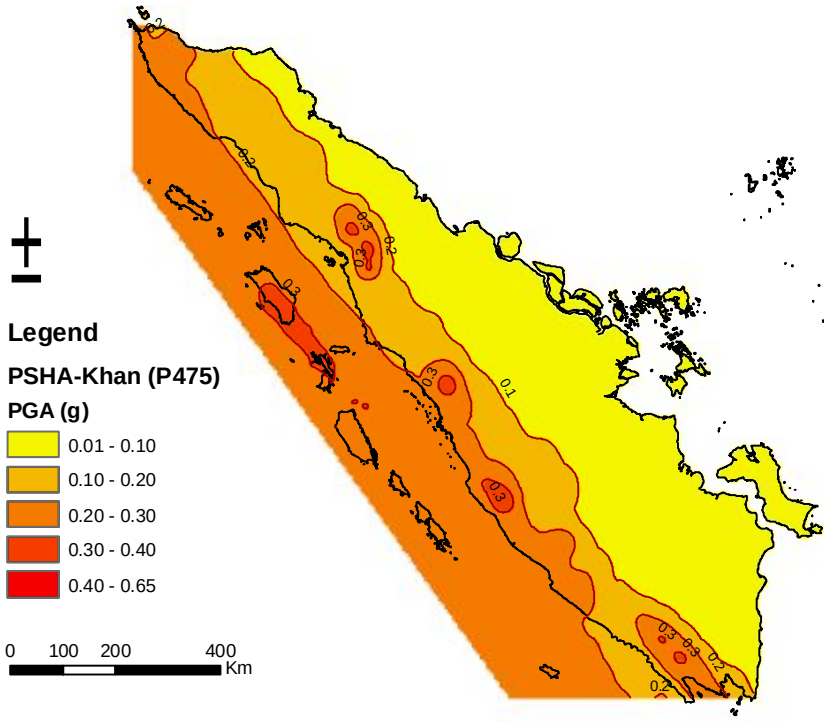

Figure 5.5. Seismic hazard maps of Sumatra for 10% probability of exceedance in 50 years based on Khan's method

On the other hand, Khan's approach seems to over-estimate the seismic hazard in the Padang segment (green box in Figure 5.6). The segment has coincidentally been

identified as a seismic gap in the Sumatra Subduction Zone (SFZ). The seismicity of the Padang segment has increased significantly since 2005 and has currently reached about 2.52 times its average long-term seismicity. It is more likely that Khan's PSHA method represents the recent seismicity of the Padang area, which results in the increment of hazard above the average long-term seismicity.

In addition, it is observed that earthquake recording in Sumatra has improved significantly since the M_w 9.1 Great Sumatra earthquake in 2004, as mentioned in Section 4.4. Hence, the increased rate of seismicity in the Padang segments becomes better documented than before.

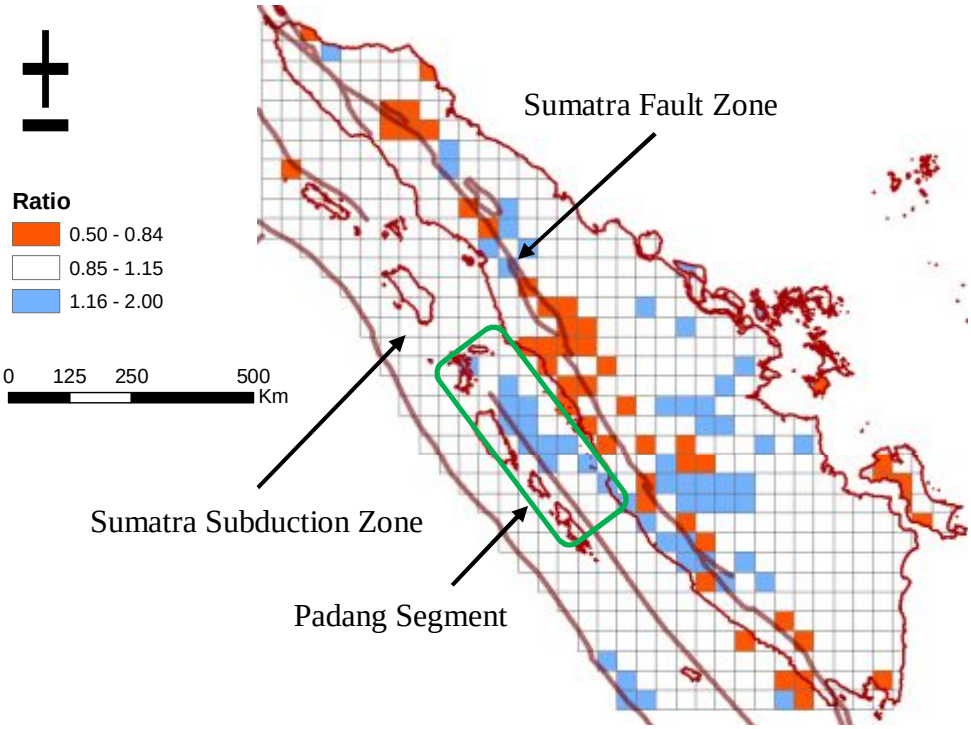

Figure 5.6. Ratio of PGA obtained from Khan's method and the new method for each grid in the case study region

5.4. THE SEISMIC HAZARD FOR PADANG CITY

Seismic hazard assessment conducted in Padang city shows that the area is likely to experience PGA of 0.24g–0.40g, as shown in Figure 5.7. The seismic hazard maps are estimated at 10% probability of exceedance in 50 years, as given in the current Indonesian seismic code for buildings (SNI 03-1726-2002, 2002). At rock site conditions, the expected PGA is around 0.24g-0.30g (Figure 5.7a), and this is

classified as "very strong" in the USGS perceived motion category (Table 5.2). However, the ground motions can be amplified by the local soil conditions (Figure 5.7b) and the most densely populated area of Padang city is likely to experience a "severe" level of ground motions of 0.35g-0.40g. The local soil condition is characterised using the geological map of Padang (Figure 4.17) and the PGA associated with the soil type of the area is determined using the attenuation relationships (see Equations 2.10 – 2.15).

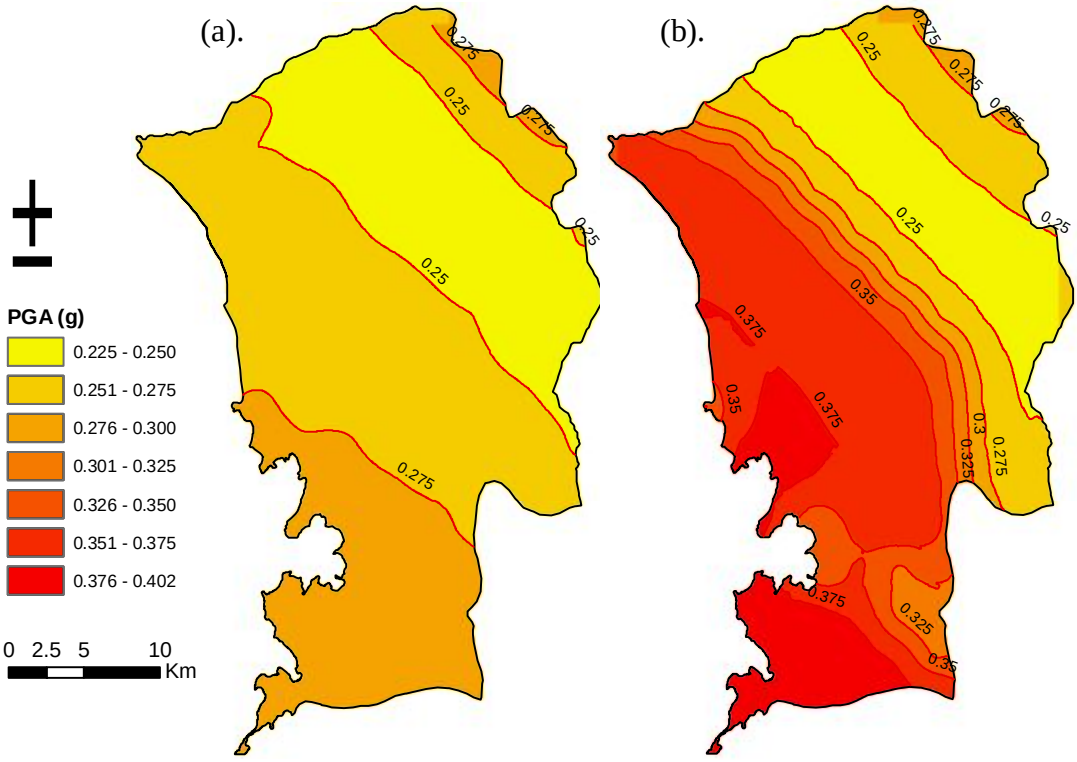

Figure 5.7. Seismic hazard map at 10% probability of exceedance in 50 years for Padang city (PGA in g): (a). on rock site condition; (b). based on the ground surface as shown in Figure 4.17.

Table 5.2. Ground motion category in terms of perceived shaking (USGS, 2009)

Perceived Shaking	PGA (g)	Perceived Shaking	PGA (g)
1. Not Felt	< 0.0017	6. Very Strong	0.1800 – 0.3400
2. Weak	0.0017 – 0.0140	7. Severe	0.3400 – 0.6500
3. Light	0.0140 – 0.0390	8. Violent	0.6500 – 1.2400
4. Moderate	0.0390 – 0.0920	9. Extreme	> 1.2400
5. Strong	0.0920 – 0.1800		

Figure 5.8 and Figure 5.9 represent the average rates of ground motions as well as their probability of exceedance in 50 years for Padang city. The average peak ground accelerations of the region are 0.23g and 0.3g for 10% and 2% probability of exceedance in 50 years, respectively. These PGA values correspond to 475 and 2500 years of return period, respectively.

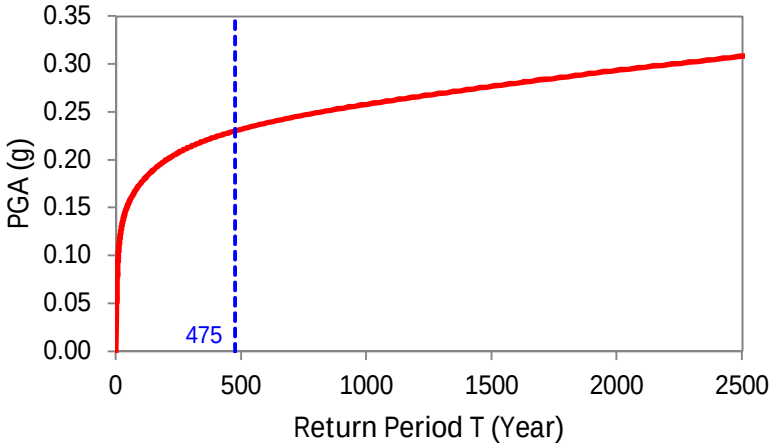

Figure 5.8. Rate of earthquake hazard for Padang city on bed rock

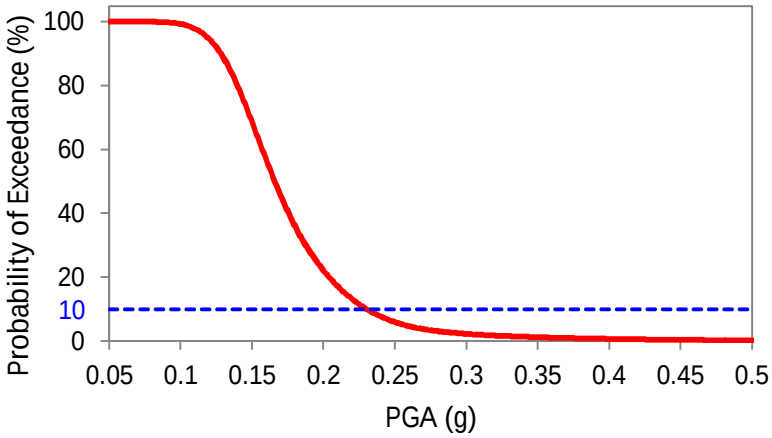

Figure 5.9. Earthquake hazard curve for Padang city for 50 years (bed rock)

The stochastic PSHA approach in this study has an advantage, in that it allows direct identification of design earthquakes that contribute to the hazard in an area. The seismic source contribution cannot be directly attained in the conventional PSHA, and therefore, a deaggregation procedure is required. As discussed in Section 2.3.2, the deaggregation procedure is known for having some issues related to the selection of bin size, the grouping of scenario and set of quantities which should be chosen as the base for the deaggregation (Abrahamson, 2006).

Figure 5.10, Figure 5.11 and Figure 5.12 show the contributions of all seismic sources, the SSZ and the SFZ to the seismic hazard in Padang, respectively. For the subduction area, the highest ground motions are mostly generated by near field events from the intraplate zone with a magnitude range of M_w 7.5-8 and focal distances of about 0-50 km from the city. The mega-thrust events on the subduction interface produce lower values of PGA. This is due to the location of the subduction interface, which is further away from the city (more than 100 km). However, the interface earthquakes are capable of producing large magnitude earthquakes with shallow focal depth, which can trigger tsunami. The earthquakes occurring on the Sumatran fault (SFZ) generally affect the eastern part of the city, which has less population and infrastructure. The significant events from this zone can be characterised as M_w 7-8 at relatively close distances to the city (around 0-100 km from Padang city).

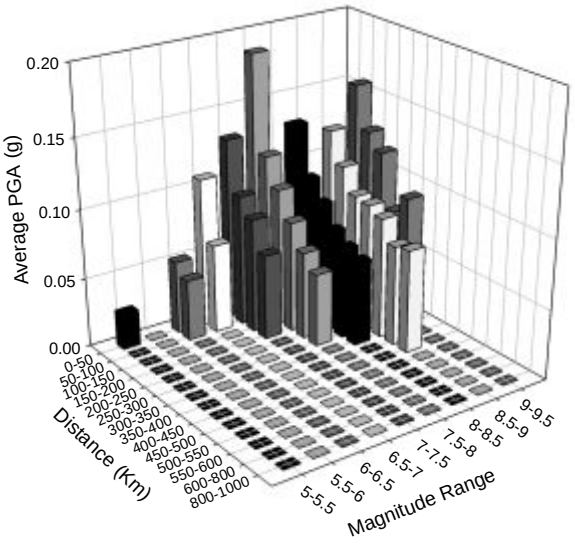

Figure 5.10. Contributions of all seismic sources to seismic hazard in Padang

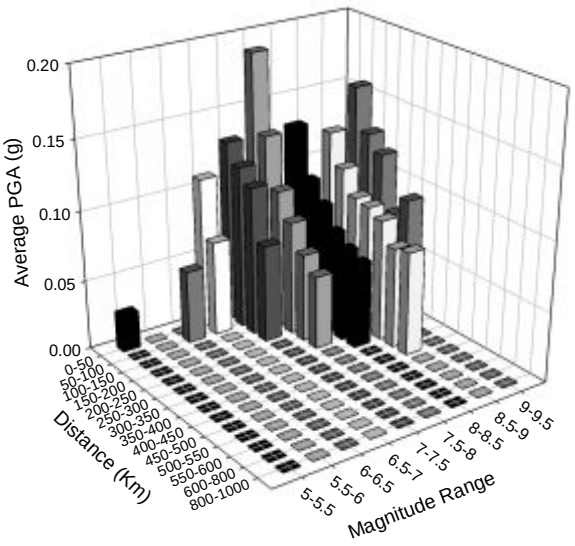

Figure 5.11. Contributions of the SSZ to seismic hazard in Padang

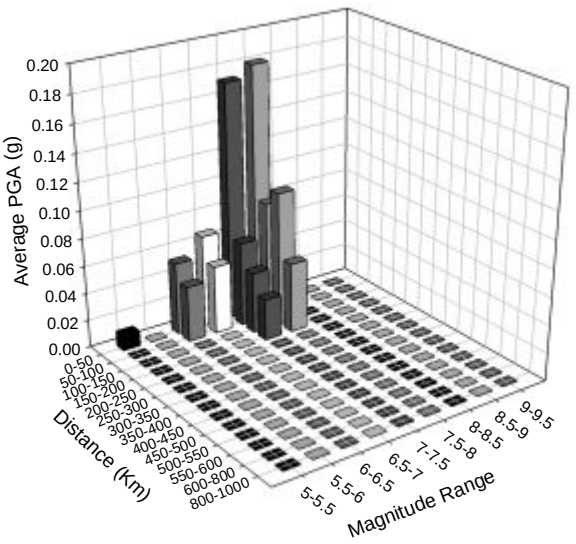

Figure 5.12. Contributions of the SFZ to seismic hazard in Padang

Previous studies show that spectral acceleration (SA) is a better parameter to represent seismic demand for buildings rather than PGA. In this study, an attempt has been made to develop uniform hazard spectra for Padang city at 475 return periods (see Figure 5.13). The hazard spectra are estimated using the attenuation equations utilised in the PSHA module (Sadigh et al., 1997; Youngs et al., 1997). For a short period ground motion (T<0.2 second), it is expected that the spectral accelerations would reach 0.76g on rock sites and 0.82g on soil. For long period ground motions (T>1 second), a lower acceleration is expected, which is 0.33g on rock sites and 0.49g on soil sites. These values are comparable with the proposed spectral

accelerations in the last revision of the Indonesian seismic code (Irsyam et al., 2010). For Padang city, the proposed code gives 0.7-0.8g and 0.3-0.4g for 0.2 second and 1.0 second of spectral accelerations, respectively. Figure 5.13 also shows the design spectrum of the 2002 Indonesian seismic code, which is assigned for Padang (Zone-5). For soil sites, it is observed that the design spectrum given in the code is still in the range of spectral acceleration obtained in this study. However, the spectral values given in the 2002 code on bed rock sites appear to be lower than those obtained in this study, particularly for short period ground motions. This problem is shown when the M_w 7.6 earthquake occurred near Padang in 2009 (Behnamfar and Afshari, 2013; Wilkinson et al., 2009). Thus, a revision of the design spectra in the 2002 seismic code is required.

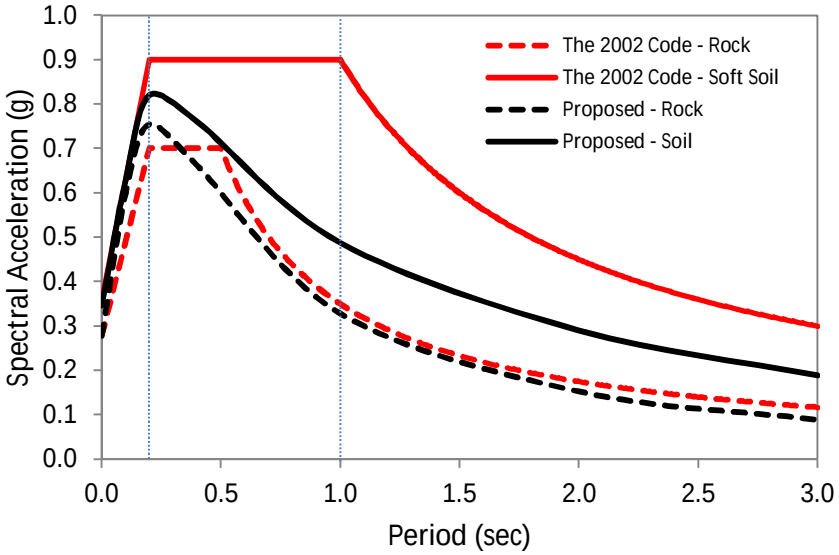

Figure 5.13. Comparison of uniform hazard spectra obtained in this study with those given in the 2002 Indonesian seismic code for Padang city (5% damping, 10% probability of exceedance in 50 years)

5.5. TIME DEPENDENT PSHA

A time-dependent PSHA is performed by modulating the seismicity about its average long-term rate. The seismicity modulation is characterised by a "varying rate" calculated using Equation 2.28. The varying rate depends on the elapsed time since the last large earthquake in a region (or fault segment), and generally, reaches its peak around large earthquakes.

In this study, the estimation of varying rates is only performed for the SSZ since the region is dominated by large magnitude earthquakes, which are assumed to have periodic recurrence intervals. Other seismic sources such as the SFZ, the Background-01 and the Background-02 zones are mostly dominated by small to moderate earthquakes, which tend to have random distribution of recurrence intervals. Moreover, unlike the SSZ, the segment boundaries of the other zones are not really apparent.

Figure 5.14 shows an example of varying rates for the Aceh Segment on the Sumatra subduction area. The last large event in the segment is the M_w 9.1 earthquake in 2004. The blue dot series in Figure 5.14 represent the varying rate estimated from the earthquake catalogue. Dashed red lines show the average of the varying rates for each 3 year period. The dashed green line shows the average of the long-term varying rate. The black line is the curve of the varying rates smoothed with a 5 year moving average window. The figure shows that the seismicity tends to decrease after the mega thrust event, and the segment is likely to experience a "varying rate" drop in the near future.

Four models are developed to observe the rates required in the time dependent approach. Model A is determined by taking the average of varying rates (the blue dot series) from 1990 to 2011, for which the $M_w \geq 4$ earthquakes are complete. Model B is the average of the varying rates between 2004 and 2011, which has been observed as the period with the highest rate. Model C and D are the exponential trends of the blue dot series and the red line, respectively, extrapolated for the next 5 years (2012-2017). The 5 year period of extrapolation is considered since the seismicity data of Sumatra are very limited and do not cover a full seismic cycle as required in the time dependent approach. For this case, a short term extrapolation is more reasonable by assuming that the seismicity does not change abruptly over a short period. The varying rates for each segment in the SSZ are summarised in Table 5.3.

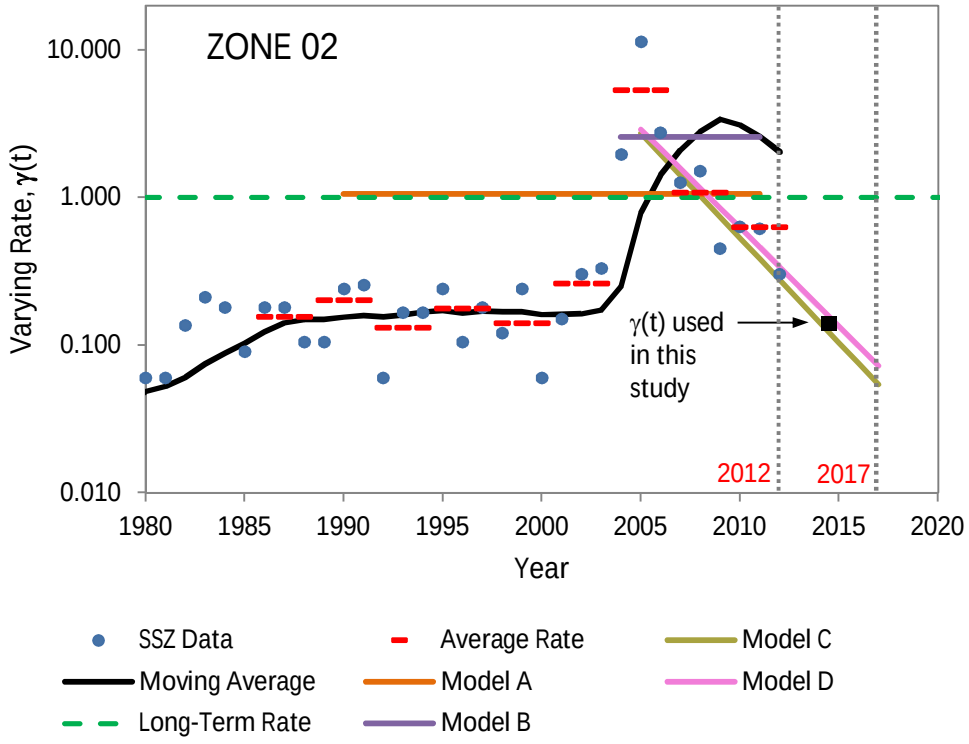

Figure 5.14. Estimation of varying rates γ(t) to modulate the seismicity on the Aceh Segment of the subduction area

Table 5.3. Extrapolation of Varying Rates

Model:	**A**	**B**	**C**	**D**	**Mean (C+D)**
Time Period	1990-2011	2004-2011	2012-2017	2012-2017	2012-2017
Method **γ(t):**	Mean	Mean	Exponential Trend (Average)	Exponential Trend (Average)	Exponential Trend (Average)
– Zone 1	3.12	7.27	0.52	0.65	0.59
– Zone 2	1.05	2.57	0.14	0.18	0.16
– Zone 3	2.17	5.49	0.83	0.76	0.79
– Zone 4	1.10	2.31	2.71	2.34	2.52
– Zone 5	0.67	1.62	2.25	1.24	1.74
– Zone 6	0.37	0.40	0.13	0.26	0.19
– Zone 7	0.43	0.55	0.82	0.43	0.62
– Zone 8	0.43	0.95	0.66	0.30	0.48

The most appropriate time dependent PSHA is the one using the average of extrapolation models C and D (see Table 5.3). The result is shown in Figure 5.15. The hazard map in the figure represents the seismicity rate of Sumatra in the next 5

years. It is observed that the middle segments of the SSZ (Zone 4 and Zone 5) are likely to experience higher ground motions in the near future in a range of 0.30-0.40g. This segment is the estimated location of the seismic gap in the subduction area (see Figure 4.5), and therefore, the time dependent approach proposed in this study is capable of capturing the non-stationary rate of seismicity in the examined area.

It should be pointed out that the time dependent PSHA in this study does not intend to predict earthquake occurrence. However, the method is aimed to look for the increasing upcoming hazard in the region; thus, appropriate mitigation strategies can be applied in the prone area.

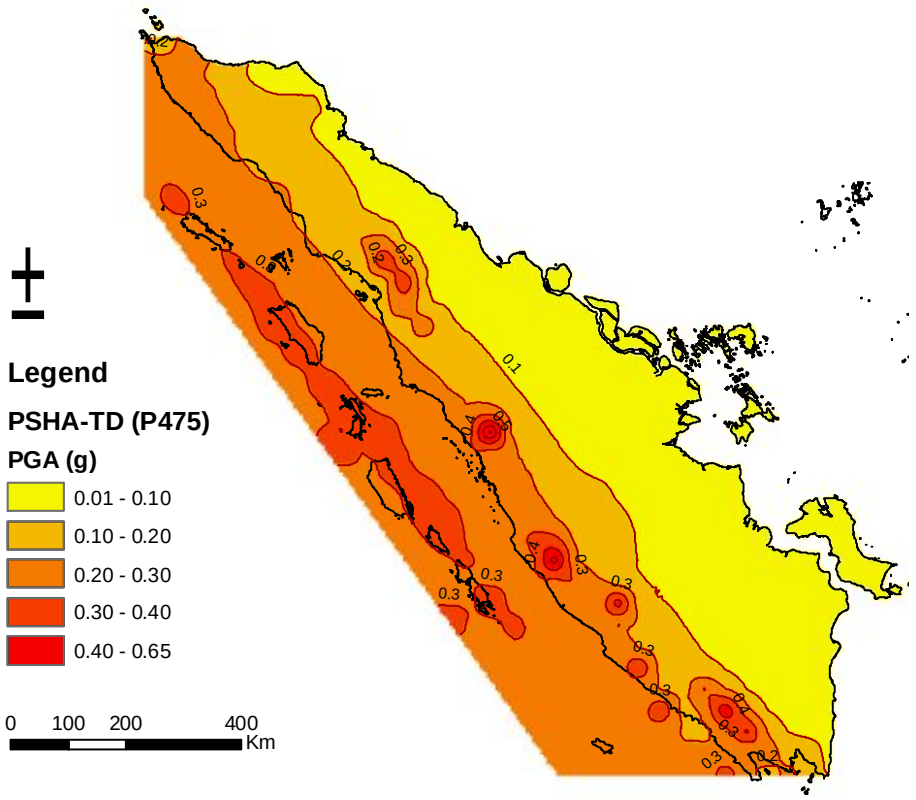

Figure 5.15. Estimated seismic hazard maps for the next 5 years at 5% probability of exceedance in 5 years

5.6. SUMMARY

- The effect of different magnitude ranges adopted in the PSHA module is investigated and appears to be negligible providing that a sufficient number of

simulations is performed. It is observed that 250 simulations are sufficient for Padang city in order to get a convergent result.

- A time independent PSHA is conducted for Sumatra and compared with those of previous studies. It is observed that the Indonesian seismic code SNI 03-1726-2002 (see Figure 2.7) applies 0.3g as the maximum PGA on bedrock in the region. However, this study finds that a maximum PGA of 0.65g on bedrock is expected in the area, which is consistent with the findings of recent studies (Irsyam et al., 2008; Irsyam et al., 2010; Petersen et al., 2004).
- For Padang city, the existing Indonesian code (SNI 03-1726-2002) applies a PGA value of 0.25g at 10% probability of exceedance in 50 years, which is about 8% higher than that obtained in this study. This study estimates an average PGA of 0.23g and 0.3g on bed rock site for 10% and 2% probability of exceedance in 50 years (see Figure 5.8 and Figure 5.9), respectively.
- It is found that uniform hazard spectra on rock site condition of this study is higher than those required in the SNI 03-1726-2002, particularly for low natural period of buildings (see Figure 5.13).
- The contributions of major seismic sources to seismic hazard in Padang are shown in Figure 5.10. The figure reveals that higher PGAs are most likely generated by near field events from the intraplate of the SSZ. However, the interface earthquakes are capable of producing large magnitude earthquakes with shallow focal depth, which can trigger tsunamis. The earthquakes occurring on the Sumatran fault (SFZ) generally affect the eastern part of the city, which has less population and infrastructures.
- A time-dependent PSHA method is developed in this study to take into account the non-stationary rate of seismicity. The method is not intended to predict earthquake, but to build more awareness to the upcoming hazards for mitigation purposes. This study finds that the middle segments of the SSZ are likely to increase (about 2.52 times for Zone 4 and 1.74 times for Zone-5) and experience higher ground motions in the near future (in a range of 0.30-0.40g).
- A time-dependent hazard map is produced for Sumatra region. The map is capable of capturing the increase rate of hazard near Padang segment, which is consistent with the location of seismic gap estimated from previous studies (see Figure 5.15).

CHAPTER 6

THE PROBABILISTIC TSUNAMI HAZARD ASSESSMENT OF SUMATRA

6.1. INTRODUCTION

The outcomes of the tsunami hazard assessment are presented in this chapter. The tsunami numerical simulations for Sumatra are first examined and the relationship between tsunami wave heights and earthquake magnitudes is discussed. The expected arrival time of tsunami waves for various distances from the coastal area of Padang is also assessed. The attained results are incorporated into a tsunami hazard framework for which the expected height of tsunami for Padang city is identified probabilistically. The expected wave height that corresponds to a 10% probability of exceedance in 50 years is determined for the Padang region.

6.2. DISCUSSION OF TSUNAMI NUMERICAL SIMULATIONS

6.2.1. The Effect of Fault Types on Tsunami Heights

The outcomes of typical tsunami simulations are presented in Figure 6.1 to Figure 6.5. The full results are shown in Appendix B. As expected, the maximum heights of tsunami are proportional to the moment magnitude (M_w) of earthquakes. The main components for determining M_w include fault rupture area and average displacement, as shown in Equations 2.35 and 2.36. The vertical component of fault displacements plays important role in producing higher tsunami waves. To verify this, two tsunami simulations with different types of ruptures (thrust and strike slip faults) are performed and the resulting wave heights are compared in Figure 6.1(a) and Figure 6.2(a). Identical earthquake magnitude as well as similar epicentral location is set for both models. It is found that the maximum wave amplitude for the thrust event is almost 5 times that of the strike slip event. Since the main tsunami source of Sumatra is the Sumatra Subduction Zone (Figure 4.7), which generates thrust events, the tsunami hazard assessment in this study only takes into account the thrust fault earthquakes from this zone.

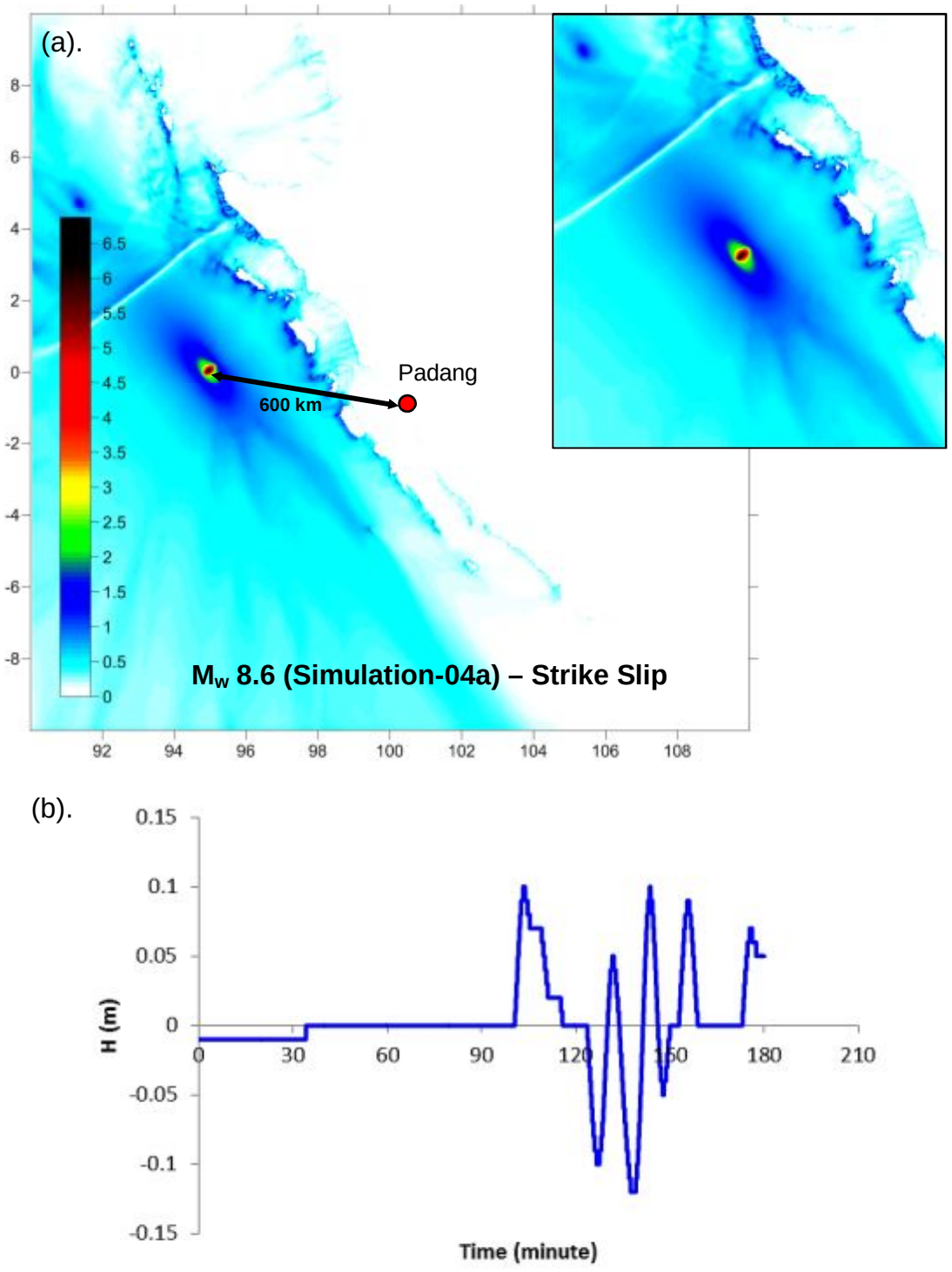

Figure 6.1. Tsunami numerical simulation for Sumatra (strike slip rupture mechanism): a). Maximum tsunami amplitudes; and b). Tsunami amplitudes with time recorded at the gauge stations in Padang area

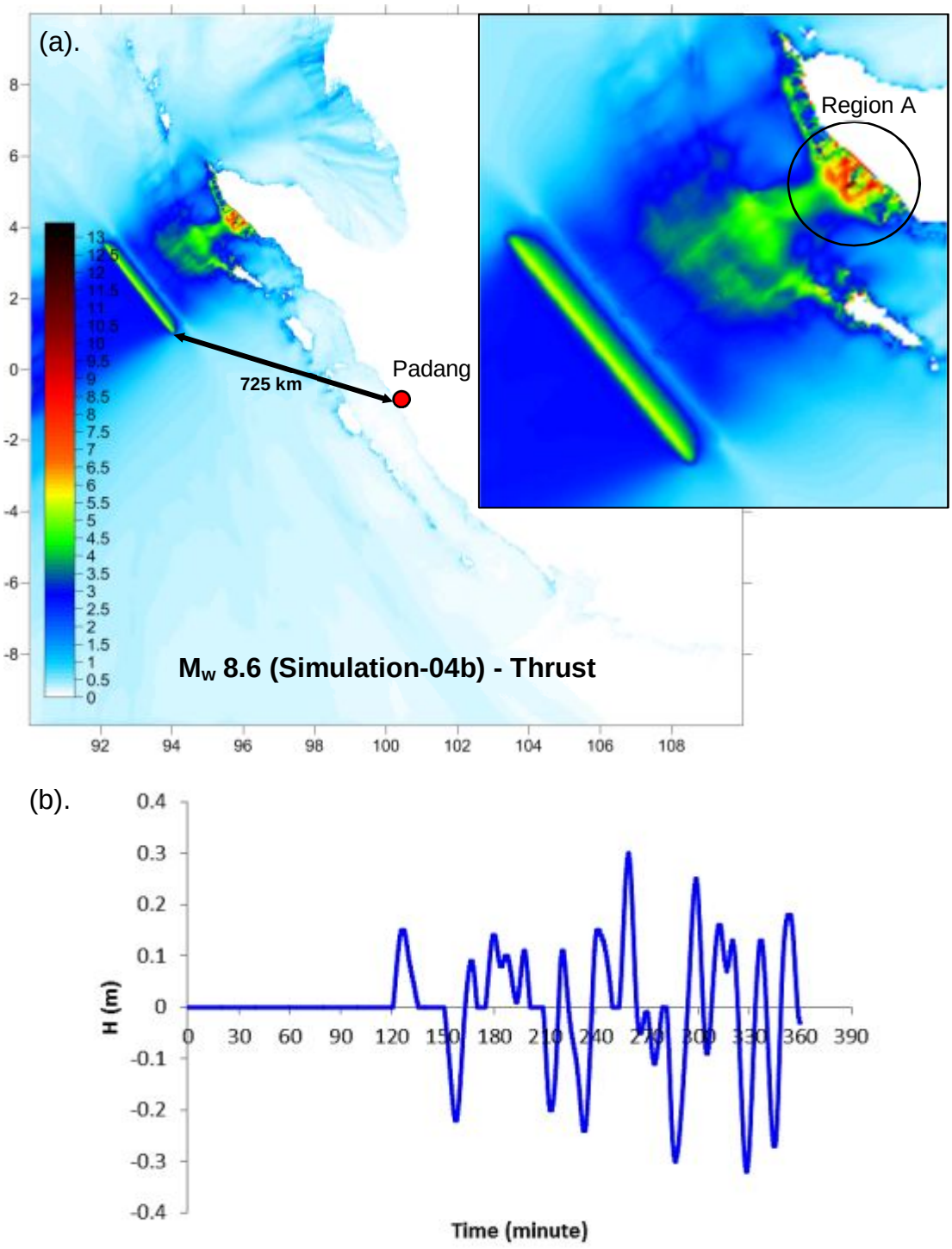

Figure 6.2. Tsunami numerical simulation for Sumatra (thrust rupture mechanism): a). Maximum tsunami amplitudes; and b). Tsunami amplitudes with time recorded at the gauge stations in Padang area

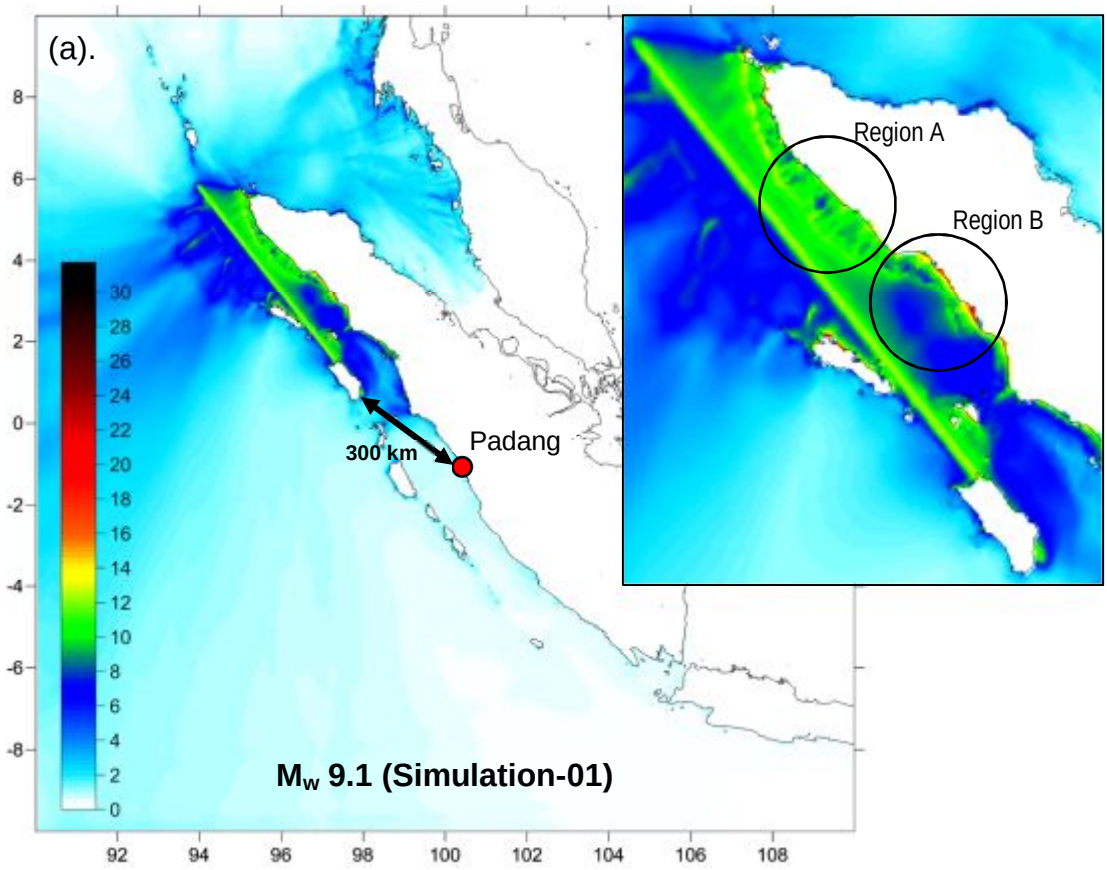

Figure 6.3. Tsunami numerical simulation for Sumatra: a). Maximum tsunami amplitudes; and b). Tsunami amplitudes with time recorded at the gauge stations in Padang area

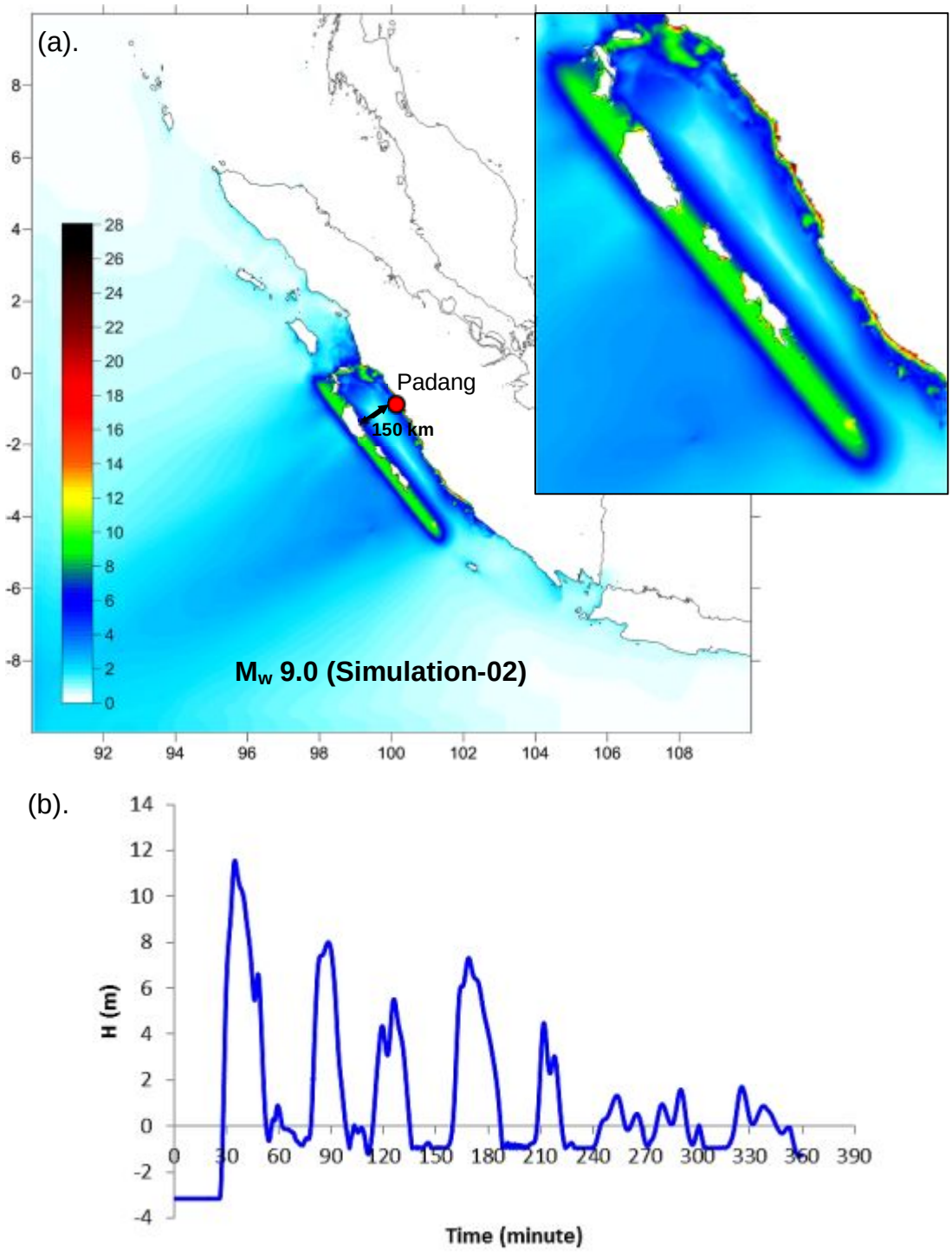

Figure 6.4. Tsunami numerical simulation for Sumatra: a). Maximum tsunami amplitudes; and b). Tsunami amplitudes with time recorded at the gauge stations in Padang area

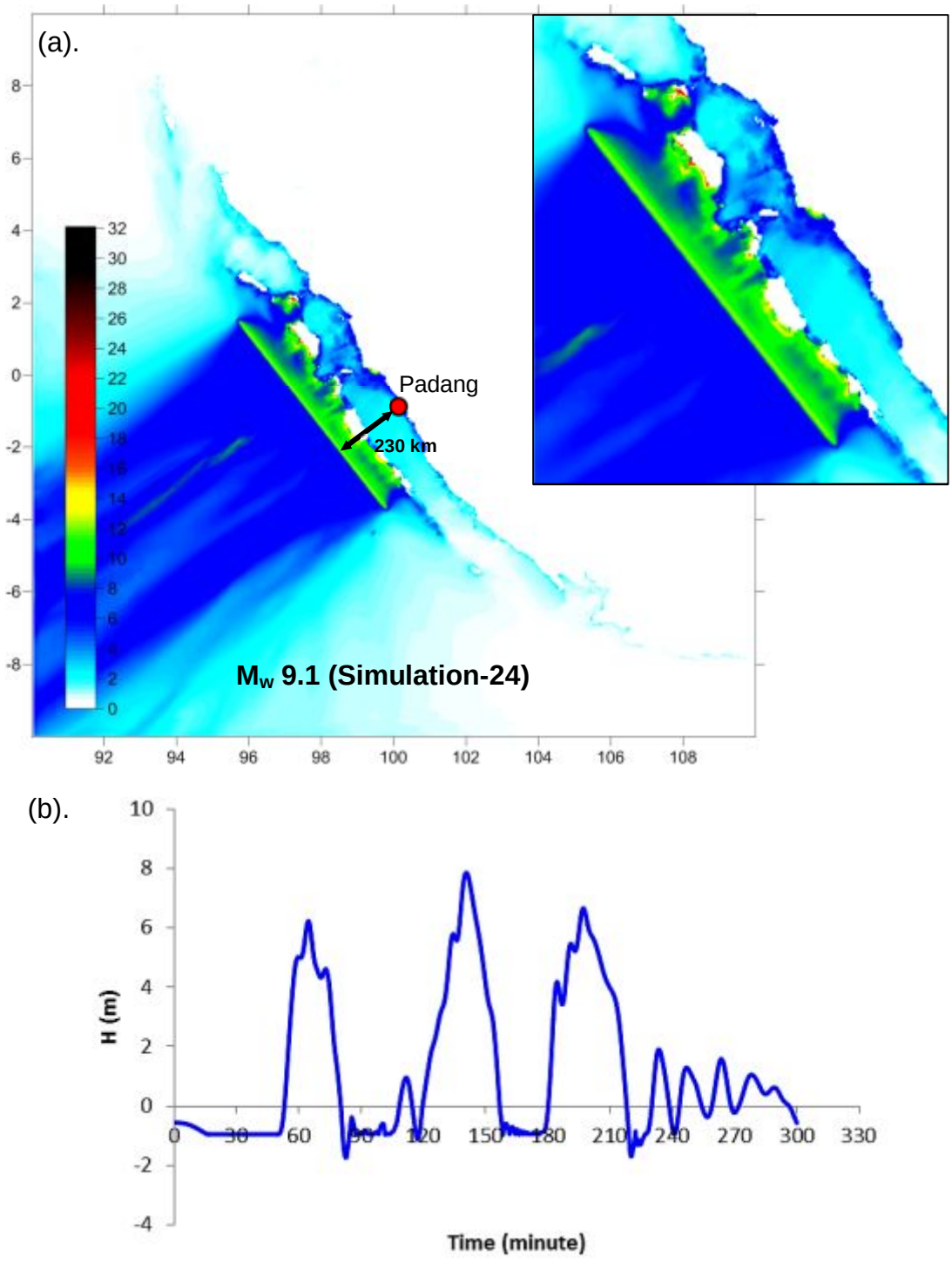

Figure 6.5. Tsunami numerical simulation for Sumatra: a). Maximum tsunami amplitudes; and b). Tsunami amplitudes with time recorded at the gauge stations in Padang area

6.2.2. Tsunami Arrival Time at Padang City

The travel time of tsunami waves to the coast of Padang city is also examined. The time histories for several simulations are shown in Figures 6.1(b) to 6.5(b), and the correlation of tsunami travelling time with distance is shown in Figure 6.6. As discussed earlier, most tsunamis in Sumatra are triggered by thrust earthquakes in the subduction zone. For the near-field intraplate earthquakes, the waves could reach the shoreline within 15 minutes following the earthquake. However, the earthquake magnitudes in the intraplate zone are generally smaller and deeper than those in the subduction interface, resulting in lower tsunami potential. For the interface events, the distance of tsunami source is around 100-300 km from the coast of Padang. Consequently, the travelling time to Padang city is approximately 25 minutes or longer, depending on the distance to the tsunami source. This finding is consistent with a tsunami study conducted by Borrero et al. (2006) for western Sumatra.

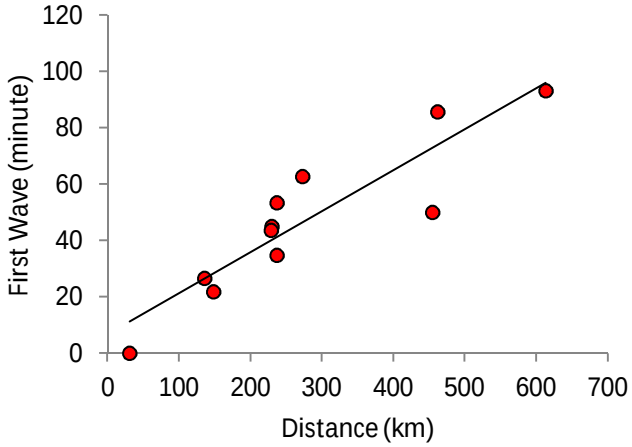

Figure 6.6. Arrival time of first tsunami waves at Padang city with distance from tsunami source

The tsunami time histories reveal that the coastal area of Padang city can be subjected to a series of tsunami waves in one tsunami event. For close distance tsunamis, the first wave is likely to have the maximum amplitude, as seen in Figure 6.4(b). However, this might not be the case for long distance tsunamis. Since tsunami waves do not travel at the same speeds, the maximum wave could reach the coastal area after several waves, as seen in Figure 6.2(b), Figure 6.3(b) and Figure 6.5(b).

6.2.3. The Effect of Bathymetry

It is also observed that the region close to the tsunami source and directly facing the rupture line is likely to experience higher tsunami waves (see Figure 6.2(a) to Figure 6.5(a)). However, maximum wave heights in different regions can vary, depending on the bathymetric profile of the oceanic floor. The tsunami waves can be shoaled, refracted or diffracted by bathymetric obstacles (i.e. islands, sea mounts, etc.) so that the tsunami energy gets focussed (or defocussed) towards a shoreline.

Figure 6.2(a) and Figure 6.3(a) show that the tsunami waves have reached maximum heights before reaching the shore. It appears that some of the tsunami energy is dissipated in the continental shelf, which results in smaller wave heights onshore. This phenomenon is likely to be caused by the bathymetric profile of the area, which has wider continental shelf. As the tsunami moves into shallow water, the waves shoal resulting in increasing wave heights. However, the wave speeds and lengths are decreased and the wave periods remain constant.

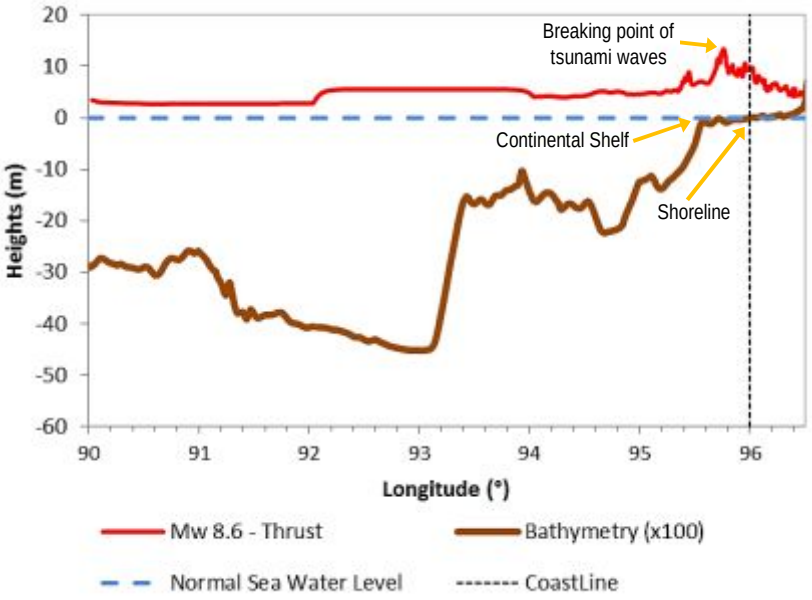

Figure 6.7. Cross section of bathymetry facing West of Aceh vs. tsunami run-up triggered by the artificial M_w 8.6 earthquake (Figure 6.2)

Figure 6.4(a) and Figure 6.5(a) demonstrate two different events of tsunami near Padang region with earthquake magnitudes of M_w 9.0 and M_w 9.1, respectively. The fault rupture of the first event is located below the Mentawai islands and the latter

event is situated close to the interface of the Sumatra subduction zone. The event illustrated in Figure 6.4(a) produces major consequences for the city of Padang. Maximum tsunami amplitude of 20 m is expected from such event. This condition might be exacerbated by steep bathymetry at the coast of Padang. Figure 6.8 reveals that, despite being closer to the tsunami source, the maximum tsunami amplitude at the Mentawai islands is comparable to that at the Padang area. This finding is in line with Abe's (1995) approach that applies constant maximum amplitudes for regions close to the tsunami source. Figure 6.5(a) reveals that the Padang area is shielded by the Mentawai islands from a tsunami event in the subduction interface. As a consequence, the tsunami heights tend to decrease in most areas of Padang. Nevertheless, significant tsunami heights are still likely to occur along the coastal area of Padang due to the refraction and the focussing effect of tsunami waves.

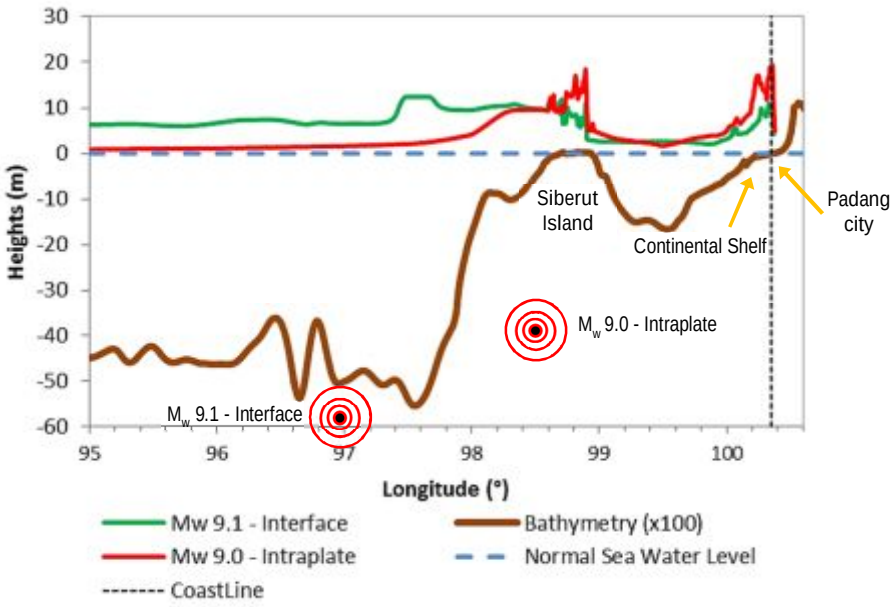

Figure 6.8. Cross section of bathymetry facing Padang city vs. tsunami run-up triggered by the M_w 9.1 (Figure 6.5) and M_w 9.0 (Figure 6.4) earthquakes

6.3. ESTIMATION OF TSUNAMI RUN-UP HEIGHTS FOR SUMATRA

The correlation between earthquake magnitude scale (M_w) and tsunami wave heights for Sumatra is estimated based on a method proposed by Abe (1979, 1981, 1985, 1995), as presented in Section 2.4.3. The results of tsunami numerical analyses for

Sumatra for four different magnitudes are utilised and compared in Figure 6.9. The figure shows the attenuation of tsunami waves with distances for the four earthquake magnitudes. The least square solutions for the results of magnitudes 9.1, 8.7, 8.5 and 7.8 produce the gradients (or "*a*" values) of 1.012, 1.034, 0.983 and 1.048, respectively. The "a" value of 1 is, therefore, adopted for Sumatra, and this is consistent with the findings of Abe (1995).

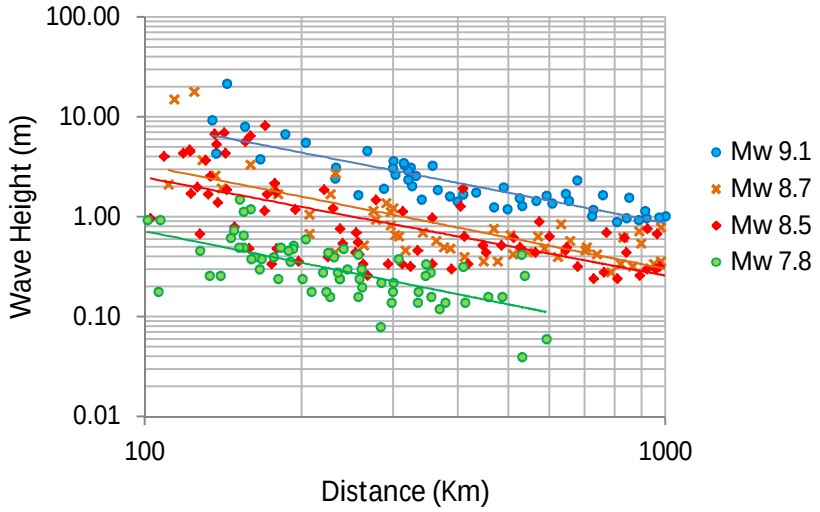

Figure 6.9. Attenuation of tsunami wave amplitudes with distances

The constant "D" in Equation 2.34 for each data series is estimated using the least square fit, which results in a value of 5.91 with a standard error of 2.77 for tsunami height. Consequently, the tsunami heights for the Sumatra region are estimated as follows:

$$\log H_t = M_w - \log(R) - 5.91 \qquad 6.1$$

where,

H_t : the heights of tsunami waves (m)

M_w : the moment magnitude of earthquake

R : the closest distance from tide station to tsunami source (km)

To avoid excessively high wave amplitude near the tsunami source, Abe (1995) suggests that the relation above should be limited to a minimum distance of "R_0" and above. The value of "R_0" is taken as the radius of a circular fault, as shown in Equation 2.38. However, this study finds that half of the fault rupture width, or $R_W/2$, defined by Wells and Coppersmith (1994), is more appropriate for limiting

the minimum distance in the investigated area. Therefore, the tsunami heights near the source can be estimated as follows:

$$R_0 = \frac{1}{2} . 10^{(0.41 M_w - 1.61)} \quad 6.2$$

$$\log H_r = M_w - \log(R_0) - 5.91 \quad 6.3$$

where,

R_0 : minimum distance (km)

H_r : limiting tsunami height near the source (m)

Figure 6.10 compares the tsunami heights (H_t) obtained using R_0 defined by Abe (1995) and R_0 proposed in this study. Abe's approach tends to underestimate the maximum tsunami height and the R_0 proposed in this study can approximate the maximum tsunami height well. The figure shows that some observed data in the brown circle appear to be significantly lower than those of the estimated relations. This deviation can be caused by the bathymetry effect of the adjacent coastline with wider continental shelf resulting in low tsunami heights.

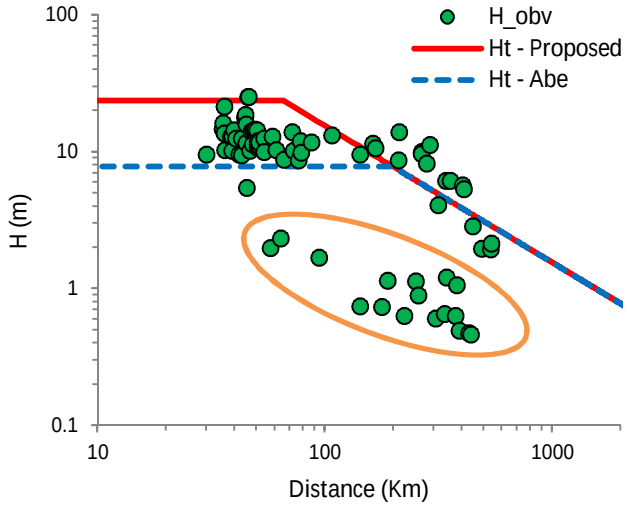

Figure 6.10. Comparison of maximum tsunami heights (H_t) estimated using R_0 proposed by Abe (1995) (dashed blue line) and R_0 proposed in this study (solid red line)

Figure 6.11 shows the correlation between tsunami magnitude and earthquake moment magnitude calculated using the equations proposed in this study.

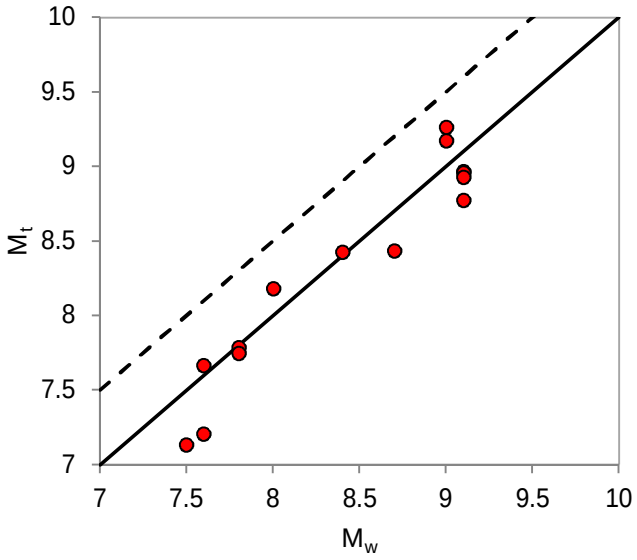

Figure 6.11. Correlation between M_t and M_w for Sumatra: the solid line expresses $M_t = M_w$ and the dash line shows a threshold for tsunami earthquake

Abe (1995) compared the tsunami height (H_t) relationship with the observation data and found that H_t statistically represented the local mean heights of tsunami; $2H_t$ characterised the maximum of local mean heights; and $2H_r$ represented the observed maximum heights or the limiting run-up heights for large earthquakes. A similar outcome is obtained in this study. However, it is found that Equation 6.1 is applicable only if the investigated areas are not directly facing the tsunami sources. This problem is shown in Figure 6.12 in which the tsunami heights, estimated with Equations 6.1 to 6.3, and the data obtained from the tsunami numerical analysis are compared. The figure shows that the data in the dashed-black boxes tend to deviate from the estimated tsunami relationships (blue and red lines). The data in the dashed-black boxes represent the events which are directly opposing the corresponding tsunami source or fault rupture line. For this case, the limiting tsunami height ($2H_r$) is more appropriate. As a consequence, this study applies $2H_r$ to estimate the maximum wave heights at areas with near-field distance ($<R_0$) or directly facing the rupture line.

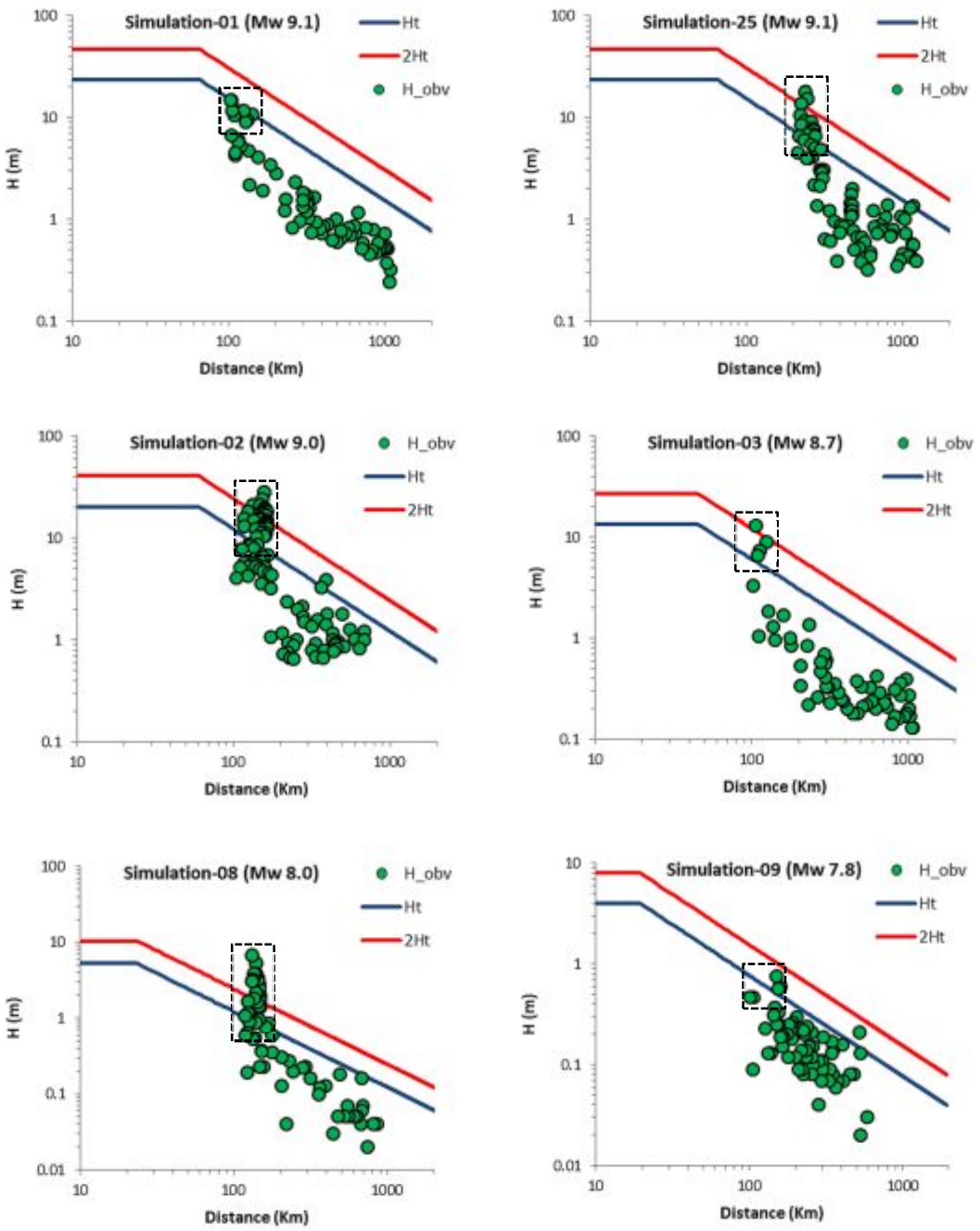

Figure 6.12. Comparison among the estimated local mean tsunami height (blue line), the estimated local maximum at each segment (red line) and the observed maximum tsunami wave heights (green circle). Most events in the dashed boxes are either located near field or directly facing the tsunami sources

6.4. PROBABILISTIC TSUNAMI HAZARD ASSESSMENT

6.4.1. Probabilistic Tsunami Hazard Analysis for Sumatra

The potency of tsunami hazard in Sumatra is assessed probabilistically based on the stochastic method presented in Section 3.3. The tsunami hazard for Sumatra at 10% probability of exceedance in 50 years (a 475 return period) is shown in Figure 6.13. The hazard is determined based on the average long-term rate of seismicity of Sumatra and, hence, it follows the time independent approach.

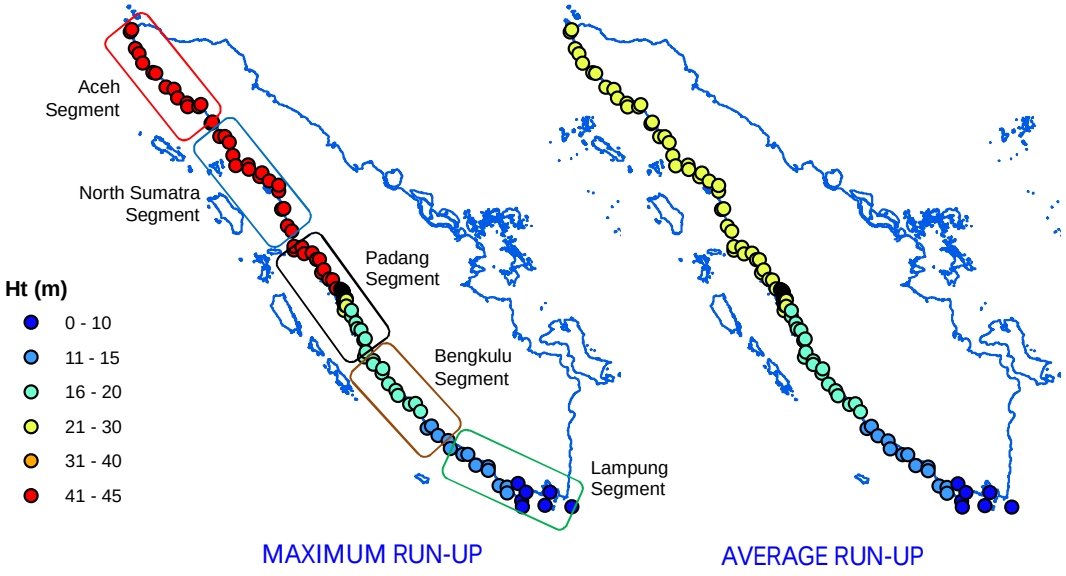

Figure 6.13. Time independent PTHA for 475 return period of tsunami

By assessing the tsunami hazard on the west coast of Sumatra, it appears that the upper sections (Aceh, North Sumatra and part of Padang segments) are more susceptible to higher tsunamis. These segments are known to have higher seismicity with historic mega magnitude earthquakes. A maximum tsunami run-up of 50.5 m was recorded in Aceh during the catastrophic Indian Ocean tsunami in 2004 (NOAA, 2011). The M_w 9.1 earthquake that triggered the tsunami had an estimated return period of about 500 years. This study obtains a maximum tsunami height of 42 m for the area. The outcome is reasonable considering that the obtained tsunami height corresponds to a return period of 475 years. In addition, Gusiakov (2012) and BMKG (2010) recorded the tsunami heights of 34.5 m and 30 m, respectively, for the event, which are comparable with the estimated average run-up for Aceh area, as shown in Figure 6.13.

The Aceh segment has deeper sea than that of the lower segments (see figures 4.24 and 4.25). A tsunami occurring at deeper sea displaces more volume of water, which can generate more energy as well as higher tsunami waves. Unlike the middle part of the island (North Sumatra and Padang segments), the Aceh segment is not shielded by adjacent offshore islands. The adjacent islands can act as a barricade and dissipate part of the tsunami energy, particularly from the events occurring at the interface of the subduction zone. This boundary condition is also occurring at Bengkulu and Lampung segments of the southern part of Sumatra.

The North Sumatra and Padang segments are situated in the middle of an active subduction zone. This might intensify the level of hazard in the areas. It is known that the rupture zone of a mega magnitude earthquake can extend to hundreds or thousands kilometres from its epicentre. As a consequence, the tsunami hazard in the North Sumatra and Padang segments may be compounded by events from their upper and lower segments.

Local bathymetry can also have an effect to the extent of tsunami hazard in an area. The North Sumatra segment is likely to experience lower tsunami heights due to its wider continental shelf along the coastline. In contrast, the Padang segment has narrower bathymetry which can lead to an increase in the impact of tsunami waves.

The Lampung segment has a relatively low level of tsunami hazard compared with the other segments. It is found that the region is mostly dominated by lower magnitude earthquakes (up to M_w 7.9) resulting in lower tsunami probability and lower level of tsunami hazard.

To take into account the non-stationary rate of seismicity with time, a time dependent tsunami hazard assessment is also performed as shown in Figure 6.14. The hazard map is produced based on the outcome of the time dependent PSHA (see Section 2.3.4). In this case, the seismicity rate of the subduction zone in the investigated area is examined and extrapolated for the next 5 years (from 2012 to 2017). The results show that the level of hazard for the Aceh segment has significantly decreased since the last tsunami in 2004. However, the hazard increases at the southern part of the island (Padang and Bengkulu segments), as shown in Figure 6.14. This finding is expected and consistent with the outcomes of the time dependent PSHA. The existence of a seismic gap in the middle part of Sumatra has increased the tsunami

hazard in those areas. As a consequence, the hazard level for the surrounding regions is also increased due to the extension of earthquake fault ruptures. This condition is shown in Figure 6.14 where the level of hazard at the lower tip of the North Sumatra segment and the upper tip of the Lampung segment is increased.

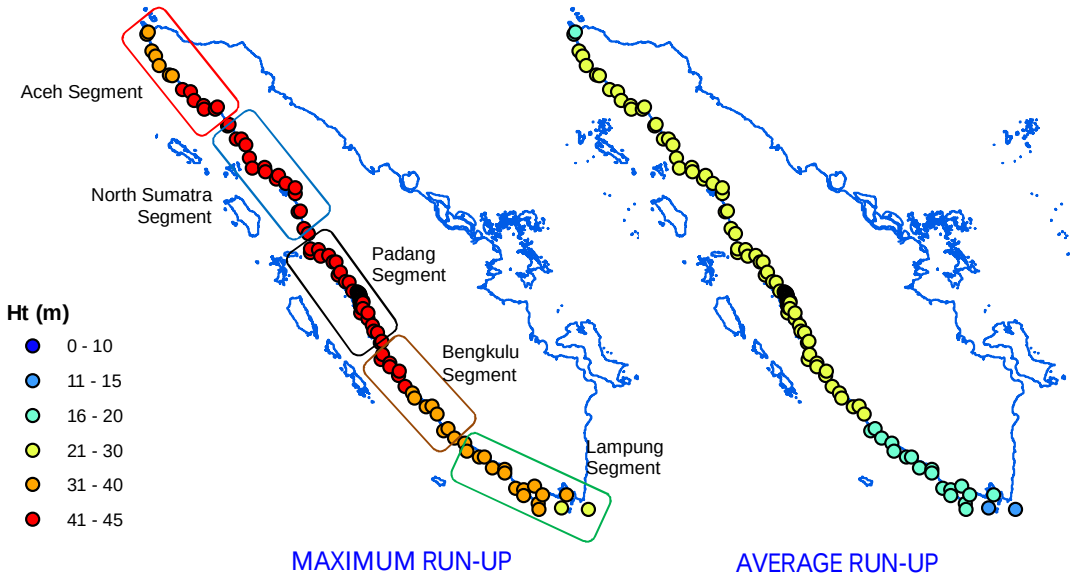

Figure 6.14. Time dependent PTHA (2012-2017) for tsunami events with a 475 return period

6.4.2. Tsunami Rate and Hazard Curve for Padang City

The probabilistic tsunami hazard assessment performed in this study reveals that the city of Padang is susceptible to an average tsunami height of 20.7 m at 10% probability of exceedance in 50 years. However, the heights of tsunami can vary across the region depending on the local bathymetry and topography in the area. Figure 6.15 shows the estimation of tsunami height above the base of structures, which is basically the difference between the average tsunami height and the ground elevations of the region. The figure highlights the high tsunami risk along the coastal area of Padang, particularly at the northern part of the city with a low lying area.

The corresponding rate of tsunami hazard is plotted in Figure 6.16, which shows that the return period of significant tsunami ($\geq$ 10 m) is relatively long, approximately 200 years. A hazard curve that implies the probability of exceedance for each tsunami height in 50 years is shown in Figure 6.17. An average tsunami height of 28 m is expected for 2500 years of return period corresponding to 2% probability of

exceedance in 50 years. The hazard curve is compulsory to determine the required tsunami height for tsunami design loads of structures.

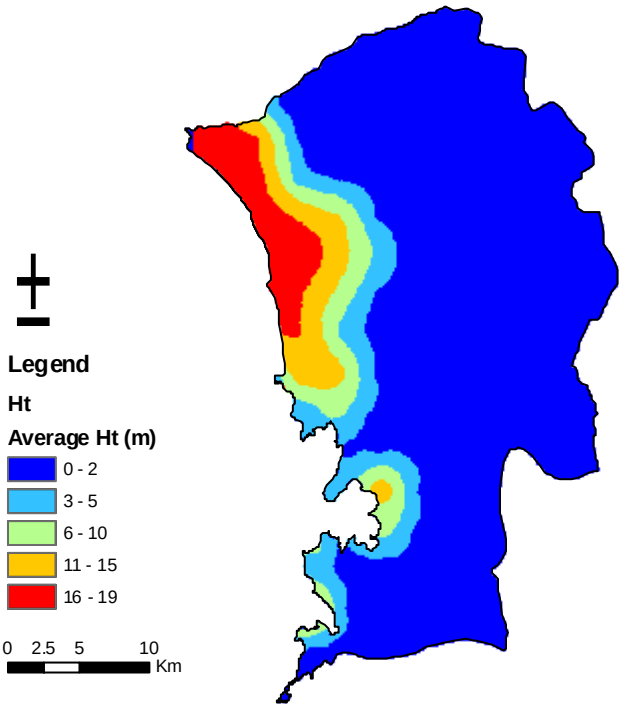

Figure 6.15. The estimated tsunami height above the base of structures for Padang city at 10% probability of exceedance in 50 years

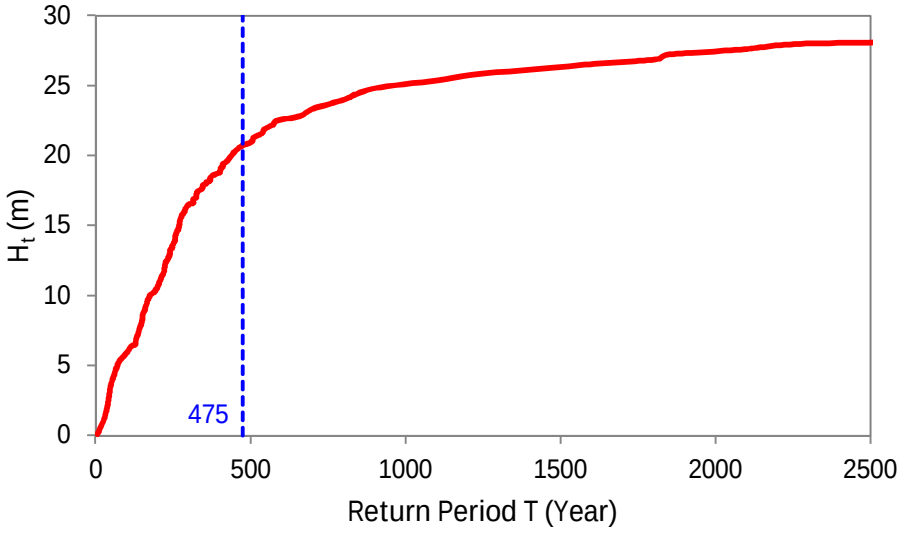

Figure 6.16. The rate of tsunami hazard for Padang city

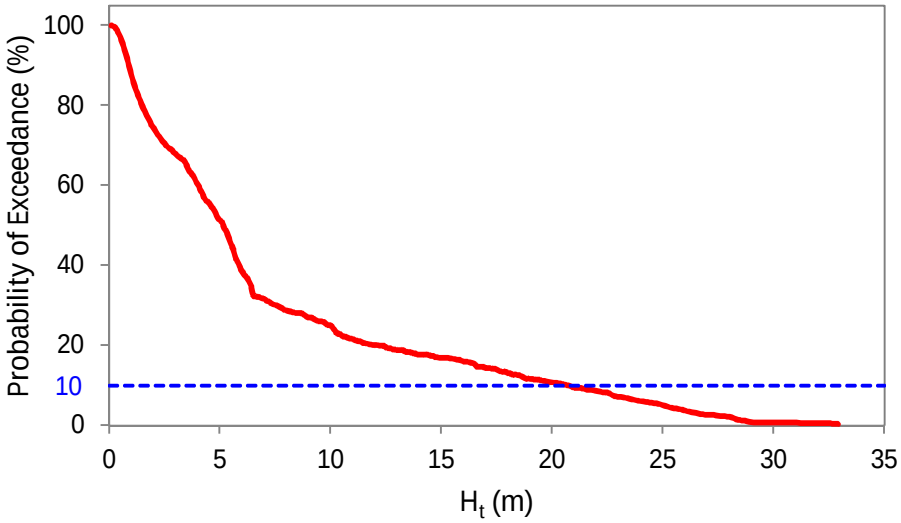

Figure 6.17. Tsunami hazard curve for Padang city for a 50 year period

6.4.3. Deaggregation of Tsunami Hazard for Padang City

Figure 6.18 shows the deaggregation of tsunami hazard for Padang city in terms of earthquake magnitudes and epicentral distances. It is observed that the near field tsunamis in the subduction intraplate zone have less contribution to the tsunami hazard in Padang city. In addition, most of the tsunamis in this zone are triggered by earthquake magnitudes of M_w 7.0 and above. It is also found that the highest tsunamis for the area are produced by earthquakes with a magnitude range of M_w 9.0-9.5 with an epicentral distance of about 150-200 km from the city. The tsunami sources of these events are located at the interface of the subduction zone, which is perpendicular to the city. Figure 6.18 also reveals that most tsunamis at the subduction interface are generated by earthquakes with $M_w \geq 8.0$ and long distance events occurring in this zone are capable of inundating the city with a considerable tsunami height. A distant tsunami, as far as 400 km from the tsunami source, can produce great consequences to the city. This finding highlights the difference between earthquake and tsunami hazard assessment. Unlike earthquake hazard assessment, tsunami hazard assessment has to take into account distant events.

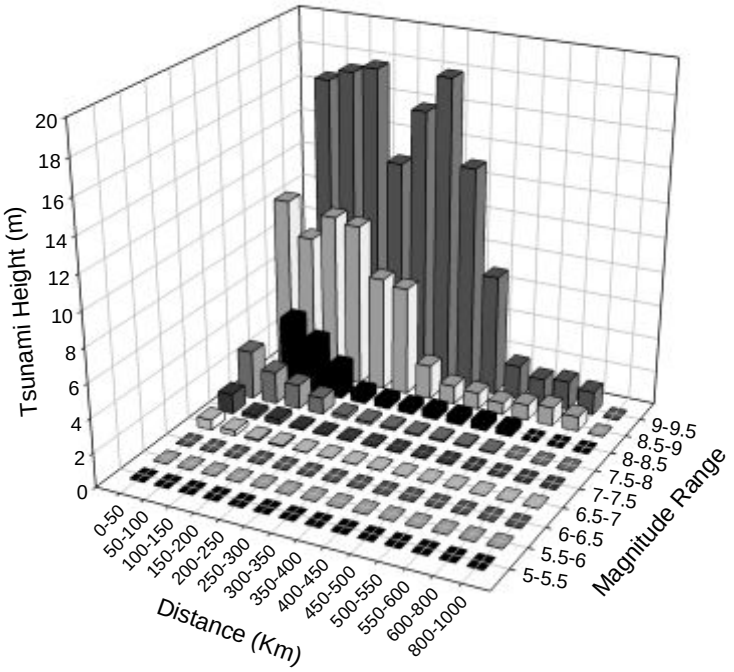

Figure 6.18. Average tsunami heights for each range of earthquake magnitudes and distances that contributes to Padang city

6.5. ESTIMATION OF TSUNAMI FORCES ON BUILDINGS

6.5.1. Determination of Tsunami Wave Parameters and Inland Penetration for Padang City

Tsunami wave parameters (i.e. velocity and distance of inundation area) can be determined by a detailed numerical model with a very fine grid size (< 10 m) in tsunami run-up zones (FEMA P646, 2008). In this study, accurate near shore bathymetry and detailed topographical data in the examined area are not available. Therefore, tsunami wave velocity as well as the distance of inland penetration is roughly estimated from tsunami height onshore, as defined in Equations 2.30 and 2.40. A return period of 475 years is adopted for the design tsunami (as used in the seismic design of buildings), as illustrated in Figure 6.19. Consequently, an average tsunami wave height of 20.7 m, at 10% probability of exceedance in 50 years, is obtained for Padang city and the average velocity onshore is roughly estimated to be 14 m/s (~50 km/hour).

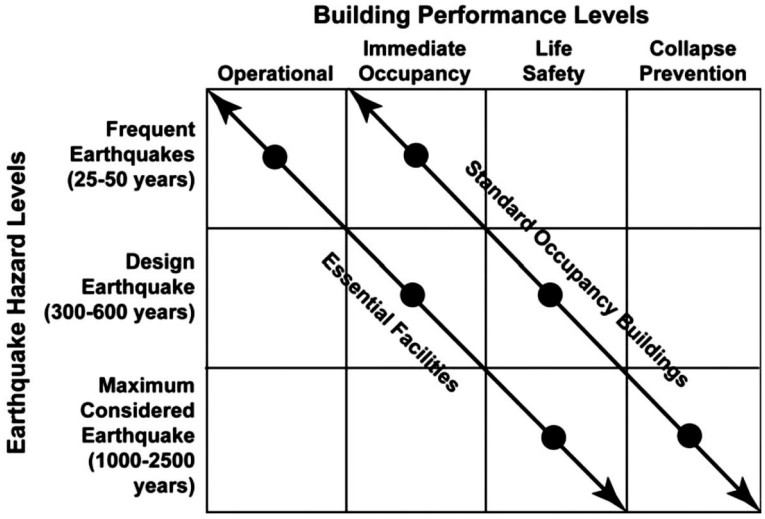

Figure 6.19. Seismic performance objectives for structural designs (SEAOC, 1995 cited in FEMA P646, 2008)

The depths of tsunami inundation vary across the region depending on the terrain condition onshore. A smooth terrain dissipates less energy; therefore, the tsunami wave can travel further inland. In contrast, a densely vegetated landscape and densely populated buildings can dissipate more tsunami energy. A rough estimation for the case study area reveals that the tsunami waves can travel up to 15 km on a smooth terrain, 3.8 km on areas covered with buildings and about 0.7 km on a densely vegetated landscape. It appears that the densely vegetated terrain is an effective environment to dissipate energy and limit the inland penetration of tsunami. Coastal vegetation as a natural barrier for tsunami can be used as an alternative for developing countries, where the cost of tsunami protection structures is prohibitive (Iimura and Tanaka, 2012; Tanaka et al., 2011; Tanaka et al., 2007).

6.5.2. Estimation of Tsunami Forces for Padang City

The catastrophic consequences of tsunami have motivated the development of vertical evacuation buildings to protect human lives in prone areas. Many tsunami design criteria were proposed for tsunami shelters (CCH, 2000; FEMA P55, 2011; FEMA P646, 2008; Lukkunaprasit et al., 2009a; Lukkunaprasit et al., 2009b; Yeh, 2007). Lukkunaprasit et al. (2009b) compared the tsunami forces obtained from the current tsunami guideline FEMA P646 (2008) with experimental works. The study revealed that the FEMA P646 approach was reasonable and produced the upper

bound of maximum tsunami design forces. Therefore, the determination of tsunami forces in this study is based on FEMA P646 (2008).

There are various assumptions adopted by FEMA P646 (2008) for estimating the tsunami forces acting on buildings. It is assumed that the fluid density of tsunami flow is 1.2 times the density of freshwater, which is equal to ρ_s=1200 kg/m^3. To take into account the significant variability in determining tsunami run-up heights, the design run-up elevation (R) is assumed to be 1.3 times the predicted maximum run-up elevation (R*). As a consequence, the design run-up elevation for Padang city is assigned as 26.9 m. To anticipate great uncertainty, any tsunami design parameters (e.g. flow velocity, depth and momentum flux) acquired from numerical simulations should not be considered less than 80% the values obtained from the analytical solutions as required in FEMA P646 (2008). The analytical solutions are derived from one-dimensional fully nonlinear shallow-water-wave theory with a uniformly sloping beach as explained in details in Appendix E, FEMA P646 (2008). The analytical solutions involve some simplifications and assumptions, which may lead to conservative values of tsunami design parameters. However, this conservatism may provide higher factor of safety in terms of structural design viewpoint, which is compulsory for tsunami evacuation buildings.

FEMA P646 (2008) specifies that the design of tsunami vertical evacuation structures has to take into account several loads including hydrostatic forces, buoyant forces, hydrodynamic forces, impulsive forces, debris impact forces, debris damming forces, uplift forces and additional gravity loads from retained water on elevated floors. However, only hydrostatic, hydrodynamic and impulsive forces are discussed here since these forces are directly correlated to the tsunami height obtained in this study.

6.5.2.1. Hydrostatic Force

Hydrostatic pressure is produced by still or slowly moving water, which acts perpendicular on a planar surface (structure or structural component). The hydrostatic forces affect mainly long structures and may not be so relevant to structures with a short width, as water can quickly flow and inundate all sides (FEMA P646, 2008; Palermo et al., 2009; Yeh, 2007). The hydrostatic force can be

estimated using Equation 6.4, and its distribution on structures is illustrated in Figure 6.20.

$$F_h = p_c A_w = \frac{1}{2}\rho_s . g . b . h_{\max}^2 \qquad 6.4$$

where,

F_h : horizontal hydrostatic force (Newton)

p_c : hydrostatic pressure (Pa)

A_w : the wetted area of the panel (m^2)

ρ_s : fluid density of tsunami flow (=1200 kg/m^3)

g : gravitational acceleration (= 9.81 m/s^2)

b : breadth or width of the wall or structural component (m)

h_{max} : maximum water height above the base of the wall at the structure location (m)

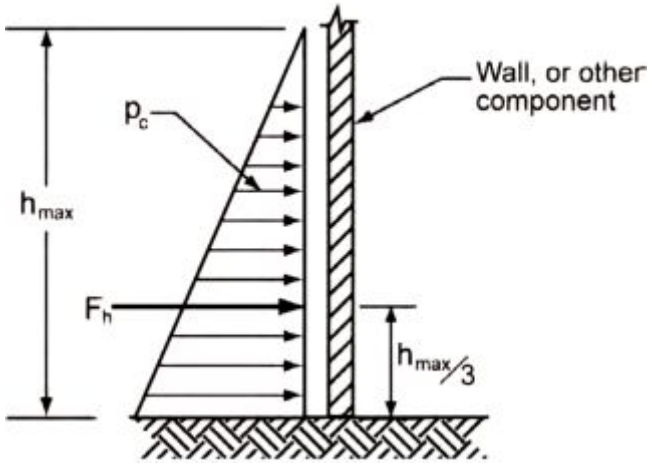

Figure 6.20. Distribution of hydrostatic force (FEMA P646, 2008)

Considering the design tsunami run-up height for Padang city, the resulting hydrostatic force per meter width on structural components can be as high as 4262 kN.

6.5.2.2. Hydrodynamic Force

Hydrodynamic force arises when tsunami bore flows around a structure with a moderate to high velocity (Palermo et al., 2009). The hydrodynamic force is also known as a drag force and is developed as a combination of lateral forces induced by the pressure from the moving mass of water and friction of forces as the water flows

around the structures (FEMA P646, 2008). The hydrodynamic force can be determined using Equation 6.5 and is illustrated in Figure 6.21.

$$F_d = \frac{1}{2}\rho_s . C_d . B . \left(h u^2\right)_{\max} \qquad 6.5$$

where,

F_s : hydrodynamic force (Newton)

ρ_s : fluid density of tsunami flow (=1200 kg/m^3)

C_d : drag coefficient (C_d = 2 for square and rectangular columns; C_d = 1.2 for cylindrical columns)

B : the breadth of structure in the plane normal to the direction of flow (m)

$(h\,u^2)_{max}$: momentum flux per unit mass (u = flow velocity; h = flow depth)

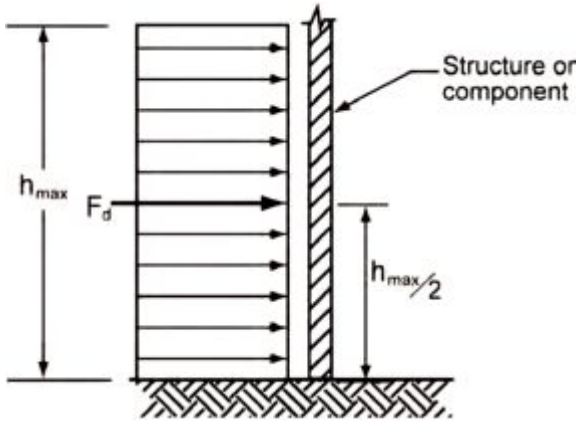

Figure 6.21. Distribution of hydrodynamic forces (FEMA P646, 2008)

The determination of hydrodynamic forces should be based on momentum flux $(hu^2)_{max}$, which represents the transfer rate of momentum per unit area. The maximum momentum flux can be obtained from detailed numerical simulation models as well as existing simulation data (FEMA P646, 2008). In the absence of the detailed tsunami model, the value of maximum momentum flux can be estimated using a relationship derived by Yeh (2006). Yeh (2006) developed envelope curves of hu^2 along a uniformly sloping beach based on an analytical solution of nonlinear shallow-water theory. Afterwards, Yeh (2007) transformed the equation to be a function of ground elevation as shown in Equation 6.6.

$$\left(hu^2\right)_{\max} = g\,R^2\left(0.125 - 0.235\frac{z}{R} + 0.11\left(\frac{z}{R}\right)^2\right) \qquad 6.6$$

where,

R : design run-up elevation (m)

z : ground elevation at the base of structure (m)

$(h\,u^2)_{max}$: momentum flux per unit mass (m^3/s^2)

Using Equations 6.5 and 6.6, the potential hydrodynamic forces for Padang city, subjected to the 475 year return period of tsunami, can be obtained, as shown by the dashed black curve in Figure 6.22. The forces obtained in Figure 6.22 are determined based on the assumption that the structure is fully submerged by a tsunami wave as high as 26.9 m. It should be noted that most regions in Padang city are situated in low lying areas with an elevation less than 5 m above mean sea level. As a consequence, the region is susceptible to experience great hydrodynamic forces of about 725-1065 kN per meter width of structures.

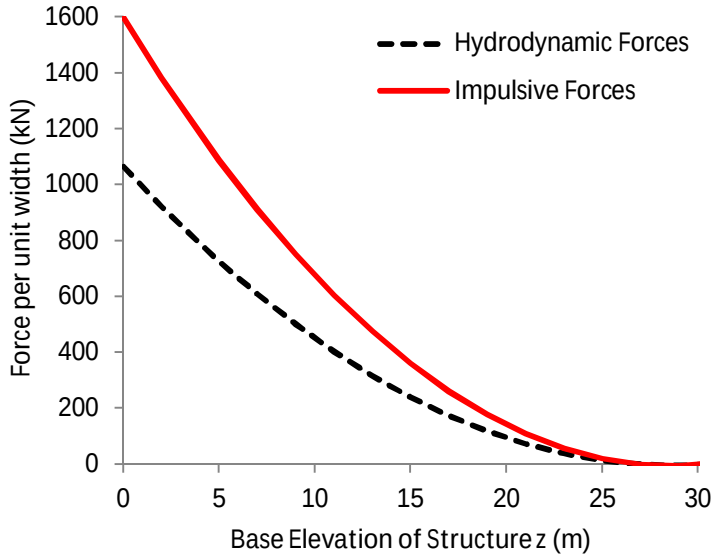

Figure 6.22. Correlation of hydrodynamic force (F_d) and impulsive force (F_s) per unit width with the ground elevation at the base of structure (z) for Padang city

6.5.2.3. Impulsive Force

Impulsive force (surge force) is produced by the leading edge of surge water that impinges the structure (Yeh, 2007). There are a few methods for calculating the impulsive force of tsunami. The first method derived the impulsive force by

summing the hydrostatic force with the change in linear momentum at the impingement of a surge front on a vertical wall (Yeh, 2007), as shown in Equation 6.7. This method is initially developed by Dames and Moore (1980 as cited in Palermo et al., 2009) and has been suggested by many studies (CCH, 2000; Okada et al., 2005; Palermo et al., 2009).

$$F_s = 4.5 \rho g h^2 \qquad 6.7$$

Where, h is surge height.

Nevertheless, Yeh et al. (2005) argued that Equation 6.7 may overestimate the surge force. Laboratory evidence from a previous study (Arnason, 2005 cited in Palermo et al., 2009) showed that the maximum surge force was approximately 1.5 times the subsequent hydrodynamic force. Therefore, FEMA P646 (2008) used this outcome to determine the impulsive force, as shown in Equation 6.8.

$$F_s = 1.5 F_d \qquad 6.8$$

Where, F_d is hydrodynamic force.

The impulsive forces for Padang city, estimated using Equation 6.8, are shown in Figure 6.22 (solid red curve), and the distribution of the impulsive force is shown in Figure 6.23.

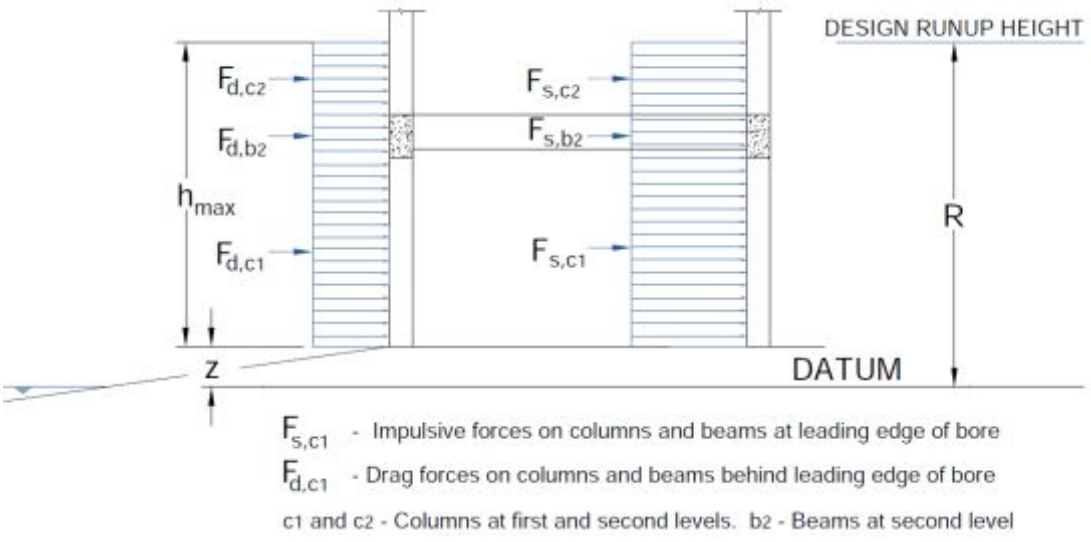

Figure 6.23. Distribution of hydrodynamic impulsive and drag forces (FEMA P646, 2008)

6.6. SUMMARY

- Tsunami hazard in Sumatra is assessed to take into account thrust earthquakes in the Sumatra Subduction Zone (SSZ). In this study, the PTHA method estimates the heights of tsunamis that correspond to tsunamigenic events in the earthquake catalogue (generated in the PSHA module).
- A relationship is developed based on tsunami numerical simulations to correlate tsunami parameters such as tsunami height, earthquake magnitude and closest distance to tsunami source in Sumatra (see Equation 6.1). The relationship is utilized for rapid estimation of tsunami heights in the PTHA module.
- It is estimated that tsunamis occurring in the intraplate of the SSZ are likely to reach the coastal area of Padang in 15 minutes (or longer) following the earthquakes. The travel time of tsunamis in the interface zone is approximately 25 minutes or longer, depending on the distance to the tsunami sources (see Figure 6.6).
- Tsunami wave heights in a region depend on the bathymetric profile of the oceanic floor and the topographic condition.
- The middle segments of the SSZ (particularly around Padang and Bengkulu segments) are susceptible to higher level of tsunami hazard in the near future due to an increased seismicity (see Figure 6.13 and Figure 6.14). In contrast, the hazard level at the Northern part of Sumatra tends to decrease after the 2004 and 2005 events.
- This study found that unlike earthquake hazard assessment, tsunami hazard assessment must consider both near-field and far-field tsunami sources. Near field tsunamis from intraplate of the SSZ are mostly generated by earthquakes located within 150 km from the coast of Padang with $M_w \geq 7.0$. Most tsunamis from the Sumatra subduction interface are generally triggered by earthquakes occurring more than 150 km from the coast with $M_w \geq 8.0$. Distant tsunamis from these interface events are capable of inundating the city with considerable tsunami heights (≥10m). The contributions of each tsunami source to tsunami hazard in Padang are shown in Figure 6.18.
- Tsunami rates and tsunami hazard curves are produced for Padang city, as shown in Figure 6.16 and Figure 6.17, respectively. It is found that the return period of significant tsunamis (≥10m) is approximately 200 years. An average tsunami

height of 20.7m and 28m is expected in the area at 10% and 2% probability of exceedance in 50 years, respectively.

- Hydrostatic, hydrodynamic and impulsive forces associated with a 475 year tsunami event are estimated for Padang city, based on a method proposed by FEMA P646 (2008). A hydrostatic force of 4262 kN per meter width of structural components is estimated for the region. It is predicted that the area can be subjected to hydrodynamic forces in the range of 725-1065 kN per meter width. The maximum surge force is approximately 1.5 times the value of the hydrodynamic forces.

CHAPTER 7

EARTHQUAKE AND TSUNAMI RISK ASSESSMENTS AND MITIGATION STRATEGIES FOR PADANG CITY

7.1. INTRODUCTION

This chapter examines and discusses earthquake and tsunami risk for Padang city. In this study, the main outcomes of the risk assessment are the estimated building losses and fatalities subjected to all probable levels of hazards. The earthquake risk model is validated against the damage data of the M_w 7.6 earthquake of Padang. The estimated annual loss for each building category in the examined region is compared with the building insurance premium tariffs from two insurance companies in Indonesia, specifically dealing with earthquake risk. The outcomes of the risk assessment are utilised to recommend earthquake and tsunami mitigation strategies for the city of Padang.

7.2. VERIFICATION OF THE SEISMIC RISK MODEL WITH A REAL EVENT

To validate the seismic risk model developed in this study, the loss due to the M_w 7.6 Padang earthquake of 30 September 2009 is estimated and compared with the existing loss data. The earthquake occurred at the intraplate of the subduction zone; and thus the focal depth was relatively deep at about 81 km. The epicentre of the event was around 60 km from the city of Padang, as shown in Figure 7.1. The predicted peak ground acceleration was estimated at 0.27g (Figure 7.2), which was consistent with the strong ground motion records obtained from BMKG, the Indonesian meteorology and geophysics agency (Wilkinson et al., 2012)

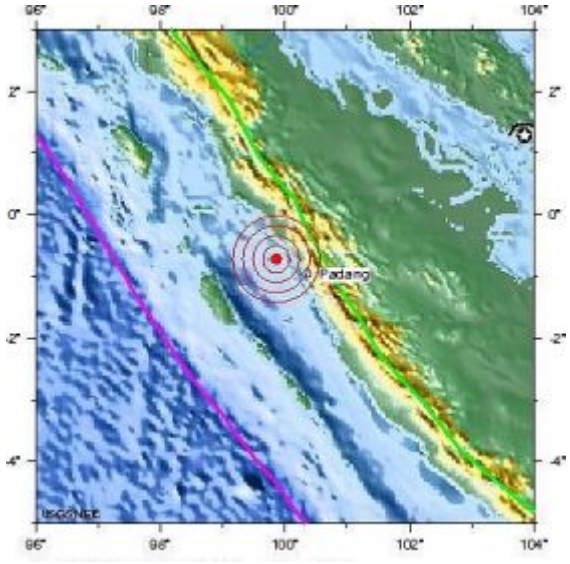

Figure 7.1. The epicentre of the M_w 7.6 Padang earthquake in 2009 (USGS, 2012)

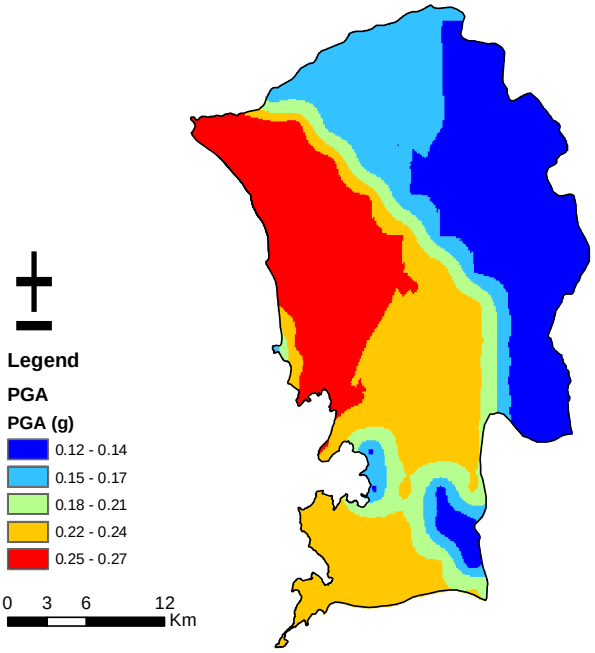

Figure 7.2. The predicted PGA of the M_w 7.6 earthquake in Padang

The Indonesian government estimated that the earthquake caused an economic loss of about Rp. 21.58 trillion (approximately £ 1.4 billion) in West Sumatra. The damaged data for Padang city was reported by the Indonesian mitigation agency, as shown in Table 7.1. Based on the data, the building loss for the area can be assessed using the building inventory information, as discussed in Section 4.13. An estimated loss of £1,179 million is obtained for the region (Table 7.2).

Table 7.1. Number of damaged buildings due to the M_w 7.6 Padang earthquake of 30 September 2009 (BNPB, 2009)

Building Function	**Number of damaged buildings**		
	Lightly Damaged	**Moderately Damaged**	**Heavily Damaged**
1. Residential	37587	38485	40406
2. Schools	1606	1038	903
3. Hospitals	9	10	2
4. Offices	59	19	14
5. Religious	238	211	169
6. Commercials	5	10	5

Table 7.2. The estimation of building loss due to the M_w 7.6 Padang earthquake of 30 September 2009

No.	Building Functions	Type	Number of Buildings	Average Area per Unit (m^2)	Unit Price[1] (GBP)	Building Loss for Each Damage Level (GBP)			Total (GBP)
						Light[2]	Moderate[3]	Heavy[4]	
1.	Residential[5]	UBM	15259	110	64.50	7,510,970.80	14,307,761.90	20,960,861.80	42,779,594.60
		CBM	60802	110	96.75	44,893,818.10	85,518,912.50	125,285,151.30	255,697,882.00
		RCI	40301	300	161.25	135,260,023.20	257,658,862.20	377,470,065.80	770,388,951.20
		Steel	116	2400	193.50	3,752,879.30	7,148,916.40	10,473,157.90	21,374,953.60
2.	Public or	UBM	64	110	64.50	23,264.30	54,829.70	122,409.10	200,503.10
	Commercial[6]	CBM	262	110	96.75	141,912.30	334,461.30	746,695.20	1,223,068.90
		RCI	3954	300	161.25	9,728,715.20	22,928,792.60	51,189,241.50	83,846,749.20
		Steel	17	2400	193.50	406,068.10	957,027.90	2,136,594.40	3,499,690.40
					Total Loss:	**201,717,651.30**	**388,909,564.50**	**588,384,177.00**	**1,179,011,393.00**

[1] Estimated building cost/m^2 in 2009
[2] Assumed 20% of MDR
[3] Assumed 40% of MDR
[4] Assumed 60% of MDR
[5] The percentage of buildings for each type of structure is determined from Table 4.2 assuming R-2 category
[6] The percentage of buildings for each type of structure is determined from Table 4.2 assuming RC-2 category

Using the seismic hazard and risk model developed in this study, it is estimated that the damages in Padang for the event reach £ 1,122 million. This value is only 4.76% lower than that obtained from the damage statistic. This difference is not significant given the approximate nature of both methods. The estimated ratio between the loss and the value of buildings is shown in Figure 7.3. By comparing Figure 7.3 and Figure 4.29, it is observed that the residential areas (R-1 and R-2 categories in Figure 4.29) are mostly affected by the earthquake. This finding is consistent with the BNPB data in Table 7.1.

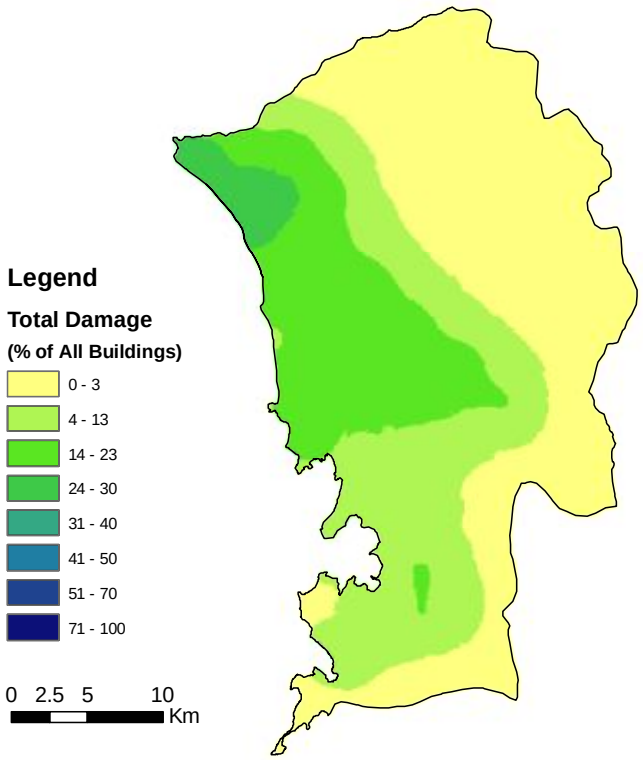

Figure 7.3. The predicted mean damage ratio (MDR) for the buildings in Padang due to the M_w 7.6 earthquake based on GESI vulnerability curves

MapAction (2009) released a damage distribution map for Padang due to the earthquake. The map was developed based on the data from Indonesian Statistical Agency, OCHA and the Indonesian Ministry of Public Works (see Figure 7.4). Considerable difference is observed between the damage distribution in Figure 7.3 and Figure 7.4, particularly at the eastern and southern part of the city. MapAction (2009) estimated a damage level of 13-100% in the areas. However, this study finds that most of the eastern and southern areas are uninhabited (or have a very limited population), and therefore, they are categorised as *"NA"* in the building inventory

database (Figure 4.27). A comparable damage distribution is observed throughout the main part of the city with the percentage of damage about 3-30%. However, Figure 7.4 shows higher values for some areas near the coast. The field survey after the earthquake revealed that liquefaction occurred near the coastal region, which exacerbated the level of damage in the area. The liquefaction effect is not taken into account in this study, and therefore, the level of damage obtained is likely to be underestimated.

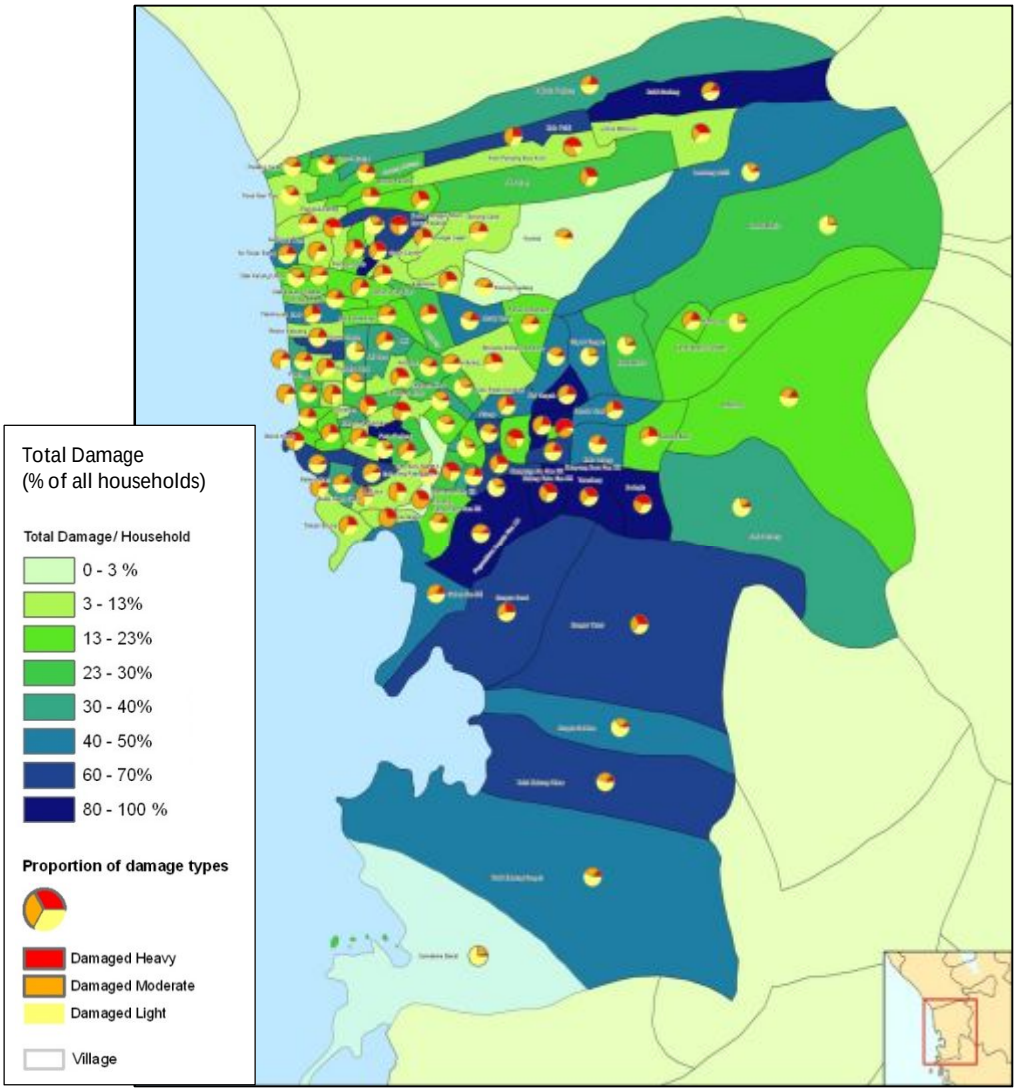

Figure 7.4. Damage level of houses due to the earthquake in Padang city (MapAction, 2009)

Figure 7.5 shows the estimated loss per m^2 of buildings in Padang subjected to the event. It is observed that the buildings in the densely populated areas are more susceptible to the earthquake (red and orange zones in Figure 7.5(a)). An average

loss of about £ 26-42 per square meter is predicted for most parts of the city. The risk model in this study estimates that about 37% of UBM structures are damaged during the event, something expected considering the poor seismic performance of the UBM structures. However, the RCI buildings have the highest loss per square meter due to their higher construction cost. The comparison of the damage and building loss/m^2 for every type of structure is shown in Figure 7.6.

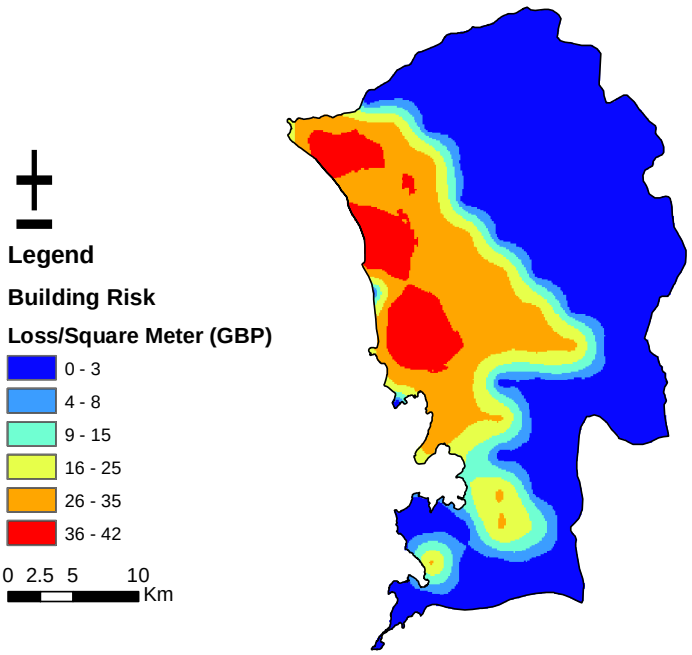

Figure 7.5. The estimated average loss/m^2 for Padang city due to the M_w 7.6 earthquake

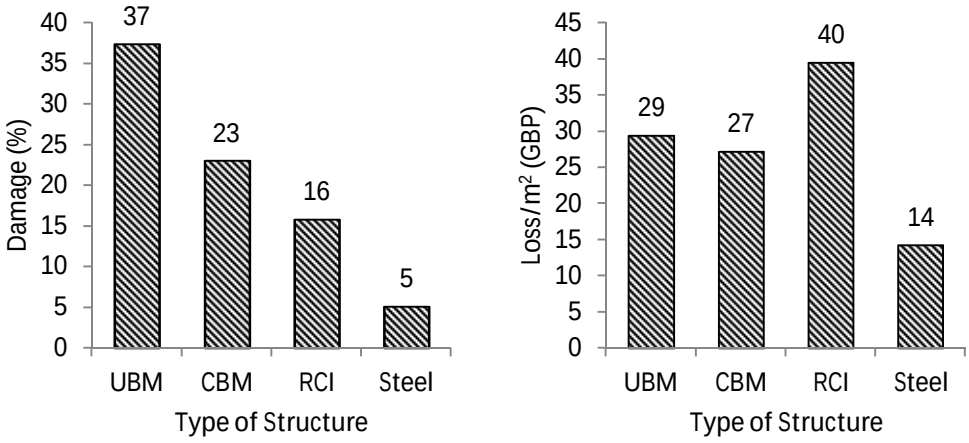

Figure 7.6. The predicted damage and unit loss for each type of structure in Padang

Figure 7.7 shows the average loss of buildings per unit grid. It appears that the worse affected regions are located near the city centre of Padang with total economic consequences up to £138 million per unit grid. This outcome is comparable with the findings of an EEFIT field survey in Padang in which the author participated as a team member (Chian et al., 2010; Wilkinson et al., 2009; Wilkinson et al., 2012). Poor quality materials, lack of seismic detailing and poor seismic design are among the main problems identified in the damaged structures. Although the Indonesian seismic design guideline for buildings was introduced since 1983, the use of seismic design in building practices was not evident. As a consequence, the structures were vulnerable, and therefore, the seismic risk was considerably high.

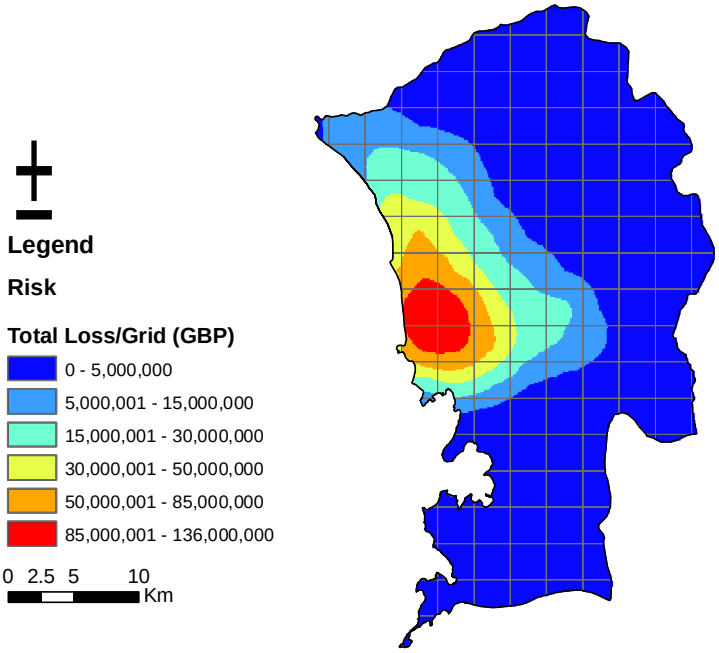

Figure 7.7. The estimated average risk in the area due to the M_w 7.6 earthquake

7.3. SEISMIC RISK FOR PADANG CITY

7.3.1. Earthquake Risk

Padang city is exposed to high earthquake risk due to the high level of hazard, high vulnerability at the existing building stock and large exposure. The city is home to almost 1 million people and is a major city in the West Sumatra province of Indonesia. The risk model in this study estimates that the earthquake risk in Padang could reach £54.5 million per annum. As previously mentioned, this considerable

risk can be attributed to poor building quality. It should be emphasised that most buildings are not constructed according to the Indonesian seismic design standard.

In this study, the risk assessment is performed considering four building categories: UBM, CBM, RCI and steel frame structures. It is assumed that most of the existing building stock in Padang is substandard with poor seismic performance, as observed during the EEFIT field survey (Wilkinson et al., 2009; Wilkinson et al., 2012). However, some seismically designed buildings are also present in the area. Therefore, the risk assessment is conducted for both substandard and seismically designed structures.

The outcomes of the risk assessment are expressed in terms of pure risk premium (PRP), as shown in Figure 7.8 and Figure 7.9. The PRP denotes estimated loss per mil (building value). Figure 7.8 reveals that the existing unreinforced brick masonry (UBM) structure is extremely vulnerable to earthquakes with an estimated PRP of 15-30‰. Although the risk decreases for a better class of UBM structure (Figure 7.9), the PRP value is still considerably high (2-10‰ for most regions). Thus, the UBM structure is not suitable for high seismicity region such as Padang due to its characteristics (rigid, heavyweight and brittle) which result in poor seismic resistance. The existing confined brick masonry (CBM) performs better than the existing UBM structure (6-15‰). However, CBM structures that comply with seismic standard can reduce the risk with estimated PRP of about 1-5‰. A PRP of 2-10‰ is also predicted for the existing reinforced concrete frame with masonry infill (RCI). However, seismically designed RCI structures show a lower risk in the range of 0.6-2‰. The existing and seismically designed steel structures show better seismic performance compared with the other building types with an estimated PRP of 1-5‰ and 0.1-0.5‰, respectively. These structures are normally light weight and used for industrial purposes.

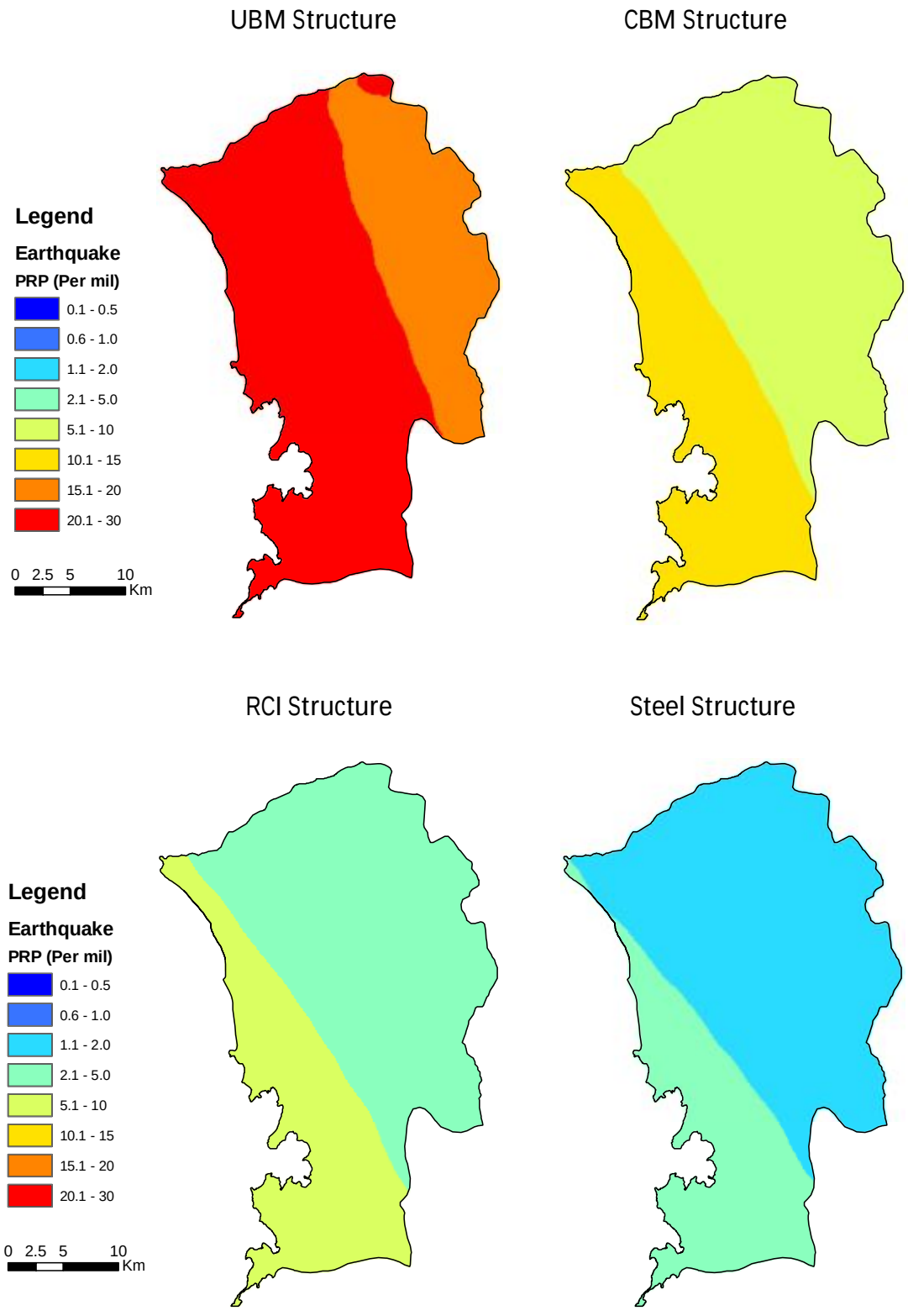

Figure 7.8. The estimated pure risk premium (PRP) for the existing building stock in Padang with poor seismic performance based on GESI (2001) vulnerability curves

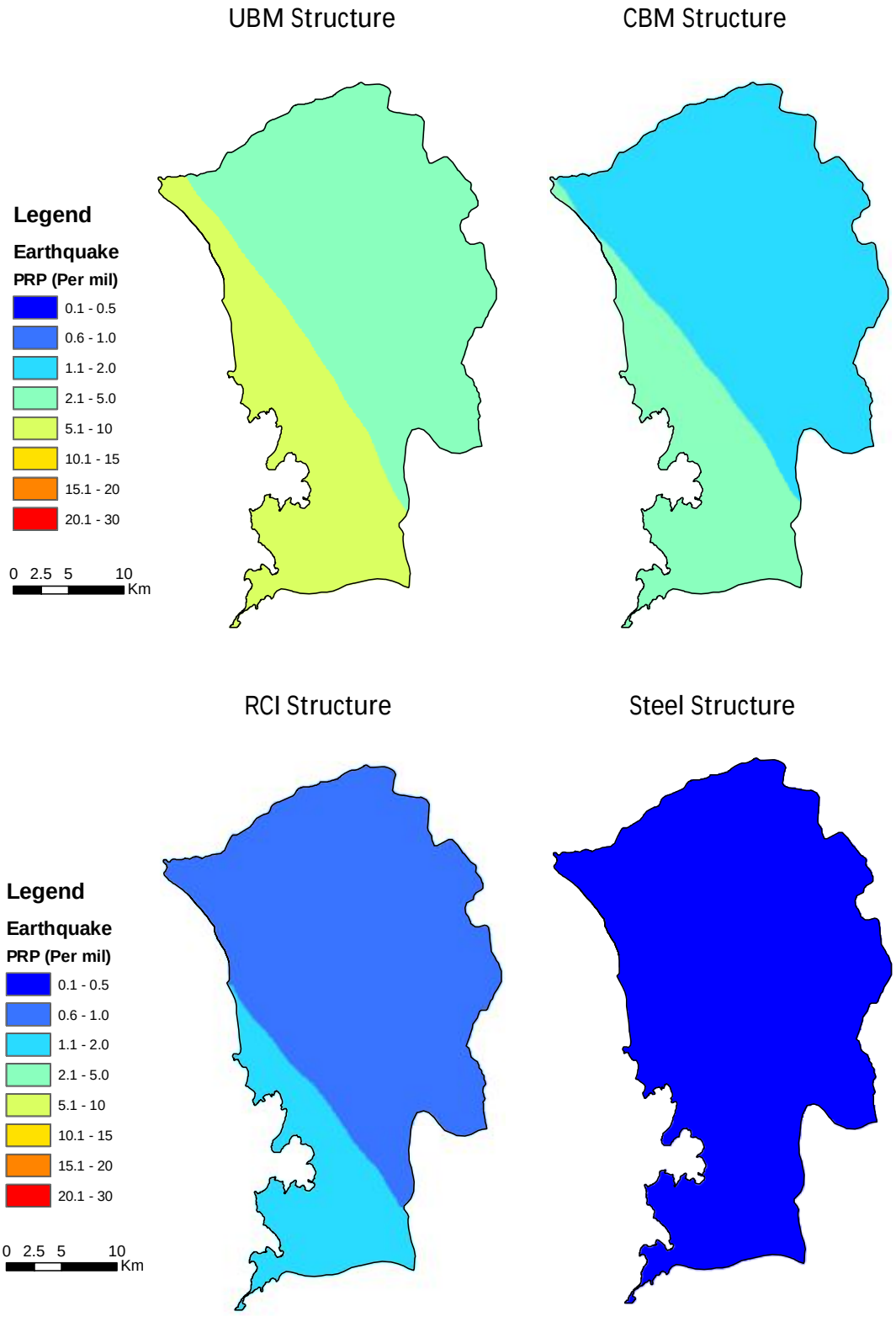

Figure 7.9. The estimated pure risk premium (PRP) for seismically designed building stock in Padang based on GESI (2001) vulnerability curves

Figure 7.10 shows the annual risk calculated using Kyriakides's vulnerability curves for RC structures. The risk is smaller than that estimated using GESI's vulnerability

functions. This result is expected because the Kyriakides's vulnerability curves apply a lower rate of damage than those of GESI's particularly at PGA ≤ 0.45g, as shown in Figure 3.12. The differences are fairly significant (approximately 27% for pre-seismic structure and even more for modern seismic buildings). In addition, the vulnerability curve for a modern seismic building proposed by Kyriakides (2007) showed a high level of seismic performance. For the modern seismic building model, Kyriakides (2007) used a concrete compressive strength of f_c' = 20 MPa, a steel yield strength of f_y' = 550 MPa and the RC structures were designed to resist a maximum ground acceleration of 0.4g (Kyriakides, 2007). These material properties are also commonly used for modern designed buildings in Indonesia. The Indonesian reinforced concrete standard for buildings (SNI, 2002) states that any structural components carrying earthquake load should have a minimum concrete compressive strength of f_c' = 20 MPa. The code has also taken into account different levels of structural ductility as required in modern seismic design standards. Therefore, with appropriate seismic detailing and supervision, the high seismic performance, as suggested by Kyriakides (2007), can actually be achieved and consequently, can further reduce the earthquake risk in Padang.

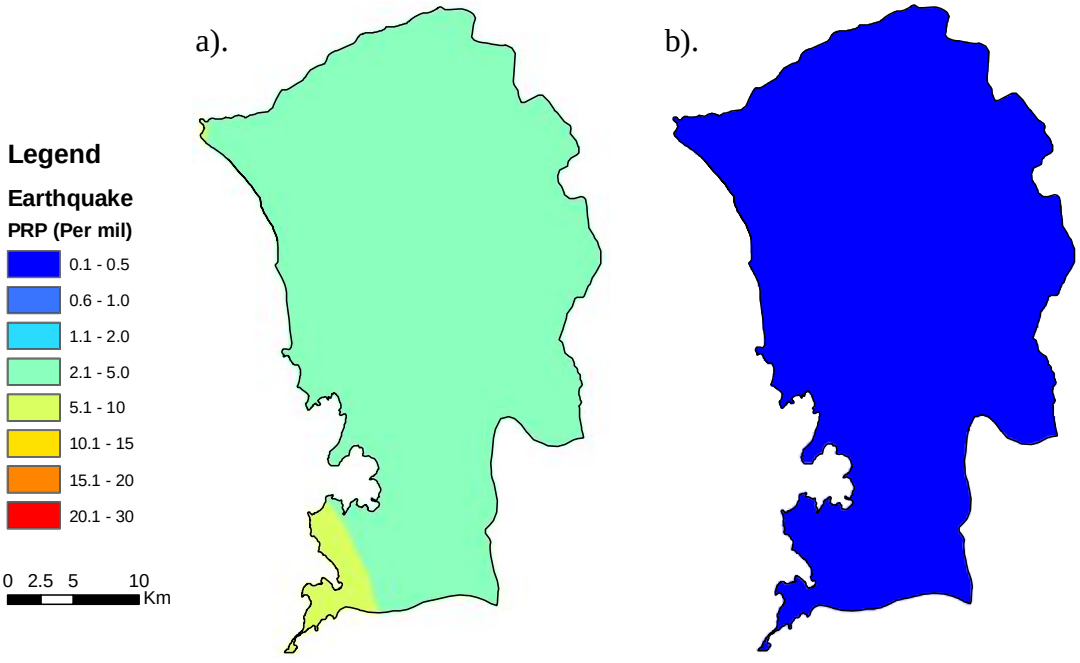

Figure 7.10. The estimated annual risk for RC structures based on Kyriakides (2007) vulnerability curves: a). pre-seismic RC buildings; and b). modern-seismic RC buildings

7.3.2. Tsunami Risk

Tsunami occurrence in Padang is infrequent due to the long return period of tsunamigenic earthquakes. However, the impact of a tsunami can be immensely devastating, as demonstrated by the 2011 tsunami of Japan. The tsunami risk in Padang is predicted to be £30.8 million per annum. The risk is lower than the predicted earthquake risk which reaches £54.5 million per annum.

As mentioned in Chapter 3, tsunami risk assessment for all building categories in this study is conducted using vulnerability curves proposed by Tinti et al. (2011). The vulnerability curves were derived empirically based on the damage data of real tsunamigenic earthquakes in Indonesia; hence, the contribution from both earthquake and tsunami has been taken into account in the vulnerability relationships. Consequently, the resulted tsunami risk represents the total risk associated with earthquake and its following tsunami.

The resulting tsunami risk is shown in Figure 7.11 and Figure 7.12 in terms of pure risk premium (PRP). As expected, the existing UBM structures are the most vulnerable buildings with a maximum PRP of 11‰. A comparable maximum PRP is obtained for CBM structures. However, it affects fewer structures closer to the coast. The RCI and steel structures show a comparable risk since an identical vulnerability curve is assigned for both building categories. A maximum tsunami risk of 3‰ per annum is predicted for the existing RCI and steel structures, and the risk decreases by 36% for the seismically designed structures.

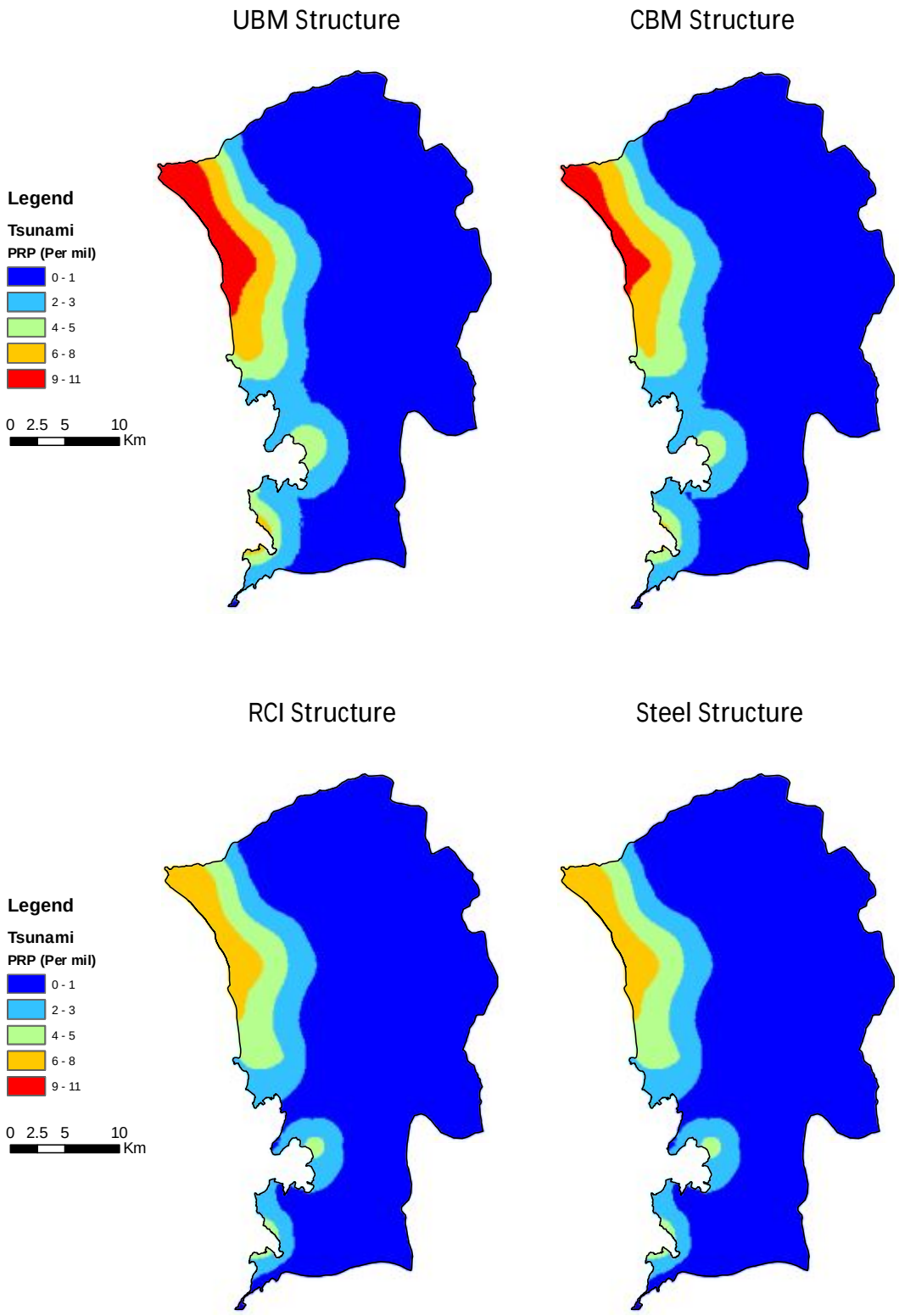

Figure 7.11. The estimated pure risk premium (PRP) for the existing building stock in Padang subjected to tsunami hazard

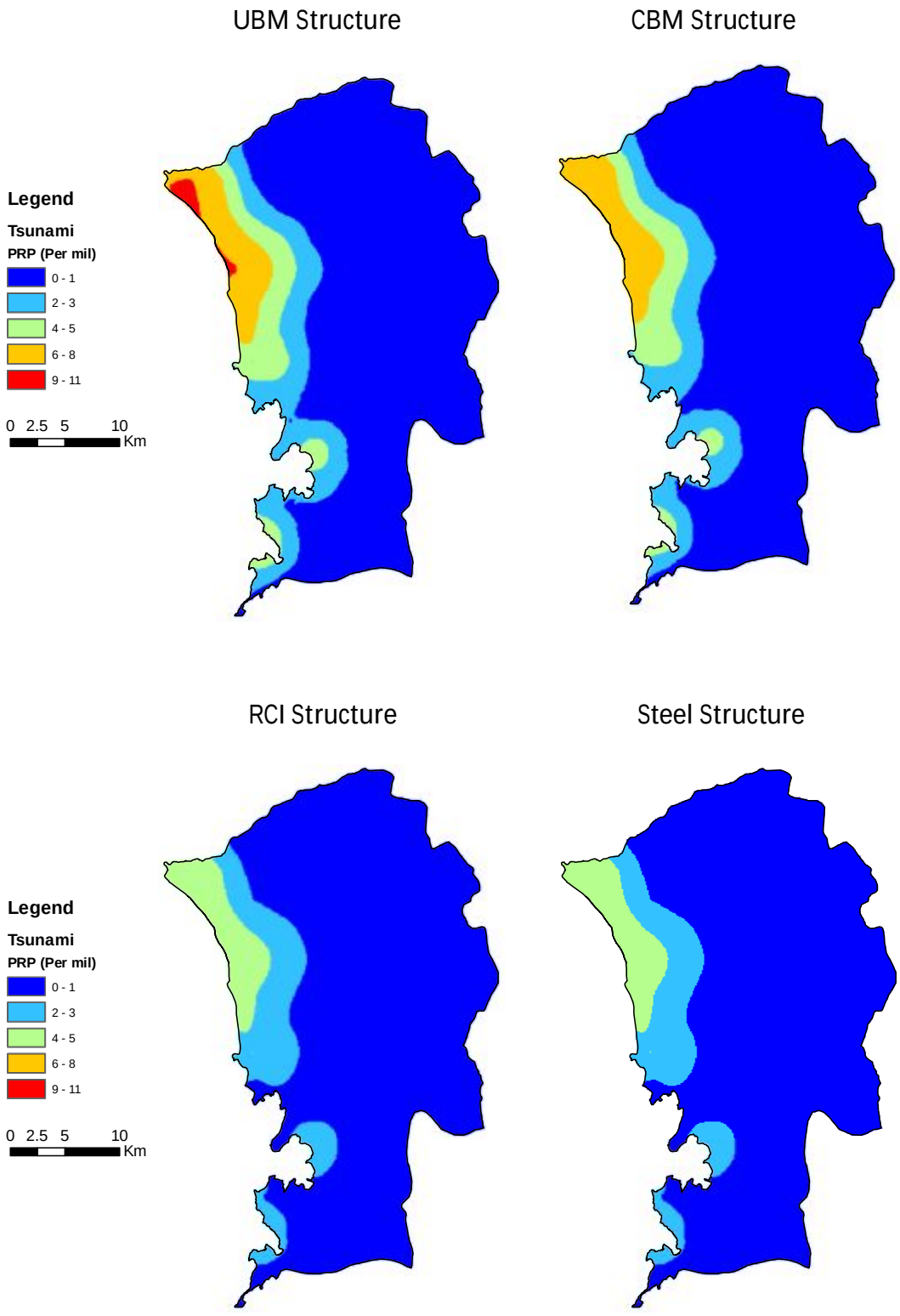

Figure 7.12. The estimated tsunami pure risk premium (PRP) for seismically designed structures in Padang subjected to tsunami hazard

7.4. FATALITY ESTIMATION FOR PADANG CITY

7.4.1. Earthquake Fatality Estimation

A detailed fatality estimation of Padang city cannot be performed due to limited population distribution data associated with the occupancy probability of the area with time. However, a rough estimation of fatalities can be conducted using fatality curves produced by various studies. In this case, fatality curves developed by Jaiswal and Wald (2010), for the USGS's Prompt Assessment of Global Earthquake for Response (PAGER) system, is adopted. The fatality curve incorporates empirical fatality data worldwide including Indonesia. It is predicted that the mean earthquake risk in Padang is approximately 8 fatalities per annum, concentrated mainly in the densely populated region (see Figure 7.13).

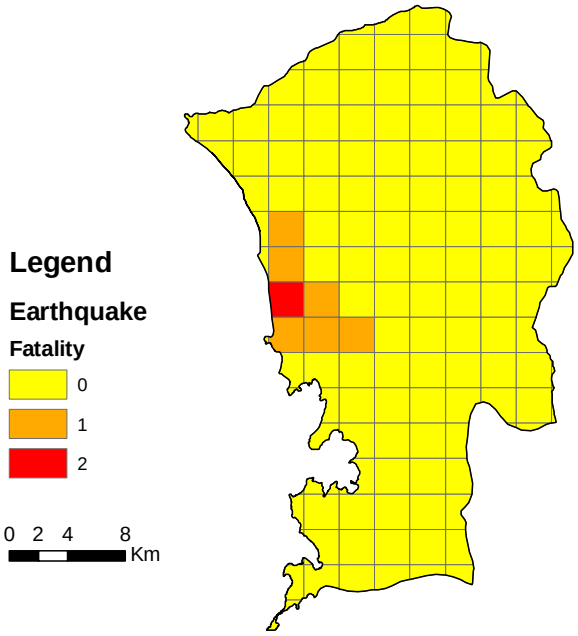

Figure 7.13. Estimated mean annual fatality for Padang city due to earthquake hazard

The estimated number of fatalities above is relatively low compared with the number of large earthquakes occurring in the region in the past decade. However, Jaiswal and Wald (2010) found that the fatality rate in Indonesia is lower than that of Iran, India and Italy, as shown in Figure 7.14. The fatality rate in Figure 7.14 only takes into account earthquake ground motion related deaths; hence, secondary effects such as fire, tsunami, liquefaction and landslide are not included (Jaiswal and Wald, 2010). Table 7.3 presents the deadly earthquakes since 1917 which affected Padang region

(USGS, 2012). It appears that the M_w 7.6 earthquake of Padang caused the highest fatality in the area within the last century. By considering the contribution of all probable earthquakes over one seismic cycle in the region, the mean annual fatality obtained in this study appears to be realistic.

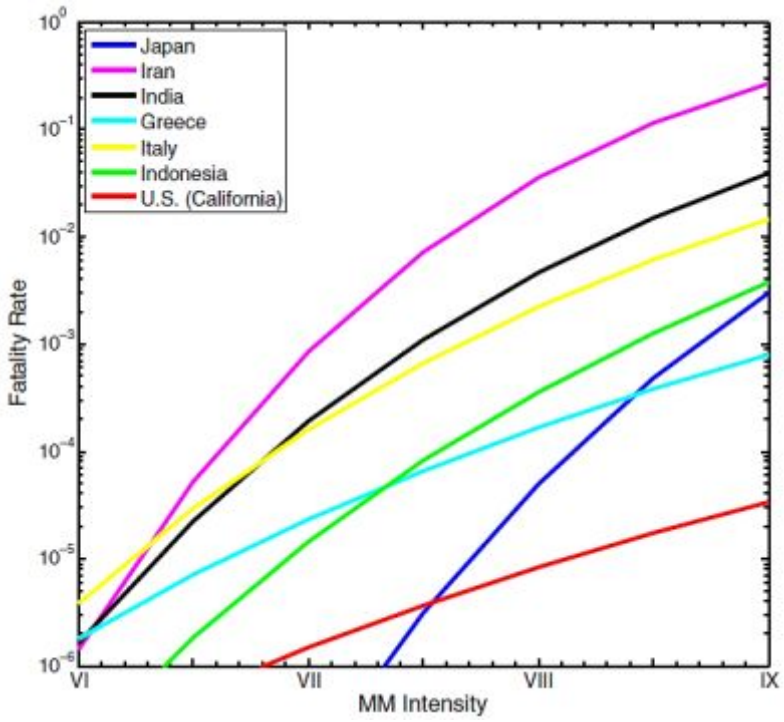

Figure 7.14. Comparison of fatality rates for different countries (Jaiswal and Wald, 2010)

Table 7.3. Recorded fatality due to recent deadly earthquakes around West Sumatra region (USGS, 2012)

Earthquake Event	Depth (km)	Location	Year	Total Fatality	Fatality in Padang
M_w 7.6 – Southern Sumatra	81	0.725°S, 99.856°E	2009	1117	313
M_w 8.5 – Southern Sumatra	34	4.520°S, 101.374°E	2007	25	1
M_w 6.4 – Southern Sumatra	19	0.512°S, 100.524°E	2007	67	-

7.4.2. Tsunami Fatality Estimation

The mean annual number of fatalities due to tsunami in Padang is assessed using the death and injury relationship defined by Reese et al. (2007). The fatality relationship is developed empirically based on the data of the 2006 tsunami event in Java,

Indonesia (see Section 2.5.2). The fatality estimation for Padang city is shown in Figure 7.15. The outcome shows that more than 2000 people in Padang may perish due to tsunami per annum. Although tsunami events in Padang are infrequent, one event can lead to great consequences. In addition, the high fatality risk is due to poor tsunami mitigation systems in the region. This can be attributed to the lack of tsunami vertical evacuation shelters in low lying coastal areas and the large distance from high ground. This finding highlights the importance of appropriate tsunami mitigation systems in Padang, which are discussed in Section 7.6.

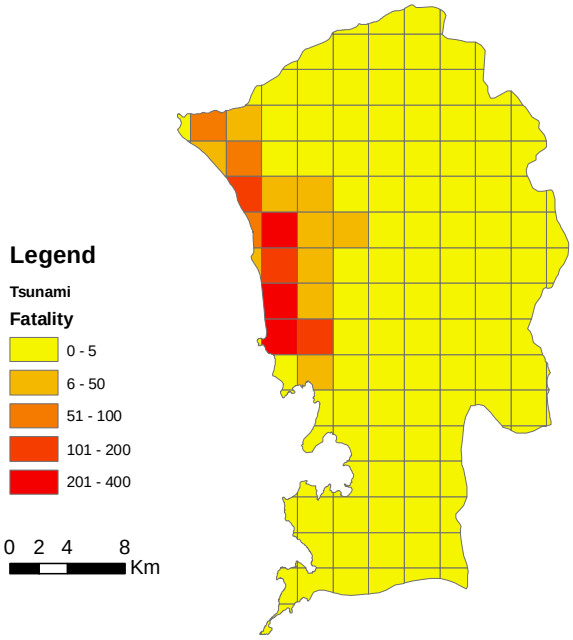

Figure 7.15. Estimated mean annual fatality for Padang city due to tsunami hazard

7.5. EARTHQUAKE AND TSUNAMI INSURANCE PREMIUM FOR BUILDINGS IN PADANG

The pure rate premiums (PRP), as discussed in Sections 7.3.1 and 7.3.2, can be utilised to determine total insurance premium (TP) for different building categories in Padang. The PRP values can be converted into insurance premium simply by including a load factor (LF), as described in Equation 2.8. The load factor takes into account hidden uncertainties, administration, taxes and profit for the insurance company (Yucemen, 2005). This study adopts a load factor of 0.4, as suggested by Yucemen (2005). The determination of earthquake and tsunami insurance premiums for buildings in Padang is discussed in the following sections.

7.5.1. Earthquake Insurance Premium

The average values of the PRP and total insurance premiums of all building categories in this study are summarised in Table 7.4. The table shows higher insurance rate for the existing UBM and CBM buildings of about 36.4‰ and 16.6‰, respectively. Better quality UBM and CBM buildings can reduce the insurance rate to be 8.1‰ and 3.1‰, respectively. The seismically designed RCI and steel structures provide better seismic resistance, resulting in lower earthquake insurance rate.

Table 7.4. Average earthquake pure rate premium (PRP) and total insurance premium (TP) for all building categories in Padang

Building Category	Existing Building Stock		Better Quality/ Seismically Designed Building Stock	
	PRP (‰)	**TP (‰)**	**PRP (‰)**	**TP (‰)**
1. Unreinforced brick masonry (UBM) structures	21.9	36.4	4.8	8.1
2. Confined brick masonry (CBM) structures	9.9	16.6	1.9	3.1
3. Reinforced concrete frame with masonry infill (RCI) structures	4.8	8.1	0.8	1.4
4. Steel frame structures	1.9	3.1	0.2	0.3

Figure 7.16 shows a comparison of the hazard between the case study area and the city of Antalya in Turkey, as cited in Deniz (2006). The level of hazard for both cities is relatively similar. Hence, it is reasonable to compare the insurance rates for both cities. Deniz (2006) estimated an insurance rate of 2.63‰ for reinforced concrete building in Antalya. This value is within the range of insurance premium for the existing and seismically designed RCI buildings in Padang (8.1‰ and 1.4‰, respectively). Therefore, the insurance rate obtained in this study is considered reasonable.

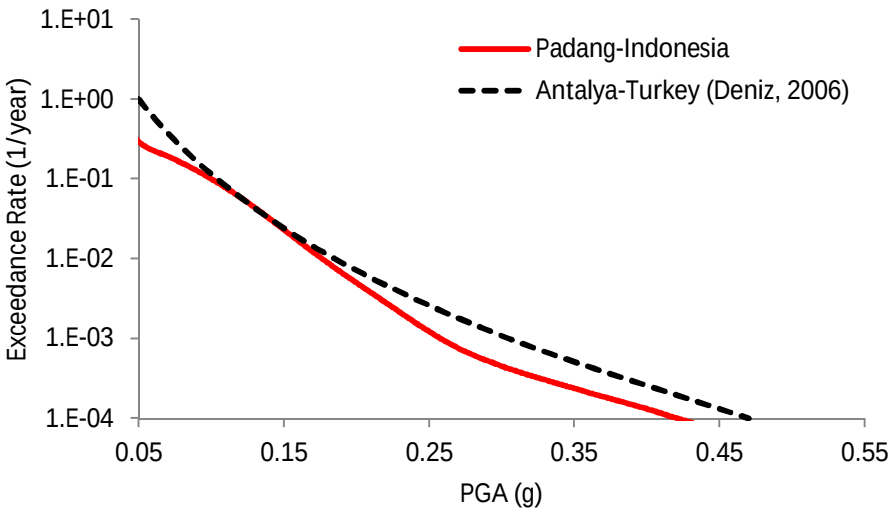

Figure 7.16. Earthquake hazard curve for Padang city in comparison with the hazard curve of Antalya City in Turkey

In addition, earthquake insurance premiums obtained in this study are compared with the insurance rates of two insurance companies in Indonesia, ACA and MAIPARK. The latter insurance company specialises in earthquake reinsurance, which was established from the Indonesian Earthquake Reinsurance Pool in 2003. MAIPARK provides earthquake statistics and sets a benchmark for earthquake insurance pricing in Indonesia (Bugl, 2005).

ACA insurance applied a flat rate of 3‰ for all building categories in Sumatra (ACA, 2011). MAIRPARK (2007) assigned a maximum earthquake insurance rate of 3.3‰ for other than RC and steel frame structures in Zone III as the highest risk zone in the area (Table 7.5). This tariff was then increased in 2010 to be 4.7‰, as shown in Table 7.6. Unlike the former tariff, the new one assumes identical rate for steel, wood and RC frame structures and categorises the Indonesian region into five zones. The risk increases from Zone I to Zone V and Padang city is categorised into Zone V. The comparison of the insurance rates obtained in this study with those given by ACA (2011), MAIPARK (2007) and MAIPARK (2011) is shown in Figure 7.17. The figure implies that, in most cases, the MAIPARK and ACA insurance rates are lower than those estimated for the existing building stock in Padang. However, the MAIPARK's rate suits the insurance premium of the seismically design structures well.

Table 7.5. Indonesian earthquake insurance rate in 2007 (MAIPARK, 2007)

Building Category	Insurance Rate (‰)		
	RC Frame	Steel Frame	Others
Zone I			
1. Manufacturing/Factory Risk	1.08	1.08	1.22
2. Other Risks:			
– Up to 3 stories	1.04	1.04	1.13
– 4 to 9 stories	1.22	1.35	2.70
– 10 stories and higher	1.35	1.49	Declined
Zone II			
1. Manufacturing/Factory Risk	1.2	1.2	1.4
2. Other Risks:			
– Up to 3 stories	1.2	1.2	1.3
– 4 to 9 stories	1.4	1.5	3.0
– 10 stories and higher	1.5	1.7	Declined
Zone III			
1. Manufacturing/Factory Risk	1.3	1.3	1.5
2. Other Risks:			
– Up to 3 stories	1.3	1.3	1.4
– 4 to 9 stories	1.5	1.7	3.3
– 10 stories and higher	1.7	1.8	Declined

Table 7.6. Indonesian earthquake insurance rate in 2010 (MAIPARK, 2011)

Building Category	Insurance Rate (‰)				
	Zone I	**Zone II**	**Zone III**	**Zone IV**	**Zone V**
1. Commercial and Industry (Non Dwelling House)					
– Steel, wood or RC frames (≤ 9 storeys)	0.90	0.95	1.25	1.50	1.90
– Steel, wood or RC frames (> 9 storeys)	1.35	1.45	1.55	1.60	2.00
– Others	1.00	1.10	1.55	3.00	4.70
2. *Dwelling House-occupation code 2976*					
– Steel, wood or RC frames	0.85	0.95	1.15	1.35	1.60
– Others	0.90	1.00	1.55	2.75	4.50

Nevertheless, MAIPARK (2011) revealed that the M_w 7.6 of Padang earthquake in 2009 caused great loss to the insurance industry in Indonesia. MAIPARK (2011) estimated that the insurance companies lost more than Rp 4.7 trillion (about £300 million) in the event. Considering that the event is not yet the highest probable earthquake magnitude of the region, the unexpected loss is likely due to the underestimation of the earthquake insurance premium. Although the rate has been

increased since then, the massive loss endured by the insurance industry are likely to be repeated if the insured buildings do not have good seismic standard, as assumed in the latest insurance tariffs.

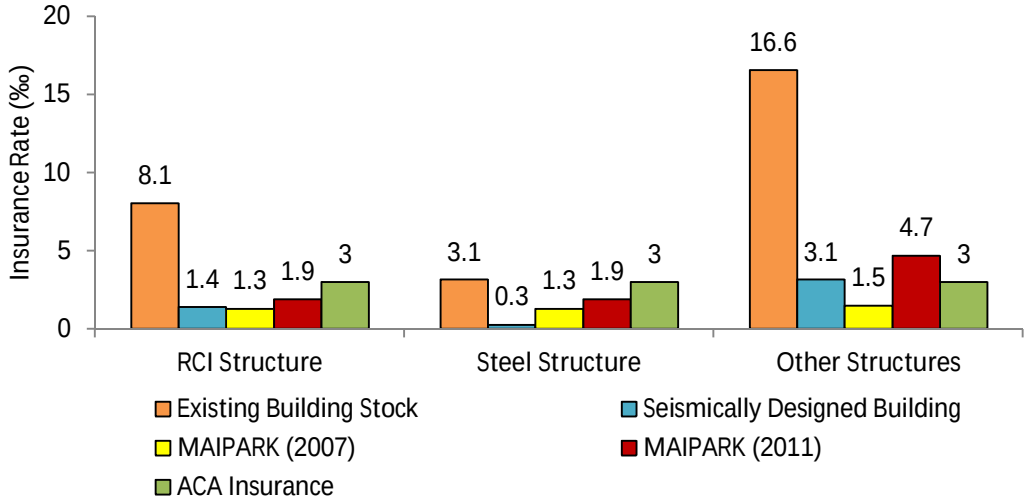

Figure 7.17. Comparison between insurance rates obtained in this study (existing and seismically design buildings) and the insurance rates applied by two insurance companies (MAIPARK and ACA insurance) for Padang city

7.5.2. Tsunami Insurance Premium

The tsunami insurance premium for Padang city is summarised in Table 7.7. The highest insurance rate applies to UBM buildings and then followed by CBM, RCI and steel structures. Equal tsunami insurance rate is estimated for RCI and steel structures. Tsunami premium data from insurance companies in Indonesia is not available, and thus, no comparison can be performed.

Table 7.7. Average tsunami pure rate premium (PRP) and total insurance premium (TP) for Padang city

Building Category		Existing Building Stock		Seismically Designed Building Stock	
		PRP (‰)	TP (‰)	PRP (‰)	TP (‰)
1.	Unreinforced brick masonry (UBM) structures	7.03	11.72	5.27	8.78
2.	Confined brick masonry (CBM) structures	5.93	9.88	4.80	8.00
3.	Reinforced concrete frame with masonry infill (RCI) structures	4.20	7.00	2.68	4.47
4.	Steel frame structures	4.20	7.00	2.68	4.47

It is observed that seismic strengthening of structures may decrease the vulnerability of buildings resulting in a lower tsunami risk. However, the difference is not very significant compared with that of earthquake hazard.

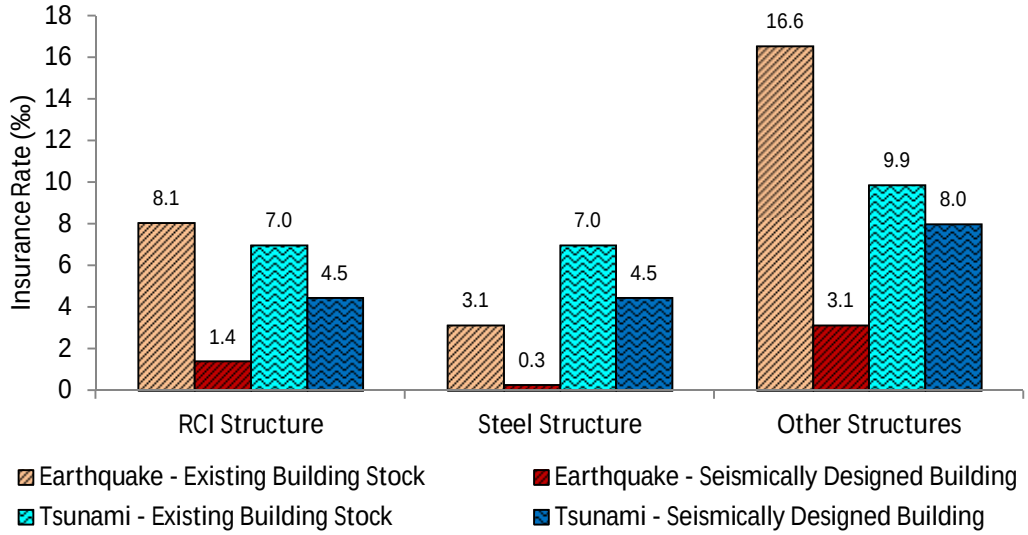

Figure 7.18. Predicted total insurance premium per 1000 building value for Padang

7.6. MITIGATION STRATEGIES

7.6.1. Seismic Provision for Buildings in Padang

Seismic provision of buildings can be adopted as a mitigation effort to reduce the earthquake risk in Padang. The seismic provision of buildings can not only reduce the vulnerability of structures, but also will reduce the number of casualties associated with the structural damage. Kythreoti (2002) used a range of 2-4% of building costs for the seismic provision of typical RC buildings in Cyprus. In Padang, a higher value of 5% can be adopted to account for seismic design. This means an additional cost of £400 million to the cost of non-seismic design buildings.

The application of a seismic provision to the existing building stock requires seismic strengthening of structures. Kanit and Altin (2010) estimated the cost of strengthening school buildings in Turkey to be in the range of 35-49% of the total cost. The examined structures were typically mid-rise RC frames with infill walls. For this study, the ratio of 35% is adopted to consider that the typical existing building stock in Padang is low to mid-rise structures. Hence, the estimated cost of strengthening the existing building stock in Padang is about £2.8 billion.

The estimated values of the seismic provision scenario above seem to be a huge investment. However, the amount is insignificant compared to the benefits. The great economic loss associated with the M_w 7.6 earthquake in Padang could have been minimised, if the vulnerable structures in the area were designed to satisfy the seismic design criteria. The earthquake risk model in this study estimates that the building loss could have been reduced from £1.122 billion to £564 million; thus lowering the loss by about 50%. As a consequence, the fatality reduction would have been much higher. The predicted loss per unit grid for seismically designed building stock due to the M_w 7.6 event is shown in Figure 7.19.

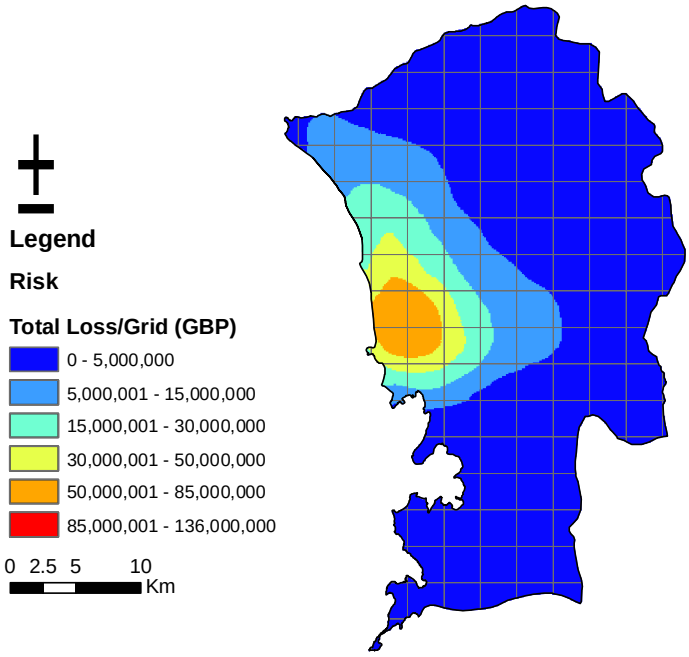

Figure 7.19. Estimated average risk in the area due to the M_w 7.6 earthquake for seismically designed building stock in Padang

Figure 7.20 shows the annual earthquake risk of the existing and seismically designed buildings in Padang. The figure reveals that the existing buildings in the area are subjected to a total risk of £54.4 million per annum. However, the risk can be significantly reduced to £11 million per annum, if the buildings follow the modern seismic design standard. Based on this outcome, it can be revealed that the break even time for the seismic provision scenario is approximately 9 years for constructing seismic design structures and about 60 years for strengthening the existing building stock. Therefore, the latter scenario is only recommended for

important buildings in the area. In addition, the new structures must be built to comply with the seismic design guideline.

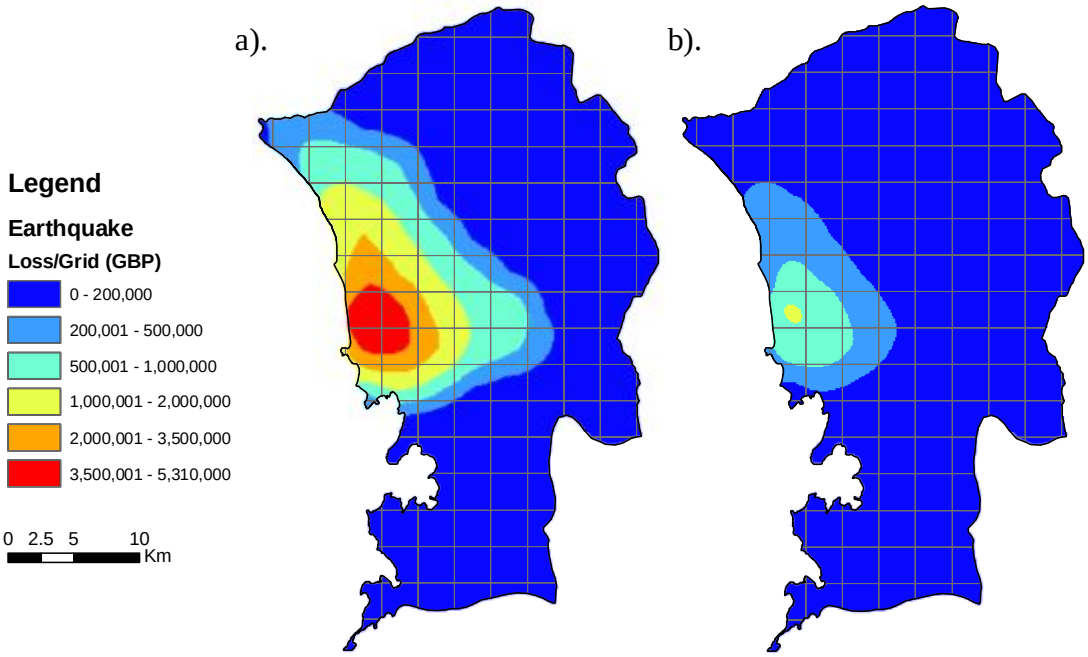

Figure 7.20. Predicted annual earthquake risk in Padang: a). existing building stock; b). seismically designed buildings

The comparison of the predicted MDR and annual risk/m^2 for the building categories in the area is shown in Figure 7.21 and Figure 7.22. It is observed that although the existing RCI structure has much lower MDR than CBM building (Figure 7.21), the risk per unit area of the RCI is slightly higher (Figure 7.22). This is due to the high cost of the RCI structures.

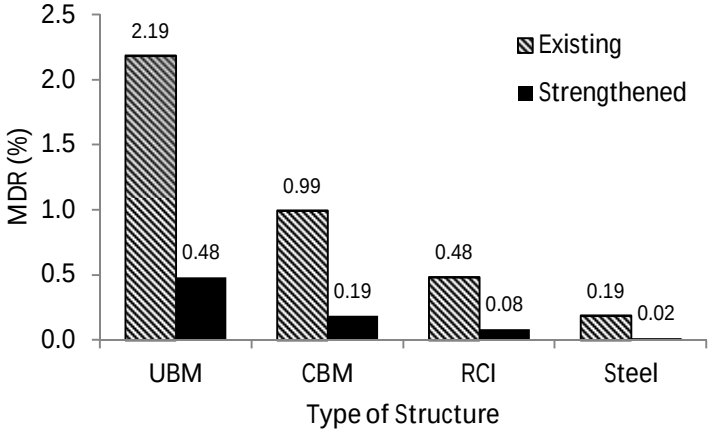

Figure 7.21. Earthquake MDR per year for building categories in Padang

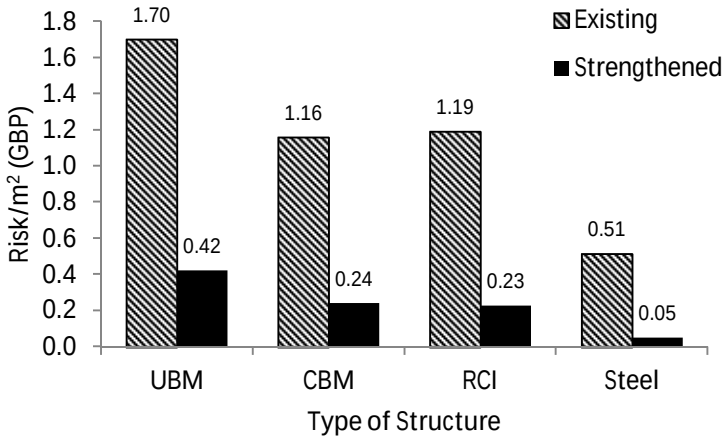

Figure 7.22. Annual earthquake risk/m^2 per year for building categories in Padang

In addition, this study finds that although the seismic design of structures is mainly aimed for earthquake risk mitigation, it can also reduce the vulnerability of buildings subjected to tsunami. The ERA Framework estimates that the seismic design of buildings in Padang can decrease the risk by up to 80% for earthquake hazard and by up to 25% for tsunami hazard. The predicted annual risk for the existing building stock and seismically designed structures due to tsunami hazard is shown in Figure 7.23.

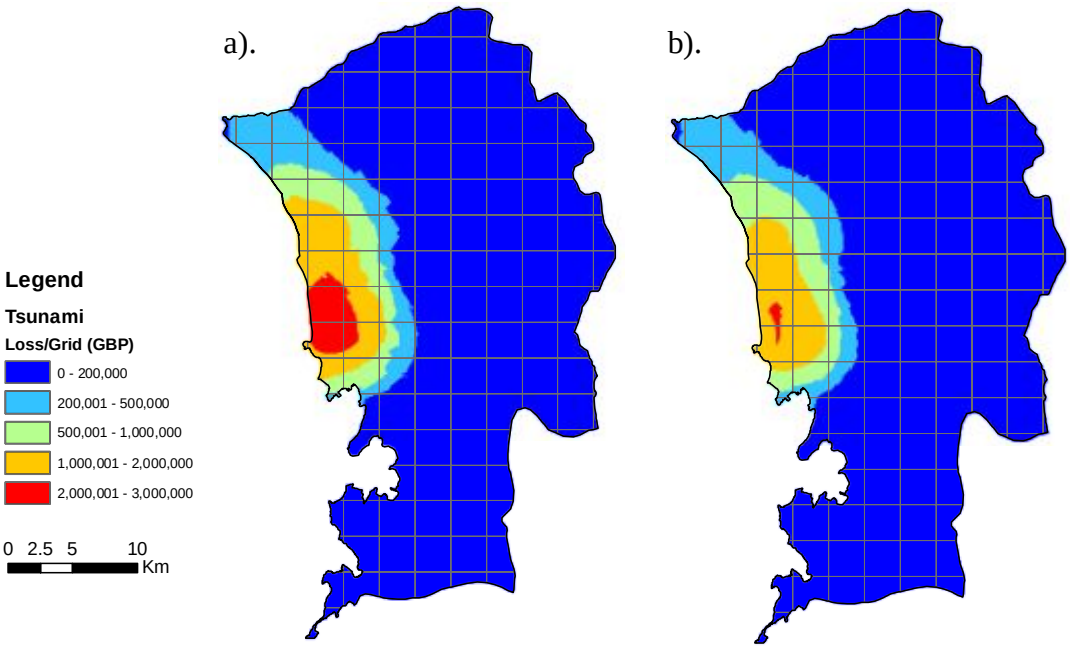

Figure 7.23. Predicted annual tsunami risk in Padang: a). existing building stock; b). seismically designed buildings

The resulted MDR and risk per unit area for all building categories in Padang subjected to tsunami hazard can be seen in Figure 7.24 and Figure 7.25. The MDR of RCI and steel structures is estimated to be similar and appears to be the lowest among other building categories. Yet, the risk of steel buildings is higher than that of RCI buildings due to the high cost of the steel buildings.

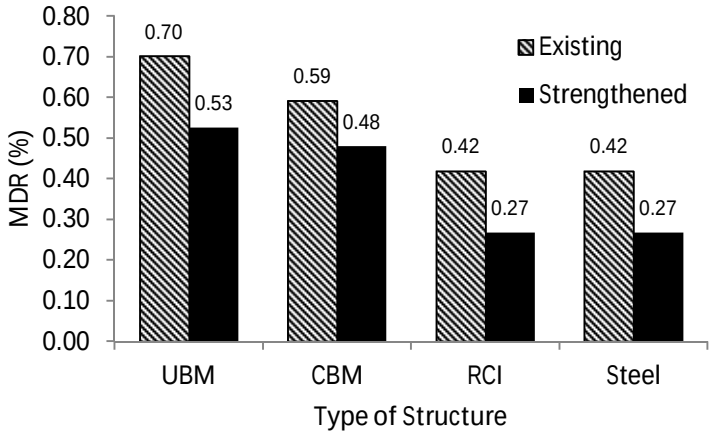

Figure 7.24. Tsunami MDR per year for building categories in Padang

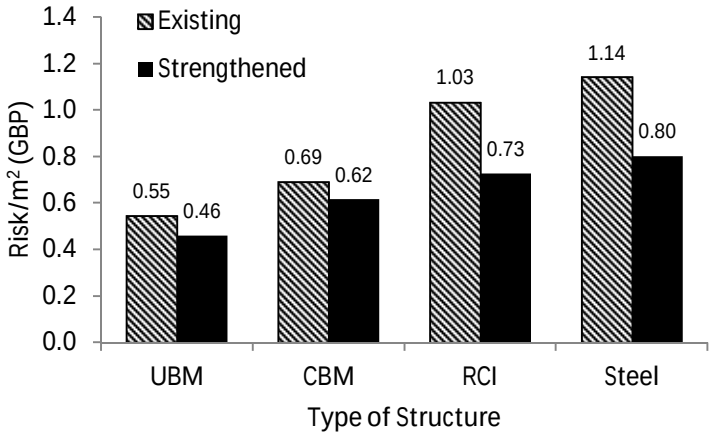

Figure 7.25. Annual tsunami risk/m^2 per year for existing building stock in Padang

7.6.2. Earthquake and Tsunami Building Insurance

The level of earthquake and tsunami hazard in most areas of Indonesia is generally high. The high reconstruction costs following earthquakes may burden the national economy. As an alternative solution, the Indonesian government can oblige seismic insurance for buildings to distribute the risk to building owners and insurance companies. The implementation of building insurance can not only reduce the

government's fiscal exposure, but also encourage the risk mitigation and safer building practice (Yucemen, 2005).

7.6.3. Tsunami Vertical Evacuation Shelters

Padang city is prone to near-field tsunami due to its close distance to one main tsunami source. Tsunami hazard assessment in this study estimates that a tsunami occurring in the Sumatra Subduction Zone is likely to hit the city in approximately 25 minutes (or longer) after the earthquake (see section 6.2.2). To minimise the casualties, the residences in the affected area have to be evacuated to higher ground before the tsunami arrival.

Despite being situated in a low lying area, Padang city has two locations of natural high grounds that can be utilised as tsunami evacuation sites. The first site, Gunung Pangilun is located around 2 km from the coast and has an area of more than 150,000 m^2 with a maximum elevation of about 50 m above the mean sea level. The site can be used to evacuate thousands of people and is relatively accessible from the city centre of Padang. The second site, Gunung Padang is a hill in the southern part of the city and located in front of the Indian Ocean. The site covers huge areas with a maximum ground elevation of about 300 m above the mean sea level. However, the site is separated from the city centre by the Batang Arau River (see Figure 7.26). The access to Gunung Padang is mainly provided by a box-girder bridge with an 8m wide and 156m span. To make the area fully functional as a tsunami evacuation site, more access bridges should be provided so that the location is more accessible to the nearby residences. Therefore, further study is required to assess the appropriate number of access bridges by considering the expected number of evacuees in the local area.

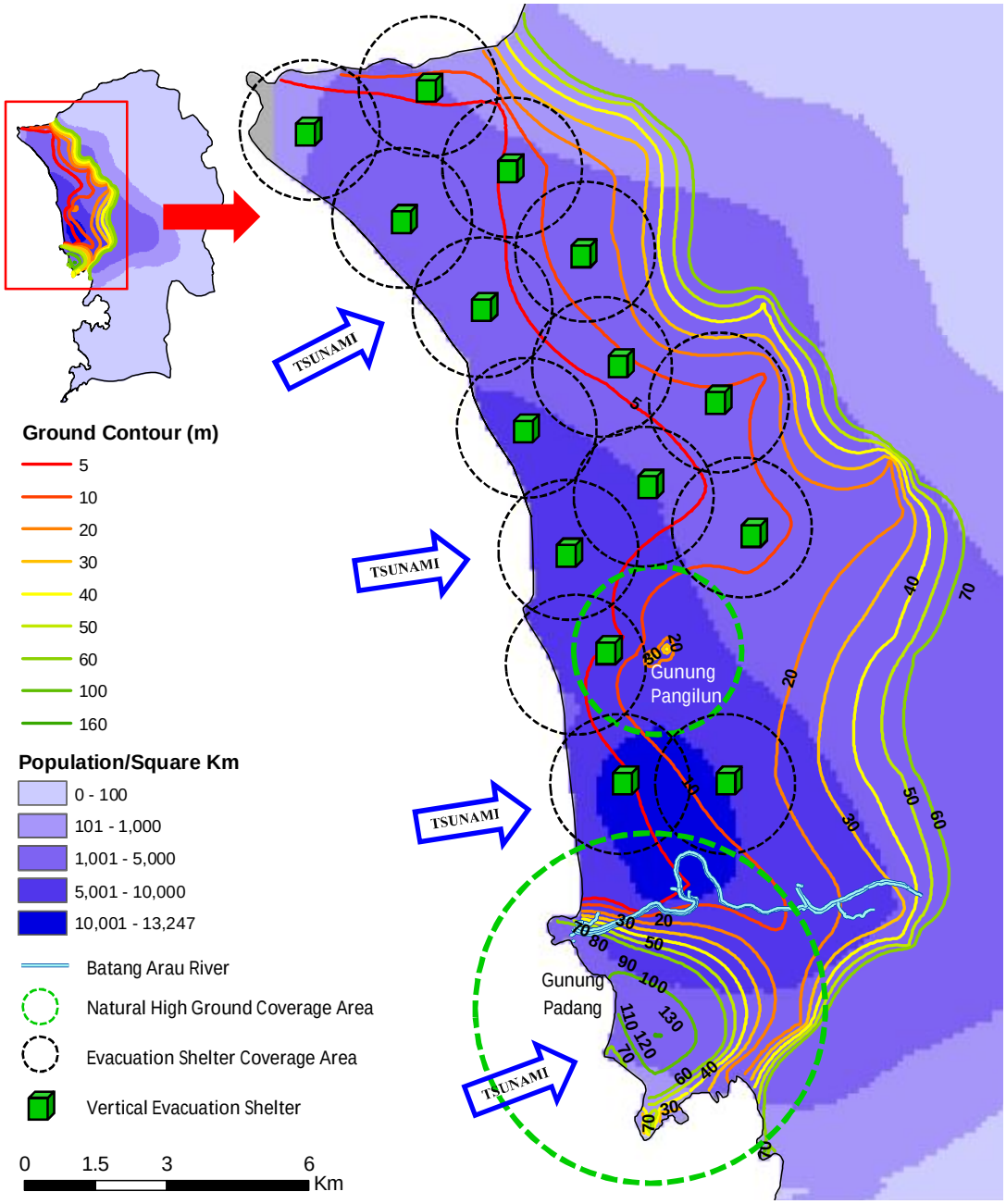

Figure 7.26. Vertical evacuation shelter plan for the city of Padang

Tsunami evacuation sites should be reachable by the evacuees within a walking distance. Park et al. (2012) developed a method to optimise the location of tsunami evacuation shelters and found that well distributed shelters produce better survival probability than that of a single optimised shelter. The method takes into account the walking speed of evacuees as well as possible evacuation delay associated with the evacuees' recognition level, as shown in Table 7.8 and Table 7.9, respectively. Park et al. (2012) found that the hazard awareness of the residences in the affected area played a significant role in the survival probability, since it was directly correlated to

the delay of evacuation process. Therefore, earthquake and tsunami evacuation drills have to be conducted regularly for the residents of Padang.

Table 7.8. Typical human walking speed (Park et al., 2012)

Age	Typical Walking Speed
Old (over 65)	1.253 m/s (4.11 ft/s)
Young (over 13)	1.509 m/s (4.95 ft/s)
Mean	1.381 m/s (4.53 ft/s)

Table 7.9. Delay time for various recognition level (Park et al., 2012)

Level	Recognition Level (%)	Delay Time (minutes)
Very Good	80-100	0
Good	50-80	2
Average	20-50	5
Poor	0-20	10

The information given by Park et al. (2012) can be utilised to develop tsunami evacuation shelters in Padang. To adopt a mean walking distance of 1.381 m/s and delay time of 5 minutes (average recognition level), the maximum distance to evacuation site in Padang is approximately 1.66 km. As a consequence, it appears that the available natural evacuation sites in Padang (Gunung Pangilun and Gunung Padang) can only be reached by a limited number of people from the immediate area, as shown in Figure 7.26. In this case, an artificial tsunami vertical system should be provided to shelter the people from tsunami.

FEMA P646 (2008) defines a tsunami vertical evacuation refuge as a building or earthen mound that can provide sufficient elevation to evacuees (above the level of tsunami inundation) and is designed and built to withstand tsunami waves. For near field tsunami, the vertical evacuation refuge should be capable of resisting both earthquake and tsunami loads, which is the case for Padang city.

Unlike earthquake load, the determination of tsunami load remains challenging. As previously mentioned in Chapter 6, tsunami loading comprises many forces including hydrostatic forces, buoyant forces, hydrodynamic forces, impulsive forces, debris impact forces, debris damming forces, uplift forces and additional gravity

loads from retained water on elevated floors (FEMA, 2008). Most of those forces depend on the tsunami inundation height, which is obtained from tsunami hazard assessment. Several studies consider that the 1797 and 1833 tsunamis represent the most plausible events for Padang in the near future (Borrero et al., 2006; Schlurmann et al., 2010). The 1797 and 1833 events are associated with earthquake magnitude of M_w 8.4 and M_w 8.8-9.2, respectively. These events inundated the coastal area of Padang in a range of 5-10 m (Ismail et al., 2008). The outcome of PTHA in this study reveals that a 10 m high tsunami has a corresponding return period of 200 years (see Figure 6.16 and Figure 6.17). The 10 m tsunami run-up can be used as a minimum threshold for designing tsunami vertical evacuation shelters in Padang. However, a higher tsunami height, corresponding to a longer tsunami return period, can also be adopted from Figure 6.16 to take into account the uncertainty in determining the design height of tsunami run-up.

Figure 7.26 shows the proposed minimum tsunami evacuation plan for Padang city. The evacuation plan is developed based on a maximum distance to the evacuation site of 1.66 km, a tsunami run-up height of 10 m, the ground-elevation level and the population density in the area. The existing natural high grounds and evacuation structures are incorporated in the tsunami evacuation system. It is observed that the city requires at least 17 tsunami evacuation points. Two of them are naturally high grounds, as shown by the dashed-green circles in Figure 7.26. As a consequence, 15 of the evacuation points should be constructed artificially (dashed-black circles).

A few examples of artificial tsunami vertical evacuation refuges are shown in Figure 7.27 ranging from a berm to a life-saving tower or building. The construction of a berm (Figure 7.27(A)) is relatively simple and cost effective. However, it requires a lot of space and is more suitable for a less populated region. For an area with a limited space, tsunami evacuation structures are more appropriate.

The use of other buildings as tsunami vertical evacuation shelters is recommended by various studies (FEMA, 2008; Yeh et al., 2005). The shelter can be selected from existing buildings in the area, which are retrofitted to resist design earthquake and tsunami loads (Figure 7.27(D)). The area of the evacuation buildings does not necessarily have to be large. The evacuation building can be designed as a refuge to one or a few families, as shown in Figure 7.27(B), or it can be constructed to

evacuate thousands of people. The type of shelter construction should have resistance to buoyant/upward forces. RC or steel structures are generally appropriate for this purpose, which are also applicable for Padang city. It should be pointed out that tsunami evacuation buildings should be located on some distance inland to avoid tsunami wave-breaking force, which is normally not taken into account in the design. Generally, the tsunami wave breaks offshore; however, detailed tsunami numerical simulations should be performed in the investigated area for better mitigation planning.

Figure 7.26 also shows that Padang has a large proportion of its population near the coast. It is observed that the population density in some areas reaches more than 10,000 people/km^2. Consequently, numerous tsunami vertical evacuation refuges have to be built in those regions, which require a lot of investment and planning. However, many strategies can be implemented by the local authorities. First, the local government can utilise and retrofit public buildings (e.g. schools, office buildings, mosques, churches, etc.) in the area as tsunami evacuation shelters. Second, the government can enforce that every building higher than 3 stories have to provide tsunami evacuation shelters in order to get building permission. Third, the government can encourage the residents to voluntarily build safe rooms as tsunami evacuation shelters with compensation in return (e.g. tax reduction, free interest loan, etc.). Guidelines for the design of tsunami shelters, and their dissemination to local engineers, are also required.

(A). Berm constructed for tsunami refuge in Aonae.

(B). Life-saving Tower.

(C). Nishiki Tower

(D). Aonae Elementary School for which the upper floors of the building are intended as tsunami evacuation shelter.

Figure 7.27. Several examples of tsunami vertical evacuation system in Japan (FEMA, 2008)

7.6.4. Tsunami Energy Dissipation Efforts

A tsunami event releases huge amounts of energy, which can cause devastating consequences to the affected coastal region. Total prevention of the tsunami wave propagation towards the coast is extremely difficult. However, many things can be done to dissipate part of the tsunami energy. Dissipating tsunami energy not only means reducing human casualties, but also decreasing economic consequences.

Jahromi (2009) suggested that high crested structures (e.g. vertical walls, rubble-mound structures), low crested/submerged structures (e.g. detached breakwater, artificial reefs), and soft structures (e.g. mangroves, sea-grasses) can be adopted to dissipate tsunami energy. Jahromi (2009) performed a study on offshore barriers

using the Steady-State Spectral Wave (STWAVE) model of the Surface Water Modelling System (SMS) and found that the offshore barrier can reduce the tsunami height by 83%.

A more eco-friendly approach of using coastal vegetation to dissipate tsunami energy was also investigated by various studies (Iimura and Tanaka, 2012; Osti et al., 2009; Sonak et al., 2008; Tanaka et al., 2011; Tanaka et al., 2007). The coastal forest reflects tsunami waves resulting in a reduction in the flow velocity, pressure and inundation depth. In addition, the coastal forest can trap debris, casualties and flotsam carried off by tsunami (Iimura and Tanaka, 2012). The efficiency of coastal vegetation for tsunami energy dissipation is proportional to the density of the vegetation (Iimura and Tanaka, 2012). Iimura and Tanaka (2012) found that an increased tree density from the coast can reduce tsunami height more than high density at the front. Based on satellite imageries and field data of the 2004 tsunami, Shelva (2005 cited in Osti et al., 2009) observed that 30 trees per 100 m^2 could reduce the maximum flow of tsunami by more than 90%.

Most of the tsunami energy dissipation methods above are feasible to be constructed in Padang. Currently, the city has approximately 8 km of rock groynes to protect the shoreline from long shore drift (see Figure 7.28(b)). The groynes can help reduce the tsunami energy. However, they may not be efficient, since the structures were not designed to resist tsunami waves. In this case, submerged structures or breakwaters can be constructed offshore of Padang. The structures should be designed appropriately so that they do not disrupt the traffic of the nearby port or sea view from the beach, which is one of the tourism assets in Padang. The bathymetry of the area shows that the sea depth of 10 m is located around 0.5-4 km from the coast line (see Figure 7.28(a)), which can be considered as the location of the submerged structures. However, further study is needed to appropriately design the structures and investigate their effect on the coast.

In addition, this study roughly estimates that the inland penetration of a tsunami with the recurrence period of 475 years in Padang can be reduced by up to 0.7 km from the coastline for an area with a densely treed landscape (see Section 6.5.1). It is observed that mangrove plants already exist in the less populated coastal area of Padang. However, the number is limited due to the rapid growth of population and

coastal deforestation. Hence, the rehabilitation of mangroves is necessary as an eco-friendly and cost effective solution to dissipate tsunami energy in the region. Osti et al. (2009) pointed out that the rehabilitation of mangrove ecosystems should take into account many aspects including the shape and the size of plants, their growth rate, life span, role in the ecosystem and benefits to communities. The coastal forest rehabilitation can be implemented at swamps or less populated areas of the city, particularly at the northern coastal area of Padang with a depth of around 0.7 km inland along the coast, as shown in Figure 7.28(b).

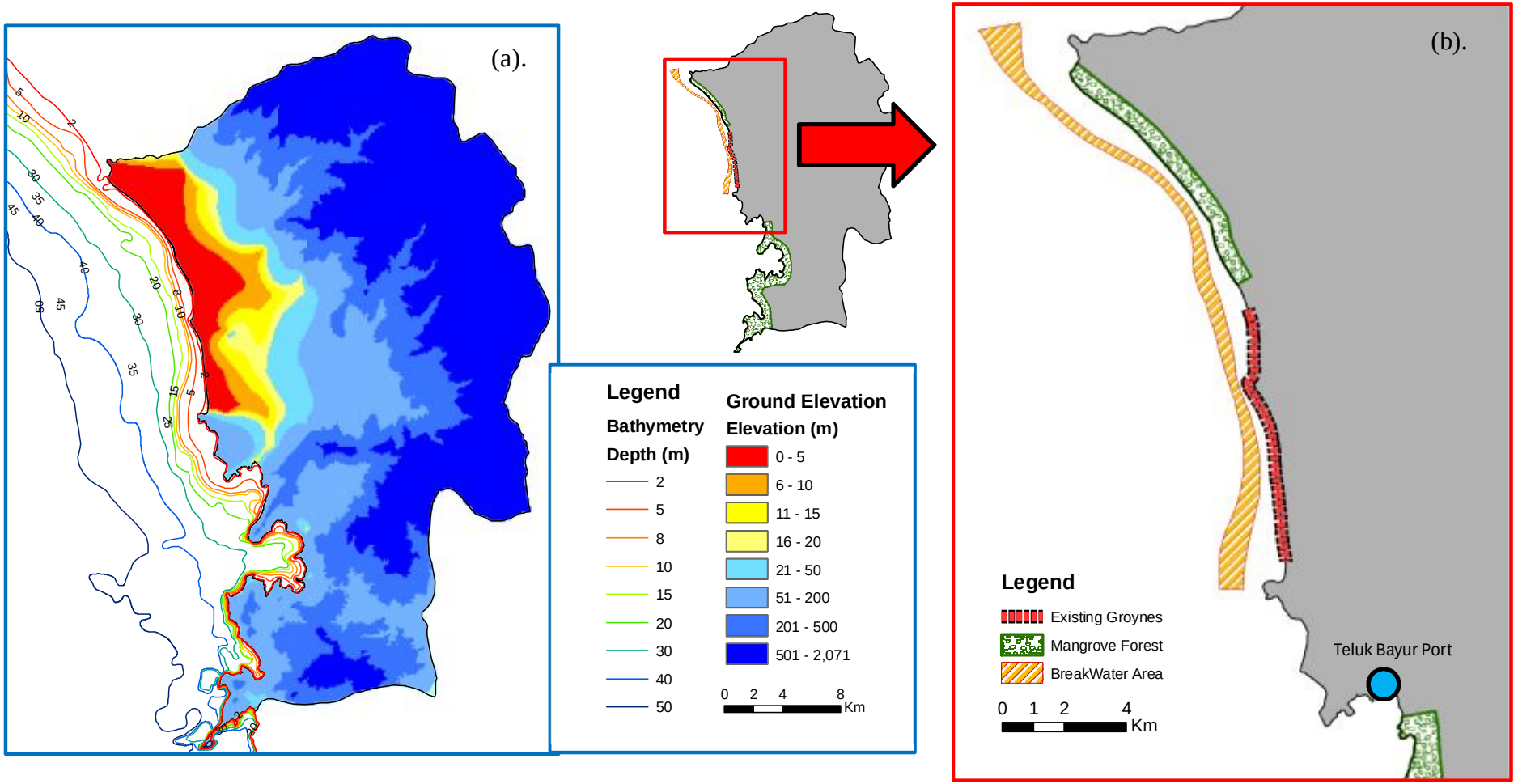

Figure 7.28. Coastal management plan for Padang city

7.7. SUMMARY

- The risk model developed in this study is verified against building damage data obtained from the M_w 7.6 of Padang. It is found that the loss estimated by the risk model is about 4.76% lower than that of the damage statistic. The results are reasonable considering that the risk model does not take liquefaction into account.
- This study reveals that existing building stock in Padang is highly vulnerable to earthquake and tsunami hazards. Estimated losses of £54.5 million and £30.8 million per annum are predicted for the building stock in Padang subjected to earthquakes and tsunamis, respectively. Building risk associated with tsunami in Padang is lower than that of earthquake due to infrequent occurrence of tsunamis in the area.
- It is found that the existing unreinforced brick masonry buildings are the most vulnerable, followed with the confined brick masonry, reinforced concrete structures with masonry infill and steel structures. However, the risk is decreased considerably if the buildings are designed according to modern seismic design standard (by 80% for earthquake and 25% for tsunami).
- This study estimates that the fatality risk due to earthquakes and tsunamis are 8 and 2000 fatalities per annum, respectively. Although tsunami events in Padang are infrequent, one event can lead to great fatalities. The high fatality risk can be attributed to poor tsunami mitigation systems in the region, including lack of tsunami vertical evacuation shelters in low lying coastal areas and the large distance from high ground.
- It is found that the earthquake insurance tariffs charged by 2 insurance companies in Indonesia are consistent with the risk obtained for seismically design structures, as shown in Figure 7.17. For RCI buildings, the total premiums obtained in this study are 8.1‰ and 1.4‰ for the existing and the seismically designed buildings, respectively. Estimated rates for steel structures are 3.1‰ for the existing building stock and 0.3‰ for buildings with good seismic performance. For other types of structures, the total premiums are estimated to be 16.6‰ and 3.1‰ for the existing and the seismically designed buildings, respectively. ACA Insurance applies a flat rate of 3‰ for all building types.

MAIPARK Insurance charges 1.9‰, 1.9‰ and 4.7‰ for RCI, steel and other structures, respectively.

- Tsunami insurance premiums for Padang are obtained. For the existing building stock, the recommended premium rates are 7‰ for RCI/steel structures and 9.9‰ for other building types. For seismically designed buildings, insurance rates of 4.5‰ and 8‰ are suggested for RCI/steel structures and other types of buildings, respectively.
- Seismic design of structures is mandatory for high seismicity region like Padang city and must be included as part of earthquake mitigation strategies. A modern seismic design standard (SNI 03-1726-2002) similar to the American UBC 1997 is available in Indonesia. However, its implementation and supervision for buildings in Indonesia are unmeasured. Therefore, the Indonesian government must enforce seismic design requirements for all buildings in the region.
- A nationwide obligatory seismic insurance for buildings can be used as an alternative to reduce the government's fiscal exposure
- Tsunami evacuation sites need to be well distributed and reachable by the evacuees within a walking distance. This study finds that the maximum distance to evacuation site in Padang is approximately 1.66 km. Therefore, at least 17 points of tsunami evacuations refuges are required for Padang city, to increase the survival probability of the residents in the area.
- Various types of refuges can be developed including earthen mounds or specially designed evacuation buildings. Earthen mounds are more suitable for less populated regions as they require a lot of space. Tsunami evacuation buildings are a better alternative for more densely populated areas.
- Design guidelines for tsunami evacuation shelters should be developed for the region.
- Many solutions to dissipate tsunami energy in Padang are proposed including the development of sea structures (e.g. vertical walls, rubble mound structures, breakwaters and artificial reefs) as well as the rehabilitation of mangrove forest along the coastal area. The latter approach is more eco-friendly and cost effective. However, it is only applicable for less populated areas.

CHAPTER 8

CONCLUSIONS AND RECOMMENDATIONS FOR FUTURE WORKS

8.1. INTRODUCTION

An Earthquake Risk Assessment Framework (ERA Framework), suitable for use in developing countries, has been developed at the University of Sheffield. A stochastic method is used with readily available seismological information. The framework was initially developed by Kythreoti (2002) and Khan (2011) to estimate earthquake hazard and risk. The framework is extended in this study to take time dependent seismicity as well as tsunami hazard into account. An integrated earthquake and tsunami risk assessment has been rarely, if ever, conducted in previous studies.

The extended ERA Framework contains three main parts: PSHA, PTHA, as well as earthquake and tsunami risk modules. The main conclusions from each part of the framework and mitigation strategies for the case study area (Padang city) are presented in the following sections.

8.2. CONCLUSIONS

8.2.1. Probabilistic Seismic Hazard Assessment (PSHA)

From the review of existing PSHA methods it can be concluded that:

- The conventional PSHA method assumes that earthquake distribution in a seismic zone is uniform. This assumption may spatially smooth the seismicity of a region and may affect the reliability of the results.
- A Poissonian (time independent) model, generally adopted in the conventional PSHA, does not appropriately characterise the observed seismicity due to its stationary hazard rate assumption.
- The integration nature of the conventional PSHA method has limited the flexibility of the method to utilize a non-Poissonian model due to mathematical and computational problems.

- The use of instrumental earthquake catalogue to characterize the seismicity of a region, as suggested by Khan (2011), may result in unrealistic hazard estimates, particularly for the areas where the instrumental catalogues are not representative of the seismicity.
- The deaggregation procedure to compute the fractional contribution of seismic sources to total hazard in the conventional PSHA method may lead to uncertainties due to the selection of bin size, the grouping of scenario and the selection of quantities utilized in the deaggregation process.

From the extended PSHA method it can be concluded that:

- The utilization of recurrence relationships and the generation of synthetic earthquakes based on the rupture areas of real events in the new PSHA method have minimized the smoothed seismicity problem, as well as the unrealistic hazard estimates associated with the incompleteness of the earthquake catalogue (see Figure 4.10).
- Seismic hazard maps corresponding to 10% probability of exceedance in 50 years are produced for Sumatra (see Figure 5.4). It is observed that the Indonesian seismic code SNI-03-1726-2002 (see Figure 2.7) applies 0.3g as the maximum PGA on bedrock in the region. However, this study finds that a maximum PGA of 0.65g on bedrock is expected in the area. This is consistent with the findings of recent studies (Irsyam et al., 2008; Irsyam et al., 2010; Petersen et al., 2004). Therefore, the implementation of a new hazard map in the Indonesian seismic standard for buildings is required.
- For Padang city, an average PGA of 0.23g and 0.3g on bed rock site is expected for 10% and 2% probability of exceedance in 50 years (see Figures 5.8 and 5.9). For 10% probability of exceedance in 50 years, the existing Indonesian code (SNI 03-1726-2002) applies a PGA value of 0.25g in the area, which is about 8% higher than that obtained in this study. However, uniform hazard spectra on rock site condition of this study shows higher spectral acceleration values than those required in the seismic standard, particularly for low natural period of buildings (see Figure 5.13).
- The deaggregation procedure to obtain hazard contribution from each seismic source is not required in the new PSHA methodology because all earthquake scenarios and associated PGAs can be obtained from the PSHA database. The

contributions of major seismic sources to seismic hazard in Padang are shown in Figure 5.10 to Figure 5.12. The figure reveals that higher PGAs are most likely generated by near field events from the intraplate of the Sumatra Subduction Zone (SSZ). However, the interface earthquakes are capable of producing large magnitude earthquakes with shallow focal depth, which can trigger tsunamis. The earthquakes occurring on the Sumatran fault (SFZ) generally affect the eastern part of the city, which has less population and infrastructure.

- A time-dependent PSHA method is developed in this study to take into account the non-stationary rate of hazard over time using the empirical varying rate of hazard. This time-dependent method is not intended to predict earthquake, but to build more awareness to the upcoming hazards for mitigation purposes. This study finds that the seismicity at middle segments of the SSZ are likely to increase (about 2.52 times for Zone 4 and 1.74 times for Zone-5) and the region may experience higher ground motions in the near future in a range of 0.30-0.40g.
- A time-dependent hazard map is produced for Sumatra region. The map is capable of capturing the increase rate of hazard near Padang segment, which is consistent with the location of seismic gap estimated from previous studies (see Figure 5.15).

8.2.2. Probabilistic Tsunami Hazard Assessment (PTHA)

Based on the probabilistic tsunami hazard assessment developed in this study it can be concluded that:

- A relationship that correlates tsunami height, earthquake magnitude and closest distance to tsunami source is established for Sumatra based on tsunami numerical simulations (Equation 6.1). The relationship is used for rapid estimation of tsunami height in the PTHA module.
- An integrated PSHA and PTHA are developed in this study. The PTHA method estimates the heights of tsunamis associated with tsunamigenic events in the earthquake catalogue generated in the PSHA module.
- Tsunami heights and arrival time for Padang city are determined. An average tsunami height of 20.7 m is obtained at 10% probability of exceedance in 50 years. It is estimated that tsunamis occurring in the SSZ will inundate the coastal

area of Padang approximately within 15 minutes and 25 minutes after the earthquakes for intraplate and interface events, respectively.

- It is found that after the 2004 and 2005 tsunamis in North Sumatra, the hazard level in the middle part of the Sumatra Subduction Zone increases, particularly around the Padang and Bengkulu segments (see Figures 6.13 and 6.14).
- This study found that unlike earthquake hazard assessment, tsunami hazard assessment must consider both near-field and far-field tsunami sources. Near field tsunamis from intraplate of the Sumatra Subduction Zone are mostly generated by earthquakes located within 150 km from the coast of Padang with $M_w \geq 7.0$. Most tsunamis from the Sumatra subduction interface are generally triggered by earthquakes occurring more than 150 km from the coast with $M_w \geq 8.0$. Distant tsunamis from these interface events are capable of inundating the city with considerable tsunami heights (≥10m). The contributions of each tsunami source to tsunami hazard in Padang are shown in Figure 6.18.
- Tsunami rates and tsunami hazard curves are drawn for Padang city, as shown in Figures 6.16 and 6.17, respectively. It is found that the return period of significant tsunamis (≥10m) is approximately 200 years. An average tsunami height of 20.7m and 28m is expected in the area at 10% and 2% probability of exceedance in 50 years, respectively.
- Hydrostatic, hydrodynamic and impulsive forces associated with a 475 year tsunami event are estimated for Padang city based on a method proposed by FEMA P646 (2008). A hydrostatic force of 4262 kN per meter width of structural components is estimated for the region. It is predicted that the area is subjected to hydrodynamic forces in the range of 725-1065 kN per meter width. The maximum surge force is approximately 1.5 times the value of the hydrodynamic forces.

8.2.3. Risk Assessment

A probabilistic risk assessment framework has been developed to estimate earthquake and associated tsunami risks. Based on the risk framework it can be concluded that:

- The earthquake risk model is verified with building damage data due to the M_w 7.6 of Padang earthquake. It is found that the loss estimated by the risk model is about 4.76% lower than that of the available damage statistic.
- Earthquake and tsunami risk assessments are conducted for Padang city for four building categories. It is found that the existing unreinforced brick masonry buildings are the most vulnerable, followed with the confined brick masonry, reinforced concrete structures with masonry infill and steel structures. The earthquake risk decreases considerably (about 80%), if the buildings are designed according to modern seismic design standard. Tsunami risk for seismic design buildings is about 25% lower than that of the existing buildings with poor seismic performance.
- The earthquake risk obtained in this study is compared with earthquake risk premium charged by 2 insurance companies in Indonesia. It is observed that the earthquake insurance tariffs are consistent with the risk obtained for seismically design structures, as shown in Figure 7.17. For RCI buildings, the total premiums obtained in this study are 8.1‰ and 1.4‰ for the existing and the seismically designed buildings, respectively. Estimated rates for steel structures are 3.1‰ for the existing building stock and 0.3‰ for buildings with good seismic performance. For other types of structures, the total premiums are estimated to be 16.6‰ and 3.1‰ for the existing and the seismically designed buildings, respectively. ACA Insurance applies a flat rate of 3‰ for all building types. MAIPARK Insurance charges 1.9‰, 1.9‰ and 4.7‰ for RCI, steel and other structures, respectively.
- Tsunami insurance premiums for Padang are obtained. For the existing building stock, the recommended premium rates are 7‰ for RCI/steel structures and 9.9‰ for other building types. For seismically designed buildings, insurance rates of 4.5‰ and 8‰ are suggested for RCI/steel structures and other types of buildings, respectively.
- Building risk associated with tsunami in Padang is lower than that of earthquake due to infrequent occurrence of tsunamis in the area. The earthquake and tsunami risk for buildings in Padang is predicted to be £54.5 million and £30.8 million per annum, respectively. However, tsunamis can cause an immensely high fatality risk than that of earthquakes. This study finds that the fatality risk subjected to earthquakes and tsunamis are 8 and 2000 fatalities per annum, respectively.

8.2.4. Mitigation Strategies

- Seismic design of structures is mandatory for high seismicity region like Padang city and must be included as part of earthquake mitigation strategies. A modern seismic design standard (SNI 03-1726-2002) similar to the American UBC 1997 is available in Indonesia. However, its implementation and supervision for buildings in Indonesia are immeasurable. Therefore, the Indonesian government must enforce seismic design requirements for all buildings in the region.
- The Indonesian code, SNI 03-1726-2002, takes into account different ductility ranges of structures, as typically found in modern seismic standards. However, this study finds that the PGA values given in the earthquake hazard map of the code are generally lower than those obtained in this study. Hence, the revision of seismic design standard and the inclusion of a new hazard map for the region are required.
- The level of earthquake and tsunami risks for most Indonesian regions is considerably high, as seen in Figures 7.8-7.12. Consequently, the reconstruction costs due to the hazard are high and may burden the national economy. A nationwide obligatory seismic insurance for buildings can be used as an alternative solution to share the burden with building owners and insurance companies in the region. Incentives (e.g. tax cuts, free interest loans, etc.) can be given in return to encourage building owners to insure their properties.
- Tsunami evacuation sites need to be well distributed and reachable by the evacuees within a walking distance. This study finds that the maximum distance to evacuation site in Padang is approximately 1.66 km. Therefore, at least 17 points of tsunami evacuations refuges are required for Padang city, to increase the survival probability of the residents in the area.
- Various types of refuges can be developed including earthen mounds or specially designed evacuation buildings. Earthen mounds are more suitable for less populated regions as they require a lot of space. Tsunami evacuation buildings are a better alternative for more densely populated areas.
- Design guidelines for tsunami evacuation shelters should be developed for the region.
- Many solutions to dissipate tsunami energy in Padang are proposed including the development of sea structures (e.g. vertical walls, rubble mound structures,

breakwaters and artificial reefs) as well as the rehabilitation of mangrove forest along the coastal area. The latter approach is more eco-friendly and cost effective. However, it is only applicable for less populated areas.

8.3. LIMITATIONS OF THIS STUDY AND RECOMMENDATIONS FOR FUTURE WORKS

- The ERA Framework needs to be extended to take into account other earthquake associated hazards such as landslide and liquefaction. The landslide and liquefaction are generally caused by the stability problems of soil mechanics for which earthquake ground motions act as external forces that destabilise the soil and trigger the hazards. To incorporate the landslide/liquefaction into the ERA Framework, the recurrence relationships of the hazard parameters need to be obtained. The main hazard parameters for landslide are sliding mass and sliding distributions; while for liquefaction, the shear wave velocity of soil and SPT (Standard Penetration Test) resistance at a specific location and a particular depth have been used as an indicator for the liquefaction potential. In the absence of detailed empirical data, the hazard parameters can be obtained by simulating the landslide (or liquefaction) events using a Finite Element Method (FEM). Based on the outcomes of the FEM simulations, a correlation between the hazard parameters with the level of earthquake ground motions can be acquired; hence, any earthquake events that are likely to trigger the landslide/liquefaction on a site can be identified. Once the distribution of the hazard rate has been attained for all grids in the case study region, a stochastic method as that adopted in the PTHA can be implemented by randomly selecting the potential events from the randomised earthquake catalogue generated in the PSHA module (see Section 3.3.3). Then, the hazard curve for landslide or liquefaction can be developed.
- The PSHA method developed in this study does not take into account fault interactions due to limited seismological information in the investigated area. A physical earthquake model can be incorporated in the PSHA module to account for the fault interactions as well as to generate long catalogue of synthetic seismicity of the region (see Section 2.3.1.4). Consequently, more detailed seismological information such as slip distribution, slip rates, frictional coefficient, stress drop, and the healing time of fault elements at the examined

area are required. The physical earthquake model encompasses the physics of fault interactions and the frictional physics of fault segments; thus, it can better approximate the seismicity of the region with incomplete period of earthquake catalogues such as that of Sumatra.

- The uncertainty associated with the lack of data (i.e. the incompleteness of earthquake and tsunami catalogues) and the incorporation of subjective information (i.e. judgemental vulnerability relationship, visual inspection of building inventory) in the ERA Framework hasn't been addressed in this study. Therefore, the incorporation of a formal statistical approach such as Bayesian method may improve the reliability of the ERA Framework in the future. Furthermore, the Bayesian method may provide a better estimate for the recurrence relationships of earthquake and tsunami in the case study region, which has relatively short time period of observations.
- The hazard and risk maps of this study were produced using the ordinary Kriging interpolation of ArcGIS software. The interpolation method assumes that the spatial variation is isotropic in all directions. However, given the presence of faults and plate boundary in the case study area with a particular direction of strike angles, the use of anisotropic Kriging interpolation should be investigated. The anisotropic Kriging takes into account spatially dependent variation associated with the directivity of seismic sources in the examined region; hence, better outcomes may be obtained.
- In this study, high resolution bathymetry and topography data of the case study area are not available. As a result, wider applications such as the development of tsunami inundation maps and a detailed estimation of tsunami forces cannot be obtained; hence, they need to be done for future works.
- Ground attenuation relationships specifically for Indonesia are not available and need to be developed. The development of the ground attenuation relationships requires strong ground motion records of earthquakes in the region, which are still lacking in Indonesia.
- A detailed vulnerability assessment for existing building stock in Indonesia does not exist and needs to be conducted to get more accurate risk estimation.
- This study uses Gutenberg-Richter relationships to characterise the seismicity of the case study region. A better model of seismicity distribution such as

characteristic earthquake recurrence model can be utilized in the PSHA module given that the geological data of the seismic sources in the region are available.

- An optimization study to determine the locations of tsunami evacuation sites hasn't been done in this study and needs to be conducted for Padang city.
- A tsunami strengthening scheme for existing buildings need to be investigated as an alternative for tsunami evacuation refuges.

REFERENCES

2007 WGCEP. (2008). The Uniform California Earthquake Rupture Forecast, Version 2 (UCERF 2) *U.S. Geological Survey Open-File Report 2007-1437 and California Geological Survey Special Report 203 [http://pubs.usgs.gov/of/2007/1091/]*.

Abe, K. (1979). Size of Great Earthquakes of 1837–1974 Inferred From Tsunami Data. *J. Geophys. Res., 84*(B4), 1561–1568.

Abe, K. (1981). Physical size of tsunamigenic earthquakes of the northwestern Pacific. *Physics of the Earth and Planetary Interiors, 27*(3), 194-205.

Abe, K. (1985). Quantification of major earthquake tsunamis of the Japan Sea. *Physics of the Earth and Planetary Interiors, 38*(4), 214-223.

Abe, K. (1989). Quantification of tsunamigenic earthquakes by the Mt scale. *Tectonophysics, 166*(1-3), 27-34.

Abe, K. (1995). Estimate of Tsunami Run-up Height from Earthquake Magnitudes *Tsunami: Progress in Prediction, Disaster Prevention and Warning* (pp. 21-35). Dordrecht, The Netherlands: Kluwer Academic Publishers.

Abrahamson, N. (2006). *Seismic Hazard Assessment: Problems with Current Practice and Future Developments.* Paper presented at the First European Conference on Earthquake Engineering and Seismology (a joint event of 13th ECEE & 30th General Assembly of the ESC), Geneva, Switzerland.

ACA. (2011). Brosur Asuransi Rumah Idaman Retrieved 05 November, 2012, from http://www.asri-aca.com/jaminan.php

Adnan, A., Hendriyawan, Marto, A., and Masyhur, I. (2005). Seismic Hazard Assessment for Peninsular Malaysia Using Gumbel Distribution Method. *Jurnal Teknologi, 42(B)*, 57-73.

Ahmad, S. (2011). *Seismic Vulnerability of Non-Ductile Reinforced Concrete Structures in Developing Countries.* PhD, The University of Sheffield, Sheffield.

Akinci, A., Galadini, F., Pantosti, D., Petersen, M., Malagnini, L., and Perkins, D. (2009). Effect of time dependence on probabilistic seismic-hazard maps and deaggregation for the central Apennines, Italy. *Bulletin of the Seismological Society of America, 99*(2 A), 585-610. doi: 10.1785/0120080053

Appuhamy, J. M. R. S. (2007). Numerical Simulation of Tsunami in Indian Ocean. Pavia: MSc. Dissertation, Rose School.

Asrurifak, M., Irsyam, M., Budiono, B., Triyoso, W., and Hendriyawan. (2010). Development of Spectral Hazard Map for Indonesia with a Return Period of 2500 Years Using Probabilistic Method. *Civil Engineering Dimension, Vol. 12, No. 1*, 52-62.

Atkinson, G., and Boore, D. M. (2003). Empirical Ground Motion Realtions for Subduction Zone Earthquakes and Their Application to Cascadia and Other Regions. *Bulletin of Seismological Society of America, Vol. 93, No. 4*, 1703-1729.

Barber, A. J., Crow, M. J., and Milsom, J. S. (2005). *Sumatra: Geology, Resources and Tectonic Evolution.* London: Geological Society, Memoirs 13.

Beetham, D. (2009). The 30 September 2009 "Padang" Earthquake. New Zealand: New Zealand Society for Earthquake Engineering Inc.

Behnamfar, F., and Afshari, M. (2013). Collapse analysis and strengthening of stone arch bridges against earthquake. *International Journal of Architectural Heritage, 7*(1), 1-25.

Blaser, L., Kruger, F., Ohrnberger, M., and Scherbaum, F. (2010). Scaling Relations of Earthquake Source Parameter Estimates with Special Focus on Subduction Environment. *Bulletin of Seismological Society of America, Vol. 6*, 2914-2926.

Blaser, L., Ohrnberger, M., Krüger, F., and Scherbaum, F. (2012). Probabilistic tsunami threat assessment of 10 recent earthquakes offshore Sumatra. *Geophysical Journal International, 188*(3), 1273-1284.

Blaser, L., Ohrnberger, M., Riggelsen, C., Babeyko, A., and Scherbaum, F. (2011). Bayesian networks for tsunami early warning. *Geophysical Journal International, 185*(3), 1431-1443.

BMKG. (2010). Query Data Tsunami. Retrieved 30/04/2012, from Badan Meteorologi Klimatologi dan Geofisika http://inatews.bmkg.go.id/query_data.php

BNPB. (2009). Laporan Harian PUSDALOPS BNPB - 19 Oktober 2009. Jakarta: BNPB.

Bommer, J. J., and Abrahamson, N. A. (2006). Why do modern probabilistic seismic-hazard analyses often lead to increased hazard estimates. *Bulletin of the Seismological Society of America, Vol. 96, No. 6*, 1967-1977.

Boore, D. M., Joyner, W. B., and Fumal, T. E. (1997). Equations for Estimating Horizontal Response Spectra and Peak Acceleration from Western North American Earthquakes: A Summary of Recent Work. *Seismological Research Letters, Volume 68, Number 1*, 128-153.

Borrero, J. C., Sieh, K., Chlieh, M., and Synolakis, C. E. (2006). Tsunami inundation modeling for western Sumatra. *PNAS, Vol. 103, No. 52*, 19673–19677.

Briggs, R. W., Sieh, K., Amindon, W. H., Galetzka, J., Prayudi, D., Suprihanto, I., . . . Farr, T. G. (2008). Persistent elastic behavior above a megathrust rupture patch: Nias island, West Sumatra. *Journal of Geophysical Research B: Solid Earth, 113*(12).

Brizuela, B. (2005). Probabilistic Tsunami Hazard Assessment of El Salvador. Pavia: MSc. Dissertation, Rose School.

Bryant, E. (2001). *Tsunami, The Underrated Hazard*. Cambridge: Cambridge University Press.

Bugl, W. (2005). *Natural Catastrophe Risk Management Policy in Indonesia* Paper presented at the Global Conference on Insurance and Reinsurance for Natural Catastrophe Risk, Istanbul.

Burbidge, D., Cummins, P. R., Mleczko, R., and Thio, H. K. (2008). A Probabilistic Tsunami Hazard Assessment for Western Australia. *Pure appl. geophys. 165*, 2059-2088.

CCH. (2000). City and County of Honolulu Building Code (CCH) *Chapter 16 Article 11*. Honolulu, Hawaii: Department of Planning and Permitting of Honolulu Hawaii.

CCOHS. (2009). Hazard and Risk, from http://www.ccohs.ca/oshanswers/hsprograms/hazard_risk.html#_1_4

Chian, S. C., Whittle, J., Mulyani, R., Alarcon, J. E., and Wilkinson, S. M. (2010). *Post Earthquake Field Investigation of the Mw 7.6 Padang Earthquake of 30th September 2009.* Paper presented at the 14ECEE, Macedonia.

Chlieh, M., Avouac, J. P., Sieh, K., Natawidjaja, D. H., and Galetzka, J. (2008). Heterogeneous coupling on the Sumatra megathrust constrained from geodetic and paleogeodetic measurements. *J. Geophys. Res., 113*.

Coburn, A., and Spence, R. (2002). *Earthquake Protection, Second Edition*. West Sussex, England: John Wiley & Sons Ltd

Cramer, C. H., Petersen, M. D., Cao, T., Toppozada, T. R., and Reichle, M. (2000). A Time-Dependent Probabilistic Seismic-Hazard Model for California. *Bulletin of the Seismological Society of America, 90, 1*, 1-21.

Deniz, A. (2006). *Estimation of Earthquake Insurance Premium Rates Based on Stochastic Methods*. MSc, Middle East Technical University, Çankaya, Ankara, Turkey.

Dominey-Howes, D., Dunbar, P., Varner, J., and Papathoma-Köhle, M. (2010). Estimating probable maximum loss from a Cascadia tsunami. *Natural Hazards, 53*(1), 43-61. doi: 10.1007/s11069-009-9409-9

Eckert, N., Keylock, C. J., Bertrand, D., Parent, E., Faug, T., Favier, P., and Naaim, M. (2012). Quantitative risk and optimal design approaches in the snow avalanche field: Review and extensions. *Cold Regions Science and Technology, 79–80*(0), 1-19. doi: http://dx.doi.org/10.1016/j.coldregions.2012.03.003

EERI. (2009). Learning from Earthquakes, The Mw 7.6 Western Sumatra Earthquake of September 30, 2009: Earthquake Engineering Research Institute (EERI) Special Earthquake Report.

Egozcue, J., and Rüttener, E. (1996). Bayesian techniques for seismic hazard assessment using imprecise data. *Natural Hazards, 14*(2-3), 91-112. doi: 10.1007/bf00128259

Ellsworth, W. L., Matthews, M. V., Nadeau, R. M., Nishenko, S. P., Reasenberg, P. A., and Simpson, R. W. (1999, 22-25 February, 1999). *A Physically-Based Earthquake Recurrence Model for Estimation of Long-Term Earthquake Probabilities.* Paper presented at the Workshop on EARTHQUAKE RECURRENCE: STATE OF THE ART AND DIRECTIONS FOR THE FUTURE, Istituto Nazionale de Geofisica, Rome, Italy.

Elnashai, A. S., and Sarno, L. D. (2008). *Fundamentals of Earthquake Engineering.* West Sussex, UK: John Wiley & Sons Ltd.

EM-DAT (Producer). (2011, October 26). The OFDA/CRED International Disaster Database. *www.emdat.be*. Retrieved from http://www.emdat.be/disaster-list

Felzer, K. R. (2008). Appendix M: Empirical Estimation of Regional Time Variation in Seismicity Rates *USGS Open File Report 2007-1437M*: U.S. Department of the Interior, USGS.

FEMA. (2003). *Multi-hazard Loss Estimation Methodology, Earthquake Model: HAZUS MR4, Technical Manual.* Washington, D.C.: Department of Homeland Security, Emergency Preparedness and Response Directorate, FEMA-Mitigation Division.

FEMA P55. (2011). Coastal Construction Manual *Principles and Practices of Planning, Siting, Designing, Constructing, and Maintaining Residential Buildings in Coastal Areas (Fourth Edition)*: Federal Emergency Management Agency.

FEMA P646. (2008). *Guidelines for Design of Structures for Vertical Evacuation from Tsunamis.* Washington, D.C.: Federal Emergency Management Agency.

FEMA. (2009). Multi-hazard Loss Estimation Methodology, Earthquake Model, HAZUS-MH MR4 User Manual. Washington, D.C.: Department of Homeland Security, Federal Emergency Management Agency, Mitigation Division.

Ferraes, S. G. (2003). The conditional probability of earthquake occurrence and the next large earthquake in Tokyo, Japan. *Journal of Seismology 7*, 145-153.

Ferson, S. (2003). Bayesian methods in risk assessment. New York.

Field, E. H. (2007). Review Article: A Summary of Previous Working Groups on California Earthquake Probabilities. *Bulletin of the Seismological Society of America, Vol. 97*, 1033-1053.

Garcia-Fernandez, M., and Egozcue, J. J. (1989). Seismic Hazard Assessment in TERESA Based on a Bayesian Technique Test Areas. *Natural Hazards, 2*, 249-265.

Gardner, J. K., and Knopoff, L. (1974). Is the sequence of Earthquakes in Southern California, with Aftershocks removed, Poissonian? *Bulletin of Seismological Society of America, Vol. 64, No. 5*, 1363-1367.

GEBCO. (2012). General Bathymetric Chart of the Oceans (GEBCO_08 Grid). from British Oceanographic Data Centre (BODC) http://www.gebco.net/

Geist, E. L., and Parsons, T. (2006). Probabilistic Analysis of Tsunami Hazard. *Natural Hazards, 37*, 277-314.

Genrich, J. F., Bock, Y., McCaffrey, R., Prawirodirdjo, L., Stevens, C. W., Puntodewo, S. S. O., . . . Wdowinski, S. (2000). Distribution of slip at the northern Sumatran fault system. *Journal of Geophysical Research B: Solid Earth, 105*(B12), 28327-28341.

GESI. (2001). Final Report: Global Earthquake Safety Initiative (GESI) Pilot Project: GeoHazards International, United Nations Centre for Regional Development.

Gisler, G., Weaver, R., and Gittings, M. L. (2006). Sage Calculations of the Tsunami Threat from La Palma. *Science of Tsunami Hazards, 24*(4), 288-301.

Google Earth. (2011). The Map of Padang City, Indonesia (Version 6.1.0.5001): Google Inc.

Goto, C., and Ogawa, Y. (1991). Numerical Method of Tsunami Simulation With the Leap-Frog Scheme, Translated for the TIME Project by Prof. Shuto, N. Sendai, Japan: Disaster Control Research Center, Faculty of Engineering, Tohoku University.

Gusiakov, V. K. (2001). Basic Pacific Tsunami Catalog and Database, 47 BC-2000 AD: Results of The First Stage of the Project. *ITS 2001 Proceedings, Session 1, Number 1-2*, 263-272.

Gusiakov, V. K. (2012). Tsunami Catalogs. Retrieved 30 April 2012, from Tsunami Laboratory, Novosibirsk, Russia tsun.sscc.ru/

Gutenberg , B., and Richter , C. F. (1954). *The Seismicity of the Earth*. Princeton, NJ, USA . Princeton University Press

Hamzah, L., Puspito, N. T., and Imamura, F. (2000). Tsunami Catalog and Zones in Indonesia. *Journal of Natural Disaster Science, Volume 22, Number 1*, 25-43.

Hanka, W., Saul, J., Weber, B., Becker, J., and Harjadi, P. (2010). Real-time earthquake monitoring for tsunami warning in the Indian Ocean and beyond. *Natural Hazards and Earth System Science, 10*(12), 2611-2622.

Heaton, T. H., Tajima, F., and Mori, A. W. (1986). Estimating Ground Motions Using Recorded Accelerograms *Survey in Geophysics, 8*, 25-83.

Hoedajanto, D. (2007). *Apakah Jakarta Aman Terhadap Gempa Desain Maksimum.* Paper presented at the Seminar HAKI: "Konstruksi Tahan Gempa Indonesia", Jakarta.

IDNDR. (1990-2000). RADIUS (Risk Assessment Tools for Diagnosis of Urban Areas Against Seismic Disasters). Geneva: United Nations Initiative Towards Earthquake Safe Cities

Iimura, K., and Tanaka, N. (2012). Numerical simulation estimating effects of tree density distribution in coastal forest on tsunami mitigation. *Ocean Engineering, 54*(0), 223-232. doi: 10.1016/j.oceaneng.2012.07.025

Imamura, F. (1989). Tsunami Numerical Simulation with the staggered leap-frog scheme (Numerical code of TUNAMI-N1): School of Civil Engineering, Asian Inst. Tech. and Disaster Control Research Center, Tohoku University.

Imamura, F., Yalciner, A. C., and Ozyurt, G. (2006). Tsunami Modelling Manual (TUNAMI Model): Disaster Control Research Center, Tohoku University., Sendai, Japan.

IOC. (2008). Tsunami Glossary, 2008. Paris: UNESCO.

Irsyam, M., Dangkua, D. T., Hendriyawan, Hoedajanto, D., Hutapea, B. M., Kertapati, E. K., . . . Petersen, M. D. (2008). Proposed Seismic Hazard Maps of Sumatra and Java Island and Microzonation Study of Jakarta City, Indonesia. *Journal Earth System Science*, 865-878.

Irsyam, M., Sengara, I. W., Aldiamar, F., Widiyantoro, S., Triyoso, W., Natawidjaja, D. H., . . . Ridwan, M. (2010). Summary of Study: Development of Seismic Hazard Maps of Indonesia for Revision of Hazard Map in SNI 03-1726-2002. Bandung: Technical Committee on Building Construction Material and civil Engineering, Ministry of Public Works of Republic of Indonesia.

Ismail, F. A., Hakam, A., Nur, O. F., and Adji, B. M. (2008). *Study on Tsunami Evacuation Route in Padang City – West Sumatra*. School of Civil Engineering, Andalas University, Padang. Padang.

Jahromi, B. E. (2009). *Design of a tsunami barrier to The North of Penang Island.* Master Thesis, Universiti Teknologi Malaysia.

Kanamori, H. (1972). Mechanism of tsunami earthquakes. *Physics of the Earth and Planetary Interiors, 6*(5), 346-359.

Kanit, R., and Altin, M. (2010). A method for the cost estimation in strengthening school buildings in Turkey. *Scientific Research and Essays, 5*(9), 923-933.

Khan, S. A. (2011). An Earthquake Risk Assessment Framework for Developing Countries: Pakistan A Case Study. Sheffield: PhD Thesis, The University of Sheffield.

Khan, S. A., Hajirasouliha, I., Guadagnini, M., and Pilakoutas, K. (2010). *A Probabilistic Seismic Hazard Assessment Method for Earthquake Risk Assessment in Developing Countries.* Paper presented at the 14ECEE, Ohrid.

Koshimura, S., Oie, T., Yanagisawa, H., and Imamura, F. (2009). Developing Fragility Functions for Tsunami Damage Estimation Using Numerical Model and Post-Tsunami Data from Banda Aceh, Indonesia. *Coastal Engineering Journal, 51*(3), 243-273.

Kyodo. (2011). Houses Destroyed (pp. Rescue workers search for Japan earthuake victims amid shattered houses in Nodamura, Iwate Prefecture, on March 14). Nodamura: Reuters.

Kyriakides, N. (2007). *Vulnerability of RC Buildings And Risk Assessment for Cyprus.* Doctor of Philosophy, The University of Sheffield, Sheffield.

Kythreoti, S. (2002). Earthquake Risk Assessment and Management. Case Study: Cyprus. Sheffield: PhD Thesis, The University of Sheffield.

Latief, H., Sengara, I. W., and Kusuma, S. B. (2008). *Probabilistic Seismic and Tsunami Hazard Analysis Model for Input To Tsunami Warning and Disaster Mitigation Strategies.* Paper presented at the International Conference on Tsunami Warning (ICTW), Bali, Indonesia.

Latief, H., Sengara, I. W., and Sunendar, H. (2009, 18-19 March). *Probabilistic Tsunami Hazard Analysis Model - For Input to Tsunami Disaster Mitigation Strategies in Banda Aceh City* Paper presented at the Estimating tsunami recurrence and its behavior in the indian ocean through tsunami sedimentation survey Tsukuba.

Levin, B., and Nosov, M. (2009). *Physics of Tsunamis*: Springer.

Li, L., Xia, J., Xu, C.-Y., and Singh, V. P. (2010). Evaluation of the subjective factors of the GLUE method and comparison with the formal Bayesian method in uncertainty assessment of hydrological models. *Journal of Hydrology, 390*(3–4), 210-221. doi: http://dx.doi.org/10.1016/j.jhydrol.2010.06.044

Løvholt, F., Kühn, D., Bungum, H., Harbitz, C. B., and Glimsdal, S. (2012). Historical tsunamis and present tsunami hazard in eastern Indonesia and the southern Philippines. *Journal of Geophysical Research: Solid Earth, 117*(B9), B09310. doi: 10.1029/2012jb009425

Løvholt, F., Pedersen, G., and Gisler, G. (2008). Oceanic propagation of a potential tsunami from the La Palma Island. *Journal of Geophysical Research: Oceans, 113*(C9), C09026. doi: 10.1029/2007jc004603

Lukkunaprasit, P., Ruangrassamee, A., and Thanasisathit, N. (2009a). Tsunami loading on buildings with openings. *Science of Tsunami Hazards, 28*(5), 303-310.

Lukkunaprasit, P., Thanasisathit, N., and Yeh, H. (2009b). Experimental Verification of FEMA P646 Tsunami Loading. *Journal of Disaster Research, 4*(6), 410-418.

MAIPARK. (2007). Statistik Gempa Bumi Indonesia 2004 - 2007: PT. Asuransi Maipark Indonesia.

MAIPARK. (2011). Indonesian Earthquake Insurance Statistic: PT. Asuransi Maipark Indonesia.

MapAction. (2009). The damage level of houses due to the earthquake in Padang City. In MA077-IDN-Sit-150k_PadangCityDamage-21Oct2009-A3-v02-300dpi.jpg (Ed.), (Vol. 3.5 Mb). Saunderton, Buckinghamshire, UK: MapAction.

Matthews, M. V., Ellsworth, W. L., and Reasenberg, P. A. (2002). A Brownian model for recurrent earthquakes. *Bulletin of the Seismological Society of America, 92*(6), 2233-2250. doi: 10.1785/0120010267

Matthews, M. V., and Reasenberg, P. A. (1988). Statistical methods for investigating quiescence and other temporal seismicity patterns. *Pure and Applied Geophysics PAGEOPH, 126*(2-4), 357-372.

McCaffrey, R. (2009). The Tectonic Framework of The Sumatran Subduction Zone. *The Annual Review of Earth and Planetary Science, 37*, 345-366.

Megawati, K., and Pan, T. C. (2010). Ground-motion attenuation relationship for the Sumatran megathrust earthquakes. *Earthquake Engineering and Structural Dynamics, 39*(8), 827-845.

Moharram, A. M., Elghazouli, A. Y., and Bommer, J. J. (2008). A framework for a seismic risk model for Greater Cairo. *Soil Dynamics and Earthquake Engineering, 28*(10-11), 795-811. doi: 10.1016/j.soildyn.2007.10.009

Mouroux, P., and Le Brun, B. (2006). Presentation of RISK-UE project. *Bulletin of Earthquake Engineering, 4*(4), 323-339. doi: 10.1007/s10518-006-9020-3

Mulyani, R., Khan, S. A., Pilakoutas, K., Guadagnini, M., and Hajirasouliha, I. (2010). *A Proposed Method of Seismic and Tsunami Hazard Assessment, Case Study Sumatra.* Paper presented at the SECED-Young Engineers Conference - 2010, London.

Münch, U., Rudloff, A., and Lauterjung, J. (2011). Postface "The GITEWS Project - results, summary and outlook". *Natural Hazards and Earth System Science, 11*(3), 765-769.

Musson, R. M. W. (2000). The Use of Monte Carlo Simulations for Seismic Hazard Assessment in The UK. *Annali Di Geofisica, Vol. 43, N. 1*, 1-9.

Musson, R. M. W. (2004). *Objective validation of seismic hazard source models.* Paper presented at the 13th World Conference on Earthquake Engineering, Vancouver, B.C., Canada.

Natawidjaja, D. H. (2002). Neotectonics of the Sumatran Fault and Paleogeodesy of the Sumatran Subduction. California: PhD Thesis, California Institute of Technology.

Natawidjaja, D. H., Sieh, K., Ward, S. N., Cheng, H., Edwards, R. L., Galetzka, J., and Suwargadi, B. W. (2004). Paleogeodetic records of seismic and aseismic subduction from central Sumatran microatolls, Indonesia. *J. Geophys. Res., 109*(B4), B04306. doi: 10.1029/2003jb002398

Newcomb, K. R., and McCann, W. R. (1987). Seismic History and Seismotectonics of The Sunda Arc. *Journal of Geophysical Research*, 421-439.

Nishenko, S. P., and Buland, R. (1987). A generic recurrence interval distribution for earthquake forecasting. *Bulletin of the Seismological Society of America, 77*(4), 1382–1389.

NOAA. (2011). Tsunami Data and Information Retrieved 08/08/2011, 2011, from http://www.ngdc.noaa.gov/hazard/tsu.shtml

Okada, T., Sugano, T., Ishikawa, T., Ohgi, T., Takai, S., and Hamabe, C. (2005). Structural design methods of buildings for tsunami

resistance (SMBTR): The Building Center of Japan, Japan.

Okada, Y. (1985). Surface deformation due to shear and tensile faults in a half-space. *Bulletin of the Seismological Society of America, 75*(4), 1135-1154.

Osti, R., Tanaka, S., and Tokioka, T. (2009). The importance of mangrove forest in tsunami disaster mitigation. *Disasters, 33*(2), 203-213. doi: 10.1111/j.1467-7717.2008.01070.x

Palermo, D., Nistor, I., Nouri, Y., and Cornett, A. (2009). Tsunami loading of near-shoreline structures: a primer. *Canadian Journal of Civil Engineering, 36*, 1804–1815. doi: 10.1139/L09-104

Parithusta, R. (2007). *New Attenuation Relation for Earthquake Ground Motions in Indonesia Considering Deep Source Events.* Paper presented at the Seminar HAKI: "Konstruksi Tahan Gempa Indonesia", Jakarta.

Park, S., van de Lindt, J. W., Gupta, R., and Cox, D. (2012). Method to determine the locations of tsunami vertical evacuation shelters. *Natural Hazards, 63*(2), 891-908.

Parsons, T., and Geist, E. L. (2009). Tsunami Probability in the Carribean Region. *Pure appl. geophys. 165*, 2089-2116.

Peiris, N. (2006). *Vulnerability functions for tsunami loss estimation*. Paper presented at the First European conference on Earthquake Engineering and Seismology: a joint event of the 13th ECEE and 30th General Assembly of the ESC, Geneva, Switzerland.

Petersen, M., Harmsen, S., Mueller, C., Haller, K., Dewey, J., Luco, N., . . . Rukstales, K. (2007a). Documentation for the Southeast Asia Seismic Hazard Maps *Administrative Report September 30, 2007*: U.S. Department of the Interior, USGS.

Petersen, M. D., Cao, T., Campbell, K. W., and Frankel, A. D. (2007b). Time-independant and Time-dependant Seismic Hazard Assessment for the State of California: Uniform California Earthquake Rupture Forecast Model 1.0. *Seismological Research Letters, Volume 78, Number 1*, 99-109.

Petersen, M. D., Dewey, J., Hartzell, S., Mueller, C., Harmsen, S., Frankel, A. D., and Rukstales, K. (2004). Probabilistic Seismic Hazard Analysis for Sumatra, Indonesia and Across the Southern Malaysian Peninsula. *Tectonophysics, 390*, 141-158.

Power, W., Downes, G., and Stirling, M. (2007). Estimation of tsunami hazard in New Zealand due to South American earthquakes. *Pure and Applied Geophysics, 164*(2-3), 547-564.

Prih-Harjadi, P. J., and Fauzi. (2009). *Development of Indonesia Tsunami Early Warning System (InaTEWS) toward Regional Tsunami Watch Provider (RTWP)*. Paper presented at the DEWS Midterm Conference, Postdam, Germany.

Puspito, N. T., and Gunawan, I. (2005). Tsunami Sources in The Sumatra Region, Indonesia and Simulation of the 26 December 2004 Aceh Tsunami. *ISET Journal of Earthquake Technology, Paper No. 459, Vol. 42, No. 4*, 111-125.

Reasenberg, P. (1985). Second-Order Moment of Central California Seismicity, 1969–1982. *J. Geophys. Res., 90*(B7), 5479-5495. doi: 10.1029/JB090iB07p05479

Reasenberg, P. A., Hanks, T. C., and Bakun, W. H. (2003). An Empirical Model for Earthquake Probabilities in the San Francisco Bay Region, California, 2002-2031. *Bulletin of the Seismological Society of America, v. 93* (no. 1), 1-13 doi: 10.1785/0120020014

Reese, S., Bradley, B. A., Bind, J., Smart, G., Power, W., and Sturman, J. (2011). Empirical building fragilities from observed damage in the 2009 South Pacific tsunami. *Earth-Science Reviews, 107*(1–2), 156-173. doi: 10.1016/j.earscirev.2011.01.009

Reese, S., Cousins, W. J., Power, W. L., Palmer, N. G., Tejakusuma, I. G., and Nugrahadi, S. (2007). Tsunami Vulnerability of Buildings and People in South Java-field Observations after the July 2006 Java Tsunami. *Natural Hazards Earth System Science, 7*, 573-589.

Robinson, R., and Benites, R. (1995). Synthetic seismicity models of multiple interacting faults. *Journal of Geophysical Research: Solid Earth, 100*(B9), 18229-18238. doi: 10.1029/95jb01569

Rossetto, T., and Elnashai, A. (2003). Derivation of vulnerability functions for European-type RC structures based on observational data. *Engineering Structures, 25*(10), 1241-1263.

Rudloff, A., Lauterjung, J., Münch, U., and Tinti, S. (2009). The GITEWS project (German-indonesian tsunami early warning system). *Natural Hazards and Earth System Science, 9*(4), 1381-1382.

Rundle, J. B. (1988). A physical model for earthquakes: 2. Application to southern California. *Journal of Geophysical Research: Solid Earth, 93*(B6), 6255-6274. doi: 10.1029/JB093iB06p06255

Rundle, J. B., Rundle, P. B., Donnellan, A., Turcotte, D. L., Shcherbakov, R., Li, P., . . . Tiampo, K. F. (2005). A simulation-based approach to forecasting the next great San Francisco earthquake. *Proceedings of the National Academy of Sciences of the United States of America, 102*(43), 15363-15367. doi: 10.1073/pnas.0507528102

Rüttener, E., Egozcue, J., Mayer-Rosa, D., and Mueller, S. (1996). Bayesian estimation of seismic hazard for two sites in Switzerland. *Natural Hazards, 14*(2-3), 165-178. doi: 10.1007/bf00128264

Sabetta, F. (2005). Probabilistic and Deterministic Seismic Hazard Assessment

Sadigh, K., Chang, C. Y., Egan, J. A., Makdisi, F., and Youngs, R. R. (1997). Attenuation relationships for shallow crustal earthquakes based on California strong motion data. *Seismological Research Letters, 68*(1), 180-189.

Satake, K. (2002). Tsunamis. In W. H. K. Lee, H. Kanamori, P. C. Jennings & C. Kisslinger (Eds.), *International Handbook of Earthquake & Engineering Seismology, Part A* (pp. 437-451): Academic Press.

Scheer, S., Gardi, A., Guillande, R., Eftichidis, G., Varela, V., Vanssay, B. d., and Colbeau-Justin, L. (2011). Handbook of Tsunami Evacuation Planning. Luxembourg: European Commision, Joint Research Centre, Institute for the Protection and Security of the Citizen.

Schlurmann, T., Kongko, W., Goseberg, N., Natawidjaja, D. H., and Sieh, K. E. (2010). *Near-field tsunami hazard map Padang, West Sumatra: Utilizing high resolution geospatial data and reseasonable source scenarios.* Paper presented at the Proceedings of 32nd international conference on coastal engineering (ICCE2010).

Schlurmann, T., and Siebert, M. (2011). The Capacity Building programmes of GITEWS - Visions, goals, lessons learned, and re-iterated needs and demands. *Natural Hazards and Earth System Science, 11*(2), 293-300.

Sengara, I. W., Hendarto, Kertapati, E., Sukamta, D., and Sumiartha, P. (2007). *3-Dimensional Source Zones Probabilistic Seismic Hazard Analysis for Jakarta and Site-specific Response Analysis for Seismic Design Criteria of 45-storey Plaza Indonesia II Building.* Paper presented at the Seminar HAKI: "Konstruksi Tahan Gempa INdonesia", Jakarta.

Shapira, A. (1983). Potential earthquake risk estimations by application of a simulation process. *Tectonophysics, 95*(1-2), 75-89.

Shimbun, M. (2011). Moment of the tsunami (pp. A wave approaches Miyako City from the Heigawa estuary in Iwate Prefecture after the magnitude 8.9 earthquake struck the area, March 11, 2011). Miyako: Reuters.

Shuto, N., Goto, C., and Imamura, F. (1990). Numerical simulation as a means of warning for near field tsunamis. *Coastal. Engineering in Japan, 33*(2), 173-193.

Sieh, K. (2005, March 31). Aceh–Andaman earthquake: What happened and what's next? *Nature 434,* 573 - 574.

Sieh, K. (2007). The Sunda Megathrust, past, present and future. *Journal of Earthquake and Tsunami, Vol. 1, No. 1,* 1–19.

Sieh, K., Natawidjaja, D. H., Meltzner, A. J., Shen, C.-C., Cheng, H., Li, K.-S., . . . Edwards, R. L. (2008, December 12). Earthquake Supercycles Inferred from Sea-Level Changes Recorded in the Corals of West Sumatra. *Science, Vol. 322,* 1674-1678.

SNI 03-1726-2002. (2002). *Tata Cara Perencanaan Ketahanan Gempa Untuk Bangunan Gedung (SNI 03-1726-2002).* Jakarta: Badan Standardisasi Nasional.

Sonak, S., Pangam, P., and Giriyan, A. (2008). Green reconstruction of the tsunami-affected areas in India using the integrated coastal zone management concept. *Journal of Environmental Management, 89*(1), 14-23.

Soong, T. T. (2004). *Fundamentals of Probability and Statistics for Engineers*. West Sussex, England: John Wiley and Sons, Ltd.

Spence, R. (2007). Saving Lives in Earthquakes: Success and Failures In Seismic Protection Since 1960. *Bulletin of Earthquake Engineering, 5*, 139-251.

Spence, R., Coburn, A., and Pomonis, A. (1992). *Correlation of ground motion with building damage: the definition of a new damage based seismic intensity scale.* Paper presented at the Proceedings of the 10th World Conference Of Earthquake Engineering, Rotterdam.

Steinmetz, T., Raape, U., Teßmann, S., Strobl, C., Friedemann, M., Kukofka, T., . . . Dech, S. (2010). Tsunami early warning and decision support. *Natural Hazards and Earth System Science, 10*(9), 1839-1850.

Strasser, F. O., Arango, M. C., and Bommer, J. J. (2010). Scaling of the Source Dimensions of Interface and Intraslab Subduction-zone Earthquakes with Moment Magnitude. *Seismological Research Letters, Volume 81, Number 6,* 941-950.

Strunz, G., Post, J., Zosseder, K., Wegscheider, S., Mück, M., Riedlinger, T., . . . Muhari, A. (2011). Tsunami risk assessment in Indonesia. *Natural Hazards and Earth System Science, 11*(1), 67-82.

Suppasri, A., Mas, E., Koshimura, S., Imai, K., Harada, K., and Imamura, F. (2012). Developing tsunami fragility curves from the surveyed data of the 2011 great east Japan tsunami in Sendai and Ishinomaki plains. *Coastal Engineering Journal, 54*(1).

Sutjipto, S. (1994). Indonesia. In M. Paz (Ed.), *International Handbook Of Earthquake Engineering: Codes, Programs, and Examples* (pp. 277-295). New York: Chapman & Hall.

Tanaka, N., Jinadasa, K., Mowjood, M., and Fasly, M. (2011). Coastal vegetation planting projects for tsunami disaster mitigation: effectiveness evaluation of new establishments. *Landscape and Ecological Engineering, 7*(1), 127-135. doi: 10.1007/s11355-010-0122-3

Tanaka, N., Sasaki, Y., Mowjood, M., Jinadasa, K., and Homchuen, S. (2007). Coastal vegetation structures and their functions in tsunami protection: experience of the recent Indian Ocean tsunami. *Landscape and Ecological Engineering, 3*(1), 33-45. doi: 10.1007/s11355-006-0013-9

Thenhaus, P. C., and Campbell, K. W. (2003). Seismic Hazard Analysis *Earthquake Engineering Handbook*. Boca Raton, London, New York, Washington D.C.: CRC Press.

Tinti, S., Tonini, R., Bressan, L., Armigliato, A., Gardi, A., Guillande, R., . . . Scheer, S. (2011). Handbook of Tsunami Hazard and Damage Scenarios, SCHEMA (Scenarios for Hazard-induced Emergencies Management), Project no 030963, Specific Targeted Research Project, Space Priority. Luxembourg: European Commission, Joint Research Centre, Institute for the Protection and Security of the Citizen.

Titov, V. V., and Gonzalez, F. I. (1997). Implemenation and testing of the method of splitting tsunami (MOST) model: NOAA/Pacific Marine Environmental Laboratory.

Tsunami Laboratory Novosibirsk. (2005). Historical Tsunami Database For The Pacific, 47 B.C. To Present. from Intergovernmental Oceanographic Commission, Russian Foundation For Basic Research, Siberian Division Russian Academy Of Sciences, Institute Of Computational Mathematics And Mathematical Geophysics http://tsun.sscc.ru/htdbpac/

USGS (Producer). (2008, October 22). Tsunamis and Earthquake: Life of A Tsunami. *Western Coastal and Marine Geology*. Retrieved from http://walrus.wr.usgs.gov/tsunami/basics.html

USGS (Producer). (2009, November 23). Historic Worldwide Earthquakes. *Earthquake Hazards Program*. Retrieved from http://earthquake.usgs.gov/earthquakes/world/historical_country.php#indonesia

Valencia, N., Gardi, A., Gauraz, A., Leone, F., and Guillande, R. (2011). New tsunami damage functions developed in the framework of SCHEMA project: application to European-Mediterranean coasts. *Nat. Hazards Earth Syst. Sci., 11*, 2835-2846. doi: 10.5194/nhess-11-2835-2011

Wallace, R. E. (1970). Earthquake Recurrence Intervals on the San Andreas Fault. *The Geological Society of America Bulletin, 81*(10), 2875-2890.

Ward, S. N. (2000). San Francisco Bay Area Earthquake Simulations: A Step Toward a Standard Physical Earthquake Model. *Bulletin of the Seismological Society of America, 90*(2), 370-386. doi: 10.1785/0119990026

Weatherill, G., and Burton, P. W. (2010). An alternative approach to probabilistic seismic hazard analysis in the Aegean region using Monte Carlo simulation. *Tectonophysics, 492*(1-4), 253-278. doi: 10.1016/j.tecto.2010.06.022

Wells, D. L., and Coppersmith, K. J. (1994). New empirical relationships among magnitude, rupture length, rupture width and surface displacement. *Bulletin of the Seismological Society of America, 84*, 974-1002.

Wesnousky, S. G. (1994). The Gutenberg-Richter or characteristic earthquake distribution, which is it? *Bulletin of the Seismological Society of America, 84*(6), 1940-1959.

WGCEP. (1988). Probabilities of large earthquakes occurring in California on the San Andreas fault: U.S. Geol. Surv. Open-File Rept.

WGCEP. (1990). Probabilities of Large Earthquakes in the San Fransisco Bay Region, California: USGS Survey circular 1053.

WGCEP. (1995). Seismic hazards in Southern California: probable earthquakes, 1994 to 2024. *Bulletin of the Seismological Society of America, Vol. 85, No. 2*, 379-439.

WGCEP. (2003). Earthquake Probabilities in the San Francisco Bay Region: 2002–2031: U.S. Department of the Interior, USGS.

Wiemer, S. (2001). A software package to annalyze seismicity: ZMAP. *Seismological Research Letters 72 (2)*.

Wilkinson, S. M., Alarcon, J. E., Mulyani, R., Chian, D., and Whittle, J. (2009). The Padang Sumatra-Indonesia Earthquake of 30 September 2009, A Field Report

by EEFIT. London: Earthquake Field Investigation Team (EEFIT)-Institution of Structural Engineers UK.

Wilkinson, S. M., Alarcon, J. E., Mulyani, R., Whittle, J., and Chian, S. C. (2012). Observations of damage to buildings from M w 7.6 Padang earthquake of 30 September 2009. *Natural Hazards, 63*(2), 521-547.

Yeh, H. (2006). Maximum fluid forces in the tsunami runup zone. *Journal of Waterway, Port, Coastal and Ocean Engineering, 132*(6), 496-500.

Yeh, H. (2007). Design Tsunami Forces for Onshore Structures. *Journal of Disaster Research, 2*(6), 531-536.

Yeh, H., Robertson, I., and Preuss, J. (2005). Development of design guidelines for structures that serve as tsunami vertical evacuation sites. Olympia, Washington: Washington Department of Natural Resources, Division of Geology and Earth Resources.

Youngs, R. R., Chiou, S.-J., Silva, W. J., and Humprey, J. R. (1997). Strong Ground Motion Attenuation Relationships for Subduction Zone Earthquakes. *Seismological Research Letters*, 58-72.

Youngs, R. R., and Coppersmith, K. J. (1985). Implications of fault slip rates and earthquake recurrence models to Probabilistic Seismic Hazard Estimates. *Bulletin of the Seismological Society of America, 75*(4), 939-964.

Yucemen, M. S. (2005). Probabilistic Assessment of Earthquake Insurance Rates for Turkey. *Natural Hazards, 35*(2), 291-313. doi: 10.1007/s11069-004-6485-8

Zaytsev, A., Yalciner, A., Chernov, A., Pelinovsky, E., and Kurkin, A. (2002). MANUAL, Tsunami Simulation/Visualization Code, NAMI DANCE versions 4.9: Middle East Technical University, Turkey and Special Research Bureau for Automation of Marine Researches, Rusia.

Appendix A. Tsunami Catalogue of Sumatra

Day	Month	Year	Time	Latitude	Longitude	Depth (Km)	Mw	Height	Intensity	Validity	Fatality	Source
-	-	1770	-	-5.00	102.00	-	6.9	1.0	0.5	3		Gusiakov
10	2	1797	-	0.00	99.00	-	8.0	5.7	3	4	300	Gusiakov
18	3	1818	-	-3.77	102.27	-	7.0	2.0	1.5	3	0	BMKG
24	11	1833	-	-2.39	99.64	75	9.0	4.0	2.5	4		Gusiakov
29	9	1837	-	5.50	96.00	-	7.3	-	0.5	3		NOAA
5	1	1843	-	1.50	98.00	70	7.1	2.8	2	4		Gusiakov
31	10	1847	-	7.33	93.67	-	-	-	-	3		NOAA
16	2	1861	-	-1.00	97.80	70	8.7	7.0	3	4	725	Gusiakov
9	3	1861	-	0.00	98.00	20	7.0	2.8	2	4		Gusiakov
26	4	1861	-	1.00	97.50	70	7.0	2.0	1.5	4		Gusiakov
17	6	1861	-	1.00	97.50	-	6.8	-	0.5	3		NOAA
25	9	1861	-	-1.50	100.00	-	6.5	2.0	1.5	3		Gusiakov
31	12	1881	-	8.52	92.43	-	7.9	1.2	-	3		NOAA
26	8	1883	-	-6.10	105.40	-	-	1.4	1	3		Gusiakov
27	8	1883	23:36:00	-6.10	105.40	-	-	35.0	4.5	4	36000	Gusiakov
4	1	1907	07:36:00	2.00	94.50	60	-	2.8	2	4	400	Gusiakov
6	2	1908	-	-2.00	100.00	130	7.5	1.4	1	3		Gusiakov
19	6	1930	-	-5.60	105.30	33	6.1	1.5	-	3		Gusiakov
25	9	1931	23:53:36	-5.00	102.75	87	7.4	1.0	-	3		NOAA
26	6	1941	20:48:00	12.50	92.50	35	7.6	1.5	-	4	5000	NOAA
26	9	1957	-	-8.20	107.30	33	5.8	1.0	-	3		Gusiakov
2	4	1964	04:47:14	5.99	95.41	133	6.9	0.0	-	3		Gusiakov
12	4	1967	20:38:48	5.07	96.22	17	7.4	2.0	1.5	3	14	Gusiakov
24	2	1982	09:04:10	4.37	97.75	52	5.4	0.1	-	4		Gusiakov
13	9	2002	11:23:48	13.04	93.07	21	7.8	0.0	0	3	0	Gusiakov
26	12	2004	23:33:22	3.30	95.98	10	9.1	50.9	4	4	226898	NOAA

Day	Month	Year	Time	Latitude	Longitude	Depth (Km)	Mw	Height	Intensity	Validity	Fatality	Source
28	3	2005	03:50:48	2.09	97.11	30	8.7	3.0	-	-	10	BMKG
10	4	2005	11:40:24	-1.64	99.61	19	6.7	0.4	-	-	0	BMKG
24	7	2005	00:00:00	7.90	92.10	33	7.0	0.0	-	-	0	BMKG
17	7	2006	07:47:29	-9.25	107.41	33	7.7	20.9	-	4	802	NOAA
12	9	2007	04:10:43	-4.44	101.37	10	8.4	5.0	-	4	-	NOAA
25	2	2008	14:37:12	-2.49	99.97	10	6.5	0.1	-	4	-	NOAA
10	8	2009	22:14:14	14.10	92.89	30	7.5	0.0	-	3	-	NOAA
16	8	2009	15:20:41	-1.48	99.49	21	6.7	0.2	-	4	-	NOAA
2	9	2009	00:00:00	-8.24	107.32	60	7.0	1.0	-	-	0	BMKG
30	9	2009	06:27:41	-0.72	99.87	81	7.6	0.3	-	4	-	NOAA
6	4	2010	06:00:36	2.38	97.05	34	7.8	0.4	-	4	-	NOAA
12	6	2010	10:44:10	7.88	91.94	17	7.5	0.0	-	4	-	NOAA
25	10	2010	16:56:48	-3.49	100.08	10	7.8	7.0	-	4	431	NOAA
4	4	2011	02:39:36	-10.01	107.69	10	7.1	0.0	-	-	0	BMKG
11	1	2012	14:46:48	2.41	93.09	10	7.1	0.0	-	-	0	BMKG
11	4	2012	15:26:48	2.31	93.06	10	8.6	0.0	-	4	-	NOAA
11	4	2012	17:16:24	0.82	92.42	24	8.1	0.0	-	4	0	BMKG

Appendix B. Parameters of the tsunami events simulated in the tsunami numerical analyses

No	Mw[1]	Depth (km)	Lon[2]	Lat[3]	Strike Angle	Dip Angle	Rake Angle	Date	H[4] (m)	I[5]	Validity	Fatality	H_t[6] (m)	time[7] (minutes)
1	9.1	10	95.98	3.30	322.98	12.00	90.00	26/12/2004	50.9	4.0	4	226898	1.8	93.4
2	9.0	30	99.64	-2.39	322.98	12.00	90.00	24/11/1833	4.0	2.5	4	-	20.1	12.0
3	8.7	30	97.11	2.09	322.98	12.00	90.00	28/03/2005	3.0	-	-	10	0.7	93.6
4[*]	*8.6*	*10*	*93.06*	*2.31*	*322.98*	*12.00*	*0.00*	*11/04/2012*	*0.0*	-	*4*	-	*0.1*	*90.0*
5	8.5	70	97.41	1.00	322.98	50.00	90.00	16/02/1861	7.0	3.0	4	725	0.4	30.1
6	8.4	10	101.37	-4.44	322.98	12.00	90.00	12/09/2007	5.0	-	4	-	1.2	60.0
7[*]	*8.1*	*24*	*92.42*	*0.82*	*322.98*	*12.00*	*0.00*	*11/04/2012*	*0.0*	-	*4*	*0*	*0.0*	*0.0*
8	8	32	99.36	-1.76	322.98	12.00	90.00	10/02/1797	5.7	3.0	4	300	3.4	21.2
9	7.8	34	97.05	2.38	322.98	12.00	90.00	06/04/2010	0.4	-	4	-	0.0	0.0
10	7.8	10	100.08	-3.49	322.98	12.00	90.00	25/10/2010	7.0	-	4	431	0.2	47.9
11	7.6	50	94.50	2.00	322.98	12.00	90.00	04/01/1907	2.8	2.0	4	400	0.0	0.0
12	7.6	81	99.87	-0.72	322.98	50.00	90.00	30/09/2009	0.3	-	4	-	0.2	2.0
13	7.5	130	100.00	-2.00	322.98	50.00	90.00	06/02/1908	1.4	1.0	3	-	0.1	7.5
14	7.4	87	102.75	-5.00	322.98	50.00	90.00	25/09/1931	1.0	-	3	-	0.0	0.0
15	7.4	17	96.22	5.07	322.98	12.00	90.00	12/04/1967	2.0	1.5	3	14	0.0	0.0
16	7.3	78	96.00	5.50	322.98	50.00	90.00	29/09/1837	-	0.5	3	-	0.0	0.0
17	7.2	70	98.00	1.50	322.98	50.00	90.00	05/01/1843	2.8	2.0	4	-	0.0	0.0
18[*]	*7.1*	*10*	*93.09*	*2.41*	*322.98*	*12.00*	*0.00*	*11/01/2012*	*0.0*	-	-	*0*	0.0	0.0
19	7.0	32	102.00	-5.00	322.98	12.00	90.00	-/-/1770	1.0	0.5	3	-	0.0	0.0
20	7.0	72	102.27	-3.77	322.98	50.00	90.00	18/03/1818	2.0	1.5	3	0	0.0	0.0
21	7.0	20	98.00	0.00	322.98	12.00	90.00	09/03/1861	2.8	2.0	4	-	0.0	0.0
22	7.0	70	97.50	1.00	322.98	50.00	90.00	26/04/1861	2.0	1.5	4	-	0.0	0.0

No	Mw[1]	Depth (km)	Lon[2]	Lat[3]	Strike Angle	Dip Angle	Rake Angle	Date	H[4] (m)	I[5]	Validity	Fatality	H_t[6] (m)	time[7] (minutes)
23	9.0	30	96.25	2.39	322.98	12.00	90.00	Synthetic	-	-	-	-	4.7	62.6
24	9.1	10	97.79	-1.07	322.98	12.00	90.00	Synthetic	-	-	-	-	10.2	39.5
25	9.1	10	94.28	3.04	322.98	12.00	90.00	Synthetic	-	-	-	-	1.8	81.4
26	9.1	10	100.52	-4.67	322.98	12.00	90.00	Synthetic	-	-	-	-	7.4	39.4

[1] The moment magnitude of earthquake

[2] The longitude of earthquake epicentre

[3] The latitude of earthquake epicentre

[4] Tsunami wave height at coastal areas of Sumatra recorded by tide gauges

[5] Tsunami Intensity

[6] Maximum tsunami height at Padang city estimated from tsunami numerical simulations

[7] Tsunami arrival time at Padang city estimated from tsunami numerical simulations

[*] Strike slip earthquake

APPENDIX C

Building inventory for Padang City

AU	Building Area (m^2)				AU	Building Area (m^2)			
	UBM	**RBM**	**RCI**	**Steel**		**UBM**	**RBM**	**RCI**	**Steel**
0	0	0	0	0	27	0	0	0	0
1	0	0	0	0	28	0	0	0	0
2	0	0	0	0	29	0	0	0	0
3	0	0	0	0	30	0	0	0	0
4	0	0	0	0	31	0	0	0	0
5	0	0	0	0	32	71.6	286.4	47.5	0
6	0	0	0	0	33	55727.4	222909.6	122927.5	0
7	0	0	0	0	34	108461.2	433844.8	239252.5	31344.14
8	0	0	0	0	35	92546.8	370187.2	204147.5	14733.17
9	0	0	0	0	36	76041.2	304164.8	167737.5	0
10	0	0	0	0	37	0	0	0	0
11	0	0	0	0	38	0	0	0	0
12	0	0	0	0	39	0	0	0	0
13	0	0	0	0	40	0	0	0	0
14	0	0	0	0	41	0	0	0	0
15	0	0	0	0	42	0	0	0	0
16	0	0	0	0	43	97.4	389.6	215	0
17	0	0	0	0	44	179857.4	719429.6	396745	0
18	0	0	0	0	45	88697.2	354788.8	195655	2161.81
19	0	0	0	0	46	94682.4	378729.6	208857.5	2171.51
20	0	0	0	0	47	0	0	0	0

AU	Building Area (m^2)				AU	Building Area (m^2)			
	UBM	**RBM**	**RCI**	**Steel**		**UBM**	**RBM**	**RCI**	**Steel**
21	4561.4	18245.6	3000	0	48	0	0	0	0
22	89666.6	358666.4	197795	0	49	0	0	0	0
23	33348.6	133394.4	73562.5	7770.93	50	0	0	0	0
24	5305.4	21221.6	3490	0	51	0	0	0	0
25	0	0	0	0	52	0	0	0	0
26	0	0	0	0	53	0	0	0	0
54	74818.4	299273.6	623487.5	0	82	0	0	0	0
55	168091.8	672367.2	1400765	0	83	0	0	0	0
56	94083	376332	207535	3603.241	84	98.4	393.6	4925	0
57	89064.6	356258.4	196465	0	85	71544	286176	3577198	61458.94
58	0	0	0	0	86	65462.2	261848.8	3273108	67241
59	0	0	0	0	87	147234.8	588939.2	1226955	146402.7
60	0	0	0	0	88	89666.6	358666.4	197795	0
61	0	0	0	0	89	89666.6	358666.4	197795	0
62	0	0	0	0	90	34669.6	138678.4	76477.5	0
63	0	0	0	0	91	0	0	0	0
64	45824.2	183296.8	381867.5	0	92	0	0	0	0
65	231212.2	924848.8	1926768	21856.27	93	35053.6	140214.4	23062.5	24161.2
66	156803.8	627215.2	103160	4555.191	94	120819.6	483278.4	266512.5	126198.7
67	129589.8	518359.2	85257.5	0	95	36276.6	145106.4	80022.5	0
68	76041.2	304164.8	167737.5	0	96	0	0	0	0
69	0	0	0	0	97	0	0	0	0
70	0	0	0	0	98	0	0	0	0
71	0	0	0	0	99	0	0	0	0
72	0	0	0	0	100	0	0	0	0
73	0	0	0	0	101	0	0	0	0

AU	Building Area (m^2)				AU	Building Area (m^2)			
	UBM	**RBM**	**RCI**	**Steel**		**UBM**	**RBM**	**RCI**	**Steel**
74	0	0	0	0	102	0	0	0	0
75	114201.8	456807.2	5710095	24813.36	103	615.2	2460.8	405	12544.28
76	54489.8	217959.2	2724493	11112.25	104	480.4	1921.6	315	0
77	157180.4	628721.6	103407.5	2573.384	105	73.4	293.6	47.5	0
78	100215.6	400862.4	65932.5	0	106	0	0	0	0
79	201017.2	804068.8	132247.5	0	107	0	0	0	0
80	0	0	0	0	108	0	0	0	0
81	0	0	0	0	109	0	0	0	0
110	0	0	0	0	127	16.2	64.8	10	0
111	230	920	152.5	0	128	117.4	469.6	77.5	0
112	1802.4	7209.6	1185	0	129	0	0	0	0
113	0	0	0	0	130	0	0	0	0
114	0	0	0	0	131	251	1004	165	0
115	0	0	0	0	132	0	0	0	0
116	0	0	0	0	133	0	0	0	0
117	0	0	0	0	134	0	0	0	0
118	0	0	0	0	135	0	0	0	0
119	0	0	0	0	136	0	0	0	0
120	1620.4	6481.6	1065	0	137	0	0	0	0
121	191.4	765.6	125	0	138	0	0	0	0
122	0	0	0	0	139	0	0	0	0
123	0	0	0	0	140	0	0	0	0
124	0	0	0	0	141	0	0	0	0
125	0	0	0	0	142	0	0	0	0
126	0	0	0	0	143	0	0	0	0

APPENDIX D

Assignment of earthquake vulnerability functions for existing building stock in Padang

Building Category	Rating Scheme[1]			Total Rate	Curve Type
	Design Quality	Construction Quality	Material Quality		
1. Existing Building Stock with Poor Seismic Performance					
– Unreinforced Brick masonry (UBM)	3	3	1	7	H
– Confined Brick Masonry (CBM)	3	3	1	7	F
– Reinforced Concrete Frame with Masonry Infill (RCI)	1	2	1	4	E
– Steel Frame (Steel)	1	2	1	4	D
2. Seismically Designed Building Stock					
– Unreinforced Brick masonry (UBM)	0	0	1	1	E
– Confined Brick Masonry (CBM)	0	0	1	1	D
– Reinforced Concrete Frame with Masonry Infill (RCI)	0	0	0	0	C
– Steel Frame (Steel)	0	0	0	0	A

[1] See APPENDIX E

APPENDIX E.1

Rating Scheme Quality for Structures (GESI, 2001)

Quality of design	
0	Engineered with seismic design
1	Engineered without seismic design, or non-engineered using seismic resistant 'rules of thumb' (e.g. lintel band for masonry)
2	Non-engineered, no seismic resistant elements, good proportions (short, wide, symmetric)
3	Non-engineered, no seismic resistant elements, poor proportions tall, narrow, or non-symmetric)

Quality of construction	
0	Excellent quality, effective supervision of seismic elements of construction
1	Good quality, some supervision of seismic elements of construction
2	Moderate quality, no supervision of seismic elements of construction but skilled workers
3	Poor quality, no supervision and unskilled workers

Quality of materials	
0	Good quality materials
1	Poor quality materials, or poor maintenance of building

APPENDIX E.2

Vulnerability Curve Assignments (GESI, 2001)

Building Types	**0**	**1**	**2**	**3**	**4**	**5**	**6**	**7**
– Wood	A	A	B	B	C	C	C	D
– Steel	A	B	C	C	D	D	E	F
– R/C	B	C	D	E	E	F	G	H
– R/C, steel infill	C	D	D	E	E	F	G	H
– Reinforced masonry	C	D	D	E	E	F	F	F
– URM	E	E	F	F	G	G	G	H
– Adobe	N/A	N/A	G	H	H	H	H	I
– Stone rubble	N/A	N/A	G	H	H	H	H	I
– Lightweight shack	N/A	N/A	N/A	H	H	H	H	I

APPENDIX E.3

The average damage state of a building for a given PGA (GESI, 2001)

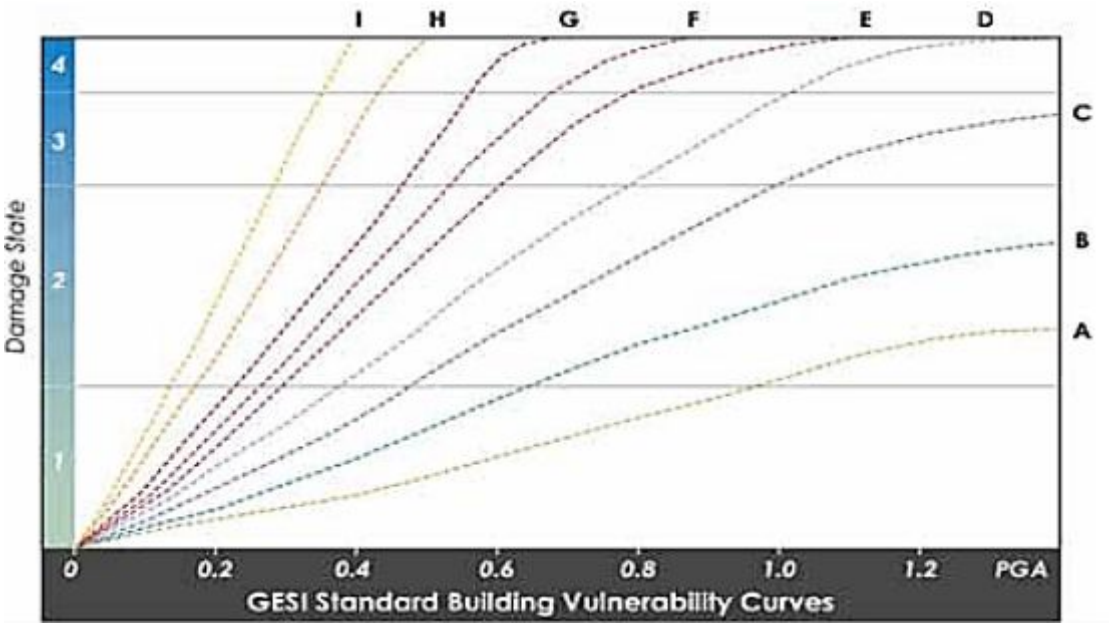

APPENDIX F[1]

TSUNAMI NUMERICAL MODEL

I. GOVERNING EQUATIONS

1.1. Shallow Water Theory

Tsunamis which are mainly generated by the movement of sea bottom due to earthquakes belong to long waves. In the theory of such waves, the vertical acceleration of water particles are negligible compared with the gravitational acceleration except for an oceanic propagation of tsunami (Kajiura, 1963). Consequently, the vertical motion of water particles has no effect on the pressure distribution. It is a good approximation that the pressure is hydrostatic.

Based upon these approximations and neglecting the vertical acceleration, the equations of mass conservation and momentum in the three dimensional problem (see Figure 1.1) are expressed by the following theory:

$$\begin{aligned}
&\frac{\partial \eta}{\partial t} + \frac{\partial u}{\partial x} + \frac{\partial v}{\partial y} + \frac{\partial w}{\partial z} = 0 \\
&\frac{\partial u}{\partial t} + u\frac{\partial u}{\partial x} + v\frac{\partial u}{\partial y} + w\frac{\partial u}{\partial z} + \frac{1}{\rho}\frac{\partial p}{\partial x} + \frac{1}{\rho}\left(\frac{\partial \tau_{xx}}{\partial x} + \frac{\partial \tau_{xy}}{\partial y} + \frac{\partial \tau_{xz}}{\partial z}\right) = 0 \\
&\frac{\partial v}{\partial t} + u\frac{\partial v}{\partial x} + v\frac{\partial v}{\partial y} + w\frac{\partial v}{\partial z} + \frac{1}{\rho}\frac{\partial p}{\partial x} + \frac{1}{\rho}\left(\frac{\partial \tau_{xy}}{\partial x} + \frac{\partial \tau_{yy}}{\partial y} + \frac{\partial \tau_{yz}}{\partial z}\right) = 0 \\
&g + \frac{1}{\rho}\frac{\partial \rho}{\partial z} = 0
\end{aligned} \qquad 1.1$$

where x and y are horizontal axes, z-the vertical axis, t-time, h-the still water depth, η-the vertical displacement of water surface above the still water surface; u, v and w are water particle velocities in the x, y and z directions, respectively, g-the gravitational acceleration, and τ_{ij}- the normal or tangential shear stress in the i-direction on the j-normal plane.

[1] The contents of this appendix are directly quoted and edited from Imamura et al. (2006) as the basis for tsunami numerical simulations adopted in this study.

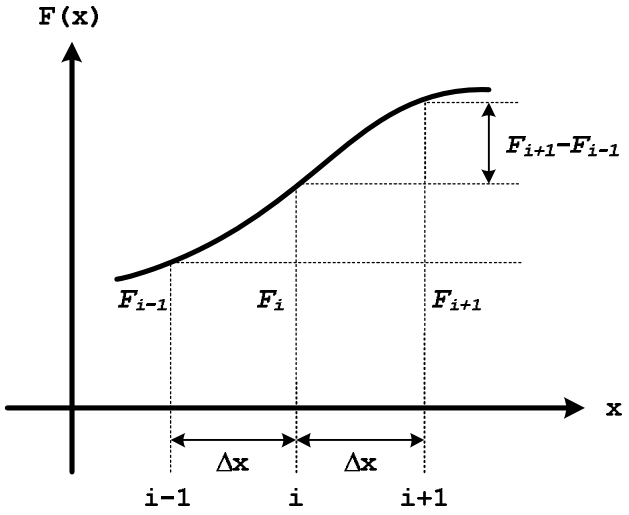

Figure 1.1. Central difference

The equation of momentum in the z-direction with the dynamic conditions at a surface that p=0 yields the hydrostatic pressure $p = \rho g(\eta - z)$

Any wave propagation problems can be solved by using the governing equations (Equation 1.1) with boundary conditions. The dynamic and kinetic conditions at surface and bottom are given as follows:

$$p = 0 \qquad \text{at } z = \eta \qquad 1.2$$

$$w = \frac{\partial \eta}{\partial t} + u\frac{\partial \eta}{\partial x} + v\frac{\partial \eta}{\partial y} \qquad \text{at } z = \eta \qquad 1.3$$

$$w = -u\frac{\partial h}{\partial x} - v\frac{\partial h}{\partial y} \qquad \text{at } z = -h \qquad 1.4$$

At this stage, Equation 1.1 can be integrated from the bottom to the surface by using Liebnitz rule. For example, the first term of the momentum equation in the x-direction is rewritten as follows:

$$\int_{-h}^{\eta} \frac{\partial u}{\partial t}\, dz = \frac{\partial}{\partial t}\int_{-h}^{\eta} u dz - u\left.\frac{\partial \eta}{\partial t}\right|_{z=\eta} + u\left.\frac{\partial(-h)}{\partial t}\right|_{z=-h}$$

With dynamic and kinetic condition - Equations 1.2-1.4, the following two dimensional equations can be obtained (this is called the shallow water theory):

$$\frac{\partial \eta}{\partial t} + \frac{\partial M}{\partial x} + \frac{\partial N}{\partial y} = 0$$

$$\frac{\partial M}{\partial t} + \frac{\partial}{\partial x}\left(\frac{M^2}{D}\right) + \frac{\partial}{\partial y}\left(\frac{MN}{D}\right) + gD\frac{\partial \eta}{\partial x} + \frac{\tau_x}{\rho} = A\left(\frac{\partial^2 M}{\partial x^2} + \frac{\partial^2 M}{\partial y^2}\right)$$

$$\frac{\partial N}{\partial t} + \frac{\partial}{\partial x}\left(\frac{MN}{D}\right) + \frac{\partial}{\partial y}\left(\frac{N^2}{D}\right) + gD\frac{\partial \eta}{\partial y} + \frac{\tau_y}{\rho} = A\left(\frac{\partial^2 N}{\partial x^2} + \frac{\partial^2 N}{\partial y^2}\right) \quad 1.5$$

Where, D is the total water depth given by $h + \eta$; τ_x and τ_y are the bottom frictions in the x and y directions; A is the horizontal eddy viscosity which is assumed to be constant in space; the shear stress on a surface wave is neglected. M and N are the discharge fluxes in the x and y directions which are given by

$$M = \int_{-h}^{\eta} u\, dz = u\,(h + \eta) = u\,D$$

$$N = \int_{-h}^{\eta} v\, dz = v\,(h + \eta) = v\,D \quad 1.6$$

1.2. Bottom friction

The bottom friction is generally expressed as follows, in an analogy to the uniform flow,

$$\frac{\tau_x}{\rho} = \frac{1}{2g}\frac{f}{D^2} M\sqrt{M^2 + N^2}$$

$$\frac{\tau_y}{\rho} = \frac{1}{2g}\frac{f}{D^2} N\sqrt{M^2 + N^2} \quad 1.7$$

Where, f is the friction coefficient. Without any detailed discussion of the value of f, it is preferred to use Manning's roughness (n) which is familiar among civil engineers. Values of n are given in Table 1.1 (Chow, 1960).

The friction coefficient (f) and Manning's roughness (n) are related by

$$n = \sqrt{\frac{f D^{1/3}}{2g}} \quad 1.8$$

This implies that f becomes rather large when the total depth (D) is small as n remains almost constant. Thus, the bottom friction terms are expressed by

$$\frac{\tau_x}{\rho} = \frac{fn^2}{D^{7/3}} M\sqrt{M^2 + N^2}$$

$$\frac{\tau_y}{\rho} = \frac{fn^2}{D^{7/3}} N\sqrt{M^2 + N^2} \qquad 1.9$$

Throughout the present model, the expression of bottom friction in Equation 1.9 is being used. The value of n should be selected depending on the condition of the bottom surface according to the Table 1.1.

Table 1.1 Values of Coefficient of Bottom Friction n
(after Linsley and Franzini, 1979)

Channel Material	n	Channel Material	n
Neat cement, smooth metal	0.010	Natural channels in good condition	0.025
Rubble masonry	0.017	Natural channels with stones and weeds	0.035
Smooth earth	0.018	Very poor natural channels	0.060

1.3. Governing equation

For the propagation of tsunami in the shallow water, the horizontal eddy turbulence could be negligible compared to the bottom friction except for run-up on the land. The following equations are therefore given as the fundamental equations in the present model.

$$\frac{\partial \eta}{\partial t} + \frac{\partial M}{\partial x} + \frac{\partial N}{\partial y} = 0$$

$$\frac{\partial M}{\partial t} + \frac{\partial}{\partial x}\left(\frac{M^2}{D}\right) + \frac{\partial}{\partial y}\left(\frac{MN}{D}\right) + gD\frac{\partial \eta}{\partial x} + \frac{gn^2}{D^{7/3}} M\sqrt{M^2 + N^2} = 0$$

$$\frac{\partial N}{\partial t} + \frac{\partial}{\partial x}\left(\frac{MN}{D}\right) + \frac{\partial}{\partial y}\left(\frac{N^2}{D}\right) + gD\frac{\partial \eta}{\partial x} + \frac{gn^2}{D^{7/3}} N\sqrt{M^2 + N^2} = 0 \qquad 1.10$$

1.4. Note on convection terms

The other expression of the shallow water equation using the averaged velocities in x and y directions (u and v) are often introduced by

$$\frac{\partial \eta}{\partial t} + \frac{\partial \overline{u}D}{\partial x} + \frac{\partial \overline{v}D}{\partial y} + \frac{\partial \overline{w}D}{\partial z} = 0$$

$$\frac{\partial \overline{u}}{\partial t} + \overline{u}\frac{\partial \overline{u}}{\partial x} + \overline{v}\frac{\partial \overline{u}}{\partial y} + \overline{w}\frac{\partial \overline{u}}{\partial z} + g\frac{\partial \eta}{\partial x} + \frac{gn^2}{D^{1/3}}\overline{u}\sqrt{\overline{u}^2 + \overline{v}^2} = 0$$

$$\frac{\partial \bar{v}}{\partial t} + \bar{u}\frac{\partial \bar{v}}{\partial x} + \bar{v}\frac{\partial \bar{v}}{\partial y} + \bar{w}\frac{\partial \bar{v}}{\partial z} + g\frac{\partial \eta}{\partial x} + \frac{gn^2}{D^{1/3}}\bar{v}\sqrt{\bar{u}^2 + \bar{v}^2} = 0 \qquad 1.11$$

It should be noted that the above equation cannot be used in a numerical model for runup because it does not satisfy conservation of momentum. For example, the convection terms in the momentum equation in the x direction in Equation 1.10 divided by D can be modified as

$$\frac{1}{D}\left\{\frac{\partial}{\partial x}\left(\frac{M^2}{D}\right) + \frac{\partial}{\partial y}\left(\frac{MN}{D}\right)\right\} = \bar{u}\frac{\partial \bar{u}}{\partial x} + \bar{v}\frac{\partial \bar{u}}{\partial x} + \frac{\bar{u}}{D}\left\{\frac{\partial(\bar{u}D)}{\partial x} + \frac{\partial(\bar{v}D)}{\partial y}\right\}$$
$$= \bar{u}\frac{\partial \bar{u}}{\partial x} + \bar{v}\frac{\partial \bar{u}}{\partial x} + \frac{\bar{u}}{D}\frac{\partial \eta}{\partial t} \qquad 1.12$$

The convection terms in Equation 1.10 are not the same as those in Equation 1.11 and even if the mass conservation equation in Equation 1.10 is applied, the third term in left side of Equation 1.12 cannot be eliminated. Note that in the case of tidal current with longer wave period than tsunami in which acceleration term, the third term in left side of Equation 1.12 is neglected.

II. NUMERICAL SCHEME

2.1. Numerical scheme for linearized equation

For the first step to describe the numerical scheme for the tsunami model, the linearized long wave equation without bottom frictions in one-dimensional propagation, Equation 2.1, is introduced.

$$\frac{\partial \eta}{\partial t} + \frac{\partial M}{\partial x} = 0$$
$$\frac{\partial M}{\partial t} + gD\frac{\partial \eta}{\partial x} = 0 \qquad 2.1$$

The finite difference method can be used to solve the above equation numerically. The finite difference method based upon the Taylor expansion series is shown as follows.

$$\eta(x, t + \Delta t) = \eta(x, t) + \Delta t\frac{\partial \eta(x,t)}{\partial t} + \frac{\Delta t^2}{2}\frac{\partial^2 \eta(x,t)}{\partial t^2}\frac{\Delta t^3}{3!}\frac{\partial^3 \eta(x,t)}{\partial t^3} + \cdots \qquad 2.2$$

Where, Δt is the grid interval. The "forward" difference can be formed by

rearranging Equation 2.2 as follows:

$$\frac{\partial \eta(x,t)}{\partial t} = \frac{\eta(x,t+\Delta t) - \eta(x,t)}{\Delta t} + O(\Delta t) \qquad 2.3$$

Where, the first term in the right side of Equation 2.3 is obviously the finite difference representation for the first order of time derivative at t = t (see Figure 1.1).

The truncation error which has the order of $\Delta t, O(\Delta t)$ is the difference between the partial derivative and its finite difference representation. Moreover, the Taylor expansion series in Equation 2.2 can be rearranged by replacing Δt by $+\Delta t/2$ and $-\Delta t/2$; thus, "central" difference with the second order of truncation error can be obtained.

$$\frac{\partial \eta(x,t)}{\partial t} = \frac{\eta\left(x,t+\frac{1}{2}\Delta t\right) - \eta\left(x,t-\frac{1}{2}\Delta t\right)}{\Delta t} + O(\Delta t^2) \qquad 2.4$$

It is interesting that although the expression of the finite difference representations in Equations 2.3 and 2.4 are similar, the order of truncation errors is different. By using the above "central" difference method with the staggered numerical points for water level and discharges, which is called the staggered leap-frog scheme, Equation 2.1 can be discretised as follows.

$$\begin{aligned} &\frac{1}{\Delta t}\left(\eta_i^{n+1} - \eta_i^n\right) + \frac{1}{\Delta x}\left(M_{i+1/2}^{n+1/2} - M_{i-1/2}^{n+1/2}\right) + O(\Delta x^2) = 0 \\ &\frac{1}{\Delta t}\left(M_{i+1/2}^{n+1/2} - M_{i+1/2}^{n-1/2}\right) + g\frac{(D_{i+1}^n + D_i^n)}{2}\frac{1}{\Delta x}(\eta_{i+1}^n - \eta_i^n) + O(\Delta x^2) = 0 \end{aligned} \qquad 2.5$$

For dealing with discrete values in numerical computations, $\eta(x,t)$ and $M(x,t)$ are expressed for the case of the staggered leap-frog scheme as

$$\begin{aligned} &\eta(x,t) = \eta(i\Delta x, n\Delta t) = \eta_i^n \\ &M(x,t) = M\{(i+1/2)\Delta x, (n+1/2)\Delta t\} = M_{i+1/2}^{n+1/2} \end{aligned} \qquad 2.6$$

where Δx and Δt are the grid sizes in x-direction and in time-t. The point schematics for the numerical scheme are illustrated in Figure 2.1. The point for water depth-h is the same as those for water elevation, η.

$$D_i^n = \eta_i^n + h_i$$

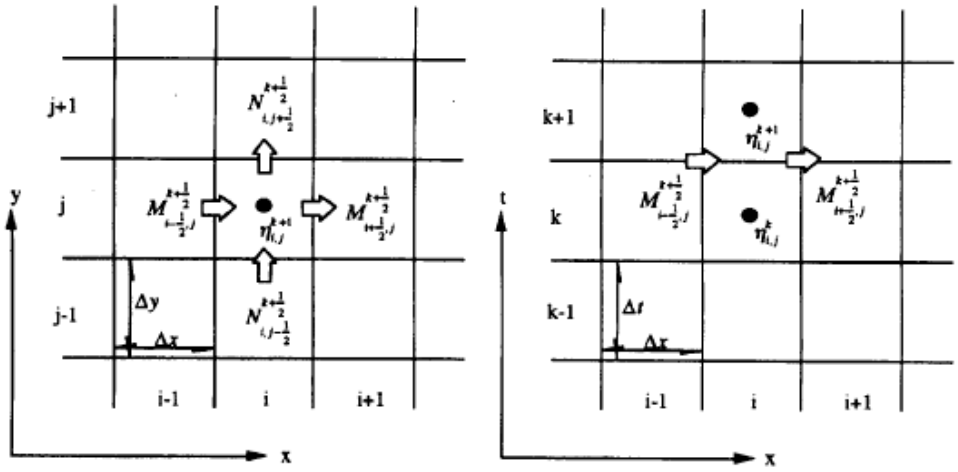

Figure 2.1 The point schematics for the numerical scheme

The above finite method provides stable result as long as the C.F.L condition is satisfied:

$$C \text{ (celerity)} < \Delta x / \Delta t$$

Details of the stable condition can be found in Chapter 3.1 of Imamura and Goto (1988) in which investigated the truncation errors in three kinds of typical scheme for long wave simulations and showed that in term of numerical accuracy the staggered leap-frog scheme is the best among them.

2.2. Numerical scheme for convection terms

In the present numerical scheme, an "upwind" difference scheme is applied to the convection terms in order to make the computation stable. The reason why this scheme ensures the stability of computation is explained by taking a simple convection equation in the following:

$$\frac{\partial F}{\partial t} + C\frac{\partial F}{\partial x} = 0 \qquad 2.7$$

Here the coefficient-C is the propagation velocity and is assumed constant. The arrangement of computation points in the present scheme requires the forward difference scheme for the first order time derivations. This yields

$$\frac{\partial F}{\partial t} = \frac{1}{\Delta t}\left(F_i^{n+1} - F_i^n\right) - \frac{\Delta t}{2}\frac{\partial^2 F}{\partial t^2} + O(\Delta t^2) \qquad 2.8$$

In addition, the central difference is applied to the space derivative.

$$C\frac{\partial F}{\partial x} = \frac{C}{2\Delta x}\left(F_{i+1}^{n} - F_{i-1}^{n}\right) + O(\Delta x^2) \qquad 2.9$$

As a result, F_i^{n+1} is given by

$$F_i^{n+1} = F_i^k - C\frac{\Delta t}{2\Delta x}\left(F_{i+1}^{n} - F_{i-1}^{n}\right) \qquad 2.10$$

The solution of Equation 2.10 is implicitly equivalent the solution of Equation 2.11 with a truncation error of $(\Delta t^2 + \Delta x^2)$. Substituting Equations 2.8 and 2.9 into Equation 2.7 yields

$$\frac{\partial F}{\partial t} + \frac{\Delta t}{2}\frac{\partial^2 F}{\partial t^2} + C\frac{\partial F}{\partial x} = 0 \qquad 2.11$$

If the second-order derivative with respect to time is rewritten by using the following relationship (this assumption is valid for the progressive waves),

$$\frac{\partial^2 F}{\partial t^2} = \frac{\partial}{\partial t}\left(-C\frac{\partial F}{\partial x}\right) = C^2\frac{\partial^2 F}{\partial x^2}$$

The solution of Equation 2.11 is the same as the solution of the following diffusion equation in which the diffusion coefficient is negative.

$$\frac{\partial F}{\partial t} + C\frac{\partial F}{\partial x} = -\frac{\Delta t}{2}C^2\frac{\partial^2 F}{\partial t^2} \qquad 2.12$$

A negative diffusion works to amplify round-off errors with time leading to instability. Therefore, Equation 2.10 is an unstable difference scheme. More details about stable and unstable scheme are discussed in chapter 3.1.

In order to obtain a stable scheme, the space derivative term is approximated by either forward or backward difference depending on the sign of coefficient-C. The forward difference can be written as

$$C\frac{\partial F}{\partial x} = \frac{C}{\Delta x}\left(F_{i+1}^{n} - F_i^n\right) - \frac{\Delta x}{2}C\frac{\partial^2 F}{\partial x^2} + O(\Delta x^2)$$

and the backward difference can be expressed as

$$C\,\frac{\partial F}{\partial x} = \frac{C}{\Delta x}\,(F_i^n - F_{i-1}^n) + \frac{\Delta x}{2}\,C\,\frac{\partial^2 F}{\partial x^2} + O(\Delta x^2)$$

The solution of the corresponding differential equations is within the truncation error of $O(\Delta t^2 + \Delta x^2)$, for the forward difference

$$\frac{\partial F}{\partial t} + C\,\frac{\partial F}{\partial x} = -\frac{C}{2}\,(C\Delta t + \Delta x)\,\frac{\partial^2 F}{\partial x^2} \qquad 2.13$$

and for the backward difference

$$\frac{\partial F}{\partial t} + C\,\frac{\partial F}{\partial x} = -\frac{C}{2}\,(-C\Delta t + \Delta x)\,\frac{\partial^2 F}{\partial x^2} \qquad 2.14$$

Therefore, to keep the virtual diffusion coefficient positive (or say to ensure the stability of the computation), the backward difference in case of positive C, and the forward difference in case of negative C, in addition to setting $\frac{\Delta x}{\Delta t} > |C|$ are used. In other words, the difference should be taken in the direction of the flow. This is the reason why this scheme is called the "upwind" difference. Although the leap-frog scheme has the truncation error of the order of Δx^2 as long as the convection term concerns, its order become large as Δx.

2.3. Numerical scheme for bottom friction term

The friction term becomes a source of instability if it is discretized with an explicit scheme. To make the discussion of instability simple, the following momentum equation without convection terms is considered:

$$\frac{\partial M}{\partial t} + gD\,\frac{\partial \eta}{\partial x} + \frac{gn^2}{D^{7/3}}\,M|M| = 0 \qquad 2.15$$

The explicit form of Equation 2.15 is

$$M^{n+1} = \left(1 - \frac{gn^2}{D^{\frac{7}{3}}}|M|\right)M^n - gD\,\frac{\partial \eta}{\partial x} \qquad 2.16$$

When a velocity become large or a total depth is small in a very shallow water, the absolute of coefficient (amplification factor) of the first term on the right hand side of Equation 2.16 become more than unity, which leads to numerical instability. In order to overcome this problem, an implicit scheme to set a

friction term can be basically introduced. For example, a simple implicit form

$$M^{n+1} = \frac{M^n}{\left(1 + \frac{gn^2}{D^{7/3}}|M|\right)} - \frac{gD\frac{\partial \eta}{\partial x}}{\left(1 + \frac{gn^2}{D^{7/3}}|M|\right)} \qquad 2.17$$

ensures numerical stability, because the amplification factor in Equation 2.17 is always less than unity. However the effect of friction in shallow water becomes so large that numerical results are dumped. Another implicit form, a combined implicit one to the friction term is given by,

$$M^{n+1} = \frac{M^n\left(1 - \frac{gn^2}{2D^{7/3}}|M|\right)}{\left(1 + \frac{gn^2}{2D^{7/3}}|M|\right)} - \frac{gD\frac{\partial \eta}{\partial x}}{\left(1 + \frac{gn^2}{2D^{7/3}}|M|\right)} \qquad 2.18$$

This scheme also gives a stable result. It is, however, noted that the above scheme causes a numerical oscillation at the wave front because the amplification factor could be negative.

The best scheme among some implicit ones should be selected to apply the bottom friction term with Manning's roughness. Considering the fact that the numerical scheme of convection terms also involves artificial or numerical dissipation, selection of Equation 2.17 causes much damping in the result. Therefore the present model uses the combined implicit scheme, Equation 2.18.